

# Insights into vector control through the modulation of *An. gambiae* G protein-coupled receptors

Author: Kimberly Regna

Persistent link: <http://hdl.handle.net/2345/bc-ir:104637>

This work is posted on [eScholarship@BC](#),  
Boston College University Libraries.

---

Boston College Electronic Thesis or Dissertation, 2015

Copyright is held by the author, with all rights reserved, unless otherwise noted.

Boston College

The Graduate School of Arts and Science

Department of Biology

Insights into vector control through the modulation of *An. gambiae*  
G protein-coupled receptors

a dissertation

by

KIMBERLY REGNA

Submitted in partial fulfillment of the requirements  
for the degree of

Doctor of Philosophy

July 2015

© copyright by KIMBERLY REGNA  
2015

## ABSTRACT

### INSIGHTS INTO VECTOR CONTROL THROUGH THE MODULATION OF *AN. GAMBIAE* G PROTEIN-COUPLED RECEPTORS

Kimberly Regna

Thesis Advisor: Professor Marc A.T. Muskavitch

Malaria is a life-threatening infectious disease caused by inoculation of the apicomplexan *Plasmodium* parasite into vertebrate hosts. Transmission of the parasite is mediated by the *Anopheles* mosquito, which has the capacity to efficiently transmit the parasite from host to host, as the disease vector. There are many factors that make anopheline mosquitoes competent vectors for disease transmission. The hematophagous (blood-feeding) behavior of the female mosquito is one of most fundamental factors in physical transmission of parasites, because the ingestion of blood from an infected host allows parasite entry into the mosquito and the completion of parasite sexual reproduction. In addition to this blood-feeding behavior, there are a host of biological (i.e., parasite replication) and behavioral factors (i.e., mosquito chemosensation, host preference) that contribute to the high vectorial capacity of these vector species.

There are over four hundred *Anopheles* species worldwide, approximately forty of which are considered epidemiologically critical human malaria vectors. *Anopheles gambiae*, the primary vector in malaria-endemic sub-Saharan Africa, is responsible for the largest number of malaria cases in the world and is therefore one of the most important vectors to study and target with control measures. Currently, vector-targeted



control strategies remain our most effective tools for reduction of malaria transmission and incidence. Although control efforts based on the deployment of insecticides have proven successful in the past and are still widely used, the threat and continuing increases of insecticide resistance motivate the discovery of novel insecticides. In this thesis, I provide evidence that G protein-coupled receptors (GPCRs) may serve as “druggable” targets for the development of new insecticides, through the modulation of developmental and sensory processes.

In Chapter II, “A critical role for the *Drosophila* dopamine 1-like receptor Dop1R2 at the onset of metamorphosis,” I provide evidence supporting an essential role for this receptor in *Drosophila melanogaster* metamorphosis via transgenic RNA interference and pharmacological methods. In *An. gambiae*, we find that the receptor encoded by the mosquito ortholog GPRDOP2 can be inhibited *in vitro* using pharmacological antagonists, and that *in vivo* inhibition with such antagonists produces pre-adult lethality. These findings support the inference that this *An. gambiae* dopamine receptor may serve as a novel target for the development of vector-targeted larvicides. In Chapter III, “RNAi trigger delivery into *Anopheles gambiae* pupae,” I describe the development of a method for injection directly into the hemolymph of double strand RNA (dsRNA) during the pupal stage, and I demonstrate that knockdown of the translational product of the *SRPN2* gene occurs efficiently, based on reductions in the levels of SRPN2 protein and formation of melanized pseudo-tumors, in *SRPN2* knockdown mosquitoes. This method was developed for rapid knockdown of target genes, using a dye-labeled injection technique that allows for easy visualization of injection quality. This technique is further utilized in Chapter IV, “Uncovering the Role

of an *Anopheles gambiae* G Protein-Coupled Receptor, GPRGR2, in the Detection of Noxious Compounds,” where the role for GPRGR2 in the detection of multiple noxious compounds is elucidated. We find that pupal stage knockdown of this receptor decreases the ability of adult *Anopheles gambiae* to identify multiple noxious compounds. While these findings provide a strong link between GPRGR2 and a very interesting mosquito behavior, they may also provide opportunities to develop better field-based strategies (i.e., insecticides baited traps) for vector control.

The goal of this thesis is to understand the functional roles of selected mosquito GPCRs that may serve as targets for the development of new vector-targeted control strategies. Exploiting these GPCRs genetically and pharmacologically may provide insights into novel vector control targets that can be manipulated so as to decrease the vectorial capacity of *An. gambiae* and other malaria vectors in the field, and thereby decrease the burden of human malaria.

## **DEDICATION**

This thesis is dedicated to my husband (Chase Miller), mother (Nancy Regna) and sister (Katie Pohlmeier), who have always shown me endless love, support and encouragement.

## ACKNOWLEDGEMENTS

There are a number of people without whom this thesis might not have been written, and to whom I am greatly indebted. First, I would like to thank my thesis advisor, Dr. Marc A.T. Muskavitch, for allowing me the opportunity to explore the field of vector biology, as well as the actual field in Africa. His enthusiastic support and encouragement throughout the years have been fundamental to my development as a scientist. I also need to thank all of the members of the Muskavitch Lab for the many interesting discussions and insights we have shared over the years – and, of course, for making every day so much fun! I especially need to thank Adam Jenkins with whom I not only explored a new area of vector research, but also new areas of the world during our travels. I also need to thank my amazing undergraduate students, Rachel Harrison and Kristin Torre, for putting in so much time and effort to make this work possible. I am extremely grateful for the all of the helpful advice and support provided by the members of my thesis committee: Dr. Michelle Meyer, Dr. Welkin Johnson and Dr. Flaminia Catteruccia.

A great deal of the work presented in this thesis was possible because of collaborations with individuals at various institutions. At Tufts Medical Center, I would like to give my sincere thanks to Dr. Isabelle Draper, Dr. Alan Kopin, Dr. Ben Harwood and Dr. Jamie Doyle for contributing so much insight and support, and for helping me advance my scientific skills in pharmacology. For all of the discussions (and mosquitoes) shared, I would like to thank Dr. Flaminia Catteruccia, Emily Lund and Dr. Rob Shaw at the Harvard School of Public Health. Members of the Garrity Lab at Brandeis University

have been very helpful in pursuing the chemosensory work, especially Dr. Gonzalo Budelli and Dr. Paul Garrity. At Kansas State University, Dr. Kristin Michel has been very generous, not only her research materials, but also with her time.

My experience at Boston College would not have been nearly as great without the friends I have made over the years. I will miss all of the Thursday Thursdays, Odd Fridays, game nights, dinner parties, etc. – hopefully we can still make some of them happen when we are “grown ups”. Michelle – thanks for all the “Sunday-funday” brunch/science dates and for being the best java buddy a person can ask for!

Last, but not at all least, I need to thank my family for being so supportive during the time I have spent pursuing this degree. Mom – thank you for allowing me to begin my career as a scientist as a little kid setting up experiments in our bathroom (laboratory). Katie – not only have you been great sister, but also a great fellow scientist to talk about my research with. Chase – I cannot put into words how thankful I am to have such an amazing husband and how lucky I am to have met you during this journey.

# TABLE OF CONTENTS

ABSTRACT .....	i
DEDICATION.....	iv
ACKNOWLEDGEMENTS.....	v
LIST OF TABLES.....	x
LIST OF FIGURES.....	xvii
LIST OF DATASETS .....	xix

## CHAPTER I: INTRODUCTION

A. Malaria as a Major Public Health Issue .....	2
B. Malaria Life Cycle .....	8
C. Malaria Vector: <i>Anopheles</i> mosquito.....	10
D. Control Strategies, Implementation and the Battle of Insecticide Resistance .....	16
E. G protein-coupled Receptors (GPCRs): Drug Targets.....	20
F. Figures and Legends .....	30

## CHAPTER II: A critical role for the *Drosophila* dopamine 1-like receptor Dop1R2 at the onset of metamorphosis

A. ABSTRACT.....	34
B. INTRODUCTION .....	35
C. RESULTS .....	38
D. DISCUSSION.....	46
E. METHODS .....	55
F. TABLES, FIGURES AND LEGENDS.....	65

## CHAPTER III: RNAi trigger delivery into *Anopheles gambiae* pupae

A. ABSTRACT.....	90
B. INTRODUCTION .....	91
C. RESULTS .....	94
D. DISCUSSION.....	95
E. METHODS (PROTOCOL) .....	99
F. FIGURES AND LEGENDS.....	105

CHAPTER IV: Uncovering the role of an *Anopheles gambiae* G protein-coupled receptor, GPRGR2, in the detection of bitter compounds

A. ABSTRACT.....	112
B. INTRODUCTION .....	113
C. RESULTS AND DISCUSSION.....	119
D. METHODS .....	130
E. FIGURES AND LEGENDS.....	136

**APPENDIX**

CHAPTER AI: Modulation of TRPA1 thermal sensitivity enables sensory discrimination in *Drosophila*

A. ABSTRACT.....	149
B. INTRODUCTION, RESULTS AND DISCUSSION.....	150
C. METHODS .....	157
D. TABLES, FIGURES AND LEGENDS.....	162

CHAPTER AII: CYP6 P450 Enzymes and *ACE-1* duplication produce extreme and multiple insecticide resistance in the malaria mosquito *Anopheles gambiae*

A. ABSTRACT.....	177
B. INTRODUCTION .....	178
C. RESULTS .....	182
D. DISCUSSION.....	188
E. METHODS .....	195
F. TABLES, FIGURES AND LEGENDS.....	204

CHAPTER AIII: Metabolic and target-site mechanisms combine to confer strong DDT resistance in *Anopheles gambiae*

A. ABSTRACT.....	223
B. INTRODUCTION .....	224
C. RESULTS .....	226
D. DISCUSSION.....	231
E. METHODS .....	235
F. TABLES, FIGURES AND LEGENDS.....	245
<b>REFERENCES.....</b>	<b>260</b>



## **LIST OF FIGURES**

**Figure 1.1:** Global distribution of malaria vector species

**Figure 1.2:** Malaria Life Cycle

**Figure 1.3:** G Protein-Coupled Receptor Signaling

**Figure 2.1:** Dop1R2 cDNA and a corresponding interference construct

**Figure 2.2:** Dop1R2 RNAi flies show decreased Dop1R2 transcript levels

**Figure 2.3:** dsDop1R2 RNAi constructs

**Figure 2.4:** Ubiquitous knockdown of Dop1R2 results in reduced adult emergence and wing and/or melanization phenotypes

**Figure 2.5:** dsDop1R2 knockdown-induced lethality is recapitulated with alternate RNAi constructs

**Figure 2.6:** Down-regulation of Dop1R2 around larval-to-pupal ecdysis leads to developmental arrest

**Figure 2.7:** Transcriptome analysis of Dop1R2 RNAi arrested flies reveals up-regulation of families of related genes

**Figure 2.8:** WEB-based GENE SeT AnaLysis (WEBGestalt)

**Figure 2.9:** STRING analysis reveals protein-protein interactions

**Figure 2.10:** RT-PCR analysis confirm differential expression of genes in Dop1R2 RNAi flies

**Figure 2.11:** Tyrosine hydroxylase expression is increased in dsDop1R2 pupae

**Figure 2.12:** Dop1R2 down-regulation using the P{GawB}332.3 driver leads to developmental arrest at the pharate adult stage

**Figure 2.13:** Progression from egg to L1 instar

**Figure 2.14:** dsDop1R2 knockdown using alternate salivary gland driver results in semi-lethality

**Figure 2.15:** Confirmation of salivary gland expression in tested driver stocks

**Figure 2.16:**  $G\alpha_s$ -targeted, but not  $G\alpha_i$ -targeted KD in the salivary glands results in pre-adult lethality

**Figure 2.17:** Dop1R2 is expressed in prepupal salivary glands and brain

**Figure 2.18:** Dop1R2 is stimulated by dopamine and antagonized by two known small molecules *in vitro*

**Figure 2.19:** Exposure of *Drosophila melanogaster* ( $w^{1118}$ ) larvae to flupenthixol dihydrochloride results in increased lethality and developmental abnormalities

**Figure 2.20:** Dop1R2 sequence motif

**Figure 3.1:** Developmental staging for pupal dsRNA injection

**Figure 3.2:** Injection position and distribution of dye-labeled dsRNA

**Figure 3.3:** Post-injection adult emergence

**Figure 3.4:** Emergence rate, sex assessment and adult survival

**Figure 3.5:** Pseudo-tumor positive control phenotype reflects successful knockdown

**Figure 3.6:** Quantification of pseudo-tumor formation and decreased SRPN2 protein levels

**Figure 4.1:** GPRGR2 sequence motif, structure and phylogeny

**Figure 4.2:** *An. gambiae* GPRGR membrane topology

**Figure 4.3:** *An. gambiae* GPRGR2 is highly expressed in multiple sensory appendages

**Figure 4.4:** Choice preference assay

**Figure 4.5:** *An. gambiae* bitter compound aversion

**Figure 4.6:** *An. gambiae* sensilla scanning electron micrographs (SEMs) and electrophysiology

**Figure 4.7:** *An. gambiae* GPRGR2 knockdown

**Figure 4.8:** *An. gambiae* GPRGR2 knockdown results in decreased bitter compound aversion

**Figure A1.1:** Reactive electrophiles cause incapacitation in *Drosophila*

**Figure A1.2:** TRPA1-dependent gustatory neurons do not respond to heat

**Figure A1.3:** Example response from labellar gustatory bristles to electrolyte-only solution in wild type and *Trpa1<sup>ins</sup>* mutants

**Figure A1.4:** TRPA1 isoform diversity yields tissue-specific channels with different thermal sensitivities

**Figure A1.5:** TRPA1(A) currents below and above the transition temperature show similar reversal potentials and voltage dependences

**Figure A1.6:** Comparison of maximum heat-responsive current amplitudes for wild type TRPA1(A) and TRPA1(B) channels from *Drosophila melanogaster* and *Anopheles gambiae*

**Figure A1.7:** TRPA1 isoform diversity determines sensory specificity of gustatory neurons

**Figure A1.8:** Example responses from labellar gustatory bristles for TRPA1 rescue and gain-of-function

**Figure A1.9:** Regulation of insect TRPA1 thermosensitivity by alternative N termini

**Figure A1.10:** Representative current recordings of wild type TRPA1 isoforms and TRPA1(A) mutants

**Figure A1.11:** Comparison of maximum current responses for wild type and mutant TRPA1 channels

**Figure A1.12:** NMM sensitivities of TRPA1(A) mutants are similar to those of wild type TRPA1(A)

**Figure A1.13:** Both agTRPA1(A) and agTRPA1(B) robustly respond to reactive electrophiles

**Figure A1.14:** Conservation of TRPA1 diversity in insect pests

**Figure A2.1:** Microarray Experimental Design

**Figure A2.2:** Genes Significantly Overexpressed (Relative to Susceptible Samples) in Tiassalé Bendiocarb Resistant Samples in Exp1, and both Tiassalé and Kovié Samples

**Figure A2.3:** Probes significantly over-expressed in Kovié

**Figure A2.4:** Microarray results for Tiassalé selected vs unexposed controls

**Figure A2.5:** Relationship between expression measured by qRT-PCR and microarrays for candidate genes

**Figure A2.6:** qRT-PCR Expression Analysis of Candidate Genes

**Figure A2.7:** Survival of transgenic *D. melanogaster* that express *CYP6M2* or *CYP6P3* in the presence of varied amounts of insecticides

**Figure A2.8:** Survival of Transgenic *Drosophila* Expressing *An. gambiae* *Cyp6M2* or *CYP6P3* in the Presence of Bendiocarb

**Figure A2.9:** *In vitro* Metabolism of Bendiocarb by Recombinant *CYP6P3* Expressed in *E. coli*

**Figure A2.10:** Insecticide Resistance Phenotypes From Dry (Blue) and Wet (Red) Seasons With and Without the Synergist PBO

**Figure A2.11:** Role of Target Site Allelic Variation and Copy Number Variation in Bendiocarb Resistance

**Figure A2.12:** Interwoven microarray experimental loop

**Figure A3.1:** Mean normalized expression of *GSTe2* in female *An. gambiae* s.s. of the DDT resistant ZAN/U strain and susceptible Kisumu strain

**Figure A3.2:** Western blot comparison of *GSTe2* protein level in the Kisumu (Kis) and ZAN/U (Zan) *An. gambiae* s.s. strains

**Figure A3.3:** Comparison of *GSTE2* catalyzed DDT metabolism for three variant recombinant proteins over a DDT dilution series

**Figure A3.4:** Crystal structure of *GSTE2* ZAN/U variant

**Figure A3.5:** Superimposition of the *GSTE2* enzymes of *An. gambiae* (ZAN/U variant generated in this study containing Thr114) and *An. funestus* (containing Ile114)

**Figure A3.6:** Subunit Interface in *GSTE2* variants

**Figure A3.7:** Dose-response curves for *Drosophila melanogaster* adults transformed with *Anopheles gambiae* *Gste2* alleles

**Figure A3.8:** Geographical variation in frequency of *Gste2*-I114T in the S and M molecular forms of *An. gambiae* across Africa

**Figure A3.9:** Summary of haplotypic association tests for the combination of four possible allele combinations at the *Vgsc*-1014 (*kdr*) and *Gste2*-114 loci with DDT susceptibility in *An. gambiae* M-form females from Benin and Burkina Faso

**Figure A3.10:** SDS PAGE gel illustrating the purity of three recombinant variants of *Gste2* isolated from *An. gambiae* s.s.

## LIST OF TABLES

**Table 2.1:** Effect of tissue-specific down-regulation of Dop1R2

**Table 2.2:**  $G\alpha_s$ , but not  $G\alpha_i$ , knockdown targeted to salivary glands/amnioserosa leads to developmental arrest

**Table 2.3:** Primer sequences

**Table 4.1:** GPRGR2 orthologs

**Table 4.2:** Bitter compounds

**Table 4.3:** Primer sequences

**Table A2.1:** Survival of transformed *D. melanogaster* expressing *CYP6M2* and *CYP6P3* exposed to the pyrethroids permethrin and deltamethrin, and for *CYP6M2* also DDT

**Table A2.2:** qRT-PCR expression results for transformed *Drosophila melanogaster*

**Table A2.3:** Generalized linear model testing the effects of insecticide type, season and PBO on bioassay mortality

**Table A2.4:** Resistance association of the G119S target site mutation, in the presence and absence of PBO following 60 min bendiocarb exposure

**Table A2.5:** qRT-PCR primer details for copy number variant analysis

**Table A2.6.** qRT-PCR primer details for gene expression analysis



**Table A3.1:** *GSTE2* allelic variants from the *An. gambiae* Kisumu and ZAN/U strain used for recombinant protein expression

**Table A3.2:** Enzyme kinetic parameters of three *GSTE2* alleles with substrate DDT

**Table A3.3:** PCR primers

**Table A3.4:** Statistics for X-ray data and model refinement

**Table A3.5:** Exact latitudes and longitudes of the sample collections

## **LIST OF DATASETS**

**Dataset 2.1:** Summary of microarray data

**Dataset 2.2:** DAVID bioinformatic analysis of dsDop1R2 differentially expressed genes

**Dataset 4.1:** TMHMM topology and TMD prediction data

# **CHAPTER I**

## **INTRODUCTION**

## A. Malaria as a Major Public Health Issue

In 2013, the World Health Organization (WHO) reported that there were approximately 200,000,000 reported cases of malaria and nearly 600,000 malaria-induced deaths (Nájera et al. 2011; World Health Organization 2014; GBD 2013 Mortality and Causes of Death Collaborators 2015). Among these reported deaths, approximately 78% percent were children under the age of five, and an estimated 96% percent of the total occurred in African countries (Petersen et al. 2011; World Health Organization 2014; Cheruiyot et al. 2014; Bartoloni & Zammarchi 2012). In 14 sub-Saharan African countries, malaria was reported as the leading cause of death (Durand et al. 2001; GBD 2013 Mortality and Causes of Death Collaborators 2015; Warhurst 2001). In addition to Africa, malaria is still a major public health concern in other geographical regions, such as South Asia, Southeast Asia, Central America, South America, the Caribbean and the Middle East (P. G. Bray et al. 1998; Snow et al. 1999; GBD 2013 Mortality and Causes of Death Collaborators 2015) (Figure 1.1). From a global perspective, approximately 3.2 billion individuals are at risk for contracting malaria (World Health Organization 2014), representing almost half of the world's current population.

Malaria is an infectious disease that is characterized by an infection in a vertebrate host by apicomplexan *Plasmodium* parasites. The vertebrate hosts currently known include humans, monkeys, rodents, birds and reptiles (Bashar et al. 2012). There are four major species within the *Plasmodium* genus that are able to infect a human host, causing malaria: *P. falciparum*, *P. vivax*, *P. ovale* and *P. malariae* (Biamonte et al. 2013; Butcher et al. 1970; N. J. White et al. 2014). Although historically considered a macaque-specific species, *P. knowlesi* has also been reported as a fifth species that is able

to infect humans (B. Singh & Daneshvar 2013; N. J. White et al. 2014). Among these five species, *P. falciparum* is the most epidemiologically prevalent and yields the highest mortality rates (Snow et al. 1999; Gething et al. 2011). In fact, *P. falciparum* is responsible for approximately 90% of malaria-related deaths in sub-Saharan Africa (World Health Organization 2014). *P. vivax*, although not as prevalent a public health concern as *P. falciparum*, is responsible for 47% of malaria-related deaths worldwide (World Health Organization 2014) and is observed over a larger geographical area due to its ability to remain dormant for years (Zucker 2009; World Health Organization 2014; Biamonte et al. 2013).

Malaria transmission almost exclusively occurs through the bite of an infected *Anopheles* mosquito, with rare transmissions occurring via blood transfusions or *in utero* transmission from mother to fetus (Bartoloni & Zammarchi 2012). The symptoms of the disease often present as flu-like (e.g., fever and chills), but can include more severe symptoms (e.g., renal failure, retinopathy, cerebral malaria and hemolytic anemia), and can prove to be fatal (Beare et al. 2006; World Health Organization 2014; Laishram et al. 2012). In young children and pregnant women, symptoms are often much more severe (e.g., cerebral malaria and miscarriage) as a result of an underdeveloped or suppressed immune system (N. J. White et al. 2014; Laishram et al. 2012). Given the potential severity of symptoms, and the risk of mortality, rapid diagnostics and prompt treatment are critical to decrease malaria case mortality rates.

Currently, malaria diagnoses can be made by quantification of parasite loads in blood smears by simple microscopy or by antigen-based rapid diagnostic tests (RDT) (Murray & Bennett 2009; World Health Organization 2014). Using RDT methods, it is

also possible to distinguish between *P. falciparum* and *P. vivax* by targeting lactate dehydrogenase (LDH) with specific antibodies (Murray & Bennett 2009; Makler et al. 1998). Because these two species show different drug resistance patterns in different geographical regions (Schneider & Escalante 2013), the ability to distinguish between these species is important, so that the appropriate drug can be administered. In addition to aiding in diagnosis and treatment, these tests have been beneficial in surveying *P. falciparum* infection prevalence and parasite rate (PfPR) to assess trends over time and better identify populations at risk (World Health Organization 2014; Gething et al. 2011).

Treatment for individuals with malaria was introduced as early as the seventeenth century, prior to understanding what actual microbial causative agent of the disease. Quinine, a compound that is found in the bark of the cinchona tree, was found to have medicinal properties that alleviate malarial fevers and was widely used for malaria treatment (Dinio et al. 2012). The mechanism by which this drug functions is still not fully resolved, but the observation that it seems to inhibit heme detoxification via hemozoin biocrystallization suggests that quinine treatment results in the cytotoxic heme accumulation within the parasite (Hempelmann 2006). Mutations in genes that encode transporter proteins such as the multidrug resistance transporter 1 (*pfMDR*) and sodium/proton exchanger 1 (*pfNHE1*) have rendered this drug less effective by inhibiting access to target sites by the rapid expelling of drugs (Petersen et al. 2011; Ibraheem et al. 2014). In the mid-1900s a new compound, chloroquine, was introduced to compensate for the decreased effectiveness of quinine (Nájera et al. 2011). Chloroquine causes parasite lethality by preventing the detoxification of free heme by binding to hematin, which leads to the buildup of heme monomers and causes excess membrane

permeabilization (Petersen et al. 2011; Cheruiyot et al. 2014). Unfortunately, within a few decades of its deployment, chloroquine-resistant parasites arose, particularly based on mutations in the *P. falciparum* chloroquine resistance transporter (*PfCRT*) gene (Durand et al. 2001; Warhurst 2001). Mutations in this gene can cause the parasite to expel the drug from acidic food vacuoles approximately 40-50 times faster than drug-sensitive parasites (P. G. Bray et al. 1998). In response to the drug resistance issues observed with chloroquine, a new sulfadoxine-pyrimethamine (SP) combination therapy that utilizes an alternate mechanism of action was introduced. Sulfadoxine and pyrimethamine are sulfa drugs that function by blocking folate biosynthesis through inhibition of dihydropteroate synthetase (*PfDHPS*) and dihydrofolate reductase (*PfDHFR*), respectively (Petersen et al. 2011; Cowman et al. 1988; Hyde 2002; Sibley et al. 2001). These enzymes play critical roles in reactions that are essential for nucleotide provision during DNA synthesis and in the metabolism of specific amino acids (Hyde 2002). However, the success of this treatment was extremely short-lived, as a result of rapid selection for mutations in both of the target enzymes, *PfDHPS* and *PfDHFR*, resulting in altered drug binding and substantial decreases in parasite susceptibility (Petersen et al. 2011; Korsinczky et al. 2004). Currently, artemisinin and artemisinin combination therapies (ACT) are the most widely used methods for the treatment of malaria (World Health Organization 2014). Artemisinin, while not fully mechanistically understood, likely works by selectively inhibiting the calcium pump PfATP6, as mutations in the gene can modulate the affinity of this pump for artemisinin (Eckstein-Ludwig et al. 2003; Shandilya et al. 2013). Recently, mutations in genes encoding proteins such as sarco-endoplasmic reticulum calcium ATPase6 (*PfSERCA*) and

multidrug resistance protein (*PfMDR1*), have been implicated in artemisinin tolerance, provoking concerns regarding ACT's efficacy (Petersen et al. 2011; Dondorp et al. 2009; Pandey et al. 1999; Eckstein-Ludwig et al. 2003). Although there is significant concern surrounding artemisinin-resistance, ACTs still serve as frontline treatments and currently constitute the most effective approach for rapid clearance of parasites and symptomatic treatment (O'Neill et al. 2010).

In addition to anti-malarial drugs, vector-targeted interventions that reduce vector-host contact and have played significant roles in decreasing malaria rates have also been challenged by the development of insecticide resistance. In fact, the control of malaria in many areas of the globe is attributed primarily to successful vector control strategies, rather than parasite-targeted treatments. During the early 1950s, the United States eradicated malaria by applying both environmental and chemical measures. Environmental management largely focused on reducing vector breeding sites and larval habitats by water drainage in areas such as swamps and ponds (Smillie 1952). Chemical control was implemented by interventions such as household indoor residual spraying (IRS) of the insecticide dichloro-diphenyl-trichloroethane (DDT) for mosquito control (Zucker 2009; L. L. Williams 1963; Andrews et al. 1950). Given the success of these interventions in the United States, the WHO established the Global Malaria Eradication Program to implement control efforts based on the use of DDT worldwide during the mid-1950s (Greenwood et al. 2008; Nájera et al. 2011). This program was unfortunately very short-lived and was ultimately discarded by early 1970s due to the emergence of insecticide resistance, as well as a lack of monetary and governmental resources in many of the endemic areas (Nájera et al. 2011; Greenwood et al. 2008). Despite the



termination of this program, insecticide-based approaches have been critical in controlling malaria rates. The distribution of pyrethroid-based insecticide-treated nets (ITNs) and the deployment of DDT-based IRS applications have played extremely important roles in decreasing malaria incidence in many malaria-endemic areas (Enayati & Hemingway 2010; Martinez-Torres et al. 1998). Similar to parasite-targeted drugs, vector control insecticides have also displayed decreased effectiveness due to the increasing prevalence of target-site mutations that confer insecticide resistance (see “Control Strategies, Implementation and the Battle of Insecticide Resistance,” below).

Global malaria control efforts are currently being implemented through organizations such as the Malaria Eradication Research Agenda (malERA), the Roll Back Malaria (RBM) Partnership and the Bill & Melinda Gates Foundation (Nájera et al. 2011; Alonso et al. 2011). With continuing advances in malaria research and information gained from previous eradication efforts, the ultimate goal is for worldwide eradication of malaria through intensive research and deployment of advanced control efforts in malaria-endemic countries. The WHO reports that between 2000 and 2013, we have already observed a 47% world-wide decrease in malaria-related deaths, largely do to the implementation of vector-targeted control strategies (World Health Organization 2014). While these statistics are encouraging, the problem is far from resolved, as this mosquito-borne disease still affects an exceedingly large number of individuals, and much more effort and many more resources will need to be deployed to reach the goal of complete malaria eradication.

## B. Malaria Life Cycle

The life cycle of the *Plasmodium* parasite occurs in a vector-host system (Figure 1.2) consisting of a primary host, the *Anopheles* mosquito vector, and a vertebrate secondary host (N. J. White et al. 2014). The hematophagous (blood-feeding) nature of the female mosquito is a critical aspect of *Plasmodium*'s life cycle, as the action of blood feeding enables vector-host parasite transfer. Only the female is involved in this biting behavior because she requires proteins obtained from the blood for egg development and completion of the gonotrophic cycle (Takken et al. 2006).

The *Plasmodium* transmission cycle begins when an infected mosquito takes a blood meal from a human host and in doing so releases sporozoite-stage parasites into the human blood stream during the transfer of saliva (Figure 1.2, A), in a process in which the mosquito injects a small amount of saliva to introduce blood anticoagulants (Stark & James 1996). Once this inoculation into a human host occurs, the sporozoites travel through the blood stream to invade the liver, where they replicate within hepatocytes (Figure 1.2, B) in the exo-erythrocytic cycle (Biamonte et al. 2013; N. J. White et al. 2014; Sinden 2002). In the liver, sporozoites will undergo maturation into the schizont stage and for most species will produce approximately 100,000 daughter merozoites within the span of roughly one week (N. J. White et al. 2014). After multiple rounds of replication, the cell will expand to an extent where it will rupture and release merozoites that will then infect red blood cells (RBCs) (Figure 1.2, C), beginning the erythrocytic cycle. While within the erythrocytic cycle, the parasites divide through asexual replication and then progress through morphologically distinct developmental stages, including ring, trophozoite, and schizont (mature and actively replicating) (Sinden

2002; N. J. White et al. 2014). After multiple rounds of division, the RBC will physically increase in size and rupture, releasing daughter merozoites that can infect still other RBCs. The majority of these merozoites will remain in an asexual form and continue to reinfect new RBCs. This leads to parasitemia involving the development of trillions of asexual parasites during the course of a single human infection (N. J. White et al. 2014; Sinden 2002). However, a smaller proportion of these parasites can develop into a sexual stage called a gametocyte (N. J. White et al. 2014), which is then ingested by another blood-feeding mosquito.

Entry into the sporogonic cycle begins within the stomach of the mosquito (Figure 1.2, D), where production of zygotes occurs when the microgametes (male gametes) penetrate the macrogametes (female gametes) (N. J. White et al. 2014; Sinden 2002). The newly formed zygotes can then adopt an elongated and motile structure and enter the epithelial midgut lining as an ookinete (Sinden 2002; N. J. White et al. 2014). The ookinete passes through the midgut epithelium and forms an oocyst on the outer surface of the midgut. After multiple rounds of replication, the oocyst will rupture to release motile sporozoites. It is at this point that thousands of sporozoites move to the salivary glands (N. J. White et al. 2014) where upon another blood meal, a small fraction will be released into a new host via the saliva of the mosquito (Sinden 2002) and reinitiate the malaria transmission cycle.

Parasite entry into erythrocytes is largely dependent on multiple pathways that are mediated by specific ligand-receptor interactions (Crosnier et al. 2011; Lo et al. 2015; Howes et al. 2011). For example, in order to enter RBCs, *P. falciparum* requires basigin, a human blood group antigen, to bind the parasite ligand reticulocyte-binding protein

(PfPRH5) (Crosnier et al. 2011). In basigin-negative individuals, the parasite is unable to enter RBCs (Crosnier et al. 2011). Additionally, for *P. vivax*, the Duffy blood group antigen is required for parasite entry into the RBC (Lo et al. 2015). These differences in receptor-ligand mediated entry impact infection rates in African areas, particular West Africa, where Duffy-negative populations are high (Howes et al. 2011). However, parasite entry is not the only critical requirement for a successful infection. Research has shown that individuals who are heterozygous for the human *globin* gene mutation that causes sickle cell anemia have a very high tolerance for *Plasmodium* (T. N. Williams 2006; Ferreira et al. 2011). Each of these examples is related to a selection process by which these mutations confer a survival advantage to those individuals who reside in malaria-endemic areas, such as Africa, by inhibiting the life cycle of the parasite.

### **C. Malaria Vector: *Anopheles* mosquito**

*Anopheles* mosquito development consists of four developmentally and behaviorally distinct stages: embryo, larva, pupa and adult. Development begins in an aqueous environment when a female mosquito lays a raft of approximately 50-200 fertilized eggs in a body of water (Clements 1992). Upon hatching, the larva will progress through four larval instars that are developmentally defined by cuticular molting events. At the completion of the fourth larval instar, the pupa is formed, and the organism undergoes metamorphosis that involves extensive morphological remodeling, resulting in a fully formed and developmentally distinct adult (Clements 1992). Developmental transitions are regulated by precisely controlled levels of ecdysteroid hormones and juvenile hormone (JH) (Riehle et al. 2002; Truman & Riddiford 2007).

After emerging from the pupal case, the adult wings expand and the cuticle undergoes sclerotization (hardening) (Dewey et al. 2004; Charles 2010). Within 48-72 hours after emergence, the adult is physiologically ready for mating (Clements 1999; Takken et al. 2006). The virgin female exhibits a pregravid state that necessitates the intake of more than one blood meal to complete the initial gonotrophic cycle (Gillies 1954). While males continue to mate throughout adulthood, females become refractory after an initial mating, usually in response to peptides secreted by the male accessory glands, and will store the sperm in the spermathecae for subsequent fertilizations (Ringo 1996; Tripet et al. 2003). Despite being able to perform subsequent fertilization using stored sperm, there is a requirement for an additional blood meal before egg-laying, allowing infected mosquitoes to transmit malaria parasites they acquired during previous bloodmeals.

There are approximately 465 known species within the *Anopheles* genus (Sinka et al. 2012). To date approximately 70 are known to have the capacity to transmit malaria, and about 40 of these are considered major malaria vectors (World Health Organization 2014; Sinka et al. 2012). Among these species, the three malaria vectors that pose a severe health concern in the most endemic area of sub-Saharan Africa are *An. gambiae*, *An. arabiensis*, (a member of the *An. gambiae* species complex) and *An. funestus* (Sinka et al. 2012; Besansky et al. 2004). *An. gambiae* is the most epidemiologically relevant vector, as it is responsible for approximately 90% of malaria cases in this region of Africa (World Health Organization 2014; Besansky et al. 2004).

Vectorial capacity is the measurement of how efficient a vector species is at transmitting a disease between hosts (Ceccato et al. 2012; Garrett-Jones & Shidrawi 1969). This concept has been developed into a mathematical model that takes into

account factors that play major roles in vectorial capacity including frequency of bites, blood-feeding preference, population density, survival and extrinsic incubation periods (Garrett-Jones & Shidrawi 1969). *An. gambiae* has the highest vectorial capacity in Africa due to its rapid breeding, ability to handle environmental changes, long life span and human biting preference (N. J. White et al. 2014). The equation for vectorial capacity is (D. L. Smith & Ellis McKenzie 2004; Garrett-Jones & Shidrawi 1969):

$$C = \frac{ma^2p^n}{-\ln(p)}$$

where:

$C$  = vectorial capacity (number of infective bites received daily by a single host)

$m$  = vector density with respect to host

$a$  = daily biting frequency

$p$  = daily survival probability of vectors

$n$  = extrinsic incubation period of parasite (days)

This model describes the capacity of a vector species to transmit malaria based on the number of potential secondary inoculations per day from an infected individual. Given the variability of different species (i.e., different biting frequencies and density), the values obtained can help to determine which local species need to be reduced in order to decrease the local intensity of malaria transmission. With the ability to calculate

vectorial capacity based on this model, scientists are now better able to understand vector dynamics across species and geography (Ceccato et al. 2012).

Environmental factors and seasonality play significant roles in the density and reproductive cycles of *Anopheles* mosquitoes, ultimately impacting malaria transmission rates. Geographically speaking, *An. gambiae* prefer wet and humid climates, while *An. arabiensis* are more often found in areas that are drier. *An. funestus* can be found in both wet and dry areas (Ayala et al. 2009). These ecological and environmental preferences allow all three species to co-dominate a large portion of western and southeastern Africa (Figure 1.1, green regions). The substantial variations in climate across portions of Africa allow for each species to become dominant in certain areas such as *An. gambiae* species in the Democratic Republic of Congo or *An. arabiensis* in Ethiopia – with *An. funestus* frequently found with both of these species (Sinka et al. 2012). *An. gambiae* is most often found in areas of Africa that are forest-free and maintain temperatures above 5°C (Snow et al. 1999).

Interestingly, the environmental temperature at which a vector processes a blood meal also greatly affects the ability of the parasite to replicate within the mosquito. At temperatures below 22°C, the incubation period that encompasses the parasite sporogonic cycle begins to approach the time that a mosquito will survive in the field (Snow et al. 1999). For example, at 18°C, *P. falciparum* will take about 55 days to complete sporogonic development, and by that time following parasite uptake, the surviving proportion of a cohort of blood-fed mosquitoes becomes extremely low (Snow et al. 1999; Martens 1998; Detinova 1962). If the temperatures fall below 16°C, the parasite replication will cease (Snow et al. 1999).

Vectorial capacity can also vary due to the behaviors of hosts that are preferentially fed upon or environmental sites that harbor these hosts. *An. gambiae* and *An. funestus* are highly endophagic (i.e., exhibit an indoor feeding preference) and anthropophagic (i.e., a biting preference for humans) (Githeko et al. 1996), making these species more likely to acquire human malaria parasites via blood feeding. However, the actual transmission rates by *An. funestus* are much lower than *An. gambiae* due to its reduced susceptibility to *Plasmodium* infections (Charlwood et al. 1997). *An. arabiensis* is considered to be a zoophilic species, having a biting preference for animals rather than humans (Githeko et al. 1996), decreasing the rate at which it transmits human malaria parasites. Given that *An. gambiae* exhibits anthropophagic and endophagic behaviors, as well as its susceptibility to *Plasmodium* infection and the ability of *Plasmodium* parasites to replicate at high rates within this primary host, this vector species displays high vectorial capacity.

Mosquito mating strategies, sites and preferences play critical roles in the vectorial capacity of a species. In particular, the mosquito population density is largely dependent on the reproductive success of the mosquito (S. N. Mitchell et al. 2015b). By understanding mosquito reproduction, and the behaviors surrounding it, we can identify additional targets for vector control. Both field and laboratory observation of *An. gambiae* mating reveal that copulation typically occurs around dusk (Dabire et al. 2013; Charlwood & Jones 1980), when large swarms (hundreds to thousands) of males form, awaiting the entry of a virgin female into the swarm and her choice of a mating partner to form a *copulae* (mating pair) (Dabire et al. 2013; Charlwood & Jones 1980; Takken et al. 2006). During this swarming process, an intricate set of auditory cues are used by



male and female mosquitoes, in a process called harmonic convergence, which involves reciprocal responses to acoustic tones that are generated by distinct wing beat frequencies (Gibson & I. Russell 2006; Cator et al. 2010). Additionally, olfactory cues such as cuticular hydrocarbons (CHC) have been shown to be involved in mating partner selection (Polerstock et al. 2002), and volatiles emitted by conspecific larvae have been shown to be involved in the identification of oviposition sites (Sumba et al. 2008). Further findings regarding the biochemistry of reproduction, such as uncovering the role of the mating plug hormone 20-hydroxyecdysone (20E) in increasing egg production (S. N. Mitchell et al. 2015b; Baldini et al. 2013) and the requirement of seminal transglutaminase (TG3) in *An. gambiae* mating plug coagulation (Rogers et al. 2009), have provided valuable information regarding mosquito mating. Understanding the biochemical factors and the underlying behaviors that are essential for mosquito mating provides opportunities for the discovery of novel insect control targets, by targeting reproduction.

It has become increasingly apparent that the vectorial success of *Anopheles* mosquitoes relies on many intricate biological, physical and behavioral features. From environmental preferences to acoustic control of mating, there are many interesting facets of mosquito biology of which we are currently aware and surely more to discover. Not only are these aspects of mosquito bionomics interesting from a basic biological perspective, but also useful in providing avenues for vector control by modulation of factors that greatly impact the vectorial capacity of the *Anopheles* mosquito.

#### **D. Control Strategies, Implementation and the Battle of Insecticide Resistance**

Current control strategies largely aim to either decrease vector-host contact by the deployment of insecticides and bed nets or target the parasite in humans by the deployment of antimalarial drugs. While both of these strategies have proven to lessen human malaria incidence, the frequent use of such compounds in both strategies has increased the prevalence of resistance in the mosquito and the parasite. In light of these issues, we need, as well, to understand the underlying genetic and molecular mechanisms that result in resistance and to discover novel compounds that can safely and efficiently reduce malaria transmission rates.

The most widely used and effective intervention methods against malaria are targeted against the vector, such as lethal insecticides or insect deterrents. In the field, these methods almost exclusively include the use of insecticide-treated bed nets (ITNs) and indoor residual spraying (IRS) (Enayati & Hemingway 2010; Martinez-Torres et al. 1998). The use of ITNs has proven to be more widely pursued in locations such as Africa due the operational ease of distributing pretreated nets, compared to the labor-intensive requirements for IRS deployment of insecticides (van den Berg et al. 2012). Currently, there are four classes of chemical compounds that have been approved for use as insecticides: organochlorines, organophosphates, carbamates and pyrethroids, which all function by inhibiting the insect nervous system (Ramphul et al. 2009; Hill et al. 2013; Hemingway & Ranson 2000). Dichloro-diphenyl-trichloroethane (DDT) (an organochloride) and permethrin (a pyrethroid) have been two of the most commonly used insecticides, as they have been shown to be highly effective in vector control (ffrench-Constant et al. 2004). Pyrethroids and organochlorides act by inhibiting voltage-gated

sodium channels (Vgsc) in insect nerve cell membranes and impede the proper functioning of the nervous system, resulting in paralysis and death (Davies et al. 2007; Ranson et al. 2009; Hemingway & Ranson 2000). Both carbamates and organophosphates impeded the functioning of the post-synaptic nerve membrane by targeting acetylcholinesterase (AChE), which is required to hydrolyze the excitatory neurotransmitter acetylcholine (Hemingway & Ranson 2000; Ranson et al. 2009). With all of these chemical classes, resistance correlates with reduced sensitivity of the insect nervous system to these toxic molecules (Martinez-Torres et al. 1998; Hemingway & Ranson 2000), making these insecticides dramatically less effective.

Insecticide resistance mechanisms become established in populations due to the action of selective pressures that result from constant exposure of insecticides. There are multiple mechanisms for resistance, including metabolic, target-site, behavioral and penetration/cuticular resistance (Ranson et al. 2011; Hemingway & Ranson 2000). Metabolic and target-site resistance are the more commonly observed mechanisms (French-Constant et al. 2004; Ranson et al. 2011).

In the case of metabolic resistance, mutation(s) are acquired that increase the ability to metabolize or detoxify insecticides (S. N. Mitchell et al. 2014; Ranson et al. 2011). Mutations often result in the ability to produce more detoxifying enzyme (e.g., increased gene copy number, gene duplication events, increased gene transcription/expression) (Daborn et al. 2002; Field et al. 1999; Schmidt et al. 2010), or by altering the kinetics and substrate specificity of the enzymes (C. J. Jackson et al. 2013). For example, mutations in glutathione *S*-transferase (e.g. *Gste2*) (Perry et al. 2011; Daborn et al. 2012; S. N. Mitchell et al. 2014; Schmidt et al. 2010) and cytochrome

P450 (e.g. *Cyp6*) (Edi et al. 2014; Daborn et al. 2002) have been shown to confer resistance to organochlorine- and carbamate-based insecticides through detoxifying mechanisms.

Target-site resistance occurs when the site of inhibitory compound binding to a target protein is altered, resulting in reduced inhibition due to inefficient inhibitor binding. For pyrethroids and DDT, mutations that are associated with resistance have been shown to involve malfunctioning of voltage-gated sodium channels (Davies et al. 2007; Ranson et al. 2011). Most notably, multiple nonsynonymous mutations have been identified in *para*, a voltage-gated sodium channel protein, that confer resistance to DDT and pyrethroid insecticides (Pinto et al. 2007; Ranson et al. 2011; Davies et al. 2007; Saavedra-Rodriguez et al. 2007). Mutations in  $\gamma$ -aminobutyric acid type A (GABA) channels have been reported to play a large role in resistance of insecticides that target the nervous system (Ramphul et al. 2009; ffrench-Constant et al. 1993). One of the first characterized target site mutations, *Rdl*, is a mutation that alters the GABA-gated chloride channel, such that the binding affinity of dieldrin (an organochlorine) is decreased (Perry et al. 2011; ffrench-Constant et al. 1993). With increased resistance to organochlorine and pyrethrioid compounds, the amounts of carbamate- and organophosphate-based insecticides used in the field have been increased (Essandoh et al. 2013). These compounds have shown efficacy in reducing malaria transmission in the field, but recent mutations in the acetylcholinesterase target-site enzyme *Ace-1* have been linked to increased insecticide resistance in *An. gambiae* (Essandoh et al. 2013; Edi et al. 2014).

Although not identified as often as the previously mentioned mechanisms, behavioral and cuticular penetration resistance can play roles in reduced insecticide

efficacy (Ranson et al. 2011). Behavioral resistance occurs when the insects avoid contact with an insecticide-treated area by altering previously normal behaviors. Behavioral changes (e.g., in resting sites, feeding locations, mating sites, breeding sites) can occur when the insect modifies its behavior to avoid physical contact (contact irritancy) or non-physical contact (spatial repellency) with insecticidal compounds (Chareonviriyaphap et al. 2013). Compounds with high volatility (e.g., DEET) (Ditzen et al. 2008) and bitter taste qualities (e.g., quinine and caffeine) (Ignell et al. 2010) can contribute to behavioral resistance (Wada-Katsumata et al. 2013), and ultimately decrease the effectiveness of insecticides by reducing insecticide contact. This type of resistance uncovers the importance of understanding not only the insecticidal compounds, but the underlying biology associated with chemosensation, as well (i.e., gustatory and olfactory systems). Cuticular penetration resistance occurs when a barrier is formed on the insect's outer cuticle, resulting in decreased insecticide absorption (Ranson et al. 2011). An example of delayed cuticular penetration has been seen with *Helicoverpa armigera* (Cotton Bollworm) in response to the deltamethrin (Ahmad et al. 2006), a common pyrethroid used in field applications for mosquito control. In *An. gambiae* and *An. stephensi*, microarray studies intended to identify differentially expressed genes in insecticide-resistant populations have revealed that a particular cuticular protein-coding gene, CPLC8, is significantly unregulated in resistant insect populations (Vontas et al. 2007; Awolola et al. 2009). Based on the sequence similarity to the *D. melanogaster* adult cuticle protein precursor (DACP1) gene, the function of CPLC8 is predicted to be involvement in thickening of the cuticle (Vontas et al. 2007). While this process of cuticle thickening may not impact the efficacy of insecticides that are delivered via

ingestion, it certainly provides protection during the cuticular contact with insecticides in ITN and IRS applications (Ranson et al. 2009).

### **E. G Protein-Coupled Receptors (GPCRs): Drug Targets**

G protein-coupled receptors (GPCRs) represent an extremely large family of cell surface receptors that function in many biological capacities, making them extremely attractive as pharmacological targets. Within the human genome, over 800 GPCRs have been identified (Lagerström & Schiöth 2008; Ghosh et al. 2015), representing approximately 2-4% of human protein-coding genes (R. Zhang & Xie 2012; Allen & Roth 2011). Likewise, GPCR families have been identified in multiple insect species. In the *An. gambiae* genome, there are currently 276 bioinformatically identified GPCRs, making up roughly 2% of the protein-coding genes in the 278 megabase genome (Hill et al. 2002). This percentage is comparable to the number of GPCRs represented in the *D. melanogaster* genome, many of which have putative orthologs within the *An. gambiae* genome (Hill et al. 2002). Many *D. melanogaster* GPCRs have already been characterized, and this has enabled the development of readily available genetic tools (i.e., transgenic fly stocks) that can provide information pertaining to functions of putative GPCR orthologs in *An. gambiae*. In this thesis, I utilized *D. melanogaster* GPCR family members *Dop1R2* and *Gr66a* to gain insight into GPCR functions for the respective orthologous receptors *GPRDOP2* and *GPRGR2* in *An. gambiae*.

The linear structure of a canonical GPCR family member includes seven transmembrane domain (7TMD) alpha helices that are linked by three extracellular and three intracellular loops (Allen & Roth 2011) (Figure 1.3). The orientation within the

membrane is typically such that the amino-terminal end resides in the extracellular space and the carboxy-terminal end in the cytoplasm. The arrangement of the seven TMD helices is stabilized by a series of intra-molecular interactions (Klabunde & Hessler 2002), and the structured GPCR then interacts with an intracellular heterotrimeric guanine-nucleotide-binding protein (i.e., G protein) complex, made up of  $\alpha$ ,  $\beta$ , and  $\gamma$  subunits (Alfredo Ulloa-Aguirre et al. 1999). Few GPCR crystal structures have been determined, due to the complexity of GPCR structures, as well as their insertion within lipid membranes. However, using currently available sequences and structures, it is notable how highly similar GPCR transmembrane regions are. For example, the  $\beta_2$ -adrenergic and rhodopsin receptors contain less than 20 percent sequence similarity, but are extremely similar in TMD structure (Tautermann & Pautsch 2011). The sequence similarities within 7TMD regions allows for the classification of GPCRs into specific subfamilies. In *Anopheles*, these classes include the rhodopsin-like (Class A), secretin-like (Class B), metabotropic glutamate-like (Class C), atypical (Class D) and chemosensory (Class E) GPCRs (Hill et al. 2002). The chemosensory GPCRs are the most abundant subfamily, including 155 receptors that are predicted to function in either olfactory or gustatory processes (Hill et al. 2002). The second largest subfamily is the rhodopsin-like class, which includes 81 GPCRs belonging to biogenic amine, glycoprotein hormone, peptide, purine, opsin or orphan GPCR subfamilies (Hill et al. 2002). In this thesis, the GPCRs that are investigated belong to both the rhodopsin-like (e.g., *GPRDOP2*) and chemosensory classes (e.g., *GPRGR2*).

GPCRs transduce signals when extracellular ligand binding initiates activation of the heterotrimeric G-protein complex. Crystal structures of GPCRs reveal that the

primary regions of sequence diversity exist within the extracellular loop regions (i.e., diversity of secondary structures and patterns of disulfide crosslinking), which are essential for ligand binding (Katritch et al. 2013; Wheatley et al. 2012). However, it is not exclusively the diversity of extracellular loops that is important for ligand binding. Changes in TMD regions and/or extracellular loops can alter the ligand-binding pocket dramatically in terms of shape, size and electrostatic properties (Katritch et al. 2013; Granier & Kobilka 2012). The act of ligand binding also stabilizes receptor conformation and promotes the exchange of guanine diphosphate (GDP) on the heterotrimeric G-protein complex  $\alpha$  subunit ( $G\alpha$ ), for guanine triphosphate (GTP), resulting in a conformational change and allowing for dissociation of the  $\beta$ - $\gamma$  dimer ( $G\beta\gamma$ ) from  $G\alpha$  (R. Zhang & Xie 2012; Allen & Roth 2011; Vanden Broeck 2001; Lagerström & Schiöth 2008; Katritch et al. 2013). Uncoupled  $G\alpha$  can then activate downstream effector molecules [e.g., adenylyl cyclase (AC), phospholipase C beta ( $PLC\beta$ ), Rho guanine nucleotide exchange factor (RhoGEF)], which then can regulate the intracellular concentrations of second messengers [e.g., 3', 5'-cyclic adenosine monophosphate (cAMP), inositol 1, 4, 5-triphosphate ( $IP_3$ ), diacylglycerol (DAG)] (Ritter & Hall 2009; R. Zhang & Xie 2012; Allen & Roth 2011). The increased levels of second messengers ultimately yield physiological responses, often by regulating downstream gene transcription. The dissociated  $G\beta\gamma$  can also bind to and regulate downstream effector molecules (e.g.,  $PLC\beta$  and ion channels) (Ritter & Hall 2009). This signal transduction will continue until the intrinsic GTPase activity of  $G\alpha$  leads to the hydrolysis of GTP to GDP, resulting in the reassociation of the heterotrimeric G-protein complex (Vanden Broeck 2001; R. Zhang & Xie 2012; Allen & Roth 2011).



Downstream signaling mechanisms and alterations in secondary messengers vary based on the type of  $\alpha$  subunit that is activated by a given GPCR-agonist (ligand) interaction. There are four major classes of  $\alpha$  subunits,  $G\alpha_s$ ,  $G\alpha_i$ ,  $G\alpha_q$  and  $G\alpha_{12/13}$ , which will modulate different intracellular effector molecules (R. Zhang & Xie 2012; Ritter & Hall 2009). GPCRs that are coupled to  $G\alpha_s$  (stimulatory) activate AC, while those coupled to  $G\alpha_i$  (inhibitory) inhibit it (X. Zhang et al. 2010; Allen & Roth 2011; Ritter & Hall 2009). The levels of AC activity directly impact the levels of cAMP produced, as AC is an enzyme required for catalyzing the conversion of ATP to cAMP. The formation of cAMP is important in a variety of cellular processes, such as activation of protein kinase A (PKA) (Beggs et al. 2011; Rosenbaum et al. 2009; Blenau et al. 1998; R. Zhang & Xie 2012; Mustard et al. 2003; Meyer et al. 2012; Reale et al. 1997; Ritter & Hall 2009).  $G\alpha_q$ -coupled GPCRs activate PLC effector molecules, which cleave  $PIP_2$  and catalyze the synthesis of two secondary messengers,  $IP_3$  and DAG.  $IP_3$  and DAG are important in modulating further downstream effectors such as  $Ca^{2+}$  and protein kinase C (PKC), respectively (Ritter & Hall 2009; R. Zhang & Xie 2012). Finally,  $G\alpha_{12/13}$ -coupled GPCR agonist binding results in modulation of RhoGEF effector molecules, in turn increasing the levels of RhoA (Ritter & Hall 2009; R. Zhang & Xie 2012).

GPCRs can be bound by many different ligands that can be either endogenous or exogenous to the cell. Endogenous ligands commonly include molecules such as biogenic amines, peptides, glycoproteins, amino acids, phospholipids, fatty acids, nucleosides, nucleotides and calcium ions, whereas exogenous ligands include molecules such as pheromones/odorants, tastants, and photons (Kristiansen 2004; Granier & Kobilka 2012). The regions to which ligands bind to a given GPCR can be predicted, in

many instances, based on the structural subfamily within which a given receptor/ligand pair reside. For example, the biogenic amine dopamine frequently binds within a transmembrane helix (TMH) pocket that includes TMH3-TMH7 (Kristiansen 2004; Liapakis et al. 2000). This hydrophobic pocket is formed from the specific interactions of the transmembrane domains (Klabunde & Hessler 2002; Allen & Roth 2011). Proteins and peptide hormones tend to bind the extracellular loops that connect TM domains, as well at the extracellular amino-terminal domain (Kobilka 2007).

G-protein coupled receptors play very important biological roles by functioning in the cellular processing of extracellular signals to elicit intracellular responses (Neubig & Siderovski 2002; Lagerström & Schiöth 2008; Hearn et al. 2002). The binding of specific ligands to these receptors regulates many important developmental and physiological processes, including development, sensory transduction and cell-cell communication (R. Zhang & Xie 2012; Gobeil et al. 2006; Ritter & Hall 2009). Understanding the roles of these receptors in mosquito development, behavior, survival and longevity can enhance our ability to develop vector-targeted pharmacological interventions, moving forward.

G protein-coupled receptors are one of the most “druggable” cellular targets, and they account for approximately forty to fifty percent of human therapeutic small molecules that are currently on the market (Rozenfeld & Devi 2010; Allen & Roth 2011; Overington et al. 2006). The ability to modulate GPCR-mediated signal transduction has enabled the identification of GPCRs and ligands that control many biologically relevant signaling pathways. The work described in this thesis investigates the role of multiple GPCRs that play important roles in the vector competence and vectorial capacity of *An.*

*gambiae*. The ultimate goal of this work is to identify potential targets for the discovery of new vector-targeted interventions that can be used in the field for vector control. These compounds include those intended to decrease mosquito survival (i.e., adulticides and larvicides), as well as those that may modulate behaviors (i.e. altering gustatory compound recognition or refractoriness to mating). Thus, understanding the roles of these receptors can enable the development of new insecticides for vector control (R. Zhang & Xie 2012; Allen & Roth 2011).

While the attractiveness of GPCRs as insecticidal targets is clear, very few advances have been made in this regard, to date. The Purdue Insecticide Discovery Pipeline (PIDP) is currently undertaking efforts toward the discovery of new mode-of-action insecticides for vector control using a genome-to-lead approaches (Hill et al. 2013; Nuss et al. 2015; Meyer et al. 2012). In fact, through this pipeline the *Aedes Aegypti* (yellow fever vector) and *Culex quinquefasciatus* (West Nile virus vector) dopamine D1-like GPCRs have been characterized at the molecular and pharmacological levels, in the attempt to advance vector insecticide development (Hill et al. 2013; Nuss et al. 2015). Given the availability of 16 recently released *Anopheles* reference genomes (Neafsey et al. 2015) and growing vector genome sequence data resources (i.e., VectorBase, <http://www.vectorbase.org/>) (Giraldo-Calderon et al. 2015), the implementation of target-based approaches for insecticide discovery is moving in a positive direction.

Given that neurohormone GPCRs, such as biogenic amine-binding receptors, play critical roles in the regulation of many insect physiological processes, and share very limited homology with human GPCRs, they are considered to be good insecticide targets (Bai & Palli 2015; Hauser et al. 2006). Within the scope of the dopamine (DA) GPCR

project, we provide evidence that the dopamine D<sub>1</sub>-like receptor, Dop1R2, is involved in pre-adult development and may serve as a promising target for insecticide development. In addition to DA being well-described as playing fundamental roles in insect behaviors (i.e., learning, locomotion, courtship) (Meyer et al. 2012; Mustard et al. 2005; Blenau & A. Baumann 2001), it is also known to be a precursor in the biochemical pathway for the production of melanin, which is required for invertebrate cuticle sclerotization (T. R. F. Wright et al. 1976; T. R. F. Wright 1987; Wittkopp et al. 2003; Shakhmantsir et al. 2013). There is also evidence suggesting that dopamine is involved in the regulation of larval and pupal ecdysis, as well as in metamorphosis (Granger et al. 2000; Park et al. 2004; Srivastava 2005; Bai et al. 2011; Meyer et al. 2012). Given these insights from previous research, we used the model organism *D. melanogaster* to evaluate the roles of a specific D<sub>1</sub>-like (stimulatory G $\alpha_s$ ) GPCR, Dop1R2, in development and survival. By using a reverse genetic approach, we uncovered requirements for Dop1R2 activity during third instar larval and pupal development – resulting in lethality and cuticle abnormalities. Investigation of the tissue/cell types associated with these phenotypes suggests that the function of this receptor in the salivary glands is critical for normal development. Furthermore, we have identified a subset of genes that are differentially expressed in response to Dop1R2 knockdown, and are required for completion of development (i.e., cuticular, immune response and stress response genes). Pharmacological treatment of larvae with the established insect/mammalian D<sub>1</sub>-like receptor antagonist flupenthixol dihydrochloride (Beggs et al. 2011; Blenau et al. 1998; Mustard et al. 2003; Meyer et al. 2012; Reale et al. 1997) results in pre-adult developmental delay or arrest. Given that this GPCR is well-conserved in arthropods, but

exhibits limited homology with mammalian dopamine receptors (Mustard et al. 2003; Mustard et al. 2005), Dop1R2 may serve as a promising candidate GPCR to control vector insects.

The RNAi trigger delivery chapter (Chapter III) describes a method that I have developed for direct injection of dsRNA into *An. gambiae* pupae and illustrates the importance of this technology for functional genomics and vector biology. Currently available methods for inducing non-transgenic RNA interference (RNAi) in mosquitoes involve direct injection of dsRNA into the adult hemolymph (Catteruccia & Levashina 2009; Garver & Dimopoulos 2007) or larval feeding of RNAi trigger-coated nanoparticles (X. Zhang et al. 2010; X. Zhang et al. 2015; Mysore et al. 2014; Mysore et al. 2013). Targeting the adult mosquito, while extremely valuable, can exclude a large number of genes that function during earlier developmental periods. Larval feeding involves a more time consuming process of preparing nanoparticles and may yield inconsistent phenotypes during the adult stage, due in part to the potential for variable protein persistence through the pupal stage. The SRPN2 target used for validation of this technique was chosen because of the easily identifiable melanotic pseudo-tumor phenotype in adult stage mosquitoes with reductions in SRPN2 levels (Michel et al. 2005; An et al. 2011), and the high expression levels of SRPN2 during the pupal stage (Suwanchaichinda & Kanost 2009). Using this method, I demonstrate high efficiency, transstadial knockdown at the levels of SRPN2 protein and phenotypic effect. The overall goal of this project was to develop a method for performing RNAi-mediated gene knockdown during pupal development, and for cell types that originate during metamorphosis, but are less accessible in adults.

The gustatory chapter of this thesis (Chapter IV) investigates behavioral, molecular and structural aspects of mosquito chemosensation. Chemosensation is a highly specialized process that allows animals to identify and respond to chemosensory information (e.g., tastants) within the environment (K. Scott et al. 2001). This study was initiated by assessing the spatial expression of *An. gambiae* GPRGR2 in tissues with high sensilla (hair-like sensory projections) densities (i.e., proboscis, palp, legs/tarsi, antennae) (K. Scott et al. 2001; Stocker 1994; Dahanukar et al. 2007; N. R. Singh 1997; Seenivasagan et al. 2009; Pitts et al. 2004; Pappas & Larsen 1976). I show that *GPRGR2* is abundantly expressed in the proboscis, legs/tarsi and antennae, all of which have been demonstrated to function in gustatory processes in many species (B. K. Mitchell et al. 1999; Pappas & Larsen 1976). Utilizing the RNAi trigger delivery method mentioned above, I pursued a functional genetic assessment of GPRGR2 function and show that this receptor is involved in the recognition of specific, bitter-tasting compounds. Reduced levels of *GPRGR2* impede the ability of *An. gambiae* to avoid imbibing bitter and potentially harmful substances. Our analysis of sensilla requirements for bitter taste sensation through ablation assays demonstrates the importance of these chemosensory structures on the labial palps. These findings provide insights into some of the molecular aspects underlying of chemosensory behaviors in vector mosquitoes and may enable the development of better feeding-based vector-targeted interventions, such as enhanced attractive toxic sugar bait (ATSB) traps (Beier et al. 2012; Muller et al. 2010).

The research presented in this thesis was undertaken to identify candidate GPCRs that may serve as novel targets for the development of new vector control strategies. I provide show that the dopamine D1-like receptor is critical for development and may

serve as a candidate for insecticide development, particularly during pre-adult stages (i.e., larvicides). I also describe the importance of chemosensation with regard to the detection of noxious compounds by the gustatory system and identify a receptor, GPRGR2, that is critical for the detection of various bitter compounds. By modulating the ability of the mosquito to detect bitter insecticides, we may be able to create more effective insecticide deployment in the field. Finally, I describe a novel method for RNAi-mediated knockdown during the *An. gambiae* pupal stage, which may provide vector biologists with a valuable tool for functional genomic analysis during additional developmental stages.

## F. FIGURES AND LEGENDS

**Figure 1.1: Global distribution of malaria vector species.** Map depicting the geographic distribution of the major *Anopheles* vector species.

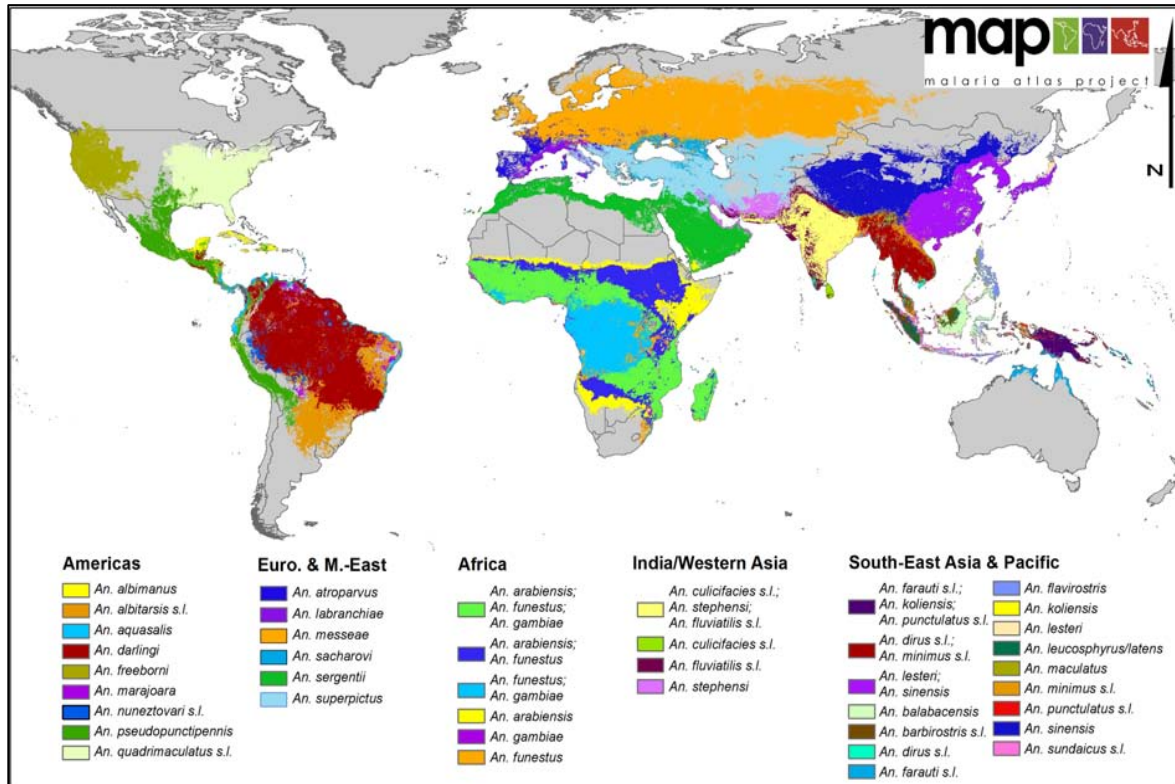


Image credit: Sinka et al. (2012)



**Figure 1.2: Malaria Life Cycle.** Illustration of the dual-host life cycle of the *Plasmodium* malaria parasite. In the human host, the parasite remains in an asexual reproductive phase during the exo-erythrocytic cycle in the liver and erythrocytic cycle in the red blood cell. Once infected blood is ingested by a female *Anopheles* mosquito, the parasite enters a sexual reproductive sporogonic cycle within the midgut of the insect host, from which it will later migrate to the salivary glands, to be transmitted during an ensuing blood meal.

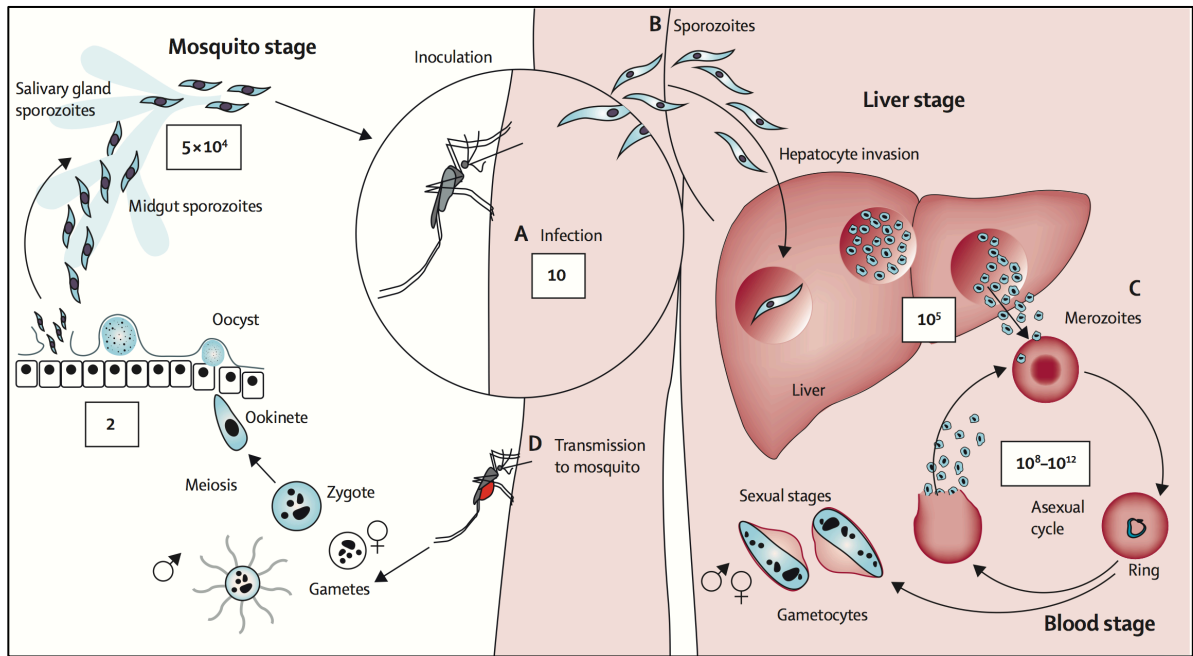


Image credit: N. J. White et al. (2014)

**Figure 1.3: G Protein-Coupled Receptor Signaling.** Schematic of GPCR signaling through the major transduction pathways:  $G_{\alpha s}$ ,  $G_{\alpha i}$ ,  $G_{\alpha q}$  and  $G_{\alpha 12/13}$ . Boxes below indicate the primary effectors (purple), second messengers (blue) and downstream effectors (green).

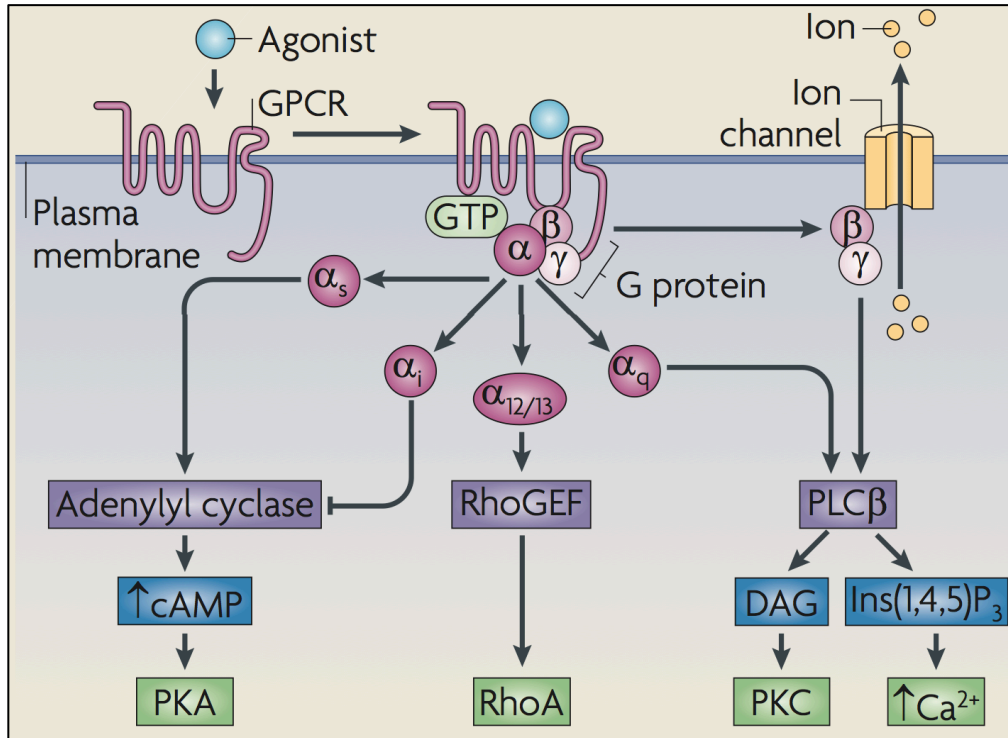


Image credit: Ritter & Hall (2009)

## **CHAPTER II**

**A critical role for the *Drosophila* dopamine 1-like receptor Dop1R2  
at the onset of metamorphosis**

## A. ABSTRACT

Insect metamorphosis relies on temporal and spatial cues that are precisely controlled. Previous studies in *Drosophila* have shown that untimely activation of genes that are essential to metamorphosis results in growth defects, developmental delay and death. Multiple factors exist that safeguard these genes against deregulated expression. By using RNAi transgene-induced gene silencing coupled to spatio/temporal assessment, we have unraveled an essential role for the *Drosophila* dopamine 1(D1)-like receptor Dop1R2 in development. We show that Dop1R2 knockdown leads to pre-adult lethality, as well as to cuticle and/or wing defects in flies that survive to adulthood. Our genetic analyses support an important function for this GPCR in the salivary glands, during the larval stage. In addition, we show that larvae treated with the high affinity D1-like receptor antagonist, flupenthixol, display developmental arrest, or morphological defects, as seen with ubiquitous or salivary gland knockdown of Dop1R2. To probe the basis for pupal lethality in Dop1R2 RNAi flies, we carried out transcriptome and RT-PCR analysis. These studies revealed up-regulation of selected families of genes that respond to ecdysone, as well as regulate morphogenesis and defense/immunity. Taken together, our findings suggest a role for Dop1R2 in the repression of genes that coordinate metamorphosis. Premature release of this inhibition, and misexpression of corresponding genes, is harmful to the developing fly.

## B. INTRODUCTION

The naturally occurring catecholamine dopamine (DA) acts as a neurotransmitter and neurohormone in the central nervous system (CNS) of vertebrates and invertebrates. DA is a precursor in the biochemical pathway for the production of melanin, which is required for invertebrate cuticle sclerotization (T. R. F. Wright et al. 1976; T. R. F. Wright 1987; Wittkopp et al. 2003; Shakhmantsir et al. 2013). Increasing evidence suggests that in insects, DA and DA receptors (DARs) are involved in the regulation of larval and pupal ecdysis, as well as in metamorphosis (Granger et al. 2000; Park et al. 2004; Srivastava 2005; Bai et al. 2011; Meyer et al. 2012).

DA metabolism has been studied extensively within many phylogenetic groups. The essential steps required for dopaminergic neurotransmission (i.e., DA synthesis, release, receptor activation, and reuptake) are conserved between flies and humans. DA synthesis is controlled by the rate-limiting enzyme tyrosine hydroxylase (TH), which is encoded in *Drosophila* by the *pale* locus (T. R. F. Wright et al. 1976; Neckameyera & Quinna 1989; T. R. F. Wright 1987; Wittkopp et al. 2003; Shakhmantsir et al. 2013). TH converts tyrosine to the precursor molecule L-DOPA, which is in turn converted to DA by the enzyme DOPA decarboxylase (DDC), encoded by the *Ddc* gene (Granger et al. 2000; Livingstone & Tempel 1983; Park et al. 2004; Eveleth et al. 1986; Srivastava 2005; Bai et al. 2011; Meyer et al. 2012). TH and DDC are required for normal development in *Drosophila*. Null mutations targeting either biosynthetic enzyme result in late embryonic lethality (Budnik & K. White 1987; Valles & K. White 1986). More recently, elegant studies have shown that selective depletion of TH in the nervous system is well tolerated

by the developing fly, and that corresponding adults have normal lifespan, albeit with some motor deficits (Riemensperger et al. 2010).

DA exerts its function by activating G protein-coupled receptors (GPCRs). The fruit fly expresses both D<sub>1</sub>-like and D<sub>2</sub>-like DA receptors, which are distinguished based on the ability of the receptor to couple to either stimulatory G $\alpha_s$  (D<sub>1</sub>-like) or inhibitory G $\alpha_{i/o}$  (D<sub>2</sub>-like) G proteins, which in turn activate downstream signaling mechanisms (Yamamoto & Seto 2014). The fly D<sub>1</sub>-like receptors include Dop1R1 (synonyms: DopR1, dDA1, dumb, Dmdop1, DA1) (Gotzes et al. 1994; Sugamori et al. 1995) and Dop1R2 (synonyms: DopR2, DAMB, DOPR99B) (Feng et al. 1996; Han et al. 1996), as well as the non-canonical DopEcR (synonym: dmDopEcR) (Ishimoto et al. 2005; Evans et al. 2014; Inagaki et al. 2012). DopEcR has a unique *in vitro* pharmacological profile and can be activated either by dopamine or by the steroid hormone 20-hydroxyecdysone (20E) (Evans et al. 2014). There is only one known *Drosophila* D<sub>2</sub>-like receptor, Dop2R (synonym: DD2R, D2R), which has also been cloned and characterized (Hearn et al. 2002).

In addition to modulating a range of receptor-mediated physiologies in insects (Draper et al. 2007; Kim et al. 2007; Andretica et al. 2008; Seugnet et al. 2008; Kong et al. 2010; Lebestky et al. 2009; Bang et al. 2011), DA acts as a precursor of metabolites involved in cuticle melanization (pigmentation) (Shakhmantsir et al. 2013), and is essential for the crosslinking of proteins and chitin during sclerotization (hardening) of the cuticle after eclosion (Friggi-Grelin et al. 2003; T. R. F. Wright 1987; Monastirioti 1999; Neckameyer et al. 2001; Birman et al. 1994). Although the importance of DA GPCRs as modifiers of adult fly behavior (including locomotor activity, memory,

arousal, temperature preference, courtship, gustation, olfaction and response to drugs of abuse) is well-documented (Draper et al. 2007; Kim et al. 2007; Andretica et al. 2008; Seugnet et al. 2008; Kong et al. 2010; Lebestky et al. 2009; Bang et al. 2011; Ueno & Kume 2014; Waddell 2013; Inagaki et al. 2012; Ishimoto et al. 2005), the contribution of DA receptors to the modulation of developmental processes has not been defined. DopEcR, which responds to both DA and ecdysone, has been shown to regulate sugar sensing, male courtship, and pheromone perception in adult insects (Abrieux et al. 2014; Evans et al. 2014; Inagaki et al. 2012). Overexpression or a significant reduction in the expression of this receptor, however, does not compromise normal development (Evans et al. 2014). The focus of our study is to define the role of the D<sub>1</sub>-like *Drosophila* DA receptor, Dop1R2, during development. This GPCR is well-conserved in arthropods, but exhibits limited homology with mammalian dopamine receptors (Mustard et al. 2003; Mustard et al. 2005), suggesting a unique function for Dop1R2 that is specific to invertebrate physiology.

We have used transgenic Dop1R2 RNA interference (RNAi) *Drosophila*, and characterized the effects of Dop1R2 knockdown (KD) using the GAL4/UAS-mediated system. We demonstrate that Dop1R2 activity is critical during the third larval instar and pupal stages to ensure completion of development through adult emergence. Our investigations of the tissue/cell types that underlie the observed Dop1R2-mediated phenotypes suggest the involvement of Dop1R2 receptors expressed in the salivary glands. The Dop1R2 RNAi-induced phenotypes observed in escaper adults are recapitulated in progeny exposed to a Dop1R2 small molecule antagonist. We have identified a subset of genes that respond to Dop1R2 KD, and are essential in

development. Our data provide the first indications that a peripheral dopamine receptor controls key developmental processes in *Drosophila*.

## C. RESULTS

### **Dop1R2 RNAi flies exhibit decreased Dop1R2 transcript levels**

Crossing UAS-dsDop1R2 RNAi transgenic flies with the Act5C-GAL4 driver strain (Figures 2.1A and 2.1B) results in progeny that ubiquitously express Dop1R2 double-strand (ds) RNA. This leads to targeted degradation of the endogenous Dop1R2 mRNA (i.e., Dop1R2 “knockdown”, or KD) in all tissues in which the receptor is normally expressed (Figure 2.1C). When primers were designed to amplify the endogenous Dop1R2 message, without amplifying the RNAi sequence, a significant and reproducible decrease in Dop1R2 expression was observed, in Dop1R2 RNAi vs. control flies (Figures 2.2A and 2.2B). When PCR primers were designed to amplify the Dop1R2 RNAi construct, a marked increase in transcript level was observed, confirming the expression of the RNAi transgene (Figure 2.2B). To assess whether expression of the Dop1R2 RNAi construct could trigger off-target effects, expression of a series of other biogenic amine receptors with closest homology (36-43% identity as assessed at the nucleotide level via ClustalW alignment [Larkin et al. 2007]) with Dop1R2 were also assayed. These included the second fly dopamine D<sub>1</sub>-like receptor Dop1R1, the dopamine D<sub>2</sub>-like receptor Dop2R, the octopamine receptor Oamb, the tyramine receptor Oct-TyrR and the serotonin receptor 5-HT1A. There was no significant change in the expression level of each GPCR gene under study in Dop1R2 RNAi vs. control flies,



except for that of Dop2R (the D<sub>2</sub>-like dopamine receptor), for which a slight increase was observed (Figure 2.2B).

### **Expression of dsDop1R2 RNAi in the developing fly results in reduced viability, wing malformation and cuticle melanization phenotypes**

Dop1R2 RNAi flies that are reared at 29°C and are ubiquitously express the Dop1R2 RNAi construct (Figure 2.3) develop normally throughout larval and early pupal stages, but fail to emerge from their pupal cases. When the flies are reared at a lower temperature (i.e., 25°C), the GAL4/UAS-mediated RNAi gene silencing is attenuated (Duffy 2002) and ‘escaper’ adults emerge (23.4% males and 54.7% females vs. control flies expressing GAL4 alone) (Figure 2.4A). The escaper flies display other phenotypes with varying degrees of penetrance, including premature death, abnormal melanization (e.g., abdominal patchiness or complete absence of melanization, Figure 2.4B), and/or failure to expand wings (e.g., curly wing, Figure 2.4C). Males showed a more pronounced phenotype, with a higher penetrance, than females (data not shown). Two independent Act5C-GAL4 driver lines (FBst0004414 and FBst0003954) led to lethal, melanization and wing phenotypes in the progeny. The lethal phenotype was recapitulated using two additional UAS-dsDop1R2 lines (Figures 2.3 and 2.5) generated by the Vienna *Drosophila* RNAi Center (i.e., 3391-GD and 10524-KK, see Materials and Methods). In addition, male escapers (obtained with VDRC driver line 3391-GD) displayed the melanization phenotype (data not shown).

### **Analysis of the temporal requirements for *Dop1R2* expression suggests a role at the third larval instar and prepupal stage**

We have utilized the well-established temperature effect on the Gal4/UAS system (i.e., more efficient at higher 29°C, vs. lower 25°C, temperature (Duffy 2002) to probe whether Dop1R2 expression is required during a specific time interval for the flies to complete development. Developing flies were shifted from high (29°C) to low (25°C) temperatures, and conversely, during different developmental stages (i.e., embryo, first/second instar larva, third feeding/wandering instar larva, early pupa, late pupa) (Figure 2.6A). Regardless of which developmental stage, or direction (high to low vs. low to high), was selected to perform the transfer, flies that were kept at the high temperature throughout the third instar larval stage later arrested at the late pupal/pharate adult stage (Figure 2.6B). These experiments indicate that expression of Dop1R2 at the third instar larval stage is critical for survival of the developing progeny (Figure 2.6C).

### **A preliminary transcriptome analysis of *Dop1R2* RNAi flies reveals up-regulation of tyrosine hydroxylase and ecdysone-related genes, as well as stress and immune response genes**

Affymetrix GeneChip<sup>R</sup> *Drosophila* genome array transcriptome expression analysis was performed in duplicate on early pupal stage *Dop1R2* RNAi flies expressing the interference construct ubiquitously under restrictive conditions, and compared to that of corresponding control pupae. Significance was assessed using Genespring array analysis software (Silicon Genetics). A total of 163 genes were identified as significantly

differentially expressed following assessment of the two independent transcriptome analyses (Dataset 2.1). Among these, only eight genes were down-regulated, with a modest -1.1 to -1.5 fold-difference of expression compared to control flies. Our focus was then shifted to 101 genes that were up-regulated with a fold-difference of  $\geq 1.6$  (compared to expression levels in control flies, Figure 2.7 and Dataset 2.1; arbitrary cutoff of 1.6). Results include a 3-fold increase in expression levels of tyrosine hydroxylase (TH) in Dop1R2 RNAi vs. control flies. The Affymetrix GeneChip<sup>R</sup> array data discussed in this publication have been deposited into the NCBI's Gene Expression Omnibus (GEO) data repository (Edgar et al. 2002) and are accessible through the GEO Series accession number GSE66496 (<http://www.ncbi.nlm.nih.gov/geo/query/acc.cgi?acc=GSE66496>). FlyBase annotation (St Pierre et al. 2014) and DAVID bioinformatic analysis (Huang et al. 2009) of the genes that are differentially expressed in response to Dop1R2 KD revealed highly significant enrichment (Benjamini corrected p-value range of 4.9E-2 to 4.8E-6) of genes falling under selected ontology (GO) term classes (i.e., heat shock response, immune response, salivary gland development, larval and pupal morphogenesis, Dataset 2.2). The related genes that exhibited up-regulation include seven members in the late ecdysone-induced Eig71E (L71) gene family, which were up-regulated ~3- to 6-fold. The expression levels of multiple stress response genes (e.g., Hsp22, Hsp26, Hsp67Bb, Hsp67Bc, Hsp68, Hsp70Bbb, Hsp70Bc, Hsf), antimicrobial peptides/innate response genes (CecA1/A2, dro2/dro3, LysX, IM1, IM2, IM3, IM4, IM10, IM23) associated with gut immune responses (Buchon et al. 2009), and structural components of the cuticle (Cpr72Eb, Cpr65Ec, PCP) also increased in the Dop1R2 RNAi arrested flies compared to controls (Figure 2.7 and Dataset 2.2). A

parallel analysis carried out using WEB-based GEne SeT AnaLysis Toolkit (WEBGestalt) (J. Wang et al. 2013a; B. Zhang et al. 2005) revealed enrichment of genes falling under similar GO term classes (Figure 2.8). The relatedness of these groupings is further supported by the many protein-protein interactions revealed using STRING analysis (Figure 2.9).

To further assess results from the microarray analysis, a subset of genes was randomly picked across the main GO categories (Figure 2.7). These included Hsp67Bc, Hsp70Bc (heat shock response), Cpr72Eb, Dro2, Dro3, CecA1, LysX (immune response), and Edg91 (ecdysone-dependent genes). Gene expression was assessed by RT-PCR in RNA preparations isolated from independent biological replicates (the corresponding Dop1R2 RNAi and control fly progeny were derived from three novel independent biological replicates (i.e. independent from each other, and from those used for the transcriptome analysis). This analysis confirmed increased transcript levels for all genes assessed [using RNA preparations from three independent Dop1R2 RNAi (and control) biological replicates, Figure 2.10]. We also included Rel in the RT-PCR validations (although it fell below the  $\geq 1.6$ -fold cutoff in the microarray analysis) since the corresponding protein is a key effector in the IMD pathway/gut immune response (Erturk-Hasdemira et al. 2009). Using RT-PCR, we observed a slight, but significant, increase in Rel expression, in dsDop1R2 RNAi (vs. control) animals, as was observed by microarray analysis. Quantitative PCR confirmed an increase (4x) in TH transcript levels, in Dop1R2 RNAi flies compared to controls (Figure 2.11).

## **Analysis of the tissue-specific requirements for Dop1R2 expression suggests a role for receptor function in the salivary gland**

To identify the tissue type(s) that underlie the observed phenotypes, Dop1R2 RNAi expression was directed to specific tissues/cell types utilizing a series of GAL4 drivers, and the effects of these genetic manipulations were monitored (Table 2.1). It is well established that Dop1R2 is abundantly expressed in the mushroom bodies (MB) (Han et al. 1996; K. Zhang et al. 2007). However, elav-mediated pan-neuronal expression of the RNAi construct and Tab2-mediated expression specifically targeted to the MB failed to compromise viability or to induce gross morphological abnormalities. The vast majority of drivers tested led to progeny with wild-type (WT) phenotypes (Table 2.1).

As a follow-up to this initial study, a more focused selection of candidate drivers was tested, based on the results of the transcriptome analysis. Of particular interest was the Eig71 defensin-like peptides, which are highly expressed in one tissue – the salivary gland – during the L3 wandering/white prepupal stage (Gorski et al. 2003). The P{GawB}332.3 line (FBst0005398), which expresses GAL4 in the salivary glands, was obtained and utilized to generate salivary gland-expressing Dop1R2 RNAi flies. P{GawB}332.3-directed Dop1R2 knockdown resulted in developmental arrest of the progeny at the pupal/pharate adult stage, as seen with ubiquitous knockdown of Dop1R2 (Figure 2.12A and 2.12C). The P{GawB}332.3 knockdown flies also exhibited poorly formed tergites and sternites, with line 1 displaying the most severe phenotype (Figure 2.12B). Because P{GawB}332.3 also targets amnioserosal cells, which have a role in germ band retraction and dorsal closure in the developing embryo (Scuderi & Letsou

2005), the fraction of Dop1R2 RNAi embryos hatching into first instar larvae was assessed and compared to that of corresponding control embryos. No evidence of embryonic lethality was found in RNAi-expressing organisms (Figure 2.13). In subsequent work, we identified two additional larval salivary gland driver lines (i.e., P{GawB}c729 – FBst0006983, which also targets glia and the proventriculus, and P{GawB}17A – FBst0008474, which also targets female follicle cells, male accessory glands, testis sheath and cyst cells) that induce semi-lethality (72.1% and 58.2% lethality, respectively) in the corresponding Dop1R2 RNAi progeny (Figure 2.14A and 2.14B). Importantly, FBst0005398 and FBst0006983 resulted in progeny displaying wing and/or cuticle abnormalities (Figure 2.14C) as was observed with ubiquitous KD of Dop1R2. For these drivers, the lethal and abnormal morphology phenotypes showed higher penetrance in male flies vs. female flies (data not shown), as was observed with ubiquitous KD of Dop1R2. As indicated in Table 2.1, one tissue that is common to all three phenotype-positive GAL4 drivers is the salivary gland. Follow-up experiments confirmed GAL4-driven GFP expression in the salivary glands of corresponding larvae (Figure 2.15), while other tissues displayed background fluorescence. A fourth salivary gland driver (FBst0006870, for which GAL4 is under the control of the *sgs3* gene promoter) did not result in reduced viability (or other phenotypes) in corresponding Dop1R2 RNAi progeny (Table 2.1).

Since Dop1R2 signals through the stimulatory G protein  $G\alpha_s$ , we performed a complementary genetic analysis inducing G protein RNAi-mediated knockdown *in vivo*. Two different UAS-ds $G\alpha_s$  (stimulatory G protein) lines, as well as one UAS-ds $G\alpha_i$  (inhibitory G protein) line, were used to generate progeny at 29°C that express dsRNA

under control of the P{GawB}332.3-GAL4 driver. Crossing either  $G\alpha_s$  RNAi line with the P{GawB}332.3 resulted in pharate adult progeny that failed to eclose, as compared to the corresponding controls. However, the  $G\alpha_i$  RNAi progeny develop normally and emerge from their pupal cases as fully formed adults (Figure 2.16, Table 2.2). These findings support the inferences that  $G\alpha_s$  signaling in the salivary glands is required for progression to the adult stage, and that the cognate GPCR(s) play an essential role in this tissue/developmental process. In contrast, the inhibitory G protein  $G\alpha_i$  does not play a critical role for development in the salivary glands. While this finding does not exclusively pinpoint Dop1R2 as the only essential  $G\alpha_s$ -coupled protein in the salivary glands, it supports the premise that we are not targeting Dop2R, which signals via  $G\alpha_i$ . As observed with Dop1R2 RNAi,  $G\alpha_s$  RNAi under the control of the *sgs3* promoter (FBst0006870) does not lead to compromised viability (data not shown). A follow-up molecular analysis confirmed expression of Dop1R2 in salivary glands of wild type prepupae (Figure 2.17), as has been documented in other insect species (i.e., cockroach, locust, tick (Troppmann et al. 2014; Gifford 1991; O. Baumann et al. 2002; Šimo et al. 2011; Šimo et al. 2014; Ali et al. 1993)).

### **Delivery of a Dop1R2 antagonist to larvae results in reduced viability, abnormal melanization and cuticle defects**

Pharmacological assessment of Dop1R2 activity *in vitro* confirmed that flupenthixol dihydrochloride, with an  $IC_{50}$  of  $2.6 \times 10^{-7}$  M (Figure 2.18), is a potent antagonist of this dopamine receptor (Hearn et al. 2002; Troppmann et al. 2014; Hill et al. 2002). Given the *in vitro* results, this compound was used to manipulate Dop1R2-

mediated signaling *in vivo*, thus providing a means to complement the RNAi genetic manipulations described above. Administering flupenthixol (within a range of 0.25 mM to 4 mM) to *Drosophila* second instar larvae resulted in a dose-dependent decrease in adult eclosion with an  $EC_{50}$  of 0.8 mM (Figure 2.19A) and developmental delay (Figure 2.19B). When flupenthixol was administered to *Drosophila* third instar feeding larvae (at either 5 mM to 10 mM), emerging adults displayed abnormal melanization and cuticle defects (penetrance ~10%-13%, Figure 2.19C), and these phenotypes were not observed in corresponding control flies (fed H<sub>2</sub>O vehicle alone). Importantly, the morphological defects resulting from drug-induced blockade of Dop1R2 are similar to those observed with genetic knockdown of Dop1R2 (Figures 2.4B, 2.12B and 2.14C).

#### **D. DISCUSSION**

Our understanding of the molecular mechanisms that orchestrate the development of an adult fruit fly continues to expand. Insect metamorphosis relies on temporal and spatial cues that mediate the transition from the larval to the adult stage. Numerous gene families are tightly regulated to ensure normal insect metamorphosis, including genes that trigger larval tissue histolysis and genes that are responsible for protecting the morphing organism against microbial assault, as well as genes that mediate the formation of new adult structures. We show that a *Drosophila* dopamine receptor, i.e., the D1-like receptor Dop1R2, plays an important role in suppressing the expression of genes, which when up-regulated, lead to developmental arrest.



By using a reverse genetic approach, we show that ubiquitous knockdown of Dop1R2 results in pre-adult lethality that is dependent on receptor function during the third instar larval stage (Figures 2.4 and 2.6). Dop1R2 RNAi adult flies that escape pre-adult lethality display multiple morphological phenotypes including hypomelanization, abnormally shaped/curly wings and defects in the cuticle (in the tergum) (Figures 2.4B, 2.4C and 2.12B). The curly wing phenotype displayed by Dop1R2 RNAi escapers is very similar to that seen in flies that overexpress (2-fold increase) tyrosine hydroxylase (TH) in dopaminergic cells (Friggi-Grelin et al. 2003). In agreement with this observation, TH is among the genes that respond to reduction in Dop1R2 knockdown (2-4 fold increase in expression levels vs. controls) (Figure 2.7, Figure 2.11, Dataset 2.1). This finding may suggest that: (i) Dop1R2 participates in the negative regulation of TH, or (ii) compensatory mechanisms are triggered to restore normal DA-mediated signaling in the dying Dop1R2 RNAi organisms. Given that DA synthesis and secretion occurs in *Drosophila* epidermal cells during molting and eclosion (Yamamoto & Seto 2014), the wing and melanization abnormalities seen in Dop1R2 RNAi escapers could be the consequence of TH dysregulation in the epidermal dopaminergic cells of the wing and cuticle. Under normal conditions, a peak of TH activity is detected in late L3 larvae/white prepupae (M. M. Davis et al. 2007; Gelbart & Emmert 2013), consistent with a role for Dop1R2 during these stages of development.

Decreased Dop1R2 function leads to increased transcription of several cuticular proteins (CPs), including *Edg91* and *PCP* (Figures 2.7 and 2.10, Dataset 2.1). Along with ecdysone, many CPs play critical roles in puparial cuticle formation and sclerotization (Charles 2010). Proteins encoded by ecdysone-dependent genes (*Edg*)

include temporally regulated CPs that are induced by increased ecdysteroid levels in the hemolymph (Charles 2010; Fechtel et al. 1989). In *Drosophila*, *Edg91* responds to 20E pulses and is abundantly expressed in the epidermis during early pupal development, at the time of exocuticle synthesis (Apple & Fristrom 1991). ‘Pupal cuticle protein’ (PCP) is also temporally regulated by 20E, and is required for a successful third larval instar to pupal developmental transition. Notably, PCP is most tightly regulated via a small 20E titer rise around the time of head eversion (Charles 2010; Doctor et al. 1985). Deregulated expression of CPs in Dop1R2 RNAi flies may also contribute to the observed abnormal phenotypes, specifically in the tergum (Figure 2.12B).

To better assess the spatial requirements underlying Dop1R2 RNAi-induced developmental arrest in *Drosophila*, we selectively drove Dop1R2 dsRNA in various tissues/cell types (Table 2.1). Our microarray analysis, which showed up-regulation of salivary glands specific genes (e.g. the *Eig71E* genes), suggested involvement of this tissue in mediating Dop1R2 effects. Consistent with this observation, although most tissue-specific drivers resulted in normal progeny, targeting Dop1R2 knockdown to salivary glands (using three different GAL4 drivers, Table 2.1) led to arrested development/abnormal tergum in corresponding pharate adults. In addition, the corresponding progeny that escaped lethality displayed melanization and/or wing defects that were highly reminiscent of the phenotypes seen following ubiquitous Dop1R2 knockdown (Table 2.1, Figure 2.4). A follow-up molecular analysis confirmed expression of Dop1R2 in salivary glands isolated from wild type prepupae (Figure 2.17). This finding correlates with previous studies in other insect species (i.e., cockroach, locust, tick), which have demonstrated dopaminergic innervation of peripheral secretory

cells in the acini, and along the ducts, of the salivary glands (Gifford 1991; O. Baumann et al. 2002; Šimo et al. 2011). More recently, D<sub>1</sub>-like dopamine receptors were found in the salivary glands of adult ticks and cockroaches, where they may play a role during the feeding phase, as well as modulate salivary secretion, myoepithelial cell contraction and effects of neuropeptides (Šimo et al. 2011; Troppmann et al. 2014; Šimo et al. 2014).

A function for Dop1R2 in salivary glands is consistent with: (i) the observed (Dop1R2 RNAi-induced) deregulation of genes that are selectively expressed in this organ (e.g., *Eig71E* genes), and (ii) the DAVID GO clustering analysis of differentially expressed genes (Figures 2.7 and 10, Dataset 2.1 and 2.2), which reveals enrichment in salivary gland biological processes. A compelling example comes from the family of *Eig71E* (aka *L71*) puff genes that are (concomitantly) induced exclusively in salivary glands, and specifically during puparium formation (they are then repressed ~12 hours later) (L. G. Wright et al. 1996). It is known that the corresponding *L71* small defensin-like polypeptides are secreted from the salivary glands between the prepupal cuticle and imaginal epidermis, to help protect the metamorphosing organism against infection (L. G. Wright et al. 1996). The *Eig71E* genes participate in the secondary response to 20E (i.e., as “late” genes), which itself depends on the expression of the early-late genes *BR-C* and *E74* (Crossgrove et al. 1996). *BR-C* expression is also up-regulated in Dop1R2 RNAi flies, and derepression of this gene could lead to subsequent induction of the *Eig71E* genes in Dop1R2 RNAi flies. Our studies support the premise that Dop1R2 acts upstream of selected late genes. Of note, the absence of phenotype in *sgs3-GAL4;UAS-dsDop1R2* progeny may be due to temporal discrepancy between the activity of the *sgs3* (glue gene) promoter and the time at which *Dop1R2* is transcribed.

Further supporting the role of this receptor in development, pharmacological treatment of larvae with the established D1-like receptor antagonist flupenthixol dihydrochloride (Beggs et al. 2011; Blenau et al. 1998; Mustard et al. 2003; Meyer et al. 2012; Reale et al. 1997) results in pre-adult developmental delay/arrest (Figure 2.19A and 2.19B), as well as induced abnormal melanization and cuticle defects (Figure 2.19C) that recapitulate those observed by genetic manipulation of Dop1R2 expression. Notably, flupenthixol and other selected compounds that also inhibit the mosquito AaDOP2 receptor, which is the *Aedes aegypti* ortholog of the fly Dop1R2 receptor, have emerged as promising candidate insecticides to control vector arthropods (Meyer et al. 2012; Conley et al. 2015). Our analysis, which documents drug-induced morphological abnormalities in adults that escape lethality, further highlights the potential of this family of compounds as potential insecticides. Such anatomical defects would likely compromise survival of these disease-transmitting vectors in the field.

Notably, analysis of genes that are differentially expressed in response to reduced levels of Dop1R2 reveals that the vast majority of them (95%) are up-regulated (Figure 2.7 and Dataset 2.1). This observation suggests that Dop1R2 may play an important role in repressing gene expression. Functional annotation analysis of the genes for which expression increases  $\geq 1.6$  times, using DAVID bioinformatic resources (Huang et al. 2009), identifies enrichment in genes implicated in several biological processes for which quantitative regulation is critical (Figure 2.7). Several of the gene clusters fall under the GO term categories defense response, immune response, and response to heat, as well as salivary gland morphogenesis and histolysis (Dataset 2.2).

Such de-regulated activation of the immune system (in response to Dop1R2 knockdown) in the developing fly may contribute to the observed lethal phenotype. It is well-established that in *Drosophila* the balance between repression and induction of the immune defense is tightly regulated, and ensures optimal growth and size at metamorphosis (Abdelsadik & Roeder 2010; K.-Z. Lee & Ferrandon 2011; Åkerfelt et al. 2010). Control of the innate immunity enables larval growth amidst the plethora of bacteria and fungi found in the natural larval feeding environment and ensures high tolerance for the larval gut commensal microbiota, which has been shown to promote development (Charroux & Royet 2012; Storelli et al. 2011; Shin et al. 2011). Conversely, de-regulated immune responses can alter normal fly growth and development. Abdelsadik and Roeder (2010) have demonstrated that chronic activation of the immune system of larval salivary glands is detrimental to fly development and survival (Abdelsadik & Roeder 2010). Similarly, Rynes *et al.* (2012) have shown that chronic inflammation of the larval gut epithelium results in developmental delay, growth retardation and lethality (Rynes et al. 2012).

Recent advances in the field have unraveled an exquisite interplay of negative regulators of the immune deficiency (IMD) pathway that together adapt the immune response to the microbiome encountered by the developing fly (dietary/beneficial or pathogenic). These factors are essential to larval growth and immune homeostasis (Erturk-Hasdemira et al. 2009; K.-Z. Lee & Ferrandon 2011; Aparicio et al. 2013; Rynes et al. 2012; Ryu et al. 2004; Myllymaki & Ramet 2013; Lhocine et al. 2008; Fernando et al. 2014; Maillet et al. 2008), and loss-of-function mutations in these negative regulators can result in larval death (Rynes et al. 2012). Our results suggest that down-regulation of

Dop1R2 leads to up-regulation of multiple antimicrobial peptides (AMPs), including the cecropins CecA1 and CecA2 (Figures 2.7 and 2.10), which are gut peptides strongly induced upon infection in an IMD/relish-dependent manner (Buchon et al. 2009; Tryselius et al. 1992). In non-pathogenic conditions, these AMPs are expressed during metamorphosis (Tryselius et al. 1992) and are regulated by ecdysone (Z. Zhang & Palli 2009). Two other AMPs, Dro2 and Dro3, together with LysX, Hsp70Bc, Hsp67Bb and Hsp22 (also on the microarray list), comprise a small group of genes that respond to changes in fly gut microbiota (Broderick et al. 2014)). LysX is a known effector of IMD response (Broderick et al. 2014). Increased expression of an entire set of *Drosophila*-specific immune-induced molecules (IMs, i.e., IM1, IM2, IM3, IM4, IM10, IM23, CG18107, CG16836 and IM2-like/CG15065) is observed in Dop1R2 RNAi animals (Figure 2.7 and Dataset 2.1). These short peptides, which are normally released into the hemolymph following septic injury, are postulated to act as chemokines (Levy 2003; Verleyen et al. 2006). Importantly, IM1, IM2, IM3, IM4, IM10, IM23, along with Dro2 and AttB (Figure 2.7 and Dataset 2.1), were recently identified within a group of 14 AMPs and IMs that are markedly up-regulated in mutant *Drosophila* deficient in *activating transcription factor 3*, *atf3*. *Atf3* plays an essential role in larval growth, and is highly expressed in the larval gut, salivary glands and Malpighian tubules (Rynes et al. 2012). The overlap between the deregulated gene set (and associated adverse effects on development) induced by Dop1R2 deficiency, and that induced by *atf3* deficiency, suggests an important role for Dop1R2 in the control of the immune response.

In addition to antimicrobial peptides, our study shows that the expression levels of multiple heat shock/stress genes increase in response to Dop1R2 deficiency, including the

major heat-inducible proteins (Hsp70Bc, Hsp70Bbc, and Hsp68), and small heat shock proteins (Hsp22, Hsp26, Hsp67Bb and Hsp67Bc) (Figure 2.7 and Dataset 2.1). These chaperones are postulated to play a role in normal development, and under non-heat shock conditions, exhibit a peak of expression during the late L3/ early pupal stages (Sirotkin & Davidson 1982; Mason et al. 1984). Expression of small hsps is regulated by a rise in the molting hormone ecdysone (Irland et al. 1982; Takahashi et al. 2010). Hsp22, Hsp67Bb and Hsp67Bc belong to a group of four hsps that regulate morphogenesis, and buffer developmental processes from environmental assault. Interestingly, the genes that encode Hsp22, Hsp26, Hsp67Bb and Hsp67Bc all cluster within a short (~5.5Kb) genomic region at cytological location 67B on chromosome 3L [FlyBase, (Ayme & Tissieres 1985)], consistent with possible co-regulation of their expression. High levels of Hsp70 in *Drosophila* (due to one extra copy of the gene) are sufficient to decrease organismal growth, development and survival to adulthood (Krebs & Feder 1997). Up-regulation of this gene alone in developing Dop1R2 RNAi flies (Figures 2.7 and 2.10) may thus contribute to the observed lethal phenotype that results from reduced Dop1R2 function.

A complementary DAVID GO clustering analysis (Huang et al. 2009) was used to identify previously published studies with data sets that best correlate with the set of differentially expressed genes in Dop1R2 RNAi flies. Intriguingly, the two most significant reports (i.e. PMID 16990270/Benjamini E-15 and PMID 16264191/Benjamini E-11, respectively, Dataset 2.2) both investigate chromatin remodeling and transcriptional activity during metamorphosis (Badenhorst 2005; Zraly et al. 2006). In both studies, the authors show that deficiency in an ecdysone-dependent transcription co-

factor affects expression of a limited subset of immune-related genes. The genes identified exhibit substantial overlap with those that respond to Dop1R2 knockdown (Figure 2.7, in ecdysone-related and immune diagrams). In support of a potential role of Dop1R2 in the regulation of transcription, sequence analysis ([http://nls-mapper.iab.keio.ac.jp/cgi-bin/NLS\\_Mapper\\_form.cgi](http://nls-mapper.iab.keio.ac.jp/cgi-bin/NLS_Mapper_form.cgi)) reveals the presence of a bipartite nuclear localization signal (the major class of NSL found in nuclear proteins), as well as a BAF1/ABF1 chromatin reorganizing factor motif (<http://www.genome.jp/tools/motif/>) (Figure 2.20), within the Dop1R2 protein. Both features are found nested in the third intracellular loop of the receptor. Interestingly, in mammals, internalization of selected GPCRs (e.g., adrenergic, catecholaminergic) in response to steroid hormone (Gonzalez-Arenas et al. 2006), their localization at the nuclear membrane and their ability to modulate gene expression (Tadevosyan et al. 2012; Vaniotis et al. 2011; Boivin et al. 2008; C. D. Wright et al. 2012) have been documented.

Taken together, our analyses strongly suggest a role for Dop1R2 in the developmental control of genes at the onset of metamorphosis. We postulate that under normal conditions, at the time of ecdysone-responsive early gene induction (i.e., during the L3 stage), Dop1R2 in the salivary glands participates in the co-repression of ecdysone-responsive late genes. We propose that the premature release of the Dop1R2 inhibitory effect (using RNAi approaches) translates into increased expression of the L71 defensin-like polypeptides, as well as a series of antimicrobial peptides, stress proteins/chaperones, cuticle and morphogenesis proteins in a de-synchronized manner. This misexpression could be highly detrimental to the developing fly, in agreement with a number of studies discussed above (Abdelsadik & Roeder 2010; Rynes et al. 2012; Krebs



& Feder 1997). During normal development, however, regulated expression of this set of genes during the molting period not only ensures the completion of adult metamorphosis, but may also provide ‘prophylactic’ protection against microbial assault and injury at a time of increased vulnerability.

The late pupal death induced by knockdown of Dop1R2 in salivary glands is reminiscent of that observed in flies that down-regulate, in the same tissue, the low abundance ecdysone receptor minor subtype EcR-A (M. B. Davis et al. 2005). Future studies comparing the levels of EcRs and their subcellular localization in Dop1R2 RNAi flies may prove informative. Our study provides a framework to further probe the molecular mechanisms, and structural domains within the receptor, that contribute to Dop1R2-induced regulation of fly development.

## **E. METHODS**

### ***Drosophila* stocks and culture**

Two independent UAS-dsDop1R2 homozygous RNAi stocks (lines 1 and 2) were originally generated at Tufts Medical Center, Boston, MA (Kopin Laboratory, the lethality phenotype was first documented with these lines). Two additional UAS-dsDop1R2 stocks (FBst0460369:  $w^{1118};P\{GD703\}v3391$  and FBst0477151:  $w^{1118};P\{KK110947\}VIE-260B$ ) were later obtained from the Vienna *Drosophila* RNAi Center (VDRC, Vienna, Austria). Two UAS-dsGα<sub>s</sub> stocks (FBst0455666:  $w^{1118};P\{GD8547\}v24958$  and FBst0477312:  $P\{KK107742\}VIE-260B$ ) and one UAS-dsGα<sub>i</sub> stock (FBst0457318:  $w^{1118};P\{GD12576\}v28150/TM3$ ) were also acquired from the

VDRC. The  $w^{1118}$  stock and all of GAL4 driver fly lines (with the exception of Bursicon- $\alpha$ -GAL4) were obtained from the Bloomington *Drosophila* Stock Center (Indiana University, Bloomington, IN): FBst0003954:  $y^1w^*$ ;P{Act5C-GAL4}17bFO1/TM6B, Tb<sup>1</sup>; FBst0004414:  $y^1w^*$ ;P{Act5C-GAL4}25FO1/CyO,  $y^+$ ; FBst0000458: P{GawB}elav<sup>C155</sup>; FBst0004440:  $w^{1118}$ ;P{GawB}Tab2<sup>201Y</sup>; FBst0003739: P{GawB}c698a, $w^{1118}$ ; FBst0006871:  $w^{1118}$ ;P{Eip71CD-GAL4.657}TP1-1; FBst0025685:  $y^1w^*$ ;P{CCAP-GAL4.P}16; FBst0037534:  $w^*$ ;P{GawB}30A/CyO; FBst0005398:  $w^*$ ;P{GawB}332.3; FBst0008474:  $w^*$ ;P{GawB}17A/CyO; FBst0006983: $w^*$ ;P{GawB}c729; FBst0006994:  $w^{1118}$ ;P{GawB}l(2)T32<sup>T32</sup>/CyO; FBst0003734:  $w^{1118}$ ;P{GawB}c381; FBst0006870:  $w^{1118}$ ;P{Sgs3-GAL4.PD}TP1; FBst0006357:  $y^1w^{1118}$ ;P{Lsp2-GAL4.H}3; FBst0007098:  $w^{1118}$ ;P{drm-GAL4.7.1}1.1/TM3,Sb<sup>1</sup>, FBst0006874:  $w^*$ ;P{UAS-2xEGFP}AH2. The Bursicon- $\alpha$ -GAL4 stock was generously provided by Dr. W. Honegger (Vanderbilt University, Nashville, TN). All stocks were maintained at 25°C in a 12 h light:12 h dark cycle on standard *Drosophila* medium (Newby & R. F. Jackson 1991). \*FBst0460369 is no longer available at VDRC; however, a corresponding RNAi line using the same RNAi target region is available: FBst0460377,  $w^{1118}$ ;P{GD703}v3392.

### **Dop1R2 RNAi construct generation and corresponding UAS-dsDop1R2 transgenic flies**

The pUAS-dsDop1R2 RNA interference ('RNAi') construct includes the yeast Upstream Activator Sequence (UAS; the binding site for the yeast transcription factor, GAL4) (Brand & Perrimon 1993), inverted repeats of a 825 bp sequence corresponding to the 3' coding region of the Dop1R2 receptor cDNA (bp 807–1631 of the Dop1R2

cDNA sequence, with bp 1 corresponding to the start of the translation initiation codon), and a SV40 polyadenylation site. Cloning of the sense and antisense cDNA repeats in the pUAST vector was performed as described previously for a Dop2R RNAi construct (Draper et al. 2007). The pUAS-dsDop1R2 RNAi transgene construct (250–300  $\mu\text{g/ml}$ ) was coinjected with the P helper plasmid p $\Pi$ 25.7wc (100  $\mu\text{g/ml}$ ) into preblastoderm  $w^{1118}$  *Drosophila* embryos, according to standard protocols (Rubin & Spradling 1982). Seven independent transformant lines containing the UAS-dsDop1R2 transgene were obtained, and maintained as homozygotes for the P[UAS-dsDop1R2] transgene.

### **Generation of Dop1R2 RNAi flies**

The interference construct was expressed under the control of the well-characterized GAL4/UAS binary system (Brand & Perrimon 1993). UAS-dsDop1R2 homozygous flies, that were either generated in the laboratory or obtained from VDRC (i.e., 3391-GD and 10524-KK, see Materials and Methods), were crossed with each of the GAL4 driver lines listed in Table 2.1. Developing progeny were reared at either 29°C or 25°C. Isogenic progeny derived from a cross between the  $w^{1118}$  control strain and the corresponding GAL4 driver line were used as control flies for all molecular and phenotypic analyses.

### **Phenotypic assessment**

Viability, melanization and wing phenotype profiles of the Act5C-GAL4/UAS-dsDop1R2 RNAi progeny were assessed versus those of Act5C-GAL4/ $w^{1118}$  control

progeny. To delineate the temporal requirements of Dop1R2 expression for adult eclosion/viability, developing flies were transferred from 25°C ('permissive' condition) to 29°C ('restrictive' condition) during different developmental stages, and emergence was monitored (as a function of developmental stage at transfer). In a complementary analysis, and to assess the spatial requirement of Dop1R2 expression for the organismal viability, Dop1R2 RNAi progeny that express the RNAi construct in specific tissues/cell types were generated at 29°C, and characterized (the corresponding GAL4 drivers used in the crosses are listed in Table 2.1).

### **Assessment of transcript knockdown in Dop1R2 RNAi**

RT-PCR analysis was utilized to assess transcript levels in Dop1R2 RNAi flies that express the Dop1R2 RNA interference construct ubiquitously vs. control flies that express the GAL4 transcription factor alone. RNA was extracted from 10-20 pooled Dop1R2 RNAi early/pale pupae and corresponding control pupae. Total RNA was isolated using Trizol reagent (Invitrogen, Grand Island, NY), and purified using the RNeasy Kit with DNase treatment (Qiagen, Valencia, CA), according to the manufacturer's recommendations. The RNA concentrations were quantified by spectrophotometry. First strand complementary DNA (cDNA) was generated from total RNA (5 ng/μl) using MultiScribe Reverse Transcriptase (Applied Biosystems, Carlsbad, CA). PCR was performed using the GeneAmp PCR core kit (Applied Biosystems, Carlsbad, CA) and the AmpliTaq Gold enzyme (Invitrogen, Grand Island, NY). Amplification was done using the GeneAmp PCR system 9700 thermocycler (Applied Biosystems, Carlsbad, CA). The conditions for PCR included: initial denaturation at

95°C x 10 min; followed by 32 cycles of amplification: 94°C x 30 sec, 58°C x 30 sec and 72°C x 1:30 min. The reaction was completed with a seven-minute final extension at 72°C. The sequences of gene specific primers are provided in Table 2.3. Dop1R2 primer pairs were designed to amplify: (i) an amplicon localized within the interference sequence (i.e., both forward and reverse primers anneal within RNAi sequence – “in/in pair”) to confirm expression of the RNAi repeats, as well as (ii) an amplicon that corresponds to a region of Dop1R2 mRNA within and outside the RNAi sequence (i.e. the forward anneals within RNAi sequence and the reverse anneal outside) – “in/out pair”) enabling assessment of endogenous Dop1R2 mRNA levels. To assess whether the RNAi construct exerted non-specific off-target effects, primer pairs corresponding to other biogenic amine receptors [i.e., Oamb (CG3856), Oct-TyrR (CG7485), 5-HT1A (CG16720), Dop1R1 (CG9652), Dop2R (CG33517)] were designed, so that the sequence with the most extensive homology (as assessed by NCBI BLAST analysis) between these transcripts and the Dop1R2 sequence was amplified for each, respectively. The primers were synthesized at the Tufts University Molecular Core (Tufts University, Boston, MA) and are listed in Table 2.3. PCR products were run on a 1% agarose gel with ethidium bromide, and photographed using a Multi Image Light Cabinet and camera (Alpha Innotech Corporation, San Leandro, CA). Alphaimager 2200 v5.04 imaging software (Alpha Innotech Corporation, San Leandro, CA) was used to visualize the bands and determine band intensity and saturation point. RT-PCR analysis was performed in triplicate using independent biological replicates. For each GPCR gene/transcript assessed, the values of the PCR signal intensities in Dop1R2 RNAi and control flies were obtained and significance evaluated using a pooled variance t-test.

## **Transcriptome analysis and RT-PCR validation**

Gene expression analysis was performed on the GeneChip<sup>R</sup> *Drosophila* genome array (DrosGenome1) using Affymetrix Gene Array technology, according to standard Affymetrix protocols (<http://www.affymetrix.com/support/technical/byproduct.affx?product=fly>). Total early pupal RNA was isolated and purified as described in ‘*Assessment of transcript levels*’ above, and double-strand cDNA was obtained using SuperScript Double Stranded cDNA Synthesis kit (Invitrogen, Grand Island, NY). *In vitro* transcription and RNA labeling was performed using Enzo BioArray High Yield RNA transcript (Affymetrix, Santa Clara, CA), according to the manufacturer recommendations. Data were analyzed using the Microarray Suite program (Affymetrix, Santa Clara, CA), as well as Genespring array analysis software (Silicon Genetics). Only genes with expression signal called as “M” (marginal present) or “P” (present) in both replicates were selected for further statically analysis. A t-test was performed to assess the significance of differential expression between the transgenic RNAi lines and the controls. Only genes that exhibited significant differences ( $p < 0.05$ ) in expression levels compared to controls in both experiments were considered for further bioinformatic analysis using DAVID (see following ‘*Bioinformatic analysis*’). The complete analysis is provided in Dataset 2.1. RT-PCR analysis was used to further assess/validate selected differentially expressed genes. Early pupae were collected, and total RNA was isolated using TRI reagent (Sigma-Aldrich, St. Louis, MO) according to manufacturer’s instructions. Synthesis of first strand cDNA was performed using 25 ng/ $\mu$ l total RNA and MMuLV Reverse Transcriptase (Invitrogen, Grand Island, NY). All primers were designed to span exon boundaries (except in circumstances of single-exon transcripts), to

avoid gDNA amplification (primer sequences are provided in Table 2.3). The conditions utilized for RT-PCR were: 95°C for 2 min, followed by 30 cycles of 95°C x 15 sec, 50-55°C x 30 sec, 68°C x 10 sec, and completed with one cycle of 72°C x 10 min. Samples were run on a 2% agarose gel with ethidium bromide and imaged to measure band intensity using ImageJ software (NIH, Bethesda, MD). The PCR products were confirmed by sequencing (Eton Bioscience Inc., Boston, MA) the corresponding amplicon excised from the gel.

### **Bioinformatic analysis**

All of the identified differentially expressed genes were used for functional annotation analysis with the DAVID Bioinformatics Resource 6.7 (Huang et al. 2009). Using the functional annotation tool for *Drosophila melanogaster*, a total of 101 genes that were up-regulated by  $\geq 1.6$ -fold were analyzed for GO class and pathway associations. For any identified gene ontology (GO) term and pathway, enrichment was considered significant if the p-value observed was  $< 0.05$  (Benjamini et al. 2001). Alternatively, the set of genes was analyzed using **WEB-based GENE SeT AnaLysis Toolkit** (WebGestalt), designed for functional genomic, proteomic and large-scale genetic studies. The program uses the hypergeometric test for enrichment evaluation analysis, and Benjamini-Hochberg multiple test adjustment, to assess enrichment significance (P.-H. Wang et al. 2013b; B. Zhang et al. 2005). In addition, protein-protein interaction analysis was performed with STRING 9.1 for all of the genes up-regulated by  $\geq 1.6$ -fold (Szklarczyk et al. 2010).

## Quantitative RT-PCR

For quantitative RT-PCR, SYBR Green fluorescence using the Quantitect SYBR Green kit (Qiagen, Valencia, CA) was used to quantify production of a PCR-generated cDNA fragment (primers sequences are listed in Table 2.3). Amplification and data analysis were performed using the ABI Prism 7700 (Applied Biosystems, Carlsbad, CA). The PCR conditions utilized for RT-PCR were: 50°C x 2 min, 95°C x 15 min, followed by 40 cycles of 95°C x 15 sec, 64°C x 45 sec.

## Analysis of Dop1R2 expression in prepupal tissues

The brain and salivary glands were dissected from prepupal *w<sup>1118</sup> D. melanogaster*. For each tissue, total RNA was isolated, and cDNA was prepared using 50 ng/ $\mu$ l total RNA (as detailed in ‘*RT-PCR validations*’, above). Dop1R2 was amplified using primers that span nucleotide positions 1521-1637 (isoforms A and C) or 1598-1711 (isoform B), with bp 1 corresponding to the start of the translation initiation codon. As an endogenous control, Act5C (CG4027) was amplified and used for normalization. To enable detection of tissue contamination, primers were designed to amplify *repo* (CG31240) cDNA (*repo* expression is enriched in glia) to provide a brain-specific probe (Watts et al. 2004), and *sgs5* (CG7596) cDNA, to provide a salivary gland-specific probe. All primers were designed to span exon boundaries (sequences are listed in Table 2.3) to avoid gDNA amplification. PCR conditions and imaging were performed as mentioned in the validation portion of ‘*Transcriptome analysis and RT-PCR validation.*’



To confirm that the amplicon corresponded to Dop1R2, DNA bands were excised from the gel and sequenced.

### ***In vitro* Dop1R2 pharmacology**

Luciferase assays were performed as previously described, with minor modifications (Harwood et al. 2013). HEK293 cells in 96-well plates were grown in serum-free Dulbecco's modified eagle medium with antibiotics. After 48 hours, cells were transfected using PEI (1  $\mu\text{g}/\text{ml}$ ) with the following constructs: the *Drosophila* Dopamine 1 receptor 2 (Dop1R2) cloned into pcDNA1.1 (4 ng/well), a CRE-LUC-HCL-PEST luciferase reporter gene (5 ng/well), and  $\beta$ -galactosidase-encoding plasmid (5 ng/well) as a transfection control. For agonist assays, cells were treated with the indicated concentrations of dopamine hydrochloride 24 hr after transfection (Product H8502, Sigma, Natick, MA). For antagonist assays, butaclamol hydrochloride (Product D033, Sigma, Natick, MA) or flupenthixol dihydrochloride (Product 4057, Tocris Bioscience, Bristol, UK) was added to cells for 15 minutes prior to the addition of 1  $\mu\text{M}$  dopamine. For both agonist and antagonist assays, cells were treated with compound for 4 hr at 37°C. Luciferase activity was quantified as an index of Dop1R2 signaling. Activity data were normalized relative to  $\beta$ -galactosidase activity as a control for transfection efficiency.

### ***In vivo* treatment of larvae with a Dop1R2 small molecule antagonist**

Adult w<sup>1118</sup> *D. melanogaster* were allowed to mate for 12 hours at 25°C to obtain developmentally synchronized eggs laid on *Drosophila* medium. All adults were removed, and larval development was allowed to continue for ~48 or ~72 hours, to obtain L2 or L3 instar larvae. Flupenthixol dihydrochloride (Product 4057, Tocris Bioscience, Bristol, UK) was prepared as a 25 mM stock solution in dH<sub>2</sub>O. The concentration of the drug that was used to feed L2 larvae ranged from 4 mM (maximum) to 0.25 mM (using two-fold serial dilutions of the drug). L3 larvae were fed flupenthixol at 5 mM or 10 mM. The drug solutions, or dH<sub>2</sub>O vehicle-only, were used to prepare instant fly food (Carolina Biological Supply Company, Burlington, NC) as follows: 0.5 g of fly food was placed into 25 x 95 mm polystyrene tubes (Dot Scientific Inc., Burton, MI) with 2 ml of solution (prepared in dH<sub>2</sub>O and 0.1% (v/v) including Fast Green Fast Green FCF dye (Product F7258, Sigma-Aldrich, St. Louis, MO). Fifty L2 or thirty L3 instar larvae were inserted gently into tubes that were kept in a humid chamber at 25°C during the course of the treatment.

## F. TABLES, FIGURES AND LEGENDS

**Figure 2.1. Dop1R2 cDNA and a corresponding interference construct.** (A) Coding sequences encompassing transmembrane domains (TMDs) 1-7 are shaded (dark gray). Knockdown region expanded, with TMDs 5-7 indicated (white boxes). UTR regions (light gray). (B) pUAS-dsDop1R2 interference construct, including the yeast Upstream Activator Sequence (UAS; binding site for the yeast transcription factor, GAL4), the Dop1R2 inverted repeats and an SV40 polyadenylation site. (C) Crosses and knockdown schematic, including Dop1R2 inverted repeat (black).

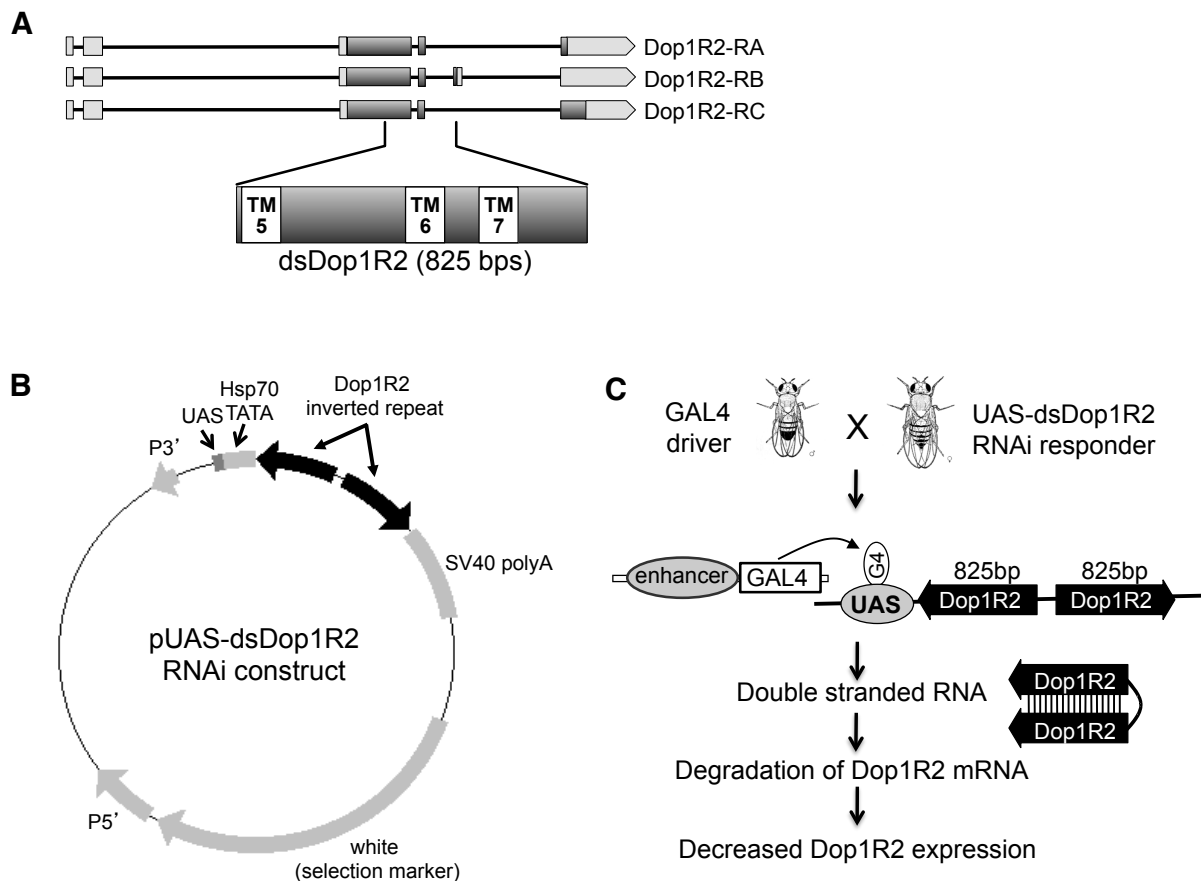


**Figure 2.2. Dop1R2 RNAi flies show decreased Dop1R2 transcript levels.** (A) Transcript levels assessed by RT-PCR. RNA from Dop1R2 RNAi and control flies was reverse transcribed, and PCR was performed in triplicate using primer sets corresponding to endogenous Dop1R2 or to Dop1R1 (as a normalization control). (B) Dop1R2 transcript levels are significantly decreased in Dop1R2 RNAi flies (genotype:  $w^{1118};UAS-dsDop1R2/+;Act5C-GAL4/+$ ), compared to controls (genotype:  $w^{1118};UAS-dsDop1R2/+;TM6B/+$ ). The average band intensity of the Dop1R2 RNAi PCR product was normalized to control PCR product for Dop1R1. Primers corresponding to Dop1R2 as well as other biogenic amine receptors (Oamb, octopamine receptor; Oct-Tyr, tyramine receptor; 5-HT1A, serotonin receptor 1A; Dop1R1, other D1-like Dopamine receptor; Dop2R, D2-like dopamine receptor) and an Actin5C control were used (Table 2.3). Error bars indicated standard variance of the mean for each gene. Significance was determined for the difference in intensity of the RNAi sample PCR band versus the control PCR band using a one-sided t-test. \*  $p < 0.05$ , \*\*  $p \leq 0.01$ , \*\*\*  $p \leq 0.001$ . Driver stock: Act5C-GAL4 (FBst0003954).

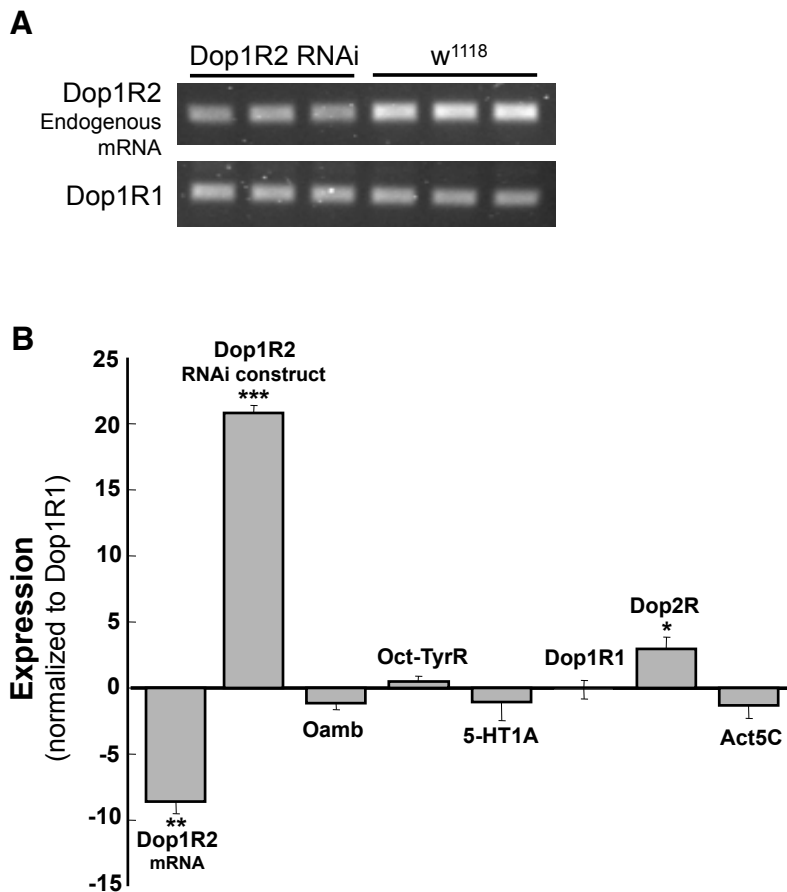
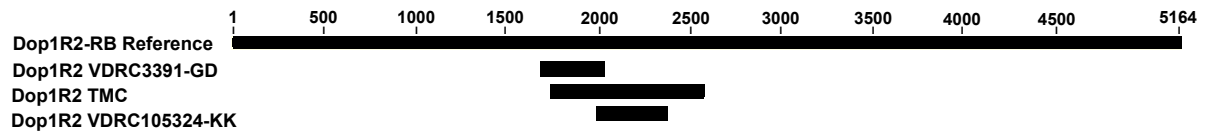


**Figure 2.3. dsDop1R2 RNAi constructs.** Sequences of the three RNAi constructs utilized in the present study, and alignment on Dop1R2-RB mRNA GenBank reference sequence. The RNAi sequences include those used to generate Vienna *Drosophila* RNAi Center (VDRC) stocks 3391-GD (FBst0460369) / construct 703 and 105324-KK (FBst0477151) / construct 110947, as well as Tufts Medical Center (TMC) Dop1R2 lines (Materials and Methods).



**Dop1R2 VDRC3391-GD**

CTGCGAGGGATGGCGAGATGCCCGCTACAAGTGCACCTTCACTGAGCACCTAGGCTATCTGGTCTTCTCGTCGACGATA  
 TCCTTCTACCTGCCGCTTCTAGTGATGGTCTTACCTACTGTGCGCATCTACAGGGCAGCCGTCATCCAGACGAGATCTCT  
 TAAGATTGGAACCAAGCAGGTGCTCATGGCTCCGGGAACTGCAGCTCACATTGCGCATTCATCGTGGTGGCACTACGC  
 GGGATCAGCAAAACCAGGTCTCCGGAGGAGGAGGTGGCGGAGGAGGAGGTGGCGGTGGCGGAGGATCTCTGAGCCACTCG  
 CACTCCCATTTCGCAC

**Dop1R2 TMC**

TCTGGTCTTCTCGTCGACGATAFCCTTCTACCTGCCGCTTCTAGTGATGGTCTTACCTACTGTGCGCATCTACAGGGCAG  
 CCGTCATCCAGACGAGATCTCTTAAGATTGGAACCAAGCAGGTGCTCATGGCTCCGGGAACTGCAGCTCACATTGCGC  
 ATTCATCGTGGTGGCACTACGCGGGATCAGCAAAACCAGGTCTCCGGAGGAGGAGGTGGCGGAGGAGGAGGTGGCGGTGG  
 CGGAGGATCTCTGAGCCACTCGCACTCCCATTCGCACCACCATCATCACAATCACGGCGGTGGCAGCAGCCTCCACGC  
 CGGAGGAGCCGGATGATGAGCCGCTATCCGCTCTGCATAACAACGGACTGGCAGCCATCGGCACATGGGCAAGAATTC  
 TCGTGTCCAGGAACTGGCGAAGTTCGCCAAGGAGAAGAAAGCGGCCAAGACGCTGGGCATCGTGATGGGCGTGTTTCAT  
 CATCTGTTGGCTGCCCTTCTTCTGTTGTTCAACTGCTGTCTGGGTTCTGCATCGAGTGCATCGAGCACGAGGAGATCGTCT  
 CGGCAATCGTCACCTGGCTCGGCTGGATCAACTCCTGCATGAATCCTGTGATTTACGCCTGCTGGAGCAGGACTTTTCGC  
 AGGGCCTTTGTGCGTCTGCTGTGCATGTGCTGTCCACGCAAGATTCGCCGCAAGTACCAGCCCAGATGCGGTTCCAAATC  
 GCAGAGATTCGCGACGCGGCGTGTACTCGACCTGCTCGCTGCACGGCATTTCAGCACGTGCGACACAACCTCTGCGAGC  
 AGACCTACATATAGTTTAGCGTAGA

**Dop1R2 VDRC105324-KK**

GCAGGCGTAAATCACAGGATTCATGCAGGAGTTGATCCAGCCGAGCCAGGTGACGATTCGCCGAGACGATCTCCTCGTGCT  
 CGATGCACTCGATGCAGAACCCAGACAGCAGGTTGACCACGAAGAAGGGCAGCCAACAGATGATGAACACGCCCATCACG  
 ATGCCAGCGTCTTGGCCGCTTTCTTCTCCTTGGCGAACTTCGCCAGTTTCTTGACAGCGAGAAGTTCTTGCCCATGTG  
 CCGATGGCGTGCCAGTCCGTTGTTATGCAGAGCGGATAGCGGCTCATCATCCGGCTCCTCCGGCGTGGAGGTGCTCGTGC  
 CACCGCCGTGATTGTGATGATGGTGGTGCGAATGGGAGTGCAGTGGCTCAGAGAT

**Figure 2.4. Ubiquitous knockdown of Dop1R2 results in reduced adult emergence and wing and/or melanization phenotypes.** (A) Ubiquitous knockdown of Dop1R2 at 29°C results in 100% of Dop1R2 RNAi (genotype:  $w^{1118};UAS-dsDop1R2/+;Act5C-GAL4/+$ ) flies failing to emerge, compared to control flies (genotype:  $w^{1118};UAS-dsDop1R2/+;TM6B/+$ ). At 25°C, 23.4-54.7% of Dop1R2 RNAi flies develop into adults ('escapers'). Escaper flies may exhibit two other phenotypes: hypomelanization and curly wing. (B) Hypomelanization phenotype appears as reduced melanization of abdominal cuticle (arrows). 25°C n = 699 and 29°C n = 117. (C) Curly wing phenotype appears as bent/curved adult wing (arrows). Driver stock: Act5C-GAL4 (FBst0003954).

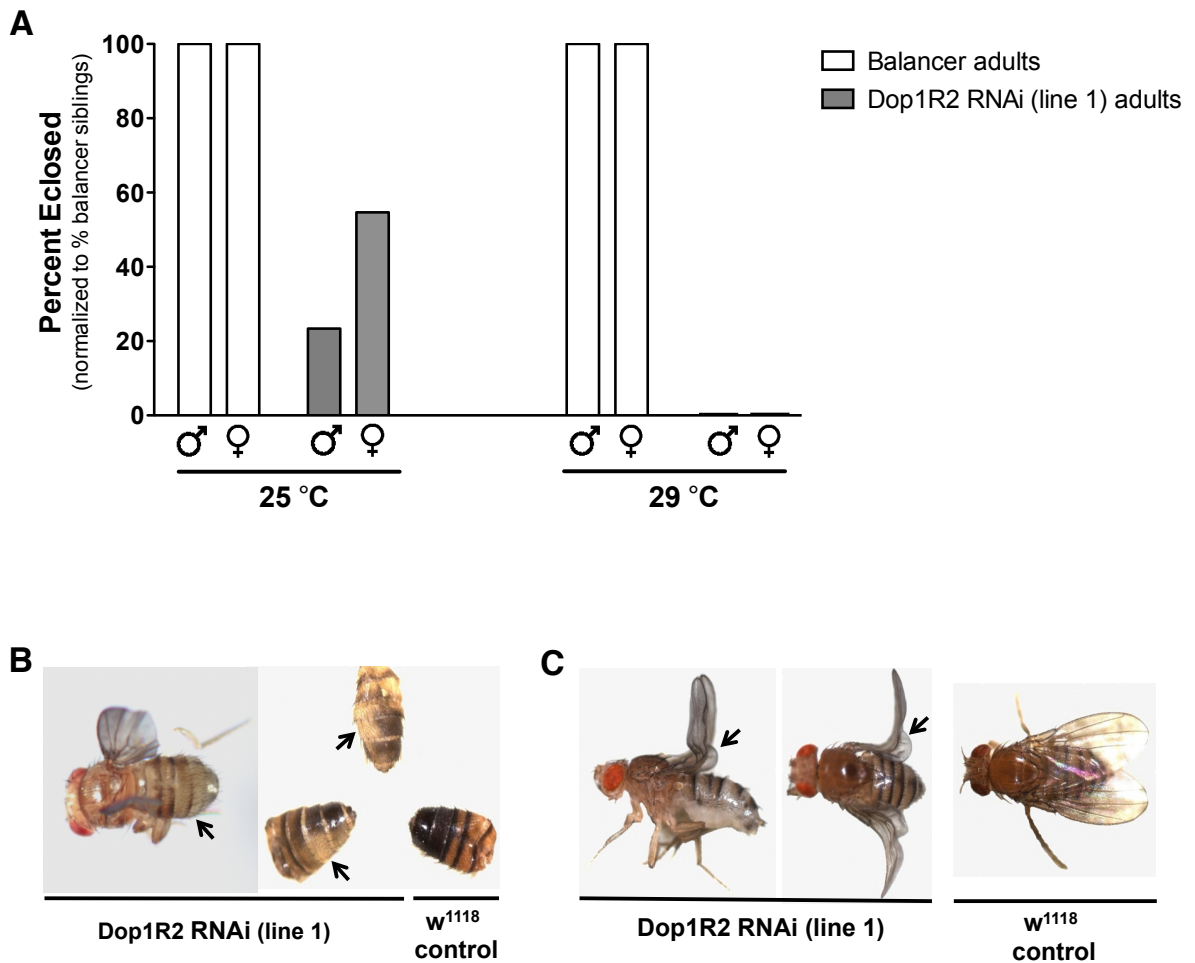


**Figure 2.5. dsDop1R2 knockdown-induced lethality is recapitulated with alternate RNAi constructs.** (A) and (B) Ubiquitous knockdown of Dop1R2. (A) VDRC 3391-GD (genotype:  $w^{1118};UAS-dsDop1R2/+;Act5C-Gal4/+$ ) results in 98% lethality at 29°C (n = 58) and 94% lethality at 25°C, or viability (n = 44). (B) VDRC 105324-KK (genotype:  $w^{1118};TM6B/+;UAS-dsDop1R2/+$ ) results in 97% lethality at 29°C (n = 59), compared to control balancer siblings (genotypes:  $w^{1118};CyO/+;UAS-dsDop1R2/+$  and  $w^{1118};CyO/UAS-dsDop1R2$ , respectively). All male escaper flies (n=4) obtained when using the VDRC 3391-GD RNAi construct exhibited the hypomelanization phenotype (described in Figure 7). (C) Salivary gland/amnioserosa targeted knockdown of Dop1R2 VDRC 3391-GD results in 68% lethality at 29°C in experimental flies (genotype:  $w^{1118};UAS-dsDop1R2/+;P\{GawB\}c729-GAL4/+$ ), compared to controls (genotype:  $w^{1118};P\{GawB\}c729-Gal4/+$ ) (n = 53). VDRC Dop1R2 knockdown stocks: 3391-GD (FBst0460369) and 105324-KK (FBst0477151). Driver stocks: Act5C-GAL4 (FBst0003954), P{GawB}17A-GAL4 (FBst0008474) and P{GawB}c729-GAL4 (FBst0006983).

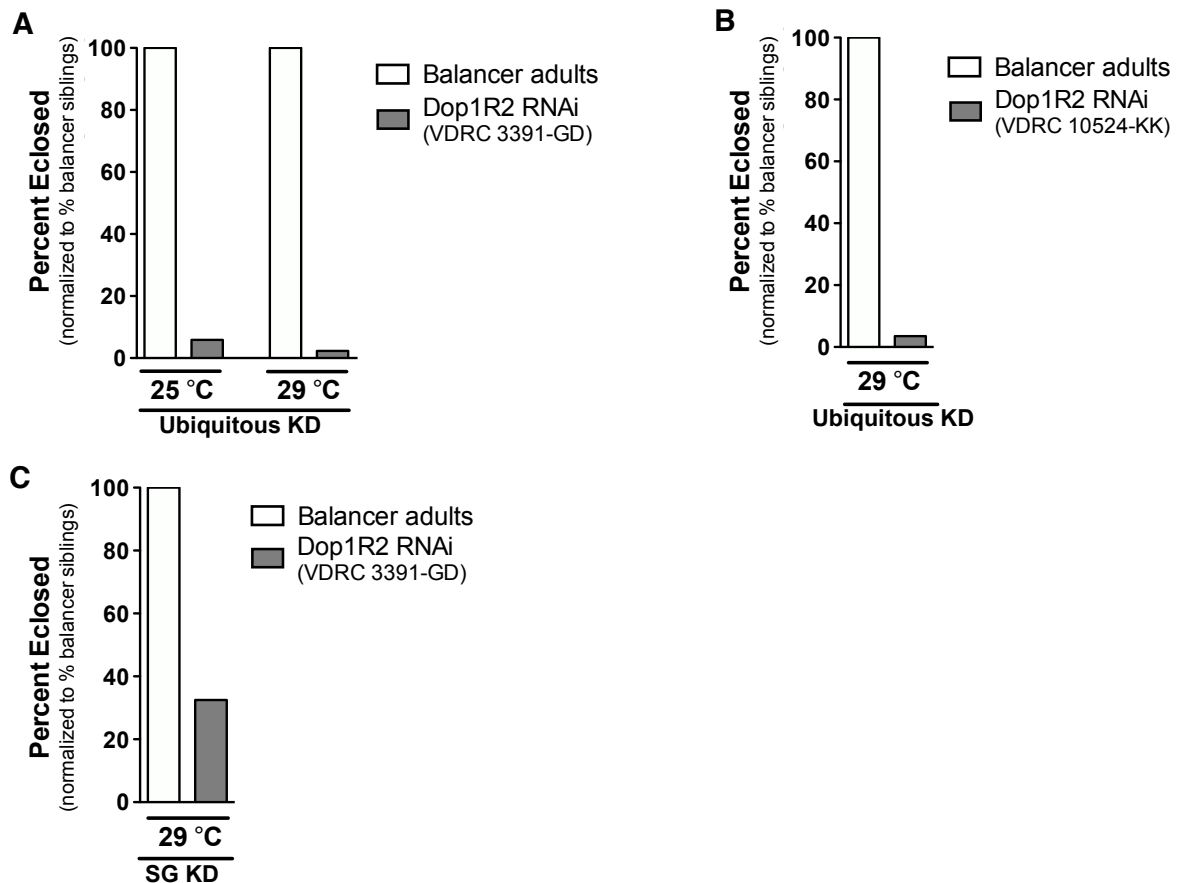


**Figure 2.6. Down-regulation of Dop1R2 around larval-to-pupal ecdysis leads to developmental arrest.** (A) Schematic of the temperature shift assay of the developing progeny. (B) Analysis of progeny that was switched from 29°C to 25°C. (C) Analysis of progeny that was switched from 25°C to 29°C. Percent of Dop1R2 RNAi (line 1 or line 2) (genotype:  $w^{1118};UAS-dsDop1R2/+;Act5C-GAL4/+$ ) that emerge vs. controls (genotype:  $w^{1118};UAS-dsDop1R2/+;TM6B/+$ ). Dop1R2 RNAi flies reared at 29°C throughout development fail to emerge as adults, while of those reared at 25°C throughout development show reduced emergence. When flies are transferred between these two temperatures at different stages of development, the time course of lethality is revealed. Growth at 25°C  $n = 1194$  (line 1),  $n = 1107$  (line 2), and growth at 29°C  $n = 1969$  (line 1),  $n = 2212$  (line 2).

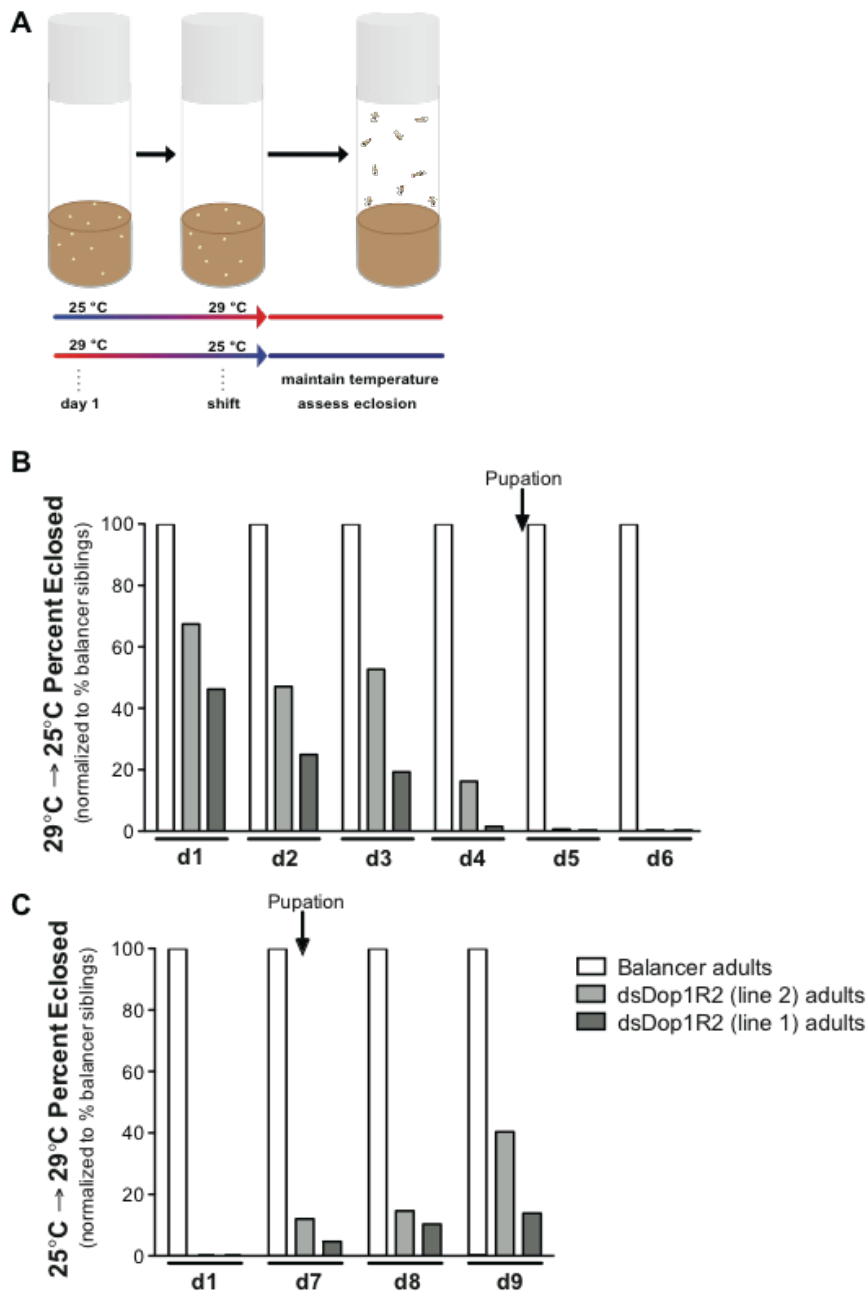




**Figure 2.7. Transcriptome analysis of Dop1R2 RNAi arrested flies reveals up-regulation of families of related genes.** Results indicate an increase in the expression of 101 genes that were significantly up-regulated by  $\geq 1.6$  times in Dop1R2 RNAi flies (genotype:  $w^{1118};UAS-dsDop1R2/+;Act5C-GAL4/+$ ), compared to control flies (genotype:  $w^{1118};UAS-dsDop1R2/+;TM6B/+$ ). The fold increase change in transcript level is indicated in parentheses. Statistical significance was determined using a t-test on the average of two independent biological replicates, with a cutoff of  $p < 0.05$ . Families were assigned by DAVID functional assignment and by manual annotation using FlyBase. Driver stock: Act5C-GAL4 (FBst0003954).

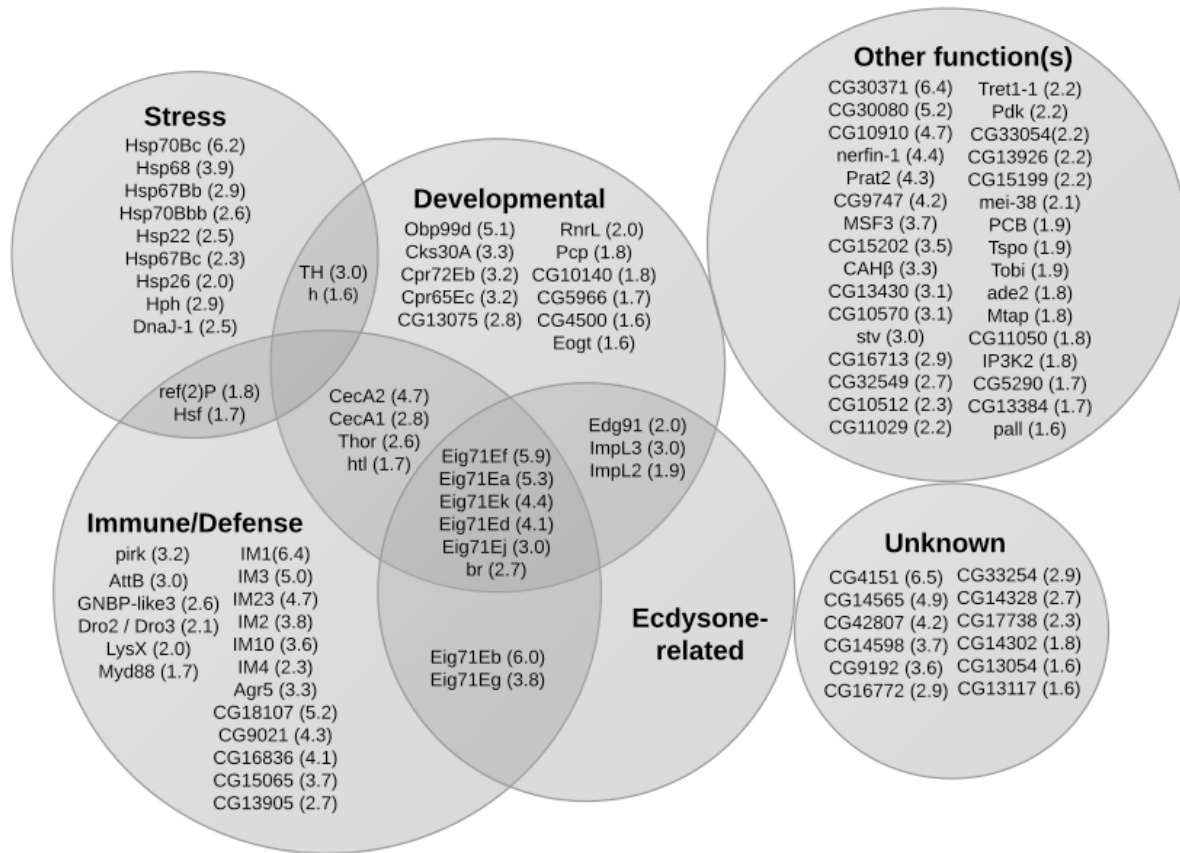


**Figure 2.8. WEB-based Gene SeT AnaLysis (WEBGestalt).** Analysis of dsDop1R2 differentially expressed genes reveals enrichment in GO categories categorized by biological process, molecular function and cellular component. The top 10 GO categories that have a Benjamini corrected p-value of < 0.05 (red) and p-value > 0.05 (brown), as well as the non-enriched parents (black), are depicted. Each node provides: GO category, gene number in category and the adjusted p-value indicating the significance of enrichment.

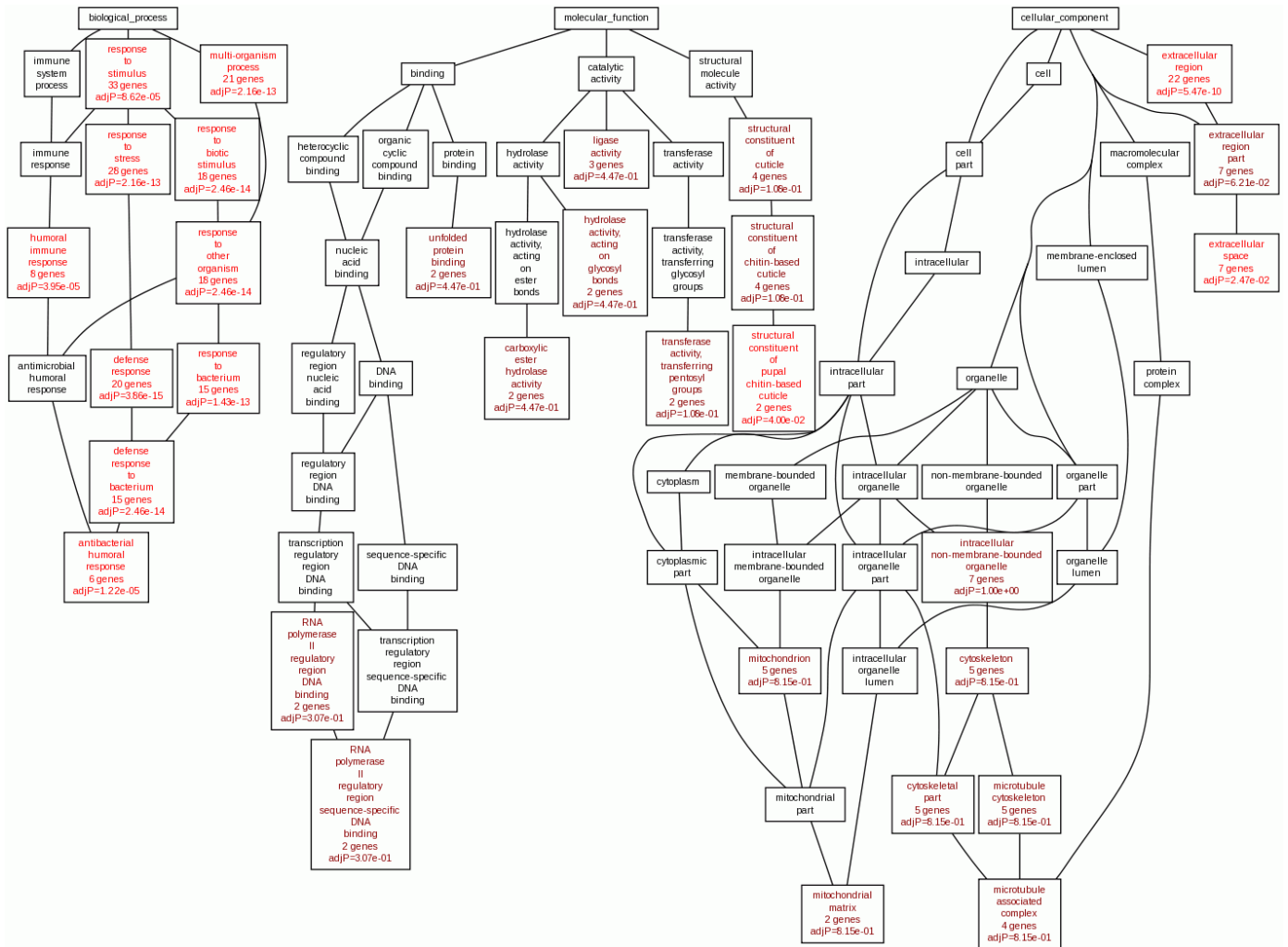




**Figure 2.10. RT-PCR analysis confirm differential expression of genes in Dop1R2 RNAi flies.** (A) Transcript levels assessed by RT-PCR. RNA obtained from Dop1R2 RNAi (genotype:  $w^{1118};UAS-dsDop1R2/+;Act5C-GAL4/+$ ) and control pupae (genotype:  $w^{1118};UAS-dsDop1R2/+;TM6B/+$ ) was reverse transcribed, and PCR was performed in triplicate using primer sets corresponding to gene of interest or to Act5C (as a normalization control). (B) Quantification of transcript levels. The average band intensity of Dop1R2 RNAi PCR products was normalized to control PCR products for Act5C. Error bars indicate SEM, and significance was determined by comparing the difference in intensities of the RNAi PCR bands versus the control PCR bands using an unpaired t-test. \*  $p < 0.05$ , \*\*  $p \leq 0.01$ , \*\*\*  $p \leq 0.001$ . Driver stock: Act5C-GAL4 (FBst0003954).

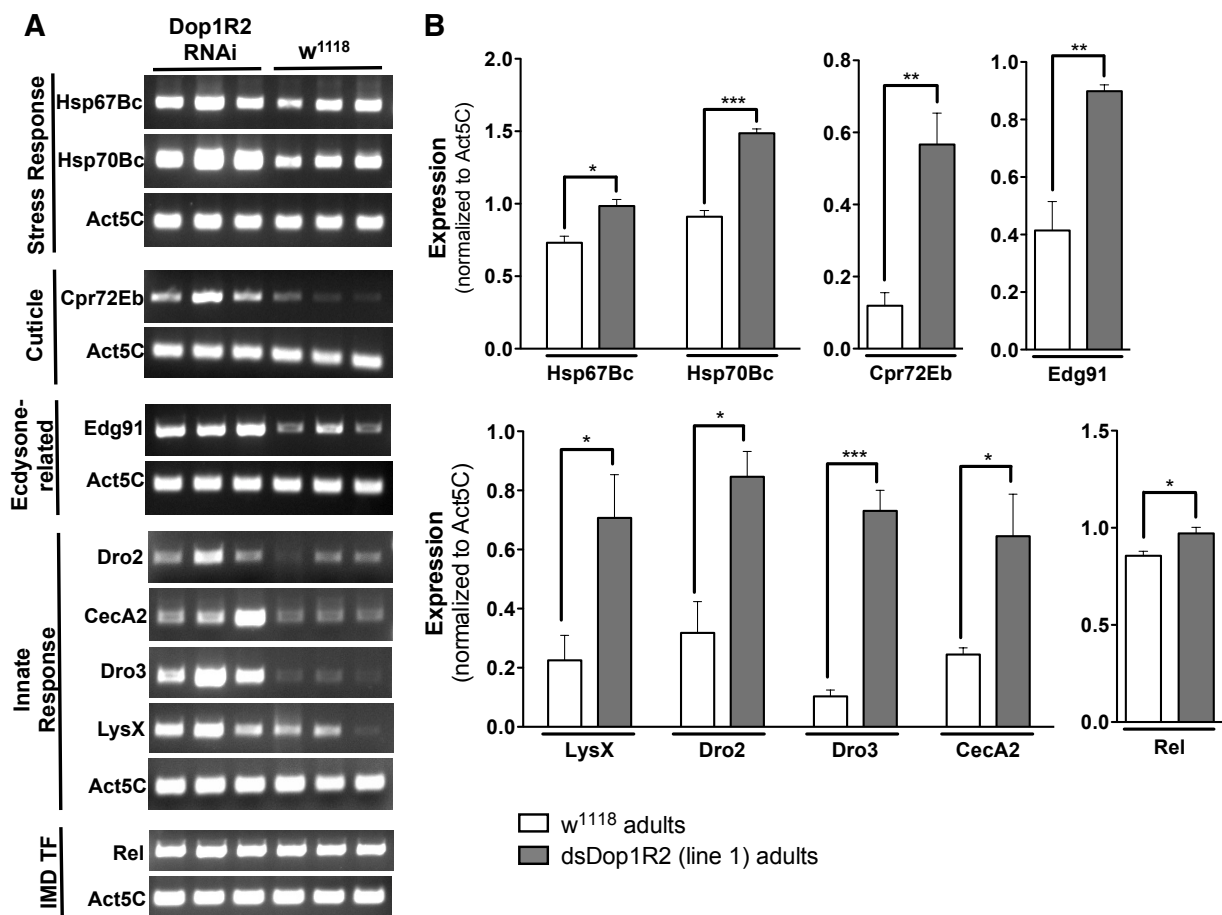


**Figure 2.11. Tyrosine hydroxylase expression is increased in dsDop1R2 pupae.** Dop1R2 knockdown pupae with the genotype  $w^{1118};UAS-dsDop1R2/+;Act5C-GAL4/+$  exhibit increased TH transcript levels compared to controls (genotype:  $w^{1118};UAS-dsDop1R2/+;TM6B/+$ ). Four-fold difference (i.e., two cycles of amplification) in TH expression is observed in Dop1R2 RNAi vs. controls using two independent biological replicates. Driver stock: Act5C-GAL4 (FBst0003954).

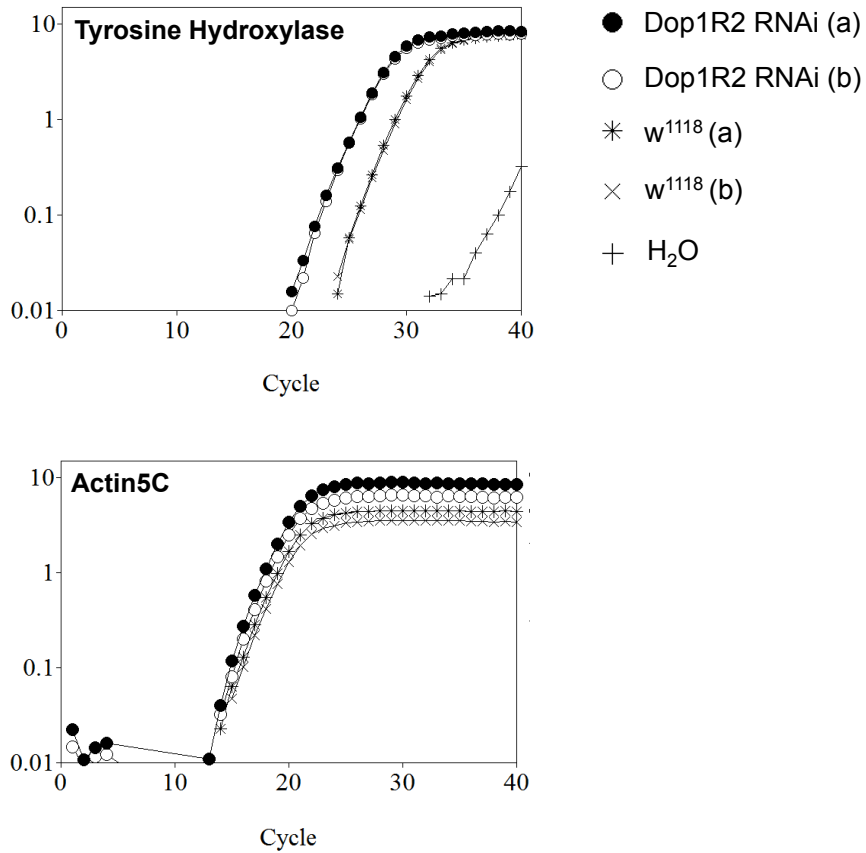


**Figure 2.12. Dop1R2 down-regulation using the P{GawB}332.3 driver leads to developmental arrest at the pharate adult stage.** (A) Expression of Dop1R2 RNAi construct under the control of the P{GawB}332.3 driver (GAL4 expressed in the salivary glands and amnioserosa), induces 99.2% lethality before eclosion. Survival of RNAi flies (genotype:  $w^{1118};UAS-dsDop1R2/P\{GawB\}332.3-GAL4$ ) is expressed as percent control progeny (genotype:  $w^{1118};TM6B/GawB-GAL4$ ).  $n = 147$  (line 1),  $n = 124$  (line 2). (B) Images of pharate adults dissected out of the pupal case suggest a poorly formed abdomen (lines 1 and line 2) or incomplete cuticle formation (line 2). (C) Analysis of progeny that were switched from 25°C to 29°C. Percent of Dop1R2 RNAi (line 1) (genotype:  $w^{1118};UAS-dsDop1R2/P\{GawB\}332.3-GAL4$ ) that emerge vs. controls (genotype:  $w^{1118};TM6B/GawB-GAL4$ ). Dop1R2 RNAi flies reared at 29°C throughout development fail to emerge as adults, while of those reared at 25°C throughout development show reduced emergence. When flies are transferred between these two temperatures at different stages of development, the time course of lethality is revealed.  $n = 543$ . Driver stock: P{GawB}332.3-GAL4 (FBst0005398).

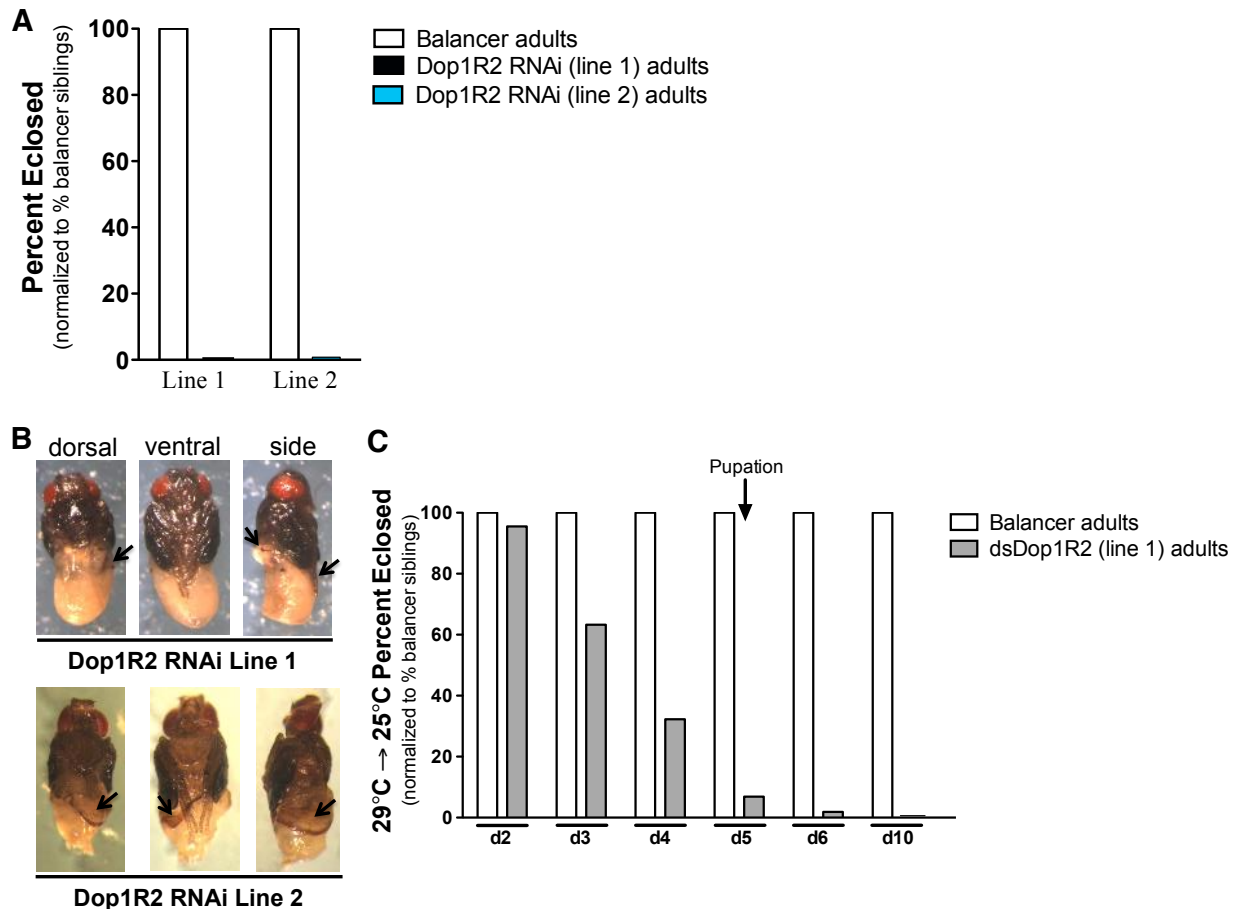


**Figure 2.13. Progression from egg to L1 instar.** Dop1R2 RNAi (line 1) or  $w^{1118}$  flies were crossed with the P{GawB}332.3 driver line [GAL4 expressed in the salivary glands and amnioserosa (Wodarz et al. 1995)] to assess completion of embryogenesis. dsDop1R2 flies (genotype:  $w^{1118}$ ;UAS-dsDop1R2/P{GawB}332.3-GAL4) showed similar progression into L1 compared to controls (genotype:  $w^{1118}$ ;P{GawB}332.3-GAL4/+) (n = 50). Driver stock: P{GawB}332.3-GAL4 (FBst0005398).

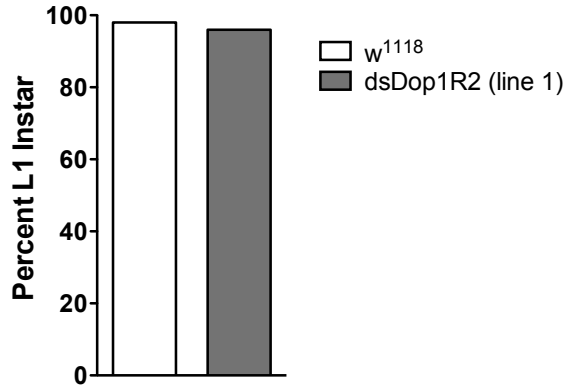


**Figure 2.14. dsDop1R2 knockdown using alternate salivary gland driver results in semi-lethality.** (A) Knockdown of Dop1R2 via TMC line 1 resulted in semi-lethality when driven by an additional larval salivary gland driver line (FBst0008474 which also targets glia and the proventriculus). At 29°C, 48.1% eclosion was observed in knockdown flies (genotype:  $w^{1118};UAS-dsDop1R2/P\{GawB\}17A-GAL4$ ) vs. control siblings (genotype:  $w^{1118};CyO/UAS-dsDop1R2$ ) (n = 397). (B) At 29°C, 27.9% eclosion was observed in knockdown flies (genotype:  $w^{1118};UAS-dsDop1R2/P\{GawB\}c729-GAL4$ ) vs. control siblings (genotype:  $w^{1118};UAS-dsDop1R2$ ) (n = 211). (C) dsDop1R2 escapers (genotype:  $w^{1118};UAS-dsDop1R2/P\{GawB\}17A-GAL4$ ) display cuticle and wing abnormalities (left and center, arrows), or fail to fully eclose from pupal case (right). Driver stocks: P{GawB}17A-GAL4 (FBst0008474) and P{GawB}c729-GAL4 (FBst0006983).

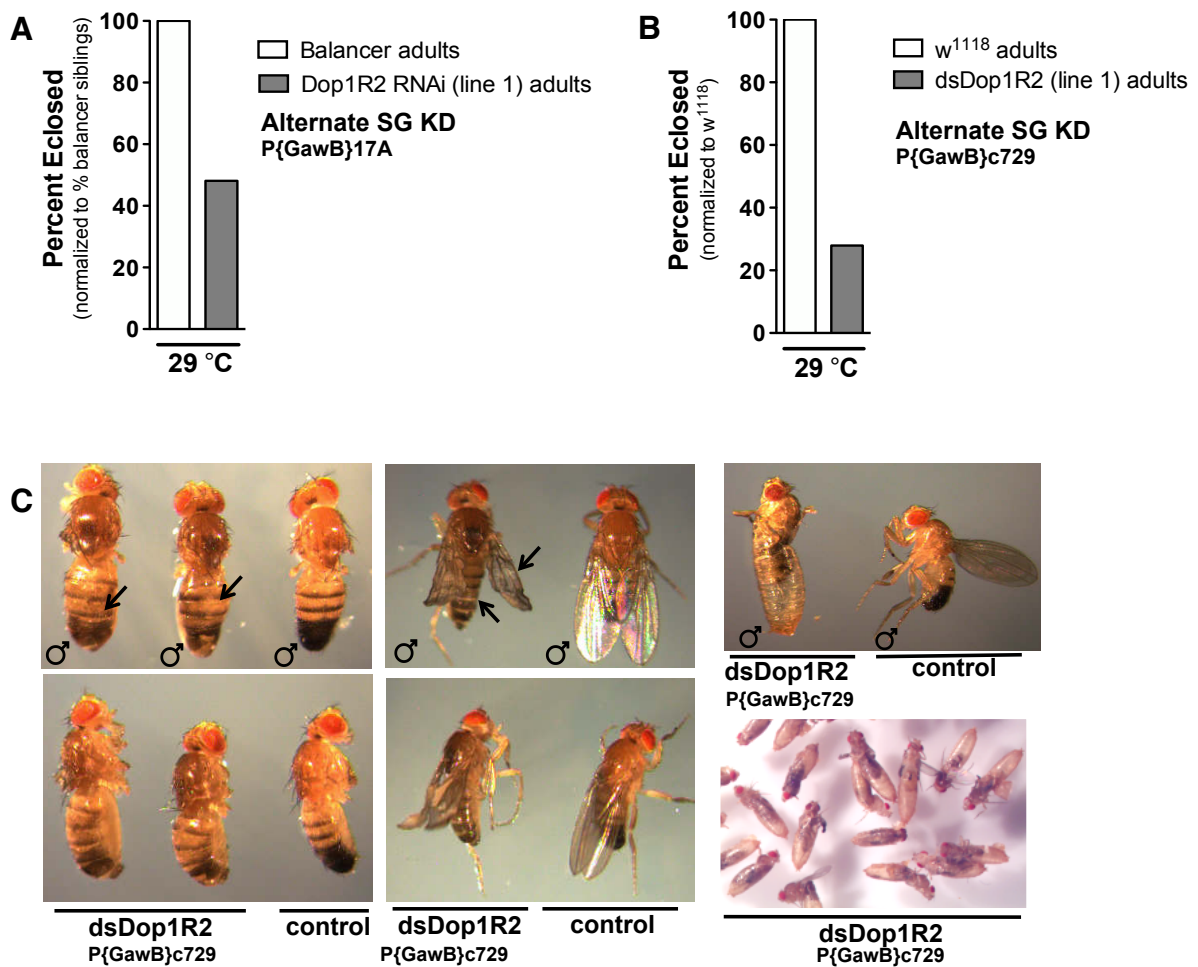




**Figure 2.15. Confirmation of salivary gland expression in tested driver stocks.** To confirm GAL4 expression in salivary glands, UAS-GFP crosses were generated using driver stocks: FBst0005398, FBst0008474, FBst0006983, FBst0006870 or  $w^{1118}$  as a control (genotype, respectively:  $w^{1118};UAS-EGFP/P\{GawB\}332.3-GAL4$ ,  $w^{1118};UAS-EGFP/P\{GawB\}17A-GAL4$ ,  $w^{1118};UAS-EGFP/P\{GawB\}c729-GAL4$  vs. control siblings (genotype:  $w^{1118};UAS-EGFP/+$ ). UAS-GFP responder stock:  $w^*;P\{UAS-2xEGFP\}AH2$  (FBst0006874). All drivers displayed GFP expression in salivary glands with no other overlapping tissue type. All drivers tested resulted in marked GFP expression in salivary glands. No overlapping fluorescence was detected in other tissue/ cell type. Control flies showed dull (background) fluorescence only. All images, magnification: 100X, image exposure: 5 msec.

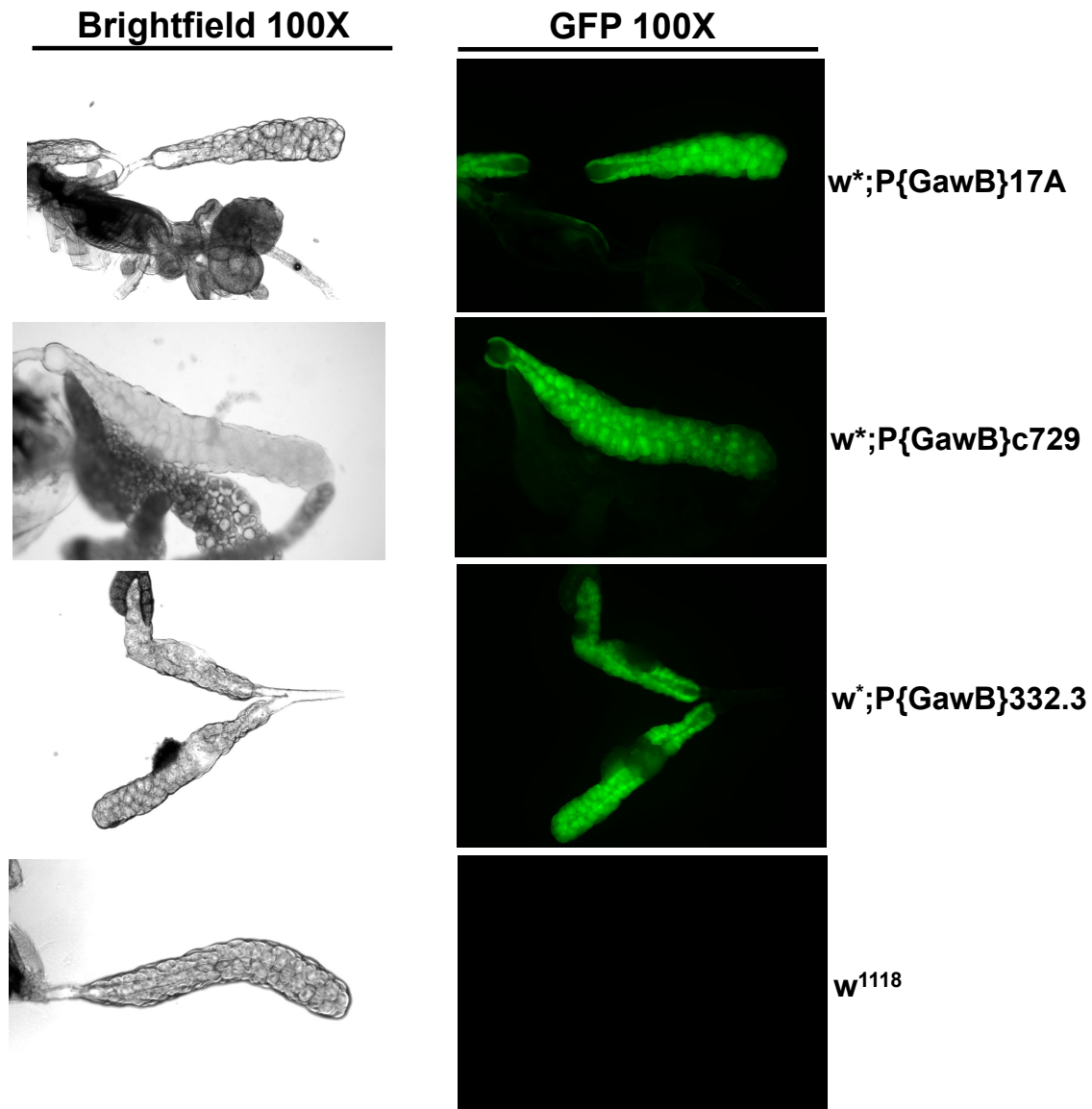


**Figure 2.16.  $G\alpha_s$ -targeted, but not  $G\alpha_i$ -targeted KD in the salivary glands results in pre-adult lethality.** Expression of either of two  $G\alpha_s$  (stimulatory G protein) RNAi constructs (Choi et al. 2012) under the control of P{GawB}332.3 driver induces lethality before eclosion (line 1 genotype:  $w^{1118};P\{GawB\}332.3-GAL4/+;UAS-dsG\alpha_s/+$ , line 2 genotype:  $w^{1118};P\{GawB\}332.3-GAL4/UAS-dsG\alpha_s$ ). Expression of the  $G\alpha_i$  (inhibitory G protein) RNAi construct, using the same driver, does not compromise viability (genotype:  $w^{1118};P\{GawB\}332.3-GAL4/+;UAS-dsG\alpha_i/+$ ). Survival is expressed as percent of balancer progeny. Driver stocks:  $G\alpha_s$  line 1: FBst0455666,  $G\alpha_s$  line 2: FBst0477321,  $G\alpha_i$  line: FBst0457318.  $G\alpha_s$  line 1:  $n = 141$ ,  $G\alpha_s$  line 2:  $n = 100$ ,  $G\alpha_i$ :  $n = 416$ .

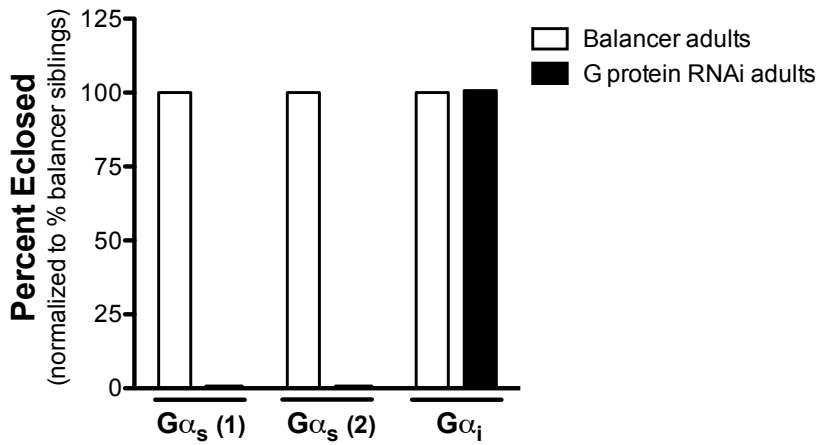


**Figure 2.17. Dop1R2 is expressed in prepupal salivary glands and brain.** (A) RNA obtained from the brain and salivary glands of  $w^{1118}$  prepupae was reverse transcribed, and PCR was performed in triplicate using primer sets corresponding to Dop1R2-RB, Dop1R2-RA/C or Act5C (as a normalization control). Transcript variants A/C and B are detected in the brain, and transcript variant B is detected in the salivary glands (the presence of a low abundance Dop1R2-RA/C transcript in salivary glands cannot be excluded). (B) Quantification of transcript levels (ImageJ software). Expression is quantified as band intensity for three biological replicates of Dop1R2-RB, or Dop1R2-RA/C, normalized to Act5C.

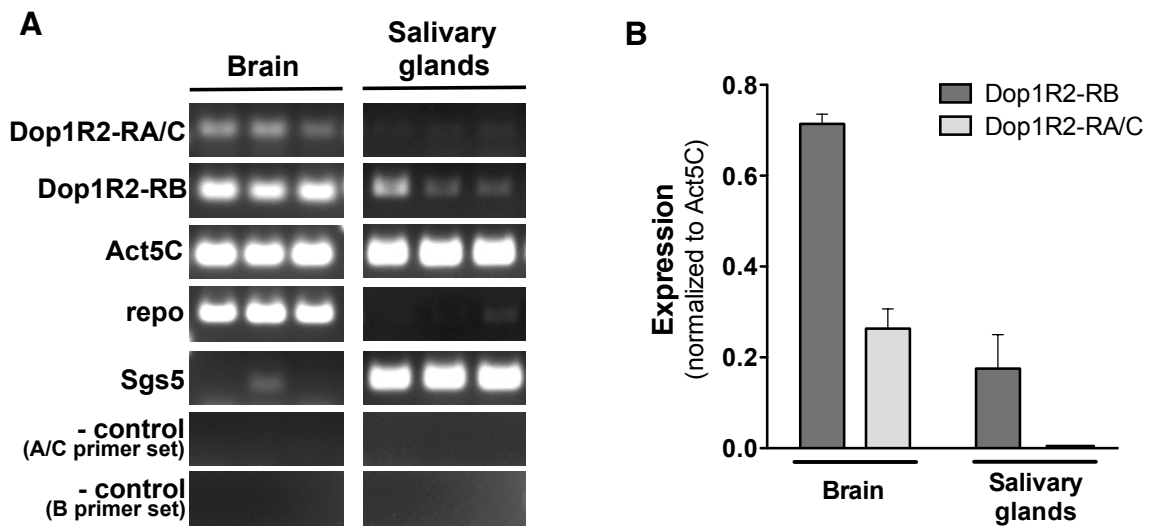


**Figure 2.18. Dop1R2 is stimulated by dopamine and antagonized by two known small molecules *in vitro*.** (A) *Drosophila* Dop1R2 protein displays concentration-dependent activity when stimulated with dopamine ( $EC_{50} = 2.7 \times 10^{-7}$  M). (B) Dop1R2 is antagonized by flupenthixol dihydrochloride ( $IC_{50} = 2.6 \times 10^{-7}$  M) and butaclamol ( $IC_{50} = 21.6 \times 10^{-7}$  M). Data represent the mean  $\pm$  SEM from three independent experiments, each performed in triplicate.

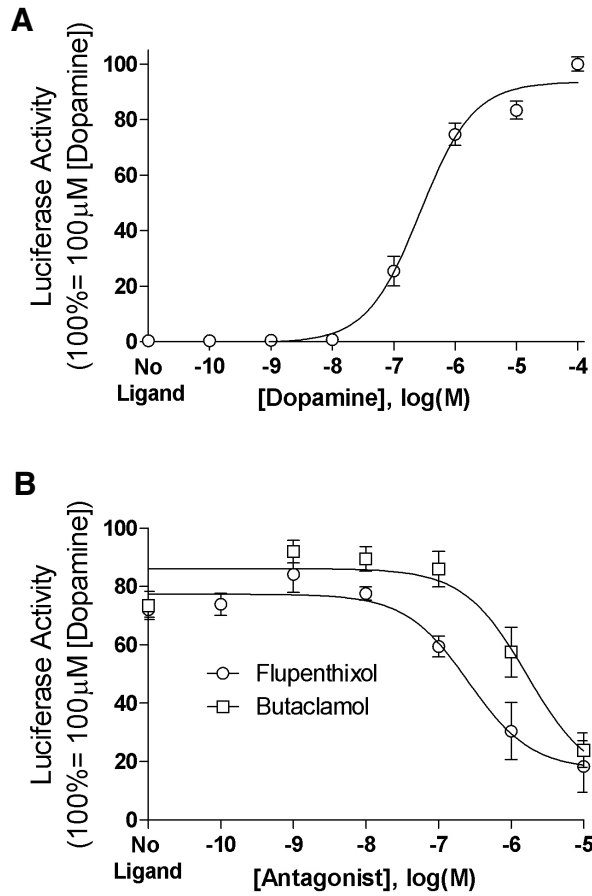


**Figure 2.19. Exposure of *Drosophila melanogaster* (w<sup>1118</sup>) larvae to flupenthixol dihydrochloride results in increased lethality and developmental abnormalities.** (A) Assessment of adult eclosion following larval exposure to flupenthixol dihydrochloride reveals a concentration-dependent effect ( $EC_{50} = 0.8$  mM). (B) Drug exposure results in developmental delay/reduced body size. Image showing representative larval body size at each drug concentration, recorded at day 6 post-treatment onset. (C) Introduction of flupenthixol pre-wandering L3 larval by feeding at 5 mM and 10 mM results in cuticle abnormalities in 13% and 10% of adults, respectively. Images shown of two day old adults (5 days post-exposure onset). n = 30 per concentration, 3 independent replicates.

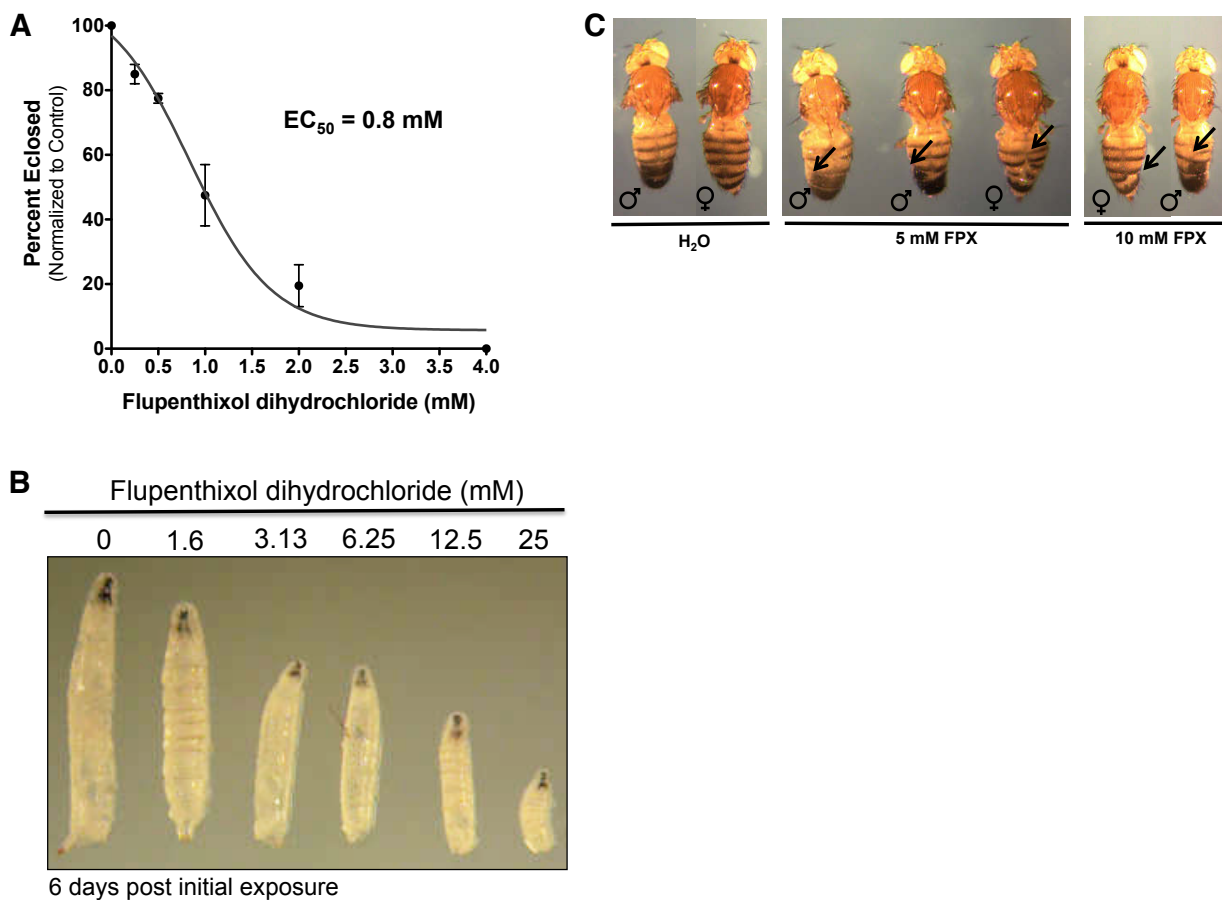


**Figure 2.20. Dop1R2 sequence motif.** (A) Sequence analysis via cNLS mapper ([http://nls-mapper.iab.keio.ac.jp/cgi-bin/NLS\\_Mapper\\_form.cgi](http://nls-mapper.iab.keio.ac.jp/cgi-bin/NLS_Mapper_form.cgi)) reveals the presence of a bipartite nuclear localization signal. (B) GenomeNet motif analysis via (<http://www.genome.jp/tools/motif/>) reveals homology to BAF1/ABF1 chromatin reorganizing factor.

**A** Appearance:

Position	337..380
Alignment	
Query	SGGGGGGGGGGGGSLSHSHSHSHHHHHHGGGTTTSTPEEPD
Database	NEDGSPGGSGDEGGHHGHNMMAHHHHHHNGHTNGHGLAEDD
Score	46.3
E-value	3e-05

Sequence:

MVDDNGSSPEVEGAEGAGAPLLALLRVDGLNQTQTRSPSPSFFGSGYNISEDVYFYFNGLP  
 TSTELVLNATTSATSATLSPAMVATGGGGTTTPEPDLSEFLALPNDRVGLLAFLFSPF  
 ATVFGNSLVILAVIRERYLHTATNYFITSLAVADCLVGLVMPFSALYEVLENTWFFGTD  
 WCDIWRSLDVLFGTASILNLCVISLDRYWAITDPFSYPMRMTVKRAAGLIAAVWICSSAI  
 SFPAIVWWRAARDGEMPAYKCTFTEHLGYLVFSSTISFYLLVMVFTYCRIRAAVIQT  
 RSLKIGTKQVLMASGELQLTLRIHRGGTTRDQQNQVSGGGGGGGGGGGGSLSHSHSHS  
 HHHHHHHHGGGTTTSTPEEPDDEPLSALHNNGLARHRHMGKNFSLSRKLAKFAKEKKA  
 LGIVMGVFIICWLPFFVFNLLSGFCIECIEHEEIVSAIVTWLWINSNMNPVIYACWSRD  
 FRRAFVRLLCMCCPRKIRRYQPTMRSKSQRFATRRCYSTCSLHGIIQVHRHNSCEQTYI

Description:

pfam04684, BAF1\_AB1, BAF1 / ABF1 chromatin reorganizing factor. ABF1 is a sequence-specific DNA binding protein involved in transcription activation, gene silencing and initiation of DNA replication. ABF1 is known to remodel chromatin, and it is proposed that it mediates its effects on transcription and gene expression by modifying local chromatin architecture. These functions require a conserved stretch of 20 amino acids in the C-terminal region of ABF1 (amino acids 639 to 662 *S. cerevisiae*). The N-terminal two thirds of the protein are necessary for DNA binding, and the N-terminus (amino acids 9 to 91 in *S. cerevisiae*) is thought to contain a novel zinc-finger motif which may stabilize the protein structure.

**B**

Predicted NLSs in query sequence	
MVDDNGSSPEVEGAEGAGAPLLALLRVDGLNQTQTRSPSPSFFGSGYNISE	50
DVYFYFNGLPTSTELVLNATTSATSATLSPAMVATGGGGTTTPEPDLSEF	100
LEALPNDRVGLLAFLFSPFATVFGNSLVILAVIRERYLHTATNYFITSL	150
AVADCLVGLVMPFSALYEVLENTWFFGTDWCDIWRSLDVLFGTASILN	200
CVISLDRYWAITDPFSYPMRMTVKRAAGLIAAVWICSSAISFP AIVWRA	250
ARDGEMPAYKCTFTEHLGYLVFSSTISFYLLVMVFTYCRIRAAVIQT	300
RSLKIGTKQVLMASGELQLTLRIHRGGTTRDQQNQVSGGGGGGGGGGG	350
GSLSHSHSHSHHHHHHGGGTTTSTPEEPDDEPLSALHNNGLARHRHMGK	400
NFSLSRKLAKFAKEKKA	450
HEEIVSAIVTWLWINSNMNPVIYACWSRDFRRAFVRLLCMCCPRKIRRK	500
YQPTMRSKSQRFATRRCYSTCSLHGIIQVHRHNSCEQTYI	539

Predicted bipartite NLS		
Pos.	Sequence	Score
391	GLARHRHMGKNFSLSRKLAKFAKEKKA	6.4

**Table 2.1. Effect of tissue-specific down-regulation of Dop1R2.** A series of GAL4 drivers was used to down-regulate Dop1R2 expression in specific tissue/cell types. The lethality observed when down-regulating expression ubiquitously was recapitulated only when using the P{GawB}332.2 driver, which expresses GAL4 in the salivary glands and amnioserosa. Semi-lethality was observed when using the P{GawB}17A and P{GawB}c729 drivers. All of the above mentioned drivers resulted in abnormal melanization and cuticle phenotypes.

GAL4 driver Symbol	Expression	Phenotype
P{Act5C-GAL4}17bFO1 <sup>1,2,3</sup>	ubiquitous	Lethal, melanization and wing defect (in escapers)
P{Act5C-GAL4}25FO1 <sup>1,2,3,4</sup>	ubiquitous	Lethal, melanization and wing defect (in escapers)
P{GawB}332.3 <sup>1,2,3</sup>	salivary glands, amnioserosa	Lethal, melanization and wing defect (in escapers)
P{GawB}17A <sup>1</sup>	salivary glands, glia, cardia	Semi-lethal
P{GawB}c729 <sup>1</sup>	salivary glands, female follicle cells, male accessory glands, testis sheath, cyst cells	Semi-lethal, melanization and wing defect (in escapers)
P{GawB}elav[C155] <sup>1</sup>	pan-neuronal	WT
P{GawB}Tab2[201Y] <sup>1</sup>	primarily in mushroom bodies	WT
P{GawB}c698a <sup>1</sup>	3IL CNS, not in discs	WT
P{Eip71CD-GAL4.657}TP1-1 <sup>1</sup>	3IL brain and epidermis	WT
Bursicon- $\alpha$ - GAL4 <sup>1,3</sup>	bursicon- $\alpha$ positive cells	WT
P{Ccap-GAL4.P}16 <sup>1,3</sup>	crustacean cardioactive peptide-secreting cells	WT
P{GawB}30A <sup>1</sup>	imaginal discs	WT
P{GawB}l(2)T32T32 <sup>1</sup>	amnioserosa, larval brain, wing discs	WT
P{GawB}c381 <sup>1</sup>	amnioserosa, embryonic PNS - stage 14	WT
P{Sgs3-GAL4.PD}TP1 <sup>1</sup>	salivary glands	WT
P{Lsp2-GAL4.H}3 <sup>1</sup>	3IL fat body	WT
P{drm-GAL4.7.1}1.1 <sup>1</sup>	gastrointestinal tract, malpighian tubules	WT

- All phenotypes were assessed on progeny that developed at 29°C
- <sup>1</sup> in combination with lab generated UAS-dsDop1R2 line 1
- <sup>2</sup> in combination with lab generated UAS-dsDop1R2 line 2
- <sup>3</sup> in combination with UAS-dsDop1R2 VDRC stock FBst0460369
- <sup>4</sup> in combination with UAS-dsDop1R2 VDRC stock FBst0477151
- WT: wild-type phenotype
- 3IL: third instar larva

**Table 2.2.  $G\alpha_s$ , but not  $G\alpha_i$ , knockdown targeted to salivary glands/amnioserosa leads to developmental arrest.**

UAS line	Description	Phenotype
UAS-ds $G\alpha_s$ (FBst0455666)	$G\alpha_s$ RNAi	Lethal
UAS-ds $G\alpha_s$ (FBst0477312)	$G\alpha_s$ RNAi	Lethal
UAS-ds $G\alpha_i$ (FBst0457318)	$G\alpha_i$ RNAi	WT

- Phenotype assessed on progeny from parental Gal4 driver line P{GawB}332.3 (FBst0005398, salivary glands/amnioserosa, see Table 2.1) and parental UAS line, as indicated
- All phenotypes were assessed on progeny that developed at 29 °C
- WT: wild-type phenotype
- ds: double-stranded



**Table 2.3. Primer sequences.**

<b>Gene</b>	<b>Forward Sequence (5' → 3')</b>	<b>Reverse Sequence (5' → 3')</b>
Dop1R2-RA/C	CAAATCGCAGTGTCACGTGG	GTGCTGCAACTGCTCAGCT
Dop1R2-RB	CCTGCGAGCAGACCTACATA	CGTGACACTTGCCATTGACT
Dop1R2 (in/in)	CACCTGGCTCGGCTGGATCAACT	CGACTTGGAACGCATCGTG
Dop1R2 (in/out)	CACGGATCCCTTTAGCTATC	CACCTGCTTGGTTCCAATCT
Act5C (set 1)	CAGCCAGCAGTCGTCTAATCC	CGACAACCAGAGCAGCAACTT
Act5C (set 2)	AACGGCTCTGGCATGTGC	ACTGGGTCATCTTCTCACGGT
repo	GTTCCCTCCACGGTGGTTAAT	AGTAAAGGTTCTCGTCTTC
sgs5	GATTGCCACAGAGAGATTCTACAG	CTGAATCCACCTCACTTAGAA
TH (set 1)	AGTTGCAGGAGATGTCCGAC	CTTGCAGAGACCGAACTCAA
TH (set 2)	AGTTGCAGGAGATGTCCGAC	AAGCTCTCGGCCACATAGTA
Dop2R (set 1)	CGAGCTGAGAGTGGTGGAC	GCTTGGCGTACTTTATTGGC
Dop2R (set 2)	GCCATGAAGCCATTGTCTT	GTCGACGTTGTAGTACCTG
Oct-TyrR	TTGCATACAGGTCTGCGTGA	ATGTAGCCCAGCCAGGTGA
Oamb	AACATCAAGGCGCAGGTGAA	TTCAAGGAGACGGACTGGC
5-HT1A	CAGAGCCACGTAGCCGACA	CGGAATCGCTGATCTGGCA
Dop1R1	GCACCGGATTCTCCACGAAT	CCGGTTCCTCACCAACTATT
CecA2	ACCACCATGAACTTCTACAACA	GGTTAACCTCGAGCAGTGG
Hsp67Bc	GGTCGTCGGTTCAACGAAC	GACGGTCAGTTCACCTGGC
Hsp70Bc	GTGAACACGTCGCTAAGCG	CCCTGGTCATTGGCGATAATCT
Edg91	GAGTTGTATGCTGGCCCTT	GAGTAACCTCCTCCTGGATAGT
LysX	GGTGTTCCTCGTGACCAGTT	CTGTTGACCCAGGACCTTTAG
Dro2	TTTCGTCTTCCTGGCTGTG	AGTATGGATTGAGCATCCTTCG
Dro3	CTATCTGGAACCTTCGGAGGTC	CCTGAAAGGCAATGCTTACG
Cpr72Eb	GTTACCCACACTAGCAGCG	GGGCAGATTGGAGGTTACATGG
Rel	GAAGTTCGGCTTTCGGTACAA	GCCGCACCTGGTTCAAG

**Dataset 2.1 – Summary of microarray data.** Spreadsheet available online in supplemental material at ProQuest.

**Dataset 2.2 – DAVID bioinformatic analysis of dsDop1R2 differentially expressed genes.** DAVID GO clustering functional analysis reveals statistically significant (yellow) genes (with Benjamin corrected p-value of  $< 0.05$ ) for biological process, cellular component, molecular function, pathway, and rank order of previously published studies that most correlate with the set of differentially expressed genes with fold-increase of  $\geq 1.6$ . Spreadsheet available online in supplemental material at ProQuest.

## **CHAPTER III**

**RNAi trigger delivery into *Anopheles gambiae* pupae**

## A. ABSTRACT

RNA interference (RNAi), a naturally occurring phenomenon in eukaryotic organisms, is an extremely valuable tool that can be utilized in the laboratory for functional genomic studies. The ability to knockdown individual genes selectively via this reverse genetic technique has allowed many researchers to rapidly uncover the biological roles of numerous genes within many organisms, by evaluation of loss-of-function phenotypes. In the major human malaria vector *Anopheles gambiae*, the predominant method used to reduce the function of targeted genes involves injection of double-stranded (dsRNA) into the hemolymph of the adult mosquito. While this method has been successful, gene knockdown in adults excludes the functional assessment of genes that are expressed and potentially play roles during pre-adult stages, as well as genes that are expressed in limited numbers of cells in adult mosquitoes. We describe a method for the injection of *Serine Protease Inhibitor 2 (SRPN2)* dsRNA during the early pupal stage and validate SRPN2 protein knockdown by observing decreased target protein levels and the formation of melanotic pseudo-tumors in *SRPN2* knockdown adult mosquitoes. This evident phenotype has been described previously for adult stage knockdown of *SRPN2* function, and we have recapitulated this adult phenotype by *SRPN2* knockdown initiated during pupal development. When used in conjunction with a dye-labeled dsRNA solution, this technique enables easy visualization by simple light microscopy of injection quality and distribution of dsRNA into the hemolymph.

## B. INTRODUCTION

Malaria is a mosquito-borne infectious disease that affects many millions of individuals every year. The World Health Organization (WHO) reports that in 2013 there were approximately 584,000 deaths due to malaria, 78 percent of which occurred in children under the age of five years (World Health Organization 2014). The pathogens that cause human malaria are apicomplexan parasites within the genus *Plasmodium* and are transmitted between their human hosts by female *Anopheles* mosquitoes. Transmission occurs when the mosquito takes a blood meal from an individual who is infected, and then deposits infective parasites into an uninfected individual in a subsequent blood meal. Within the genus *Anopheles*, *Anopheles gambiae* is the species with the greatest vectorial capacity and is the most prominent malaria vector in sub-Saharan Africa (World Health Organization 2014; Kelly-Hope & McKenzie 2009; The malERA Consultative Group on Vector Control 2011).

Currently, mosquito vector control by deployment of insecticides continues to be the major method employed to reduce the burden of human malaria. Although the use of insecticides since the 1960s has proven to be extremely successful, the rise of insecticide resistance has driven a need for development of novel insecticides and alternative vector control strategies (Enayati & Hemingway 2010; Edi et al. 2014; S. N. Mitchell et al. 2014; Knox et al. 2014). During 2010, a total of 49 of 63 countries reporting to the WHO indicated the occurrence of insecticide resistance in malaria vectors (World Health Organization 2014). Additionally, the IR Mapper tool, which utilizes peer-reviewed literature to assess resistance data in Afrotropical regions, reports that between 2001 and

2012 there were 46% and 27% increases in resistance to pyrethroids and dichlorodiphenyltrichloroethane (DDT), DDT, respectively (Knox et al. 2014).

RNA interference (RNAi) was identified in the early 1990s as a technique that could be employed to inactivate genes in the *Petunia* plant (Napoli et al. 2002; Sen & Blau 2006) and in the fungus *Neurospora crassa* (Sen & Blau 2006; Romano & Macino 1992). Shortly thereafter, in 1998, RNAi was first documented in *Caenorhabditis elegans* (Sen & Blau 2006; Fire et al. 1998) as a means of reducing gene expression in an animal model by introduction of antisense or double-strand RNA (dsRNA) via injection or feeding methods (Sen & Blau 2006; Fire et al. 1998). Since its discovery, RNAi has revolutionized the pursuit of functional genomics by allowing researchers to utilize reverse genetics to rapidly investigate the functional roles of genes of interest via a highly selective post-transcriptional gene silencing mechanism. In some organisms, such as *Drosophila melanogaster*, the use of transgenic organisms that express interfering RNA constructs has been widely successful for gene knockdown (KD). Although the use of transgenes in *An. gambiae* for RNAi has been utilized and may prove useful for large-scale screens, the generation of transgenic mosquito strains is both labor intensive and time intensive, generally taking two to three months to go from the identification of a gene of interest to the generation of an appropriate transgenic stock (Catteruccia & Levashina 2009). Currently, the primary method of gene KD in *An. gambiae* is by injection into the hemolymph, during the adult stage, of dsRNA specific for a given gene (Catteruccia & Levashina 2009; Garver & Dimopoulos 2007). This process typically takes about one month to go from identification of a gene of interest to assessment of gene KD, proving to be much more rapid than transgenic methods (Catteruccia &

Levashina 2009). A method for larval-stage RNAi has been established recently in *An. gambiae* and *Aedes aegypti* via nanoparticle feeding (Mysore et al. 2013; Mysore et al. 2014; X. Zhang et al. 2010; X. Zhang et al. 2015), offering opportunities to perform functional genomic analysis during early stages of development. In direct injection and nanoparticle delivery methods, dsRNA is taken up autonomously by the target cell and cleaved by the enzyme Dicer into ~21-25 nucleotide-long “short interfering RNAs” (siRNAs) (Huvenne & Smaghe 2010; Burand & W. B. Hunter 2013). These siRNAs are then incorporated into the RNA-induced silencing complex (RISC), from which one strand will be discarded, allowing the RNA-bound RISC complex to bind to and cleave the target mRNA and thereby reduce its level and inhibit its translation (Huvenne & Smaghe 2010; Burand & W. B. Hunter 2013).

Many intrinsic features of basic mosquito biology modulate vectorial capacity, including host preference (e.g., olfaction, gustation), mating, reproduction and immunity. Given the importance of these biological processes, it is likely that their modulation on a genetic or pharmacological level will offer new opportunities for vector control, including circumvention of insecticide resistance, and provide additional tools for more broadly integrated approaches to vector management. The use of functional genomics to assess the roles of genes underlying these intrinsic biological features will enable identification of novel targets and provide new insights into how we can effectively create new, more effective control strategies. We describe the development and use of a rapid method to induce RNAi during the pupal and adults stages of *An. gambiae*, based on pupal injection of an RNAi trigger that enables observation of resultant phenotypes in adults. This methods enables gene knockdown beginning during the pupal

developmental interval and extending into adult stages, such that gene knockdown initiated during pupal development can persist and affect adult hemolymph-accessible cell types, as well as cell types that are more hemolymph-accessible during metamorphosis than in the adult, such as sensory neurons found in adult appendages following emergence.

### **C. RESULTS**

Pupal injection for gene KD yields optimal results when injection is performed during the early pupal stage, when cuticle tanning levels are low (Figure 3.1A, left and 1B). Increased tanning and hardening of cuticle, generally after 24 hours, results in increased pupal death following injection (Figure 3.1A, center and right). The rate of pupal development can vary depending on insectary conditions and animal density (Lyimo et al. 1992; Benedict 2014); therefore, it is best to assess pigmentation visually.

During the injection process, the capillary needle is inserted into the dorsal cuticle at an angle of approximately 30° in the anterior to posterior direction (Figure 3.2A). Once the needle is inserted and the dsRNA + 0.01% (w/v) FGD is dispensed, the distribution of dye is evident throughout the hemolymph (Figure 3.2B).

Assessment of adult emergence for pupae injected with 0.01% (w/v) FGD revealed an average rate of 70% emergence, compared to 96.7% emergence of non-injected controls (Figure 3A). Of note, partial emergence from the pupal case was observed for a large number of non-surviving mosquitoes (Figure 3.3B). Injected animals exhibit no delays in emergence time (Figure 3.4A) or biased impact on either



gender (Figure 3.4B). Additional assessment of adult survival carried out up to day 10 post-emergence reveals no evident impact on post-emergence adult survival (Figure 3.4C).

Validation of KD quality was assessed by the melanotic pseudo-tumor phenotype associated with *SRPN2* knockdown (Michel et al. 2005; An et al. 2011) as a positive control for knockdown and the absence of phenotypes associated with *dsLacZ* injection as a negative control. Adult mosquitoes that emerged were assessed at day 8 post-injection. Melanotic pseudo-tumors were observed through the cuticle of 93.5% of the *dsSRPN2* vs. 0% of the *dsLacZ* adult mosquitoes (Figure 3.5A and 3.5B). Clusters of darkly melanized tissue were identified upon dissection of pigmented patches (Figure 3.5C). Pseudo-tumors were also present in a subset of *dsSRPN2* hemolymph and gut tissues (data not shown).

#### **D. DISCUSSION**

Current methods for inducing non-transgenic RNAi in mosquitoes involve direct injection of dsRNA into the adult hemolymph (Catteruccia & Levashina 2009; Garver & Dimopoulos 2007) or larval feeding of RNAi trigger-coated nanoparticles (X. Zhang et al. 2010; X. Zhang et al. 2015; Mysore et al. 2014; Mysore et al. 2013). Targeting the adult mosquito, while extremely valuable, can exclude a large number of genes that function during earlier developmental periods. Knockdown initiated by larval feeding may yield inconsistent phenotypes during the adult stage due, in part, to the potential of

variable protein persistence through the pupal stage. Therefore, introducing an additional method that is aimed specifically at initiating RNAi during pupal development will provide a means to more fully assess gene functions during pre-adult developmental stages, as well as enhanced abilities to assess gene function during adult stages. As with gene knockdown approach based on dsRNA injection or expression, the persistence of gene knockdown cannot be predicted. Therefore, transcript or protein levels should be assessed for gene of interest during developmental periods of interest. Although we observe a continuation of decreased protein levels at day 5 post-injection for *SRPN2* in *SRPN2* dsRNA-injected animals, factors such as protein turnover and half-life can differ for different targets.

We describe a method for the initiation of RNA interference during the pupal stage of *An. gambiae* development. This method relies on the introduction via microinjection of dsRNA directly into the hemolymph of an early pupae and allows for assessment of injection quality by the use of dye-labeled dsRNA. The ability to visualize injection quality constitutes a critical enhancement for ensuring successful knockdown and constitutes an aspect of injection-based gene knockdown that has not been considered in most previously reported dsRNA-based protocols focusing on the adult stage. By targeting the pupa at the onset of this developmental period, genes that might play a role during this critical developmental interval, or during the early stages of adulthood can be evaluated functionally. Additionally, this method may enable dsRNA delivery to cells, and establishment of RNA interference in cells that are accessible during metamorphosis, but less accessible in fully formed adult mosquitoes.

A recent microarray analysis by Harker *et al.* (2012) identified 560 *An. gambiae* transcripts that were up-regulated or down-regulated by at least 4-fold during distinct developmental stages, ranging from the embryo to adult. Of the 560 transcripts identified, a set of 309 was up-regulated during pupal development (Harker *et al.* 2012). These findings suggest that there are many requirements for differential gene expression throughout mosquito development, including those that occur during the pupal stage, an interval during which the organism undergoes metamorphosis. In many insect species, including *An. gambiae*, genes involved in processes such as development (i.e., pupal cuticular and chitin-binding proteins) (Harker *et al.* 2012; Dotson *et al.* 1998; Hopkins *et al.* 1999; Liang *et al.* 2010; Zhou & Riddiford 2002) and immune response (i.e., Toll receptor-like proteins) (Harker *et al.* 2012; Luna *et al.* 2002; Tauszig *et al.* 2000; Tryselius *et al.* 1992) are highly expressed during the pupal stage. Once a fully formed adult has emerged, there is continued gene expression in response to environmental and physiological changes (Goodisman *et al.* 2005). Notably, during early adult development, there is an increase in the expression of developmental genes (i.e., adult cuticular and sarcoplasmic proteins) (Cook & Sinkins 2010), as well as other key genes (i.e., sperm specific protein and cytochrome P450 metabolism enzymes) (Harker *et al.* 2012; Cook & Sinkins 2010).

The positive control used in the development of this protocol, *SRPN2*, is an *An. gambiae* serine protease inhibitor (serpin). *SRPN2* plays an important role in the negative regulation of insect melanization, a broad spectrum innate immune response in insects (Michel *et al.* 2005; An *et al.* 2011). Knockdown of *SRPN2* in adult mosquitoes results in pseudo-tumor formation (Michel *et al.* 2005; An *et al.* 2011), a phenotype that is easily

observed by use of light microscopy. Given that this distinct phenotype can be easily scored in live insects, we used *SRPN2* for initial pupal stage RNAi injections. In addition, *SRPN2* is expressed during all developmental stages (Suwanchaichinda & Kanost 2009), thereby providing a good target for pupal stage RNAi injection and assessment of function in the early adult. We demonstrate that the method we have developed is capable of inducing adult melanotic pseudo-tumor formation as a consequence of dsRNA injections performed during the pupal stage of development. In developing this protocol, we have observed that injection during early pupal development (i.e., the first 24 hours after the larval-pupal molt) is critical for obtaining optimal adult emergence. In the event that poor emergence is obtained post-injection, we recommend staging larvae with greater accuracy so as to obtain pupae with less extensive cuticle hardening and assure early pupal stage injection is achieved.

With the extensive experiences of many laboratories with the performance of adult mosquito injections, previously identified microinjection approaches can be adapted with simple protocol modifications for use in pupal RNAi experiments. Overall, the goal of this method is to provide researchers the ability to expand the timeframe during which reverse genetic analyses can be performed, further enabling research that will support the development of novel vector control strategies. Interestingly, experiments in other species, such as *Rhodnius prolixus* and *Spodoptera frugiperda*, reveal that gene silencing effects tend to be much greater when initiated during pre-adult stages (Griebler et al. 2008; Araujo et al. 2006). During all stages of development, RNAi-mediated gene knockdown is subject to considerations regarding the rapidity and persistence of gene silencing, and the stability of proteins encoded by targeted genes. The ideal RNAi target

genes tend to be those that encode a protein or RNA that has a short half-life and high turnover rate (J. G. Scott et al. 2013; Fire et al. 1998).

While transgenic RNAi strategies can also be employed to address considerations regarding rapidity and persistence of RNAi during pre-adult stages, transgenic techniques have many drawbacks (e.g., time required for the generation of transgenic lines, experimental time-frames for mosquito matings to generate insects with regulated dsRNA expression, and maintenance of transgenic stocks). By contrast, our protocol affords an easier and faster method for initiating gene knockdown during pupal development and in cell types that originate and are accessible during metamorphosis but are less accessible in adults. The use of dye-labeled dsRNA suspensions allows for easy assessment of injection success and dispersal of introduced material within pupae. This method enables initiation of gene knockdown during a previously under-studied developmental period (i.e., pupal development), and our dye labeling method may also prove useful for the development of new larval injection protocols, due to the translucent nature of the cuticle during all larval instars. In summary, this method provides a valuable pupal stage RNAi protocol and expands the functional genomic tools available for use within the vector insect research community.

## **E. METHODS (PROTOCOL)**

### **1. Synthesis and preparation dsRNA.**

1. Identify a 200 – 800 bp knockdown region (to generate the corresponding dsRNA) within the gene of interest that is predicted to have no identifiable off-

target effects (e.g., no sequence homology  $\geq 18$  bp within another gene) and a negative control (e.g., a heterologous sequence that is not present within target insect genome, such as the *Escherichia coli lacZ* gene). A positive control can also be used (e.g., which yields an easily observed phenotype, such as *SRPN2*). A *SRPN2* knockdown region is defined in Michel *et al.* (2005). Note: E-RNAi is an open-source bioinformatic resource that is useful for the identification of such regions and for the process of designing oligonucleotide primers (<http://www.dkfz.de/signaling/e-rnai3/>) (Horn & Boutros 2010).

2. Perform standard PCR amplification (i.e., performed with Taq DNA polymerase using ~30-35 cycles) using a genomic DNA or cDNA template to obtain insert DNA flanked by a T7 promoter sequence (5'–TAATACGACTCACTATAGGG–3') and proceed with dsRNA using a commercial kit, as per manufacturer's instructions. *SRPN2* PCR amplification conditions and primer information are presented in Michel *et al.* (2005).
3. Quantify RNA amplicon yields by ultraviolet absorbance spectroscopy at wavelength of 260 nm and adjust to the desired concentration (e.g., 3  $\mu\text{g}/\mu\text{l}$ ) in RNase-free water.
  - 3.1. For troubleshooting low RNA concentrations, reduce liquid volume by spinning samples down in a vacuum centrifuge at room temperature or by lyophilizing samples and reconstituting in smaller volumes of water. The time required for sample lyophilization will vary depending on initial sample volumes and dsRNA concentrations.

4. Check the quality and length of the dsRNA on a 1% agarose gel prepared with 1X TBE or TAE buffer and stained with ethidium bromide (EtBr), along with the template DNA used for the transcription reaction. The dsRNA will migrate more slowly than template DNA. Quality and length can be assessed by assuring there are no non-specific dsRNA products and by comparing products with a standard DNA marker, respectively. Note: The dsRNA is extremely concentrated and  $\leq 0.5 \mu\text{l}$  of the  $3 \mu\text{g}/\mu\text{l}$  sample is sufficient for visualization.
5. Store dsRNA at  $-20^{\circ}\text{C}$  until needed. Multiple freeze/thaw cycles can cause degradation, so aliquots should be prepared for large volumes of dsRNA.

## **2. Prepare Fast Green FCF dye (FGD) tubes.**

1. Dilute Fast Green FCF dye (Product F7258, Sigma-Aldrich, St. Louis, MO) from stock solution ( $\geq 85\%$  dye content) to 0.1% (v/v) (working solution) in RNase-free water.
2. Pipette  $1 \mu\text{l}$  of dye into the bottom of a 1.5 ml microcentrifuge tube.
3. Place tubes in a  $65^{\circ}\text{C}$  heat block for approximately 3 hours to evaporate liquid, then place tubes at room temperature for at least 30 minutes, to cool before using. This dry solid dye will reconstitute in dsRNA resuspension solution.

## **3. Pull injection needles.**

1. Pull borosilicate glass needles (Product 3-000-203-G/X, Drummond, Broomall, PA) using a heated needle puller (Product: PB-7, Narishige, East Meadow, NY) to a tip diameter of 10-30 microns. Pull settings correspond to: Heater adjustment no. 1 = 100, Heater adjustment no. 2 = 70.

2. To avoid damage to the fine tip of the needle, place all pulled needles in a Petri dish on a strip of molding putty.

#### **4. Prepare injection station.**

1. Collect materials required: glass microcapillary needles pulled to fine tip, Drummond Nanoject II microinjector (Product 3-000-204, Drummond, Broomall, PA), thin filter paper (Product 1001-090, GE Healthcare, Wilmington, MA) and thick filter paper (Product 107-3931, BioRad, Hercules, CA), Petri dishes (Product FB0875713A, Fisher Scientific, Pittsburg, PA), transfer pipettes (Product 1371150, Thermo Scientific, Tewksbury, MA), paint brush and dissecting light microscope.
2. Prepare the microinjector as instructed in the microinjector manual, and set injection volume to desired volume per pulse (e.g., Nanoject II maximum of 69 nl per pulse).
3. On a platform that is easy to maneuver under a microscope (e.g., flat side of a styrofoam tube rack), stack the two filter paper sheets with the thin filter paper on top, and secure with tape around the edges.
4. Resuspend 10  $\mu$ l of each dsRNA solution in separate colored dye tubes, and place on ice.

#### **5. Collect pupae for injection.**

1. Fill a small 60 mm x 15 mm Petri dish with 10 mL of deionized H<sub>2</sub>O, and collect ~50 pale pupae (during the first 24 hours after pupation) from an insectary tray using a disposable plastic transfer pipette.



2. Remove any pupae that have medium to dark cuticle tanning. Note: Once the cuticle begins to tan, it becomes more difficult to penetrate the cuticle, and injection results in much higher lethality.

#### **6. dsRNA injection.**

1. Under the dissecting microscope, break off the distal tip of the injection needle with a pair of fine forceps.
2. Prepare the injection needle by filling with mineral oil (using a syringe with a 3 inch, 30 gauge needle) and expelling the oil with the microinjector.
3. Fill injection needle with maximum amount of dsRNA, and eject one pulse under the microscope to ensure the dispensing of liquid. In the event that no liquid is taken up and/or expelled, check the distal tip of the needle for any blockage and ensure that the needle is firmly secure in the microinjector.
4. Pick 1-3 pupae, and place them onto the filter paper.
5. Using the paintbrush, position the pupae on the filter paper with dorsal side facing upward, and use the paintbrush to push on filter paper and absorb of excess water.
6. Stabilize the pupa with the tip of the paintbrush, and insert the needle into the dorsal cuticle between the thorax and abdomen at an angle of approximately 30° in relation to the dorsal surface of the pupa. Injection should be directed toward the posterior end of the pupa.
7. Inject two pulses (69 nl per pulse) of 3 µg/µl dsRNA solution into the hemolymph, and check for the distribution of color throughout the body. If no color is identified, shift the injection needle position slightly to clear the tip from obstruction and repeat liquid delivery.

8. Use the wetted paintbrush to gently move pupa from the needle into water for culturing. The pupa should stick to the paintbrush upon light contact.

#### **7. Post-injection conditions.**

1. Place Petri dish with injected pupae into a mosquito cage with suitable airflow (e.g., mesh cage or container with mesh lid).
2. Prepare a 10% (w/v) glucose solution, and place a solution-saturated cotton ball on the mosquito cage mesh for adult feeding.

#### **8. Assess knockdown**

1. At desired time-point(s), assess phenotypes in experimental dsRNA-injected animals, compared to controls.
  - 1.1. *dsSRPN2* and *dsLacZ* animals are assessed daily by chilling down adults for ~2-3 minutes at -20 °C, transferring them to a cold plate at 2 °C and identifying any pseudo-tumor formation by utilization of a dissecting microscope with brightfield illumination. After assessment, adults are returned to insectary conditions (27 °C and 80% humidity).
  - 1.2. The experimental and control dsRNAs employed in this protocol are *dsSRPN2* and *dsLacZ*, respectively. There are many options suitable for controls; however, it is suggested that a positive control for which phenotype and/or expression is easily visualized (e.g., by dissecting microscopy) and/or quantified [e.g., quantitative real-time PCR (qRT-PCR), Western blot] should be used when learning this technique. *SRPN2* protein and transcript quantification via Western blot and qRT-PCR, respectively, are described in Michel *et al.* (2005).

## F. FIGURES AND LEGENDS

**Figure 3.1: Developmental staging for pupal dsRNA injection.** Early pupal injection of dsRNA results in optimal survival and progression into adult stage. Low levels of cuticle pigmentation (A, left and B) can be observed within the first 0-24 hours following pupation. Tanning of the pupal cuticle preceding injection (A, center and right) results in moderate to poor survival.

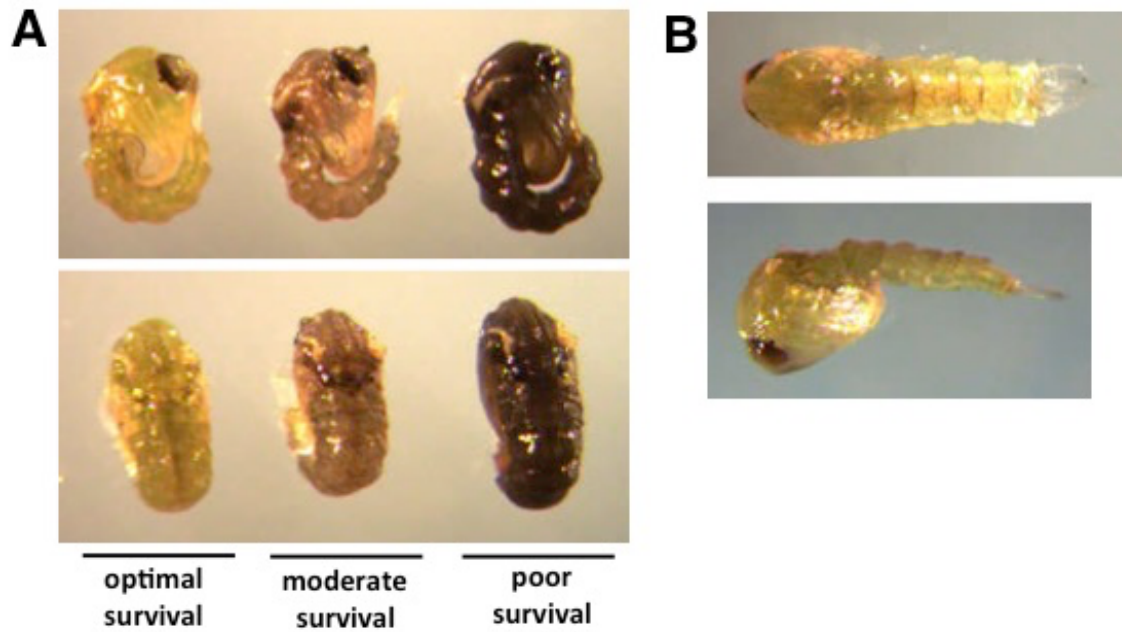


**Figure 3.2: Injection position and distribution of dye-labeled dsRNA.** (A) Capillary needle injection of dye-labeled dsRNA into the dorsal cuticle at an angle of approximately 30°, in anterior to posterior direction. (B) The dye is visibly distributed in the pupal hemolymph. dsRNA injection volume of 138 nl, labeled with 0.01% FGD (w/v).

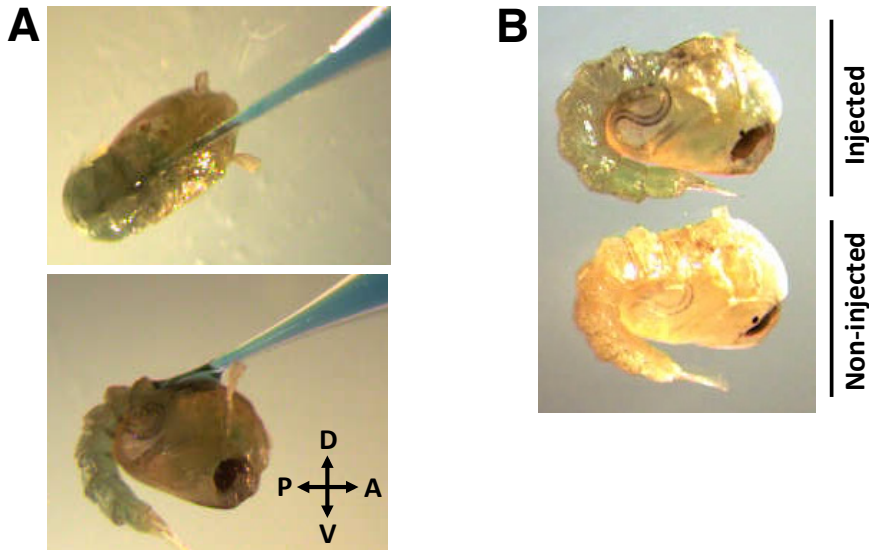


**Figure 3.3: Post-injection adult emergence.** (A) 70% of pupae injected with 0.01% FGD (w/v) successfully emerged (n = 60), compared to 96.7% of non-injected controls (n = 60). Three biological replicates were performed. (B) Partial emergence from the pupal case was observed for a large number of non-surviving mosquitoes.

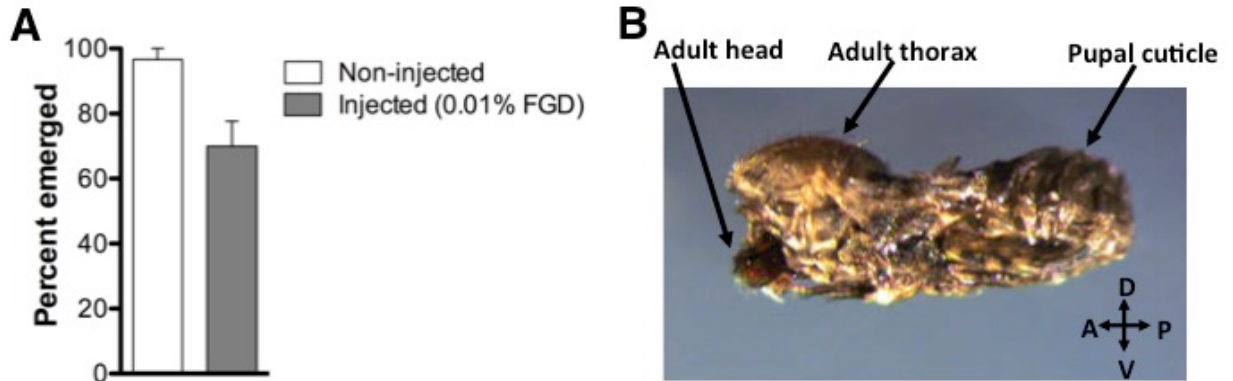


**Figure 3.4: Emergence rate, sex assessment and adult survival.** (A) Comparable emergence times were observed following pupal injection with 0.01% FGD (24hr: 80% and 48hr: 20%), as compared to non-injected pupae (24hr: 83% and 48hr: 17%). (B) Approximately equal male and female adult emergence was observed for 0.01% FGD injected pupae (female: 48% and male: 52%) and non-injected pupae (female: 52% and male: 48%). (C) Survival analysis reveals that injection with 0.01% FGD does not impact adult survival, assessed up to day 10 post-emergence. Results represent data from three independent experiments with 0.01% FGD injected (n = 60) and non-injected (n = 60) pupae (equal numbers of males and females).

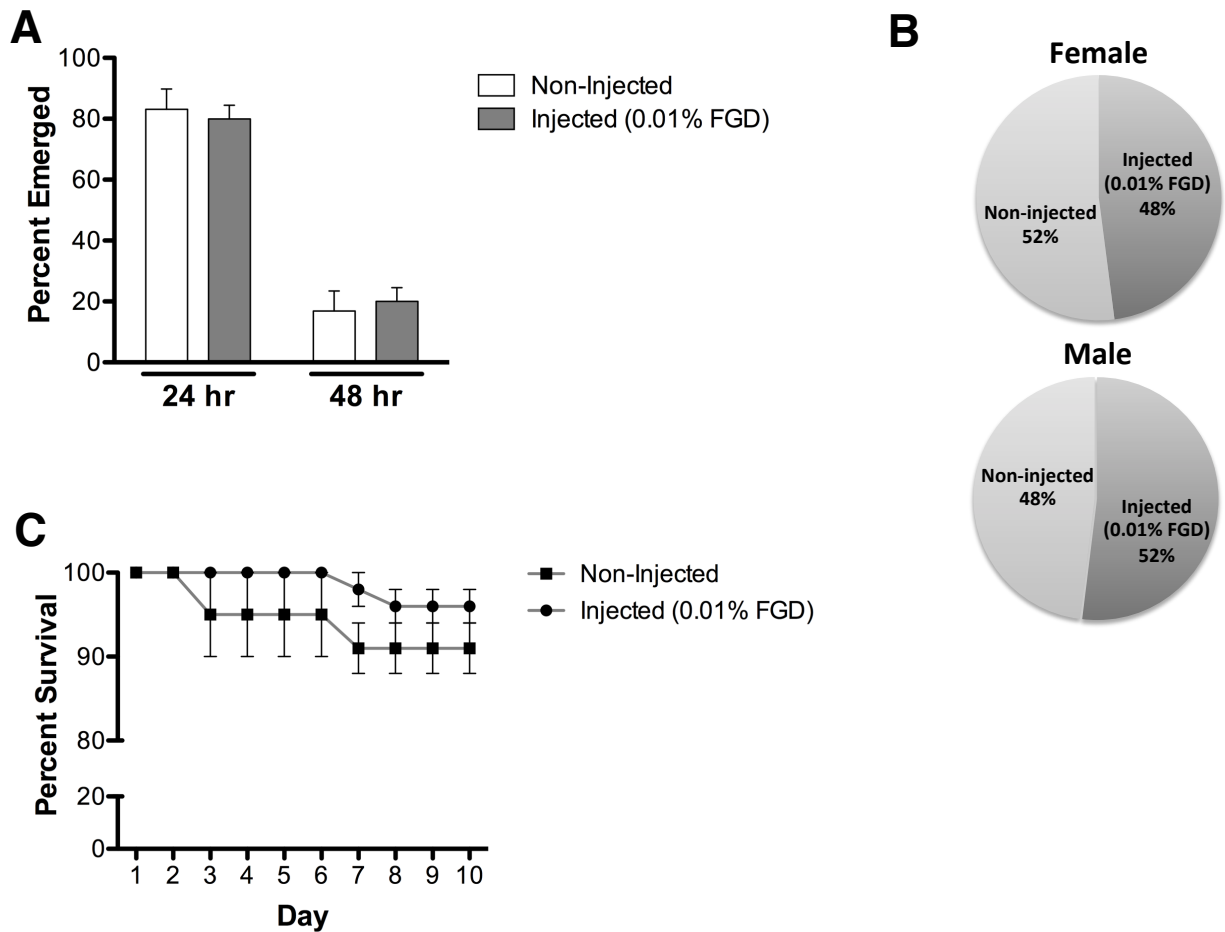


**Figure 3.5: Pseudo-tumor positive control phenotype reflects successful knockdown.** Pseudo-tumors were observed on the (A) abdominal and (B) thoracic cuticle of *dsSRPN2*-injected, but not *dsLacZ*-injected adult mosquitoes at day 8 post-injection. (C) Higher magnification (400X) imaging (a) of cuticle and dissection of pigmented patches (b) reveals clusters of darkly melanized cells.

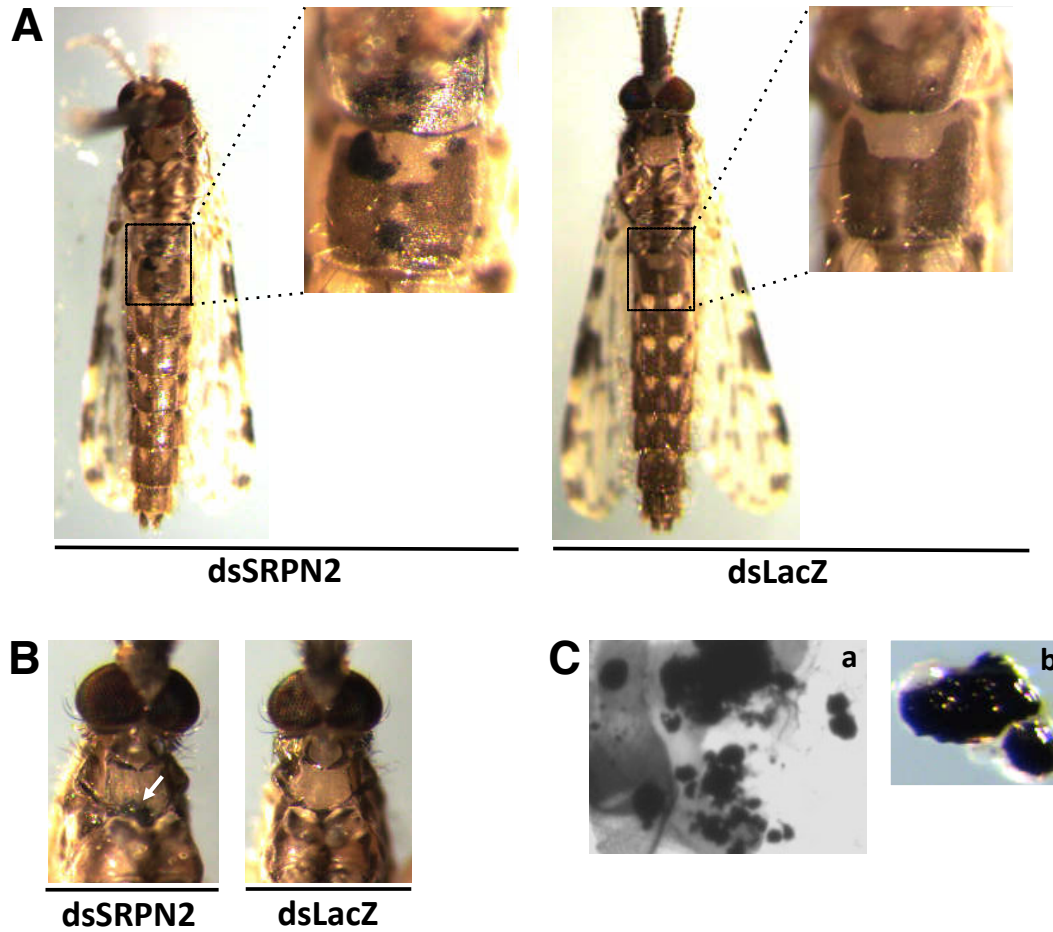
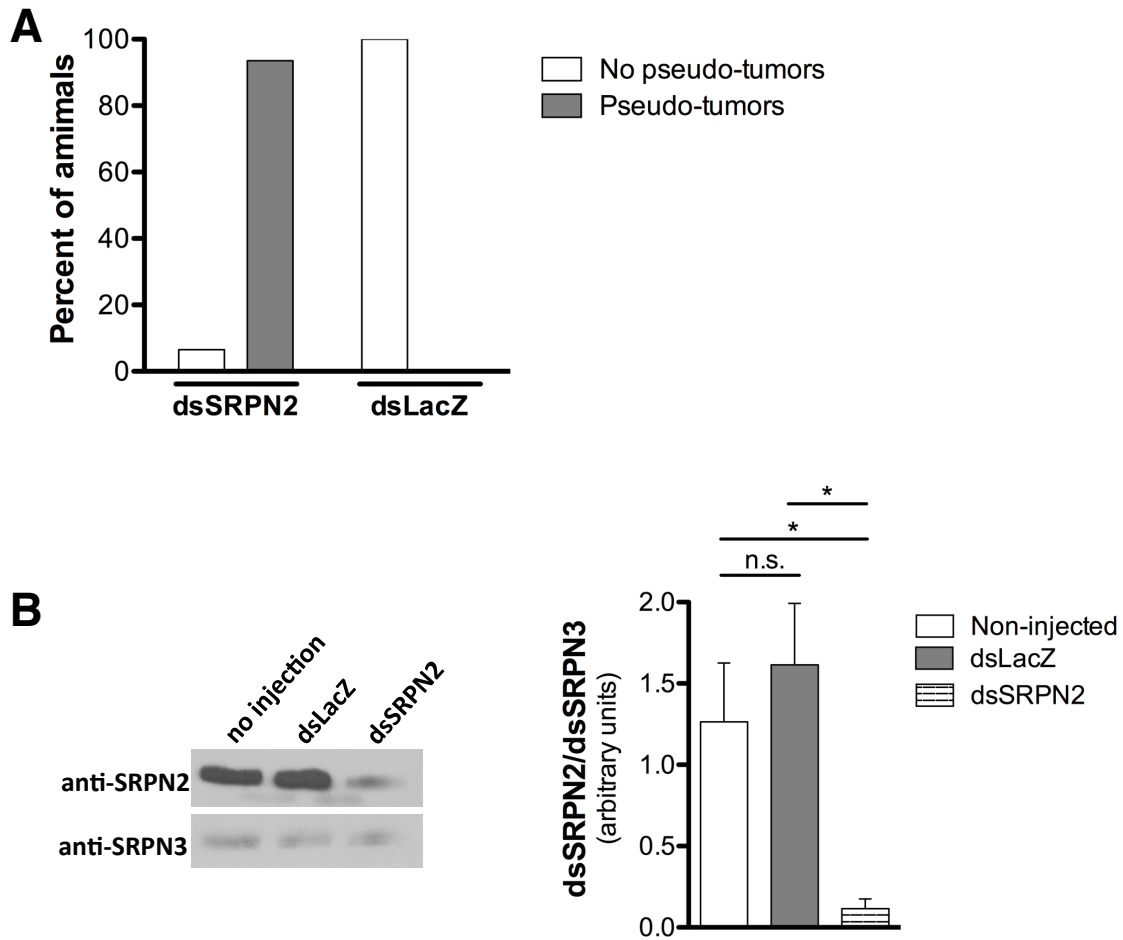


**Figure 3.6: Quantification of pseudo-tumor formation and decreased SRPN2 protein levels.** (A) Pupal stage injections result in pseudo-tumor formation in 93.5% of *dsSRPN2* adults (n = 21) compared to 0% of *dsLacZ* controls (n = 19). Results obtained day 8 post-injection. (B) Western blot (left) shows decreased SRPN2 levels in *dsSRPN2*, but not *dsLacZ* or non-injected hemolymph protein isolates (day 5 post-injection). Results based on three independent experiments. Anti-SRPN2 (Michel et al. 2005) and anti-SRPN3 (Michel et al. 2006) antibody dilutions used were 1:1000 and 1:2000, respectively. Goat anti-rabbit IgG-HRP (Product sc-2004, Santa Cruz Biotechnology, Dallas TX) was used at 1:5000. All protein levels were quantified (right) by band intensity (ImageJ Software, NIH, Bethesda, MD), normalized to SRPN3, and statistically compared by unpaired *t* test (GraphPad Software, La Jolla, CA).  $P < 0.05$ : \*,  $P \geq 0.05$ : n.s. (not significant).





## **Chapter IV**

**Uncovering the role of an *Anopheles gambiae* G protein-coupled receptor, GPRGR2,  
in the detection of bitter compounds**

## A. ABSTRACT

Investigating basic behaviors of mosquitos is essential for advancing our understanding of the bionomic factors that make these insects such competent vectors for the transmission of many infectious diseases. G protein-coupled receptors (GPCRs) are known to mediate developmental, sensory and other physiological pathways that are fundamental to mosquito survival and vectorial capacity. GPCRs that function as chemoreceptors play fundamental roles in mosquito gustation and olfaction, and are central to the abilities of insects to identify sugars, blood sources and detect bitter/noxious compounds in the environment. Despite the importance of these behaviors, surprisingly little is known about mosquito gustation, particularly in the case of the major African malaria vector, *Anopheles gambiae*. Here we investigate the ability of *An. gambiae* to detect various bitter compounds when given a choice between a sugar meal or a sugar/compound meal, employ spatial expression studies, and utilize RNAi-mediated knockdown to identify GPRGR2 as an important gustatory receptor. We characterize the set of currently annotated gustatory GPCRs phylogenetically, topologically and with regard to physiological response. Our characterization of *An. gambiae* GPRGR2 provides insights into bitter compound recognition and may provide an avenue for advanced vector control strategies.

## B. INTRODUCTION

The mosquito is one of the most successful arthropods that mediates the transmission of infectious diseases. Malaria is among the most virulent diseases transmitted by the mosquito, resulting in substantial human morbidity and mortality every year. The World Health Organization (WHO) reports that during 2013 there were an estimated 600,000 deaths as a result of malaria. Of these, 78 percent were in children under the age of five years (World Health Organization 2014). Apicomplexan parasites within the genus *Plasmodium* are the pathogens that cause human malaria, and they are transmitted between their human hosts by female *Anopheles* mosquitoes. *Anopheles gambiae* is the most epidemiologically relevant species due to its relationship to high human malaria morbidity rates, and it is the most prominent malaria vector in sub-Saharan Africa (World Health Organization 2014; Kelly-Hope & McKenzie 2009; The malERA Consultative Group on Vector Control 2011). Currently, insecticide delivery via indoor residual spraying of insecticide-treated bednets is the most successful method employed to reduce the burden of human malaria by decreasing vector mosquito populations and by reducing vector-human contact. While vector-targeted approaches remain the most effective control strategy, the increase of insecticide resistance has driven the need for the discovery of novel methods for vector control (Enayati & Hemingway 2010; Edi et al. 2014; S. N. Mitchell et al. 2014).

Chemosensory processes are fundamentally important to the relationship between an organism and its environment. Chemoreception in insects, as in most vertebrate organisms, can be divided into two separate modalities that include gustation (taste) and olfaction (smell). These two processes are critical for the ability of the organism to detect

soluble or volatile molecules, respectively (World Health Organization 2014; Stocker 1994; Kelly-Hope & McKenzie 2009; Heimbeck et al. 1999; The malERA Consultative Group on Vector Control 2011). Chemosensation is a highly specialized process that allows animals to identify and respond to chemosensory information within the environment (Enayati & Hemingway 2010; K. Scott et al. 2001; Edi et al. 2014; Bargmann 2006; S. N. Mitchell et al. 2014; Garcia-Sainz et al. 2009). Insects are dependent on chemosensation for many behaviors, such as foraging for food, reproduction, and avoidance of potentially harmful substances in the environment. The olfactory system largely mediates recognition of volatile molecules (McIver et al. 1980; K. Scott et al. 2001; Dahanukar et al. 2007; N. R. Singh 1997) that are emitted by plants or animals, and provides information required for the location of a food source in the surrounding environment (Foster 1995; Kessler et al. 2013). Upon locating a potential food source, gustatory chemoreception aids in deciding whether the mosquito imbibes a particular substance, after coming into physical contact with the compound(s) (N. R. Singh 1997; Pappas & Larsen 1978). If a compound is perceived as bitter, a characteristic of many toxins, signaling to the central nervous system (CNS) by gustatory (taste) cells will likely result in feeding rejection (Weiss et al. 2011).

The *D. melanogaster* gustatory receptors (GRs) Gr66a, Gr33a and Gr93a have been shown to mediate bitter compound recognition and aversive responses. Among the compounds evaluated, Gr66a has been shown to function in the identification of caffeine and the insecticide L-canavanine (Moon et al. 2006; Y. Lee et al. 2012), whereas Gr33a mediates detection of a larger range of bitter compounds (Thorne et al. 2004; Moon et al. 2009). Gr93 has been studied to a lesser extent, but has also been shown to function in

caffeine aversion (Y. Lee et al. 2012). The ability to successfully locate an adequate sugar meal is critical for survival, as sugar is required to build metabolic energy reserves (Clements 1955; Louis-Clement Gouagna et al. 2010). In *D. melanogaster*, two essential gustatory receptors have been shown to be essential for identifying sugars of specific classes. Gr5a functions as a receptor for glucose and trehalose (Dahanukar et al. 2001; Chyb et al. 2003), whereas Gr64a is required for identification of fructose and sucrose (Dahanukar et al. 2007). In addition to food recognition, insects utilize gustatory chemical cues to locate a mating partner and potential oviposition (egg-laying) sites (Freeman et al. 2014; Lacaille et al. 2007). In *D. melanogaster*, *Gr68a* has been shown to be expressed in gustatory bristles on the forelegs and is important in deterring male-to-male courtship (S. Bray & Amrein 2003) by sensing of male-specific bitter-tasting cuticular hydrocarbons (Lacaille et al. 2007), and the sweet taste receptor Gr5a has been shown to be essential for identification of oviposition sites (C. H. Yang et al. 2008). By modulating behaviors such as food-seeking, compound aversion, and reproduction, these receptors exert substantial influences on insect survival and reproductive capacity (Stone et al. 2012; Ignell et al. 2010).

The peripheral GRs that underlie the chemosensory system belong to a family of membrane-bound G-protein-coupled receptors (GPCRs) that mediate signal transduction through G-protein activation (Pitts et al. 2004; Takken et al. 2001; Hill et al. 2002; Sparks et al. 2013; Buck & Axel 1991; Clyne et al. 1999; Clyne 2000). In the *An. gambiae* genome, 155 putative chemoreceptors have been identified, of which 76 are predicted to function as gustatory receptors and 79 as olfactory receptors (Hill et al. 2002). Among the 76 gustatory receptors identified, 60 have been fully annotated within the major

vector bioinformatics resource VectorBase (Giraldo-Calderon et al. 2015). The genome of *D. melanogaster* has a similar numerical makeup of 62 odorant receptors and 68 gustatory receptors (Clyne et al. 1999; Vosshall et al. 1999), suggesting that fairly small numbers of receptors may be responsible for the intricate chemosensory processes that control many essential behaviors, in both species.

Upon landing on a feeding surface (i.e., plant or vertebrate), contact is made by sensilla (sensory hairs) that are located on the terminal tarsal segments, and is followed by an exploratory phase during which the mosquito contacts the surface repeatedly with the tip of the labellum, for evaluation of available resources (Clements 1992). Sensilla are chemosensory structures that are present on most insects and are widely dispersed on the exterior of the cuticle. The body regions that tend to show the highest sensillar densities are the proboscis, maxillary palp, legs/tarsi, wings and genitalia (K. Scott et al. 2001; Stocker 1994; Dahanukar et al. 2007; N. R. Singh 1997; Seenivasagan et al. 2009; Pitts et al. 2004; Pappas & Larsen 1976). In most insects, the detection of volatile chemical signals occurs in neurons that innervate sensilla on the antenna and maxillary palps, while tastants tend to stimulate those that are located on the proboscis or tarsi (Stocker 1994; Ling et al. 2014; Meunier et al. 2003).

The physical structure of a sensillum is made up of a hollow projection that is innervated with dendrites of sensory neurons surrounded by sensillum lymph (Galindo & D. P. Smith 2001). These sensory structures contain a dendritic chamber that is typically innervated with two to four sensory neurons and a single mechanosensory neuron (Falk et al. 1976; B. K. Mitchell et al. 1999). At the distal tip of taste sensillum is a pore that allows chemicals to enter and come into contact with the dendrites that are located within

the sensillar lumen (Stocker 1994). Tastants can activate one or more gustatory receptors, resulting in a neuronal response that will send action potentials down the axonal processes to suboesophageal ganglion (SOG), which is the primary gustatory center (Miyazaki & Ito 2010). Gustatory receptor neuron (GRN) stimulation has been shown to mediate physiological responses in the presence of different compound types (e.g., sugars, bitter, pure water and salt) (Moon et al. 2006; Meunier et al. 2003; Rodrigues & Siddiqi 1978; Fujishiro et al. 1984).

Extensive research has been employed to unravel the roles of GPCRs in bitter compound detection/aversion in *D. melanogaster* (Moon et al. 2009; Moon et al. 2006; Hiroi et al. 2004; Y. Lee et al. 2012; Y. Lee et al. 2009), however very little is known about how this process operates in the mosquito. Recent chemosensory work investigating this process in the yellow fever vector, *Aedes aegypti*, has started to answer some of these questions regarding aversive response to various bitter tastants. The findings from this work have revealed that taste receptors that are located on mouthparts (i.e., the labellum) display sensitivity to compounds (e.g., quinine or the commonly used insect repellent DEET) and elicit a physiological and behavioral response by activating a bitter-sensitive gustatory cell (Sanford et al. 2013). While it has been already established that DEET deters insects by interacting with the olfactory receptor cells (Vosshall et al. 1999; Ditzen et al. 2008), these findings suggest that DEET also interacts with a specific gustatory receptor (Sanford et al. 2013). In both *An. gambiae* and *Ae. aegypti*, expression data for the chemosensory GPCRs has become available recently and may provide opportunities to better investigate this critical family of proteins (Sparks et al. 2013; Pitts et al. 2011). The *An. gambiae* array showed very low expression of the GR family, and

no evident expression of GPRGR2 in the tissues assessed (i.e., maxillary palps and antenna) (Pitts et al. 2011), which in part may be due to the selected tissue types, which are primarily olfactory tissues (Bargmann 2006). Interestingly, the GPRGR2 and Gr66a *Ae. Aegypti* ortholog *AeGPRGR14* displayed very high expression in the labellum (Sparks et al. 2013).

Understanding how gustatory processes influence feeding and aversive behaviors is an important question in insect chemosensory biology. Although extensive work in *D. melanogaster* has provided valuable insights into gustation-related behavioral and physiological responses at the neurological level, we still have little understanding regarding the genetics that underlie these aversive behaviors in the mosquito. Here we investigate the behavioral aversion of *An. gambiae* to a series of known bitter compounds via colorimetric tastant detection. We have identified a mosquito gustatory receptor, GRPGR2, that shares sequence homology with the previously characterized *D. melanogaster* gustatory bitter receptor, Gr66a. This fly receptor has been shown to play an important role in the detection of bitter compounds, particularly in the response to caffeine (Thorne et al. 2004; Y. Lee et al. 2009). We have evaluated the membrane topology, spatial expression and functional genomics of GPRGR2 to assess alterations in aversive behaviors in receptor knockdown animals exposed to a subset of previously characterized bitter compounds. Manipulating this aversive behavior of *An. gambiae* by targeting GRs that are essential to gustation may serve as method to decrease vectorial capacity, by increasing the effectiveness of attractive toxic sugar bait (ATSB) interventions currently being developed (Beier et al. 2012; Muller et al. 2010).



## C. RESULTS AND DISCUSSION

### **Bioinformatic analysis of gustatory GPCR topology and identification of a candidate *An. gambiae* bitter receptor**

Within the past decade, a great deal of work has been done to elucidate the chemosensory systems of insects by defining the functional roles of GPCRs. This chemoreceptor family includes a large number of gustatory (GR) and odorant (OR) receptors from many insect species, including *An. gambiae* and *D. melanogaster* (Hill et al. 2002; Robertson et al. 2003). All of the GR and a subset of OR protein sequences contain a signature motif of hh(G/A/S)(A/S)hhTYhhhhhQF, where “h” represents a hydrophobic residue (Louis-Clement Gouagna et al. 2010; Clyne 2000; K. Scott et al. 2001; Robertson et al. 2003; Kent et al. 2007). In fact, the presence of this motif in both GRs and ORs suggests that these chemosensory families have diverged from a single structural gene family, and further suggests that ORs evolved from the GR family (K. Scott et al. 2001; Robertson et al. 2003). When assessing the phylogeny of vertebrate vs. insect chemoreceptors, the evolutionary origin is very distant (Bargmann 2006). In addition, vertebrate chemosensory GPCRs are structurally distinct, as insect receptor structure often consists of an inverted topology (i.e., intracellular amino terminus) (Benton 2009; Garcia-Sainz et al. 2009) and have actually been described as possibly being more closely related to 6 TMD ion channels (Bargmann 2006). Given the vast differences in vertebrate vs. insect chemoreceptors, it is possible that sensory receptor-targeted interventions that are targeted specifically toward insects can be employed.

In 2006, Moon *et al.* identified the *D. melanogaster* receptor Gr66a as a GPCR that is required in the process of bitter compound detection (Moon et al. 2006). To identify and study a probable ortholog of Gr66a in the *An. gambiae*, we utilized the OrthoDB database, which contains a catalog of orthologous protein-coding genes for arthropods and vertebrates (Kriventseva et al. 2015), as well as the National Center for Biotechnology Information (NCBI) HomoloGene database (Wheeler et al. 2007). The results revealed the most likely *An. gambiae* ortholog of Gr66a to be GPRGR2, and revealed no vertebrate ortholog (Table 1). We also looked for orthologs in two other major human malaria vectors, *An. funestus* and *An. arabiensis*, as well as the yellow fever vector *Ae. Aegypti*, and found AfGPRGR, AaGPRGR, and AeGPRGR14, respectively, to be the most likely candidates (Table 1). All of these receptors fall into the same InterPro identification grouping of seven transmembrane (7TM) chemosensory receptors and have the same gene ontology (GO) biological process of sensory perception of taste (A. Mitchell et al. 2015a) (Table 1). We then performed NCBI BLASTP analysis using the BLOSUM62 scoring matrix (Altschul et al. 1990) with the Gr66a receptor as a query, to assess the similarity of the sequences of Gr66a and GPRGR2. The query showed that the *An. gambiae* receptor GPRGR2 yields the highest sequence identity (35% protein identity, max score: 302, total score: 302, query coverage: 99%, E-value: 2e-95) with Gr66a. A reciprocal best BLAST using GPRGR2 as the query likewise returned the *D. melanogaster* Gr66a as the top hit. While this computational prediction does not directly imply that GPRGR2 functions in the same capacity as Gr66a, the extent of sequence identity encouraged us to further investigate GPRGR2 as a candidate bitter compound receptor.

To better visualize the sequence homology of the two receptors, we used Geneious Software (Biomatters Inc., San Francisco, CA) to compare the identities of specific protein regions (e.g., transmembrane domains, intracellular space and extracellular space). The protein region with the highest pairwise identity maps within the intracellular C-terminal region (Figure 4.1A). This finding is not unexpected, as gustatory GPCRs exhibit a conserved C-terminal motif that contains an amino acid sequence of hh(G/A/S)(A/S)hhTYhhhhhQF (Louis-Clement Gouagna et al. 2010; Clyne 2000; K. Scott et al. 2001; Robertson et al. 2003; Kent et al. 2007). Both the GPRGR2 and Gr66a receptor sequences contain this characteristic motif in the high-identity region encompassed by amino acids 449-463 and 464-478, respectively (Figure 4.1B).

Next we assessed the genetic relationships of GPRGR2 within the currently annotated gustatory family of GPCRs in *An. gambiae*. We performed a phylogenetic analysis with Geneious Software (Biomatters Inc., San Francisco, CA) for the 60 *An. gambiae* GPRGRs annotated in VectorBase (Giraldo-Calderon et al. 2015), including the *D. melanogaster* Gr66a receptor. We included, as well, three human bitter receptors TAS2R10, TAS2R14, and TAS2R46, which have been shown to be responsive to an extremely large set of bitter compounds (Meyerhof et al. 2010) and are expressed in the circumvallate papillae of the tongue, where taste recognition occurs (Behrens et al. 2007). The phylogenetic assessment shows that Gr66a is more closely related to the GPRGR2 and that the human receptors are not closely related to the insect receptors (Figure 4.1C). It is likely that more than one GR is responsible for bitter gustation in *An. gambiae*, as has been demonstrated for *Drosophila* (Moon et al. 2009; Moon et al. 2006; Thorne et al. 2004), and it will be of interest to explore whether there is any bitter GR clustering within

phylogenetic clades. However, it is possible that we will observe phylogenetic dispersion of bitter receptors because unlike sugar receptors, which exist in phylogenetic clades, both bitter taste and pheromone receptors reside within divergent subfamilies (Garcia-Sainz et al. 2009).

To investigate the membrane topology of *An. gambiae* GRs, we used Geneious Software (Biomatters Inc., San Francisco, CA) and employed the transmembrane domain (TMD) algorithm TMHMM (Krogh et al. 2001) to predict the orientation within the membrane for the 60 annotated GR sequences. Among the 60 annotated GRs, 53 are predicted to possess an intracellular N-terminus (Figure 4.2, Dataset 4.1), which is consistent with GR and OR topologies in other species (H.-J. Zhang et al. 2011; Benton 2009; Garcia-Sainz et al. 2009; Bargmann 2006). GR2 is predicted to be within the smaller proportion of GRs that exhibit an extracellular N-terminus (including GPRGR2, GPRGR 5, GPRGR 13, GPRGR 15, GPRGR 43, GPRGR 44 and GPRGR 54), which is consistent with the typical topology of a GPCR (Brody & Cravchik 2000; H.-J. Zhang et al. 2011; Benton et al. 2006). Given that this algorithmic prediction is based on sequence characteristics, confirmation of the predicted membrane topology would require experimental validation.

### **Spatial expression of GPRGR2 in adults**

The gustatory system of *D. melanogaster* has been extensively studied behaviorally, morphologically, physiologically and at the genetic level (Clyne 2000; Dunipace et al. 2001; Falk et al. 1976; Glendinning 2008; Weiss et al. 2011; H.-J. Zhang et al. 2011).

Although we have some insights into the behaviors and morphology associated with gustation in the mosquito, we know very little regarding the underlying genetics that are responsible for these essential behaviors. In *Drosophila*, it has been shown that GR receptors are expressed predominantly in gustatory organs (i.e., proboscis and legs), and in some olfactory structures (i.e., antennae) (García-Sainz et al. 2009). In *D. melanogaster*, Gr-GAL4 mediated expression based on Gr66a regulatory sequences has revealed that a distinct population of approximately twenty neurons respond to various bitter compounds that elicit aversive behaviors (Thorne et al. 2004; Z. Wang et al. 2004; Marella et al. 2006). We know that the *D. melanogaster* bitter receptor Gr66a is co-expressed with a large number of other GRs, including Gr22b, Gr22e, Gr22f, Gr28bE, Gr32a, Gr33a, Gr39aD, Gr47a, Gr59b, Gr59f, Gr93a (Isono & Morita 2010). Of these, Gr33a and Gr93a have been shown to be involved in bitter compound gustation (Moon et al. 2006; Y. Lee et al. 2009). Given that these three bitter receptors are expressed in the same cell, it is possible that identification of multiple GRs expressed in the same cell as GPRGR2 may serve to identify additional *An. gambiae* bitter receptors. Further assessment of GR co-expression, by immunohistochemical experiments would aid in identifying such receptors.

A recent RNAseq-based transcriptome analysis of chemosensory receptor expression in *An. gambiae* identified GPRGRs that are expressed in specific chemosensory tissues (i.e., maxillary palps and antenna). Of the sixty GRs assessed, very few showed expression that was detectable, including GPRGR1, GPRGR22, GPRGR23, GPRGR24, GPRGR33, GPRGR48, GPRGR49, GPRGR50 and GPRGR52 (Pitts et al. 2011). Work performed on Gr expression in *Drosophila* predicts that chemosensory GRs

expression would be highest in the proboscis and legs (García-Sainz et al. 2009). Using these insights, we set out to evaluate GPRGR2 expression in a wider set of chemosensory tissue types that have high sensillar densities, which are expected to contain innervating chemosensory and often mechanosensory neurons (Figure 4.3A). Our spatial expression analysis via quantitative RT-PCR (qRT-PCR) revealed significantly increased expression of GPRGR2 in gustatory chemosensory appendages. The leg, antenna, proboscis and maxillary palp, respectively, showed 46-fold, 39-fold, 35-fold and 5-fold increased levels of expression, compared to the midgut, which lacks sensillar structures (Figure 4.3B). These findings imply that contact with the leg, antenna and/or proboscis may be important for identification of bitter compounds. Lower expression of a GR in maxillary palp is not unexpected as this tissue has been described as a sensory organ that may function exclusively in olfaction (de Bruyne et al. 1999).

### ***An. gambiae* compound aversion and physiological response**

Behavioral observations imply that the mosquito makes an assessment of food and/or blood source via landing and repeatedly contacting the surface of the plant or animal host using the distal region of the labellum to evaluate nutritive resources (Clements 1992). In addition to these behaviors, our observations of *An. gambiae* G3 colony have revealed that this exploratory behavior frequently involves a brushing motion, in which the tips of labellum are swept over the feeding surface repeatedly (data not shown). To assess the aversive response of *An. gambiae* to bitter tastants, we selected five compounds that have been previously characterized as bitter by assessment of their behavioral effects on multiple insect species and are known to be perceived as bitter by

humans (Table 4.2) (Z. Wang et al. 2004; Thorne et al. 2004; Meunier et al. 2003; Marella et al. 2006). These compounds include three naturally occurring alkaloids (berberine chloride, caffeine, and quinine), one imide electrophilic small molecule (N-methylmaleimide) and an ammonium salt that is the most bitter compound currently known (denatonium benzoate). Using a color-labeled meal assay (Figure 4.4A), we were able to analyze the color-labeled contents of the gut through the abdominal cuticle by using light microscopy (Figure 4.4B) and by dissection of the gut (Figure 4.4C). Experiments were designed to determine whether adult mosquitoes exhibited an aversive response to known bitter compounds (i.e., choosing to feed on sugar vs. sugar plus the bitter compound). We observed significant aversion (as assessed by unpaired *t*-test) for both male and female adult mosquitoes for all five of these compounds when mosquitoes were provided with a choice between the bitter compound + 10% glucose and 10% glucose alone (Figure 4.5). For NMM (10 mM), quinine (1 mM), denatonium benzoate (1 mM), berberine chloride (1 mM) and caffeine (10 mM) the percentage of combined male and female feeding adults that preferred the sugar meal ranged from 79% to 62% (Figure 4.5). This confirmation of bitter compound recognition supports the use of these compounds for the physiological assessment of sensillum stimulation and in functional genomic assays to determine whether RNAi-mediated knockdown (KD) of GRPGR2 will interfere with bitter compound-induced aversion.

The stimulation of a given sensillum is completely dependent on the type(s) of neurons by which it is innervated. For example, in *D. melanogaster*, most sensilla contain four taste neurons that respond to sugars, low concentrations of salt, water and bitter compounds/high concentrations of salt (Falk et al. 1976; Fujishiro et al. 1984; Hiroi

et al. 2004; Rodrigues & Siddiqi 1978; Weiss et al. 2011). Structurally, there are three types of sensilla located on the *Drosophila* labellum, which are distributed in a stereotyped pattern and are categorized by length: long (l-type), intermediate (i-type) and short (s-type) (Weiss et al. 2011; Hiroi et al. 2002; Shanbhag et al. 2001). Typically, the i- and s-type sensilla respond very strongly to bitter compounds, whereas the l-type sensilla produce stronger responses to sugars. While research involving *Ae. aegypti* has demonstrated taste receptors that respond to bitter stimulation (Sanford et al. 2013), the location and distribution of sensilla containing bitter-sensitive neurons is still unknown in the *Anopheles* mosquito. Given these insights from *D. melanogaster* and *Ae. aegypti* studies, we assessed the structure and stimulation potential of sensilla located on the labellum of *An. gambiae*. Our SEM images reveal a stereotyped distribution of ~24 sensilla located on the labellum all of which have a size (~20-30  $\mu\text{m}$ ) and structure similar to those described as sensilla chaetica in *Aedes albopictus* (Seenivasagan et al. 2009) (Figure 4.6A). This type of sensillar structure is described as a thick-walled and sharp-pointed sturdy bristle that protrudes from a socket. We also observe sensilla chaetica on terminal tarsal segments in *An. gambiae*, with one distinct sensillum protruding beyond the claw (Figure 4.6B).

Electrophysiology has been used extensively to evaluate chemically-induced neurological responses in *Drosophila* (Moon et al. 2006; Meunier et al. 2003; Rodrigues & Siddiqi 1978; Fujishiro et al. 1984). Recently, Sanford *et al.* showed that sensilla on the labellum of *Ae. aegypti* can be stimulated by sugar and bitter compounds (Sanford et al. 2013). We used similar techniques to evaluate if it is possible to stimulate various sensilla with a bitter compound. Our result show that stimulation of labellum sensilla



results in a neurological response to 50 mM sucrose (Figure 4.6C, blue arrow indicates stimulated sensillum) and an initial test compound, 10 mM NMM (Figure 4.6B, blue arrow indicates stimulated sensilla). This is the first report of stimulation of *Anopheles* sensilla by exposure to an initial bitter compound. It will be interesting to assess further compounds, as well as to determine whether bitter compounds also inhibit activity of the sugar cells and water cells, which has been documented in *Ae. aegypti* (Sanford et al. 2013). Additionally, it will be of value to assess whether it is possible to stimulate tarsal sensilla, given that this is the initial contact tissue.

### **Genetic manipulation of GPRGR2 in *An. gambiae***

During the search for a food source, insects utilize chemosensory cues to identify metabolites (e.g., sugars, salts, amino acids, alkaloids and quinolines) in places such as floral/extrafloral nectaries, rotting fruit, honeydew and tree sap (Weiss et al. 2011; Ignell et al. 2010; Foster 1995; Gary & Foster 2004; C. B. Russell & F. F. Hunter 2002). Among these metabolites, the latter two examples are chemical classes produced by a variety of plants and roots to ward off insects from feeding (Sala Junior et al. 2008; Ignell et al. 2010). Chemosensory cues come into play when the mosquito is determining whether it should imbibe a sugar meal, relying heavily on the gustatory system to identify non-volatile substances. The response of *D. melanogaster* to bitter substances has been extremely well-characterized for numerous compounds (Moon et al. 2009; Moon et al. 2006; Thorne et al. 2004; Meunier et al. 2003; Hiroi et al. 2004). Behavioral responses to a subset of our tested compounds have been described in mosquitoes, including denatonium benzoate, quinine and berberine *An. gambiae* aversion and quinine and

caffeine *Ae. aegypti* aversion (Kessler et al. 2013; Ignell et al. 2010). Although we are beginning to understand mosquito behavior with regard to bitter compound aversion, it remains unclear which receptors may be involved in these processes.

To investigate the potential role of the *An. gambiae* GPRGR2 receptor in detection and aversion of bitter compounds, we proceeded in a functional genomic direction. A dsRNA was designed to target a 154 base pair region of the receptor mRNA, which displayed no off-target hits (i.e., no 18mer or greater matches within the genome). This region targets Exon 2, which encodes part of TMD 4 and all of TMD 5 (Figure 4.7A and 4.7B). RNA interference was initiated during the early pupal stage (see Chapter III for methodology), as my previous attempts of KD during the adult stage were unsuccessful (data not shown), possibly due to the lack of access of injected dsRNA to required cells or other factors in adults. Using whole head RNA isolation of adults 3 days post-emergence, following dsRNA injection, we were able to detect a decrease on GPRGR2 mRNA levels of ~40% by qRT-PCR, compared to control heads 3 days post-emergence. Due to the variability in the four biological replicates assessed (dsLacZ: 2.10, 3.08, 4.76, 8.92 and dsGPRGR2: 1.69, 2.19, 2.90, 4.77), additional experimental replicates must be performed to obtain a result with clear statistical significance.

To address the question of whether this particular receptor plays a role in detection of bitter compounds, we selected a series of chemicals that have been previously used in *D. melanogaster*, *Ae. aegypti*, and *An. gambiae* behavioral and physiological assays (Kang et al. 2010; Weiss et al. 2011; Kessler et al. 2013; Ignell et al. 2010) (Table 4.1). GPRGR2 knockdown adults displayed decreased aversion to four of the five compounds tested, when compared to LacZ dsRNA-injected controls (Figure

4.8), based on assessment using our dye-labeled choice preference assay (Figure 4.4). The compounds for which significant reduction in aversion was observed were berberine chloride, N-methylmaleimide, quinine, and denatonium benzoate. Caffeine aversion did not appear to be altered significantly. The results from these assays were unexpected since the *D. melanogaster* ortholog Gr66a has been shown to mediate caffeine detection (Moon et al. 2006), while Gr33a has been shown to mediate detection of all of the other compounds (except for NMM, which was not assessed for Gr33a) (Moon et al. 2009). Future RNA interference-based studies evaluating the role of the Gr33a mosquito ortholog, GPRGR43, alone and in combination with GPRGR2 knockdown in *An. gambiae*, would further elucidate the respective roles of these two receptors, highlighted based on orthology to *Drosophila*, in bitter compound gustation. Co-expression of these two GRs may be required in some sensilla for bitter compound gustation, just as co-expression of GPRGR22 and GPRGR24 in antennal sensilla has been demonstrated as a requirement for CO<sub>2</sub> detection in *An. gambiae* (Isono & Morita 2010). In addition to the proteins categorized as gustatory receptors, there may be other non-GR proteins involved in bitter gustation. For example, in *D. melanogaster* the transient receptor potential cation channel protein TRPA1, has been shown to play a role bitter compounds mediated responses at the physiological and behavioral levels (Kang et al. 2011; Kwon et al. 2006), in addition to its previously characterized role in thermal-sensing (Kang et al. 2010). More interestingly, the two isoforms of the *An. gambiae* TRPA1 receptor have been shown to respond to respond to NMM when expressed in oocytes (Kang et al. 2011).

Taken together, these data provide a foundation to better understand the genetics that underlie the detection of bitter compounds by *An. gambiae* and identify GPRGR2 as

an important component in this biological process, which is critical for insect survival. Not only will these insights prove useful in understanding the basic bionomics of this vector, but also may enable the development of tools for masking the sensing of compounds that would be otherwise aversive. Applications utilizing these insights could help advance the development of enhanced attractive toxic sugar bait (ATSB) interventions (Beier et al. 2012; Muller et al. 2010), targeted against *An. gambiae* and other vector insects.

## **D. METHODS**

### **Rearing and maintenance**

*Anopheles gambiae* (G3 colony) were reared at  $27 \pm 3^\circ\text{C}$ ,  $75 \pm 5\%$  humidity, under a light:dark cycle of 16:8 hours, including crepuscular periods. Larvae were provided a diet of 1.4% (w/v) Tetramin fish flakes (United Pet Group, Blacksburg, VA) and 0.4% cichlid pellets (w/v) (Kyorin Food Ind. Ltd., Himeji, Japan) and 0.4% algae wafers (w/v) (Kyorin Food Ind. Ltd., Himeji, Japan), prepared in dH<sub>2</sub>O. Adults were maintained on a diet of 10% (w/v) glucose (Sigma-Aldrich, St. Louis, MO) *ad libitum*, and females were periodically provided with human blood using a membrane feeding apparatus for egg development. Two days post-blood meal, oviposition cups were placed in cages, and eggs were collected at 24 and 48 hours to allow for hatching in trays containing dH<sub>2</sub>O.

### **RNA isolation and cDNA synthesis**

Total RNA was isolated from adult mosquito antenna, proboscis, maxillary palp, leg and midgut with TRI reagent (Sigma-Aldrich, St. Louis, MO) and treated with DNase I (Fisher Scientific, Pittsburg, PA). Synthesis of first strand cDNA was performed using total RNA, oligo(dT) primers and reverse transcriptase (Invitrogen, Grand Island, NY). Gene-specific cDNA was amplified using the primers listed in Table 4.3. cDNA was cloned into pCR2.1-TOPO vector (Invitrogen, Grand Island, NY), and recombinant clones were identified via sequencing with M13 reverse primer.

### **Quantitative reverse transcription polymerase chain reaction (qRT-PCR)**

Amplifications were performed using one-step SYBR Green PCR mastermix (Affymetrix, Santa Clara, CA). Experimental samples were run with *An. gambiae* *RSP7* as an endogenous reference and control. Expression levels were calculated by a relative standard curve method and quantified by using analysis software from Applied Biosystems (Foster City, CA). Primers were designed to span intron junctions, to distinguish from gDNA and are listed in Table 4.3.

### **Double-stranded RNA synthesis and delivery**

Template DNA was prepared using GPRGR2::pCR2.1-TOPO and amplified using dsRNA primers to add 5' T7 promoter sequences (5'–TAATACGACTCACTATAGGG–3') onto dsDNA template. dsRNA was prepared by using the dsDNA template and the Ambion MEGAscript RNAi Kit, following modified kit instructions. Modification

included an increased transcription reaction time (~18 hours) and purification via phenol/chloroform extraction. Pupal injections were performed using dsRNA at a concentration of 3 µg/µl, and injecting 2 pulses of 69 nl, with 0.1% Fast Green FCF Dye (Sigma-Aldrich, St. Louis, MO) to visualize injection quality (see Chapter III for detailed methodology).

### **Dual-choice feeding assay**

Adult *An. gambiae* (48 hours post-emergence) were starved of sugar for 16-18 hours (to empty the gut and encourage feeding) and anaesthetized by exposure to cold (4°C). Adults were placed into a cardboard container with mesh netting on top and presented with each of two solutions via one-half of a bisected hollow-bodied cotton swab (Johnson & Johnson Co, City, State), respectively. A volume of 180 µl of sugar solution was introduced into the plastic stem and saturated the swab. One blue swab and one yellow swab were placed through small openings in the netting, and containers were transferred immediately into a dark chamber for 6 hr under insectary conditions. The inverse color/sugar combination was set up in a side-by-side assay to correct for possible dye bias. The imbibed solutions were visually identified via midgut dissection by using blue and yellow dye. In addition to external visual inspection, the gut was punctured with an insect pin on a piece of white filter paper to allow a more thorough assessment of dye color. For bitter compound-sugar combinations, sugar was presented at 10% (w/v) in both control (glucose only) and experimental (bitter compound + glucose) swabs. Compounds were used at the following concentrations: 1 mM Berberine chloride (Sigma-Aldrich, St. Louis, MO), 10 mM N-methylmaleimide (Sigma-Aldrich, St. Louis, MO), 10 mM

caffeine (Fisher Scientific, Pittsburg, PA), 1 mM denatonium benzoate (Fisher Scientific, Pittsburg, PA) and 1 mM quinine (Fisher Scientific, Pittsburg, PA).

### **Aversive Behavior Data Analysis**

Statistical software (Prism, GraphPad, La Jolla, California) was used to assess significance of the choice indices, based on the pairwise choices provided. Using the data from three independent replicates ( $n = 100$  per replicate) and performing a Welch's  $t$ -test, the  $p$ -values were determined.  $p \leq 0.05$  was considered statistically significant. To calculate the choice index (C.I.), the formula from Ignell *et al.* (Ignell et al. 2010) was used:

$$C.I. _A = [(n_A) + (n_{A+B})] / n_{total}$$

$$C.I. _B = [(n_B) + (n_{B+A})] / n_{total}$$

Mosquitoes that died were not scored, and those that had refrained from feeding were scored as non-feeding (included in total number). Mosquitoes were scored by gender, as well, to determine if any gender-bias could be observed.

### **Phylogenetic Analysis**

Geneious software (Biomatters Inc., San Francisco, CA) was used to generate ClustalW alignments of the 60 annotated gustatory receptors (sequences obtained from VectorBase, <http://www.vectorbase.org/>), *D. melanogaster* Gr66a bitter receptor (sequences obtained

from FlyBase, <http://flybase.org/>) and three human bitter receptors TAS2R10, TAS2R14, TAS2R46 (sequences obtained from UniProt, <http://www.uniprot.org/>). For genes encoding multiple splice variants, the longest open reading frame was used to generate the alignment. ClustalW alignments were used to generate a phylogenetic tree using Jukes-Cantor genetic distance model and neighbor-joining with Geneious Software (Biomatters Inc., San Francisco, CA).

### **Electrophysiology**

Gustatory sensilla on the labellum of female adults 0-24 hours post-emergence were used for electrophysiological recordings as previously described in Hodgson *et al.* (Hodgson et al. 1955). All recordings were performed from a single sensillum type near the distal tip of the labellum. Recordings were performed by immobilization of the mosquito (wings and legs removed) on a glass slide by use of two-sided tape. A tungsten wire electrode was inserted into the head to serve as a ground. The recording/stimulating electrode was prepared by inserting a silver wire into a glass capillary pulled to a tip diameter just large enough to fit over the end of one single sensillum. A contact chemoreceptive sensillum preamplifier (Taste Probe, Syntech, Kirchzarten, Germany) was used to generate electrical signals that were stored and analyzed using LabCharts software (ADI Instruments, Colorado Springs, CO). Prior to any experimental recordings, sensilla were stimulated with the control solution of 10 mM KCl to ensure appropriate contact was made. Recordings were performed for a minimum of 10 seconds to ensure continued stimulation and assess any stimulation as a result of physical contact.



### **Scanning electron microscopy (SEM)**

Tissues were fixed overnight with 2.5% glutaraldehyde in PBS, pH 7.4. Following fixation, tissues were washed twice with PBS and twice with distilled water and subsequently, followed by dehydration in ascending grades of ethanol (70%, 95%, 100%; 30 min each). All tissues were stored in 100% ethanol until dried using a critical point dryer (Tousimis Autosamdri-815B, Rockville, MD). Samples were immediately mounted on glass slides and coated in a thin film of gold (~5-10 nm) via Hummer 6.6 sputter deposition (Anatech, Union City, CA). Samples were imaged using scanning electron microscopy (SEM) with a NeoScope benchtop JCM-6000 SEM (JEOL, Peabody, MA).

## E. FIGURES AND LEGENDS

**Figure 4.1: GPRGR2 sequence motif, structure and phylogeny.** (A) Protein sequence identity (green) for the *D. melanogaster* (GR66a) and *An. gambiae* (GPRGR2) orthologs. Transmembrane regions (blue). (B) The GRs are defined by a conserved C-terminal motif: hh(G/A/S)(A/S)hh(T/S)YhhhhhQF, where “h” is a hydrophobic residue. (C) Phylogenetic tree depicting the relationships among 60 annotated *An. gambiae* GPRGR receptors (blue), *D. melanogaster* Gr66a (orange) and human bitter GPCRs TAS2R10, TAS2R14, TAS2R46 (red).

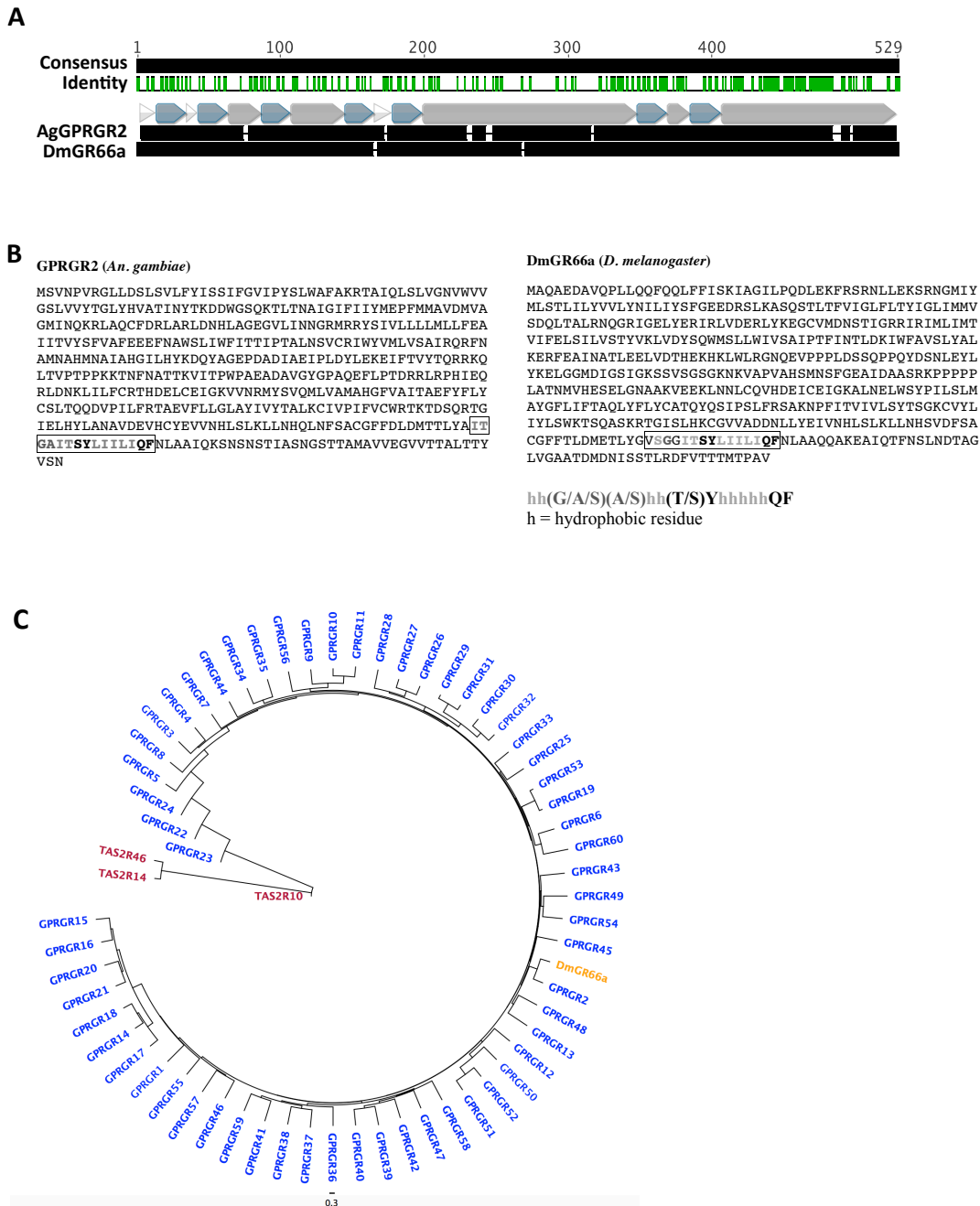


**Figure 4.2: *An. gambiae* GPRGR membrane topology.** Of the 60 currently annotated *An. gambiae* GPRGRs, TMD predications using a TMHMM algorithm (Krogh et al. 2001) revealed that the majority of receptors (53 of the 60) are oriented in an inverted manner (i.e., cytoplasmic N-terminal domain). GPRGR2 is one of the few that exhibit a typical GPCR topology (i.e., extracellular N-terminal domain).

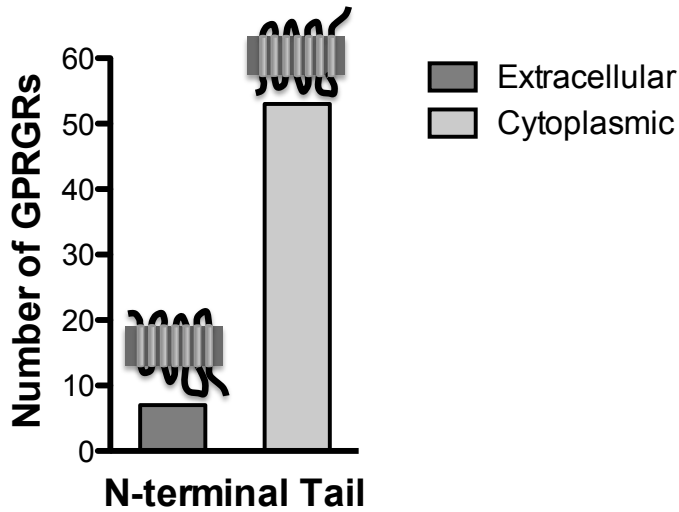


**Figure 4.3:** *An. gambiae* GPRGR2 is highly expressed in multiple sensory appendages. (A) Sensilla with potential innervating sensory neuron types. (B) Spatial analysis of transcript levels shows that GPRGR2 is abundant in the proboscis, leg and antenna (all tissues containing sensilla), when compared to midgut (no sensilla). \* =  $P < 0.05$ , \*\* =  $P \leq 0.01$ , \*\*\* =  $P \leq 0.001$

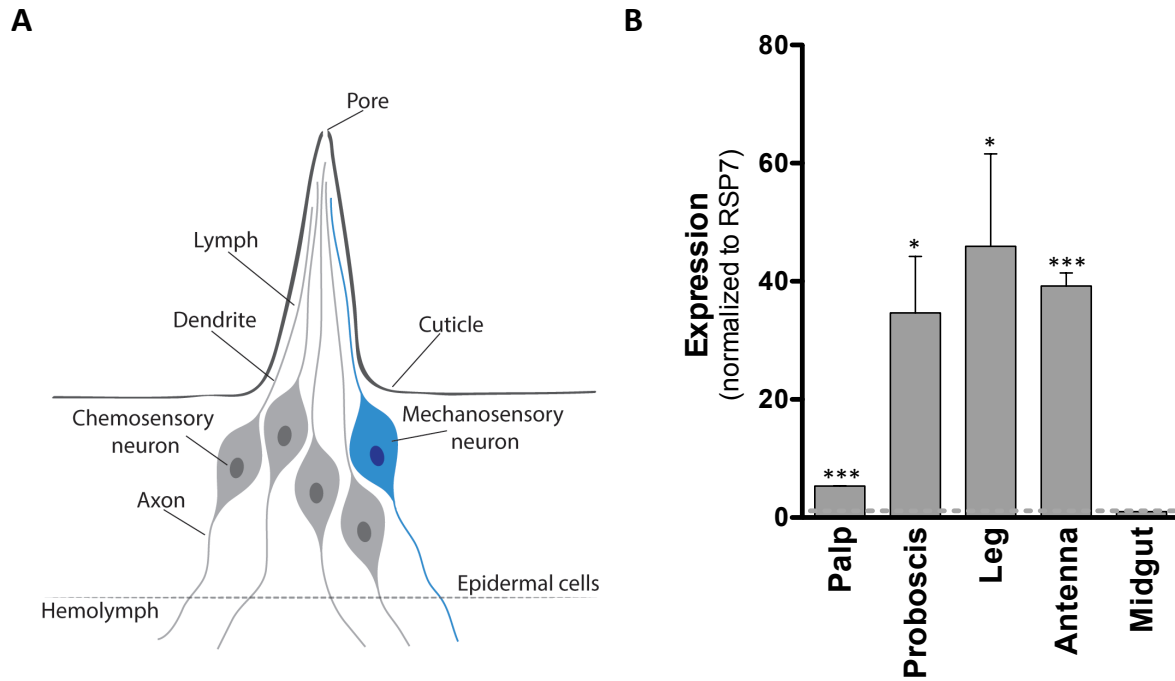


**Figure 4.4: Choice preference assay.** (A) Dual-choice feeding apparatus. Two sugar options are presented to the mosquitoes for a 6 hr time period (in a dark chamber) post-starvation. Colored dye allows for detection of sugar option(s) imbibed. Inverse options (as depicted above) are provided to adjust for any potential color bias. (B) Microscopy images of *An. gambiae* after imbibing dye-labeled sugar meal. Illumination of the abdominal region shows colored sugar solution in the gut. (a) Imbibed blue 10% glucose meal. (b) Imbibed yellow 10% glucose meal + bitter compound. (c) Imbibed both blue and yellow solutions (as indicated by green gut color). (C) Dissection of gut post-imbibition of a dye-labeled sugar meal. Image show is a male scored as feeding on both blue and yellow meals.

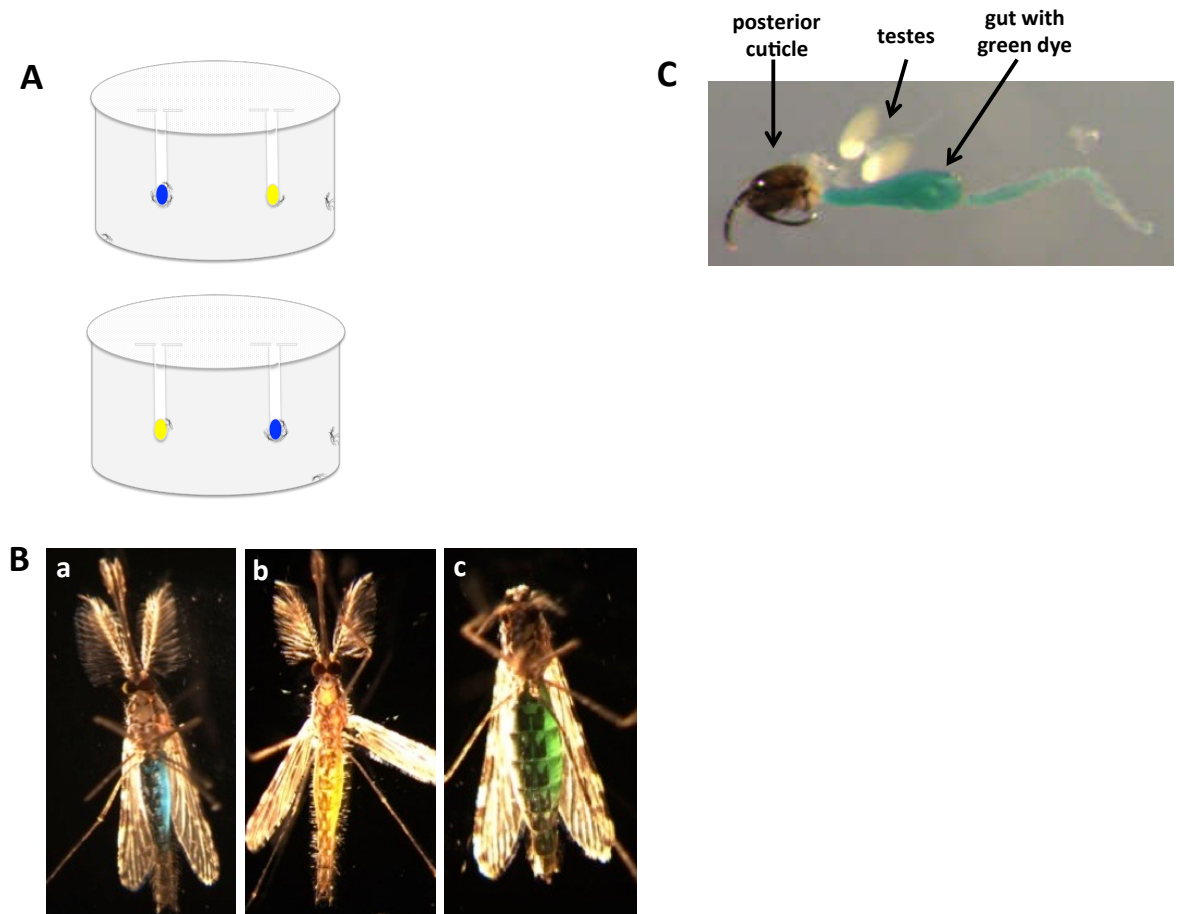


**Figure 4.5: *An. gambiae* bitter compound aversion.** Adult *An. gambiae* mosquito meal choice when provided 10% glucose (Glu) or 10% glucose + bitter compound. Compounds assessed are: (A) 10 mM NMM, (B) 1 mM berberine chloride (Ber), (C) 1 mM denatonium benzoate (Den), 1 mM quinine (Qui) and (D) 10 mM caffeine (Caf). For each compound, three replicates were performed with  $n = 100$  adults (equal numbers of males and females). Colored bars represent proportion of male (blue) and female (red) that fed on meal. Significance assessed via unpaired  $t$ -test, where  $*$  =  $P < 0.05$ ,  $**$  =  $P \leq 0.01$ ,  $***$  =  $P \leq 0.001$ .

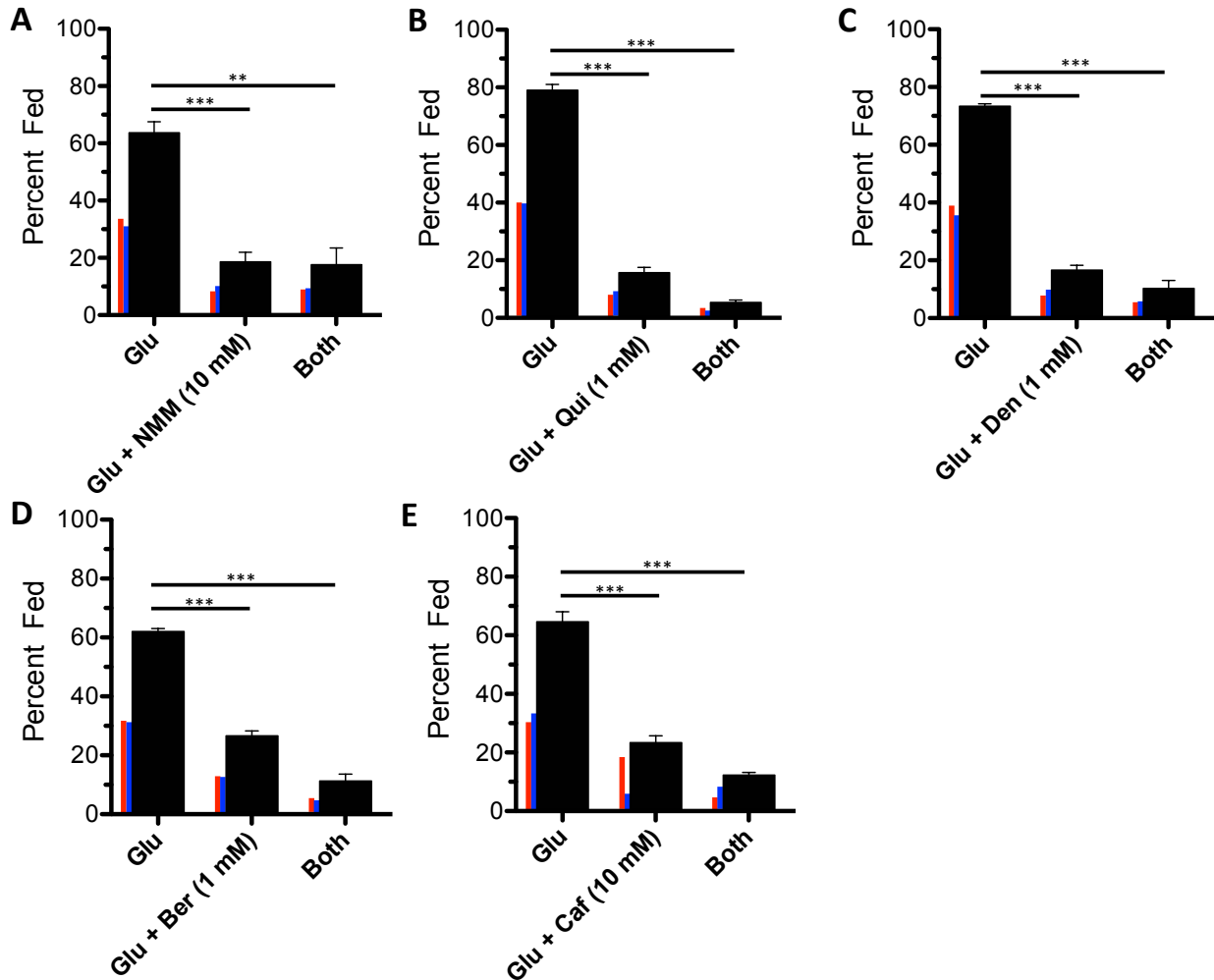


**Figure 4.6: *An. gambiae* sensilla scanning electron micrographs (SEMs) and electrophysiology.** (A) SEM images showing sensilla chaetica of an adult *An. gambiae* mosquito labellum at 240X (left) and 1100X (right). Blue arrows indicate representative sensilla from which electrophysiological recordings were performed. White asterisk indicates sensillum pore. (B) SEM image of an adult terminal tarsal segment showing a sensillum chaetica protruding beyond the claw. (C) Electrophysiological recordings using 50 mM sucrose. (D) Electrophysiological recordings using 10 mM NMM. Sensilla were stimulated with 50 mM KCl for normalization, prior to sugar or NMM exposure.

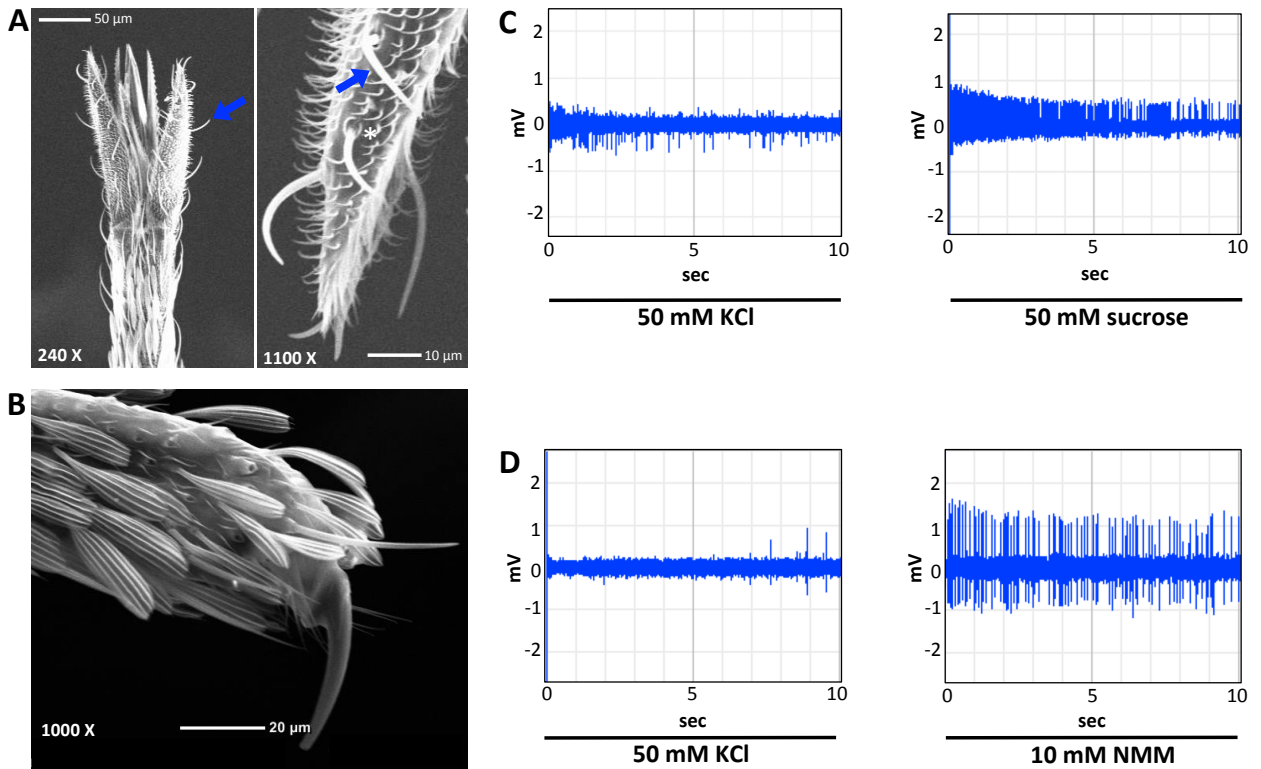
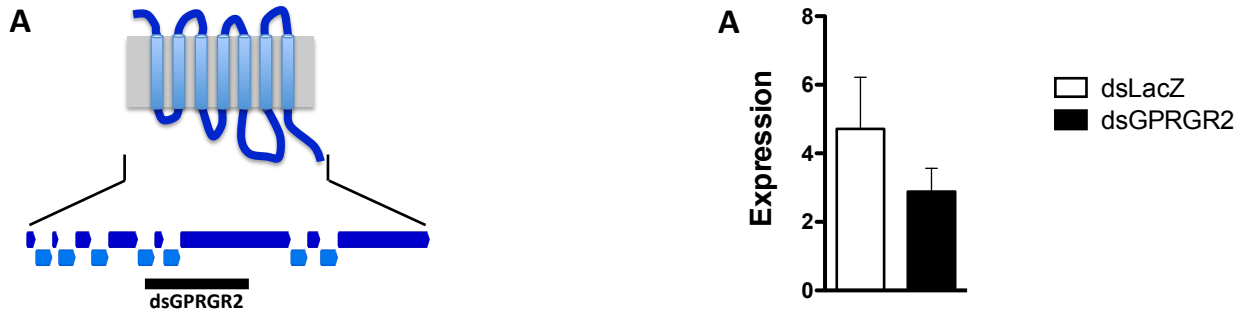


**Figure 4.7: *An. gambiae* GPRGR2 knockdown.** (A) Schematic of GPCR indicating the location of the 154 bp knockdown region. Dark blue: intra- and extra-cellular loops, light blue: TMDs, gray: membrane. (B) GPRGR2 CDS with KD region (gray highlight) indicated. (C) Quantitative PCR analysis following dsGPRGR2 injection shows approximately 40% reduction in transcript levels, compared to dsLacZ injection (control).



**B** ATGTCGGTTAATCCGGTTCGCGGGTTGCTCGATTGCTGCTCCGTGCTGTTTTACATCTCC  
TCCATCTTTGGCGTCATTCCTACTCGCTGTGGGCGTTTGCCAAGCGCACCGCAATACAG  
CTCTCCCTAGTCGGCAATGTGTGGGTAGTTGGCAGCCTGGTCGCTACACGGGCTGTAC  
CATGTGGCAACAATCAACTACACGAAAGACGATTGGGGATCGCAAAGACGCTCACGAAT  
GCGATTGGCATCTTCATCATCTACATGGAACCGTTTATGATGGCGGTGGACATGGTGGCG  
GGTATGATCAATCAGAAACGACTGGCCAGTGCTTCGATCGGCTGGCCCGCTCGACAAC  
CATCTGGCCGGGAGGGCGTGTGATCAACAACGGGCAATGCGCCGGTACAGCATCGTG  
CTGTTGCTGCTGATGCTGCTGTTTCGAGGCGATCATCACCCTGTACAGCTTTGTGGCGTTT  
GAGGAAGAGTTTAAACGCTGGTCTGATCTGGTTCATCACGACCATACCGACCGCACTG  
AACTCGGTGTGCCGCATCTGGTACGTGATGCTGGTGTCCGCCATCCGGCAGCGCTTCAAC  
GCAATGAACCGCACATGAACGCGATCGCCACGGCATACTGCACTACAAGGACCAGTAC  
GCGGGCAACCGGACCGGACATTCGCCAGATACCGCTCGACTATCTGGAGAAGGAGATA  
TTCACCTGTACACGACGCGCCGAAGCAGCTGACGGTGGCGACTTCFCCCAAGAAGACG  
AACTTCAATGCCACCACCAAGGTGATCACCCCGTGGCCCGCCGAAGCAGACGAGTCGGG  
TACGGTCCGGCTCAGGAGTTCCTGCCGACCGATCGCGGGCTACGGCCCCACATCGAGCAA  
CGGCTGGACAACAAGCTGATACTGTTCTGCGGACGCACGACGAGCTGTGCGAGATCGGC  
AAGTCTGTAACCGGATGTACAGCTGCAGATGCTGGTGGCGATGGCGACGGGTTTGTGTC  
GCCATTACGGCCGAGTTTACTTTCTCTACTGCAGCCTCACGACGAGGACGTCGCCGATA  
CTGTTCCGAACGGCGGAAGTGTTCGCTCGGGCTGGCGTACATCGCTACACGGCGCTC  
AAGTGTATCGTGCCGATCTTTGTGTGCTGGAGGACGAAAACCGACTCGCAGCGAACCGGC  
ATCGAGCTGCACTATCTGGCGAACGCGTFCGACGAGGTCCACTGTTACGAGGTGGTTAAC  
CATCTGTCGCTGAAGCTGCTAAACATCAGCTTAACTTTAGTGCCTGTGGCTTTTTCGAC  
CTGGACATGACGACACTGTACGCGATAACGGCGCAATCACCAGCTACCTGATCATACTG  
ATCCAGTTCAATCTTGCAGCGATACAGAAATCGAACAGCAACTCAACGATCGCCTCGAAT  
GGCAGCACCGCCATGGCGTGTGGAGGGCGTCTTACCACCGCACTAACGACGTAC  
GTTTCCAATTGA



**Figure 4.8: *An. gambiae* GPRGR2 knockdown results in decreased bitter compound aversion.** (A-D) Knockdown adults (dsGPRGR2) exhibit no significant differences in feeding preference for sugar versus sugar + bitter compound, whereas control (dsLacZ) show significant aversion. (E) Both knockdown and control adults show significant aversion to bitter compound. For each compound, three replicates were performed with adults that emerged after the injection of 50 pupae (see Chapter III for methodology). Number of emerged adults varied per injection round. As the number of adults tested varied for each assay, the significance was assessed by Welch's *t*-test, to increase stringency. \* =  $P < 0.05$ , \*\* =  $P \leq 0.01$ , \*\*\* =  $P \leq 0.001$ , ns =  $P > 0.05$ .

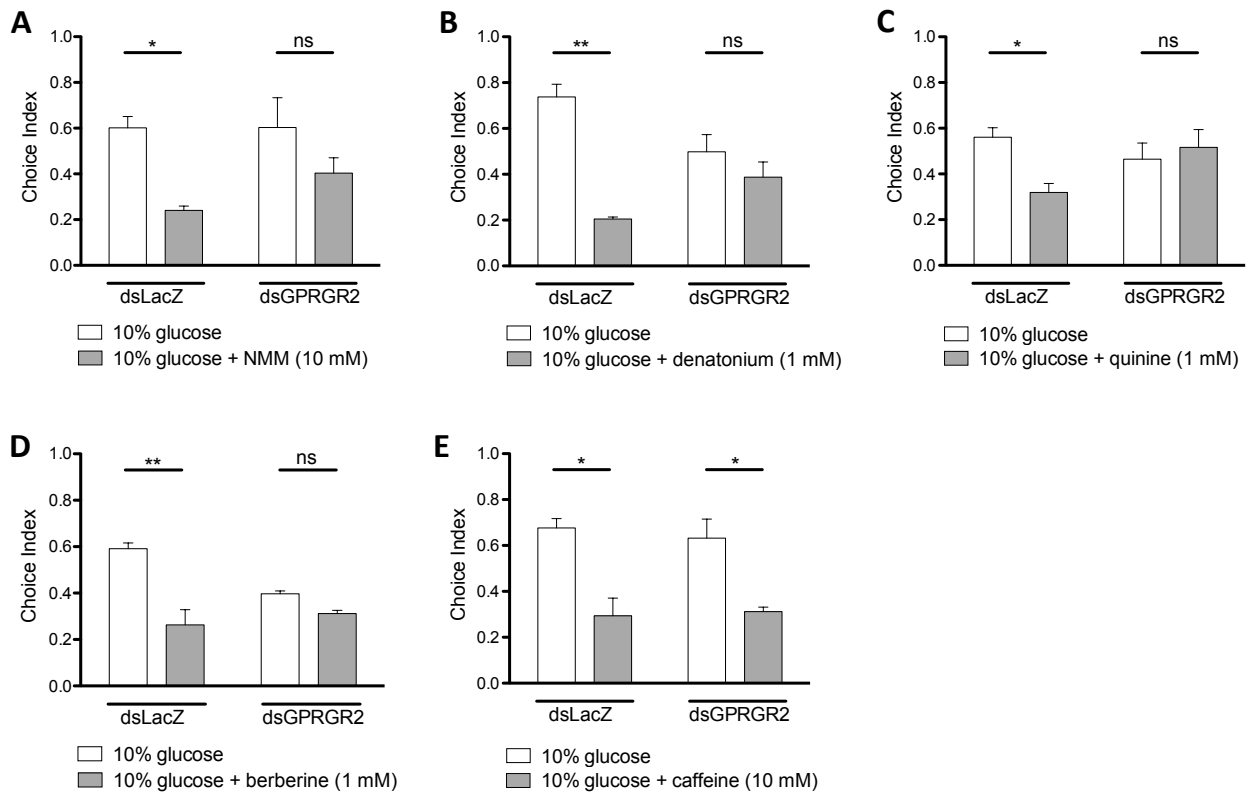


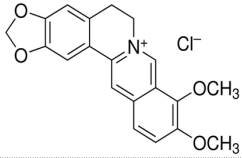
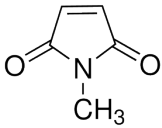
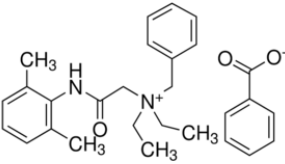
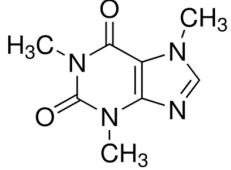
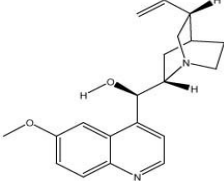
**Table 4.1. GPRGR2 orthologs.**

Organism	Protein ID	Gene Name	InterPro ID	GO Term: Biological Process
<i>Drosophila melanogaster</i>	FBpp0289508*	Gr66a	IPR013604 (7TM chemoreceptor)	Sensory perception of taste
<i>Anopheles gambiae</i>	AGAP002275-PA#	GPRGR2	IPR013604 (7TM chemoreceptor)	Sensory perception of taste
<i>Anopheles funestus</i>	AFUN002184-PA#	GPRGR	IPR013604 (7TM chemoreceptor)	Sensory perception of taste
<i>Anopheles arabiensis</i>	AARA004056-PA#	GPRGR	IPR013604 (7TM chemoreceptor)	Sensory perception of taste
<i>Aedes aegypti</i>	AAEL011571-PA#	GPRGR14	IPR013604 (7TM chemoreceptor)	Sensory perception of taste

\* FlyBase identification number

# VectorBase identification number

**Table 4.2. Bitter Compounds.**

Chemical Name	Empirical Formula	Chemical Structure	Chemical Properties
Berberine chloride	$C_{20}H_{18}ClNO_4$		<ul style="list-style-type: none"> <li>· Alkaloid</li> <li>· Quaternary ammonium salt</li> <li>· Bitter tastant</li> <li>· Found in plant roots &amp; bark</li> </ul>
N-methylmaleimide	$C_5H_5NO_2$		<ul style="list-style-type: none"> <li>· Imide</li> <li>· Electrophilic small molecule</li> <li>· Bitter tastant</li> </ul>
Denatonium benzoate	$C_{21}H_{29}N_2O \cdot C_7H_5O_2$		<ul style="list-style-type: none"> <li>· Ammonium benzoate</li> <li>· Quaternary ammonium salt</li> <li>· Bitter tastant</li> </ul>
Caffeine	$C_8H_{10}N_4O_2$		<ul style="list-style-type: none"> <li>· Alkaloid</li> <li>· Bitter tastant</li> <li>· Found in plants &amp; fruits</li> </ul>
Quinine	$C_{20}H_{24}N_2O_2$		<ul style="list-style-type: none"> <li>· Alkaloid</li> <li>· Bitter tastant</li> <li>· Found in plant roots &amp; bark</li> <li>· Known antimalarial</li> </ul>

**Table 4.3. Primer sequences.**

<b>Gene</b>	<b>Primer Sequences 5' -&gt; 3'</b>
	<b>cDNA</b>
GPRGR2	F': GCGAGTGTGCAAAAATCATGTCCG R': GGAGGCATGCTGGCTTCAATTGG
	<b>dsRNA*</b>
GPRGR2	F': taatacgactcactatagggCACCGTGTACAGCTTTGTGG R': taatacgactcactatagggGTTTCATTGCGTTGAAGCG
LacZ <sup>#</sup>	F': taatacgactcactatagggCTCGAGGTCGACGGTATCG R': taatacgactcactatagggCGGCCGCTCTAGAACTAG
	<b>qRT-PCR</b>
GPRGR2	F': GCTGCTAAACCATCAGCTTAAC R': CGGTTATCGCGTACTGTGTC
Rsp7	F': TCGCTCTTTTTCCGGGCAT R': TTGCCGGCTTTGATCACCTT

\* lowercase regions indicate T7 promoter site.

<sup>#</sup> primers designed using flanking regions in pLL10-GFP plasmid (containing LacZ)

**Dataset 4.1. TMHMM topology and TMD prediction data.** Spreadsheet available online in supplemental material at ProQuest.

## **APPENDIX**

## **CHAPTER AI**

### **Modulation of TRPA1 thermal sensitivity enables sensory discrimination in *Drosophila***

Kyeongjin Kang, Vincent C. Panzano, Elaine C. Chang, Lina Ni, Alexandra M. Dainis, Adam M. Jenkins, Kimberly Regna, Marc A. T. Muskavitch & Paul A. Garrity. Modulation of TRPA1 thermal sensitivity enables sensory discrimination in *Drosophila*. *Nature* **481**, 76–80 (2011).

## A. ABSTRACT

Discriminating among sensory stimuli is critical for animal survival. This discrimination is particularly essential when evaluating whether a stimulus is noxious or innocuous. From insects to humans, transient receptor potential (TRP) channels are key transducers of thermal, chemical and other sensory cues (Dhaka et al. 2006; Wu et al. 2010). Many TRPs are multimodal receptors that respond to diverse stimuli (Dhaka et al. 2006; Wu et al. 2010; Daniels & McKemy 2007), but how animals distinguish sensory inputs activating the same TRP is largely unknown. Here we determine how stimuli activating *Drosophila* TRPA1 are discriminated. Although *Drosophila* TRPA1 responds to both noxious chemicals (Kang et al. 2010) and innocuous warming (Hamada et al. 2008), we find that TRPA1-expressing chemosensory neurons respond to chemicals but not warmth, a specificity conferred by a chemosensory-specific TRPA1 isoform with reduced thermosensitivity compared to the previously described isoform. At the molecular level, this reduction results from a unique region that robustly reduces the channel's thermosensitivity. Cell-type segregation of TRPA1 activity is critical: when the thermosensory isoform is expressed in chemosensors, flies respond to innocuous warming with regurgitation, a nocifensive response. TRPA1 isoform diversity is conserved in malaria mosquitoes, indicating that similar mechanisms may allow discrimination of host-derived warmth—an attractant—from chemical repellents. These

findings indicate that reducing thermosensitivity can be critical for TRP channel functional diversification, facilitating their use in contexts in which thermal sensitivity can be maladaptive.

## **B. INTRODUCTION, RESULTS AND DISCUSSION**

Highly temperature-responsive TRP cation channels, thermoTRPs, mediate thermosensation from insects to mammals (Dhaka et al. 2006; Wu et al. 2010) and are important for human pain and inflammation (Patapoutian et al. 2009). Like mammalian thermoTRPs, *Drosophila melanogaster* TRPA1 is both a thermal and chemical sensor, responding to innocuous warmth (above ~25–27°C) (Hamada et al. 2008; Viswanath et al. 2003) and noxious chemicals (Kang et al. 2010). TRPA1 acts in thermosensors within the brain to modulate thermal preference over 18–32°C (Hamada et al. 2008), innocuous temperatures compatible with fly survival (Cohet 1975), and in gustatory chemosensors to inhibit ingestion of electrophiles (Kang et al. 2010), reactive chemicals like allyl isothiocyanate (AITC, found in wasabi) and N-methylmaleimide (NMM) that rapidly incapacitate flies (Figure A1.1). The responsiveness of TRPA1 to both innocuous and noxious stimuli raises the question of how these stimuli are distinguished to elicit distinct behavioral responses. Mammals face similar issues; for example, TRPM8 transduces both innocuous and noxious cold (Dhaka et al. 2006; Wu et al. 2010; Daniels & McKemy 2007).

We previously reported TRPA1-expressing chemosensors in the labral sense organ (Kang et al. 2010); using improved immunostaining conditions, we now also detect



specific TRPA1 protein expression in labellar chemosensors (Figure A1.2a, b). Extracellular tip recording (Hodgson et al. 1995) indicated these neurons were TRPA1-dependent chemosensors; they responded to the electrophile NMM with robust spiking in wild type but not *TrpA1* mutants (Figure A1.2c and Figure A1.3). The mutant defect was electrophile specific, as *TrpA1* mutants responded like wild type to berberine chloride (Figure A1.2c), a bitter compound that also activates these neurons (Weiss et al. 2011). In contrast, warming to  $\sim 39^{\circ}\text{C}$ , from innocuously warm to the noxious range, elicited no spiking in these cells (Figure A1.2d, e). This is notable as the effectiveness of TRPA1 in conferring warmth sensitivity has led to its use as a thermogenetic tool (Hamada et al. 2008; Philipsborn et al. 2011). Thus, despite the known sensitivity of TRPA1 to both temperature and chemicals, these chemosensors are warmth insensitive.

In addition to the previously characterized transcript, *TrpA1(B)*, a transcript with an alternative 5' end, *TrpA1(A)*, has been annotated (Graveley et al. 2011) (Figure A1.4a). These transcripts encode protein isoforms with distinct amino termini, but the same ankyrin and transmembrane domains (Figure A1.4b). Polymerase chain reaction with reverse transcription (RT-PCR) demonstrated differential expression: *TrpA1(A)* was expressed in the proboscis, which houses the TRPA1-expressing chemosensors, whereas *TrpA1(B)* predominated elsewhere in the head, where TRPA1-expressing thermosensors are located (Figure A1.4c).

Examined in *Xenopus* oocytes, TRPA1(A) was much less thermosensitive than TRPA1(B), as reflected in its temperature coefficient ( $Q_{10}$ ), the fold change in current per  $10^{\circ}\text{C}$  change (Dhaka et al. 2006; Wu et al. 2010). Arrhenius plot analysis (Vyklícký et al. 1999) yielded a  $Q_{10}$  of  $\sim 9$  for TRPA1(A) versus  $\sim 116$  for TRPA1(B) (Figure A1.4d-f).

In addition, whereas TRPA1(B) was essentially inactive at low temperatures, TRPA1(A)-dependent currents were observed  $\leq 15^{\circ}\text{C}$ , further reducing the temperature-dependent activity differential of TRPA1(A) (Figure A1.5). The maximum heat-activated current for TRPA1(A) was also significantly lower (Figure A1.6). Lastly, the transition (or threshold) temperature for increased temperature responsiveness was  $29.7 \pm 0.3^{\circ}\text{C}$  for TRPA1(A) versus  $27.8 \pm 0.4^{\circ}\text{C}$  for TRPA1(B) ( $P < 0.01$ , t-test). As the innocuous warm temperature range in *Drosophila* is of particular behavioral relevance, the  $Q_{10}$  from 27–37°C (below the  $\sim 38^{\circ}\text{C}$  nociceptive threshold in *Drosophila*) (Tracey et al. 2003) was also calculated, yielding  $6.2 \pm 0.5$  for TRPA1(A) and  $90 \pm 8$  for TRPA1(B) (Figure A1.4f). Other properties were largely unaffected; both channels responded robustly to electrophiles and had similar voltage sensitivities (Figure A1.4g, h). TRPA1(A) and TRPA1(B) had similar maximum current amplitudes at 300 mM NMM, with half-maximum effective concentration ( $EC_{50}$ ) values of  $176 \pm 12$  and  $128 \pm 9$  mM, respectively (Figure A1.4i).

The reduced thermosensitivity of TRPA1(A) could account for the chemosensors' warmth insensitivity. But although TRPA1(A) is less temperature sensitive than TRPA1(B), its  $Q_{10}$  resembles several TRPs implicated in warmth sensitivity (Talavera et al. 2005; Gracheva et al. 2011; Gracheva et al. 2010). To assess whether TRPA1(A) could confer warmth sensitivity upon *Drosophila* chemosensors, each isoform was used to rescue a *TrpA1* mutant. We previously demonstrated that expressing TRPA1(B) in TRPA1-dependent chemosensors using Gr66a-Gal4 rescues the *TrpA1* mutant behavioral defect (Kang et al. 2010). Using electrophysiology, we found both isoforms restored NMM responsiveness (Figure A1.7a and Figure A1.8a, b), but only TRPA1(B) conferred

warmth sensitivity (Figure A1.7b, c). These differences did not require properties unique to TRPA1-dependent chemosensors. Each isoform was expressed ectopically in sweet-responsive chemosensors using Gr5a-Gal4 (Marella et al. 2006). Both isoforms conferred electrophile sensitivity upon these normally electrophile-insensitive neurons, but only TRPA1(B) conferred thermosensitivity (Figure A1.7d–f and Figure A1.9c, d). The inability of TRPA1(A) to confer warmth sensitivity on fly chemosensors emphasizes that although a  $Q_{10}$  above 5 makes TRPA1(A) more thermally sensitive than most ion channels, *in vivo* testing is important in evaluating whether a channel is sufficiently thermosensitive to make a specific neuron warmth responsive.

These data support a model in which the specificity of TRPA1-expressing gustatory neurons for chemicals is established by their selective expression of TRPA1(A), an isoform unable to confer warmth sensitivity. In contrast, the chemical sensitivity of TRPA1(B) should render TRPA1-dependent thermosensors sensitive to reactive chemicals. However, the location of TRPA1-dependent anterior cell thermosensors inside the head (Hamada et al. 2008) should minimize exposure to environmental irritants. Interestingly, multiple TRPV1 and TRPM1 isoforms are present in humans and other mammals (Wu et al. 2010; Gracheva et al. 2011; Lu 2005; Vos et al. 2006), suggesting the potential generality of isoform diversity in modulating TRP functions.

The behavioral significance of discriminating noxious from innocuous TRPA1 activators was examined by testing gustatory responses of *TrpA1* mutants rescued by chemosensor expression of each isoform. *TrpA1* mutants exhibit decreased avoidance of reactive-electrophile-containing food (Kang et al. 2010). Each isoform rescued this

behavior (Figure A1.7g). However, TRPA1(B) also triggered a nocifensive response to innocuous warming. When allowed to ingest water to satiation and warmed to  $\sim 32^{\circ}\text{C}$ , neither wild-type nor TRPA1(A) rescue animals showed detectable gustatory responses (Figure A1.7h, i). However, warming TRPA1(B) rescue flies caused  $\sim 75\%$  to regurgitate (Figure A1.7h, i). Thus, substituting TRPA1(B) for TRPA1(A) in chemosensors disrupts discrimination of noxious from innocuous stimuli and demonstrates the negative behavioral consequence of misregulated thermosensitivity.

To probe how the alternative N termini in TRPA1 confer distinct properties, conserved residues within these regions were mutated (Figure A1.9a). Mutating either a cysteine (C105) or two basic residues (R113, R116) in TRPA1(A) markedly increased temperature responsiveness (Figure A1.9a–c and Figure A1.10 and A1.11). Whereas the  $Q_{10}$  of wild-type TRPA1(A) was  $<10$ , the TRPA1(A) mutants exhibited  $Q_{10}$  values of  $>50$  (Figure A1.9b, c), greater than the reported  $Q_{10}$  values of canonical thermoTRPs like TRPM8 ( $\sim 24$ ) (Brauchi et al. 2004) and TRPV1 ( $\sim 40$ ) (Liu et al. 2003). In addition, the TRPA1(A) mutants conducted little current below the threshold, increasing the temperature-dependent activity differential (Figure A1.9c and Figure A1.12). The enhanced sensitivities of the mutants seemed to be temperature specific, as NMM sensitivity was not increased (Figure A1.12) These data indicate that TRPA1(A) retains all the requirements for robust thermosensation, but contains a modulatory region preventing those elements from exerting their full effect.

For TRPA1(B), mutating either a conserved tryptophan or two basic residues in the N terminus yielded channels retaining robust thermo-sensitivity ( $Q_{10} >50$ ; Figure A1.9b and Figure A1.10). The thresholds of the TRPA1(A) and TRPA1(B) mutants were

all ~30–34°C, within the innocuous warm range but above the ~28°C value for wild-type TRPA1(B) (Figure A1.9b, c). Thus, although TRPA1(B)-specific sequences are unnecessary for robust responsiveness to innocuous warming, they may tune channel threshold within this range.

In insect disease vectors, TRPA1 orthologs have been implicated in detecting both warmth and chemical repellents (G. Wang et al. 2009; Maekawa et al. 2011; Kang et al. 2010), cues with opposing effects on host seeking. We found the malaria mosquito *Anopheles gambiae* also contains TRPA1(A) and TRPA1(B) isoforms of differing thermosensitivity (Figure A1.9d–h). In oocytes, the  $Q_{10}$  of *A. gambiae* TRPA1(A) was ~4 versus a  $Q_{10}$  of ~200 for *A. gambiae* TRPA1(B); from 27–37°C, the  $Q_{10}$  of *A. gambiae* TRPA1(A) was ~2 versus ~60 for *A. gambiae* TRPA1(B) (Figure A1.9h). *A. gambiae* TRPA1(A) yielded lower maximum heat-induced current than *A. gambiae* TRPA1(B) (Figure A1.6) and had a higher threshold ( $34.2 \pm 1.8^\circ\text{C}$  versus  $25.2 \pm 0.9^\circ\text{C}$ ,  $P < 0.01$ ). *A. gambiae* TRPA1(A) also exhibited significant conductance below threshold (Figure A1.4f, g). Both channels responded to electrophiles (Figure A1.13). TRPA1(A) and TRPA1(B) are conserved in other haematophagous insects including *Aedes aegypti* and *Culex quinquefasciatus* mosquitoes and *Pediculus humanus corporis* lice (Figure A1.9a and Figure A1.14), which transmit dengue, West Nile fever and typhus, respectively. The functional diversity of TRPA1 provides a potential explanation for how insect vectors discriminate noxious chemicals from host-derived warmth, indicating that TRPA1 presents two distinct molecular targets for disrupting pest behavior.

TRPA1-based electrophile detection appears to have emerged  $\geq 500$  million years ago in a common vertebrate/invertebrate ancestor (Kang et al. 2010). However, the larger

TRPA family extends to choanoflagellates, separated from animals  $\geq 600$  million years (Kang et al. 2010). As divergent TRPA clades contain highly temperature-sensitive channels (Dhaka et al. 2006), thermosensitivity may be ancestral. In this scenario, the specialization of TRPA1 for noxious chemical detection would necessitate reducing thermosensitivity, consistent with the effect of the N terminus in TRPA1(A). The ability of N-terminal variation to sculpt channel properties is intriguing as the N terminus is the most divergent region of TRPA1 within insects and from insects to mammals (Hamada et al. 2008).

TRPs are a large family of channels, with 27 human and 13 *Drosophila* members, which vary greatly in thermosensitivity and function (Wu et al. 2010). Considerable diversity is evident even among closely related TRPs. In mammals, for example, TRPM8 ( $Q_{10} \sim 24$ ; ref. 21) mediates thermosensation (Daniels & McKemy 2007), whereas the less thermosensitive TRPM4 and TRPM5 ( $Q_{10} \sim 8.5-10$ ; ref. 15) mediate insulin secretion (Uchida & Tominaga 2011) and TRPM7 (with no reported thermal sensitivity) is implicated in ion homeostasis (Wu et al. 2010). The mechanisms underlying such diversification are unclear. Whereas studies of thermal sensing by TRPs have focused on identifying regions promoting thermosensitivity (Dhaka et al. 2006; Grandl et al. 2008; Grandl et al. 2010; F. Yang et al. 2010; Yao et al. 2011), our work indicates that regions reducing thermosensitivity are also critical. Here we find that selectively reducing the thermosensitivity of *Drosophila* TRPA1 facilitates its use in a context in which thermosensitivity is undesirable. Similar mechanisms could mediate functional diversification not only among isoforms of a single TRP, but also contribute to the remarkable functional diversification observed between different TRP family channels.

## C. METHODS

### Fly Strains and Immunohistochemistry

UAS-TrpA1(B) and Gr66a-Gal4 transgenic strains and the TrpA1<sup>ins</sup> mutant have been described (Kang et al. 2010). The UAS-TrpA1(A) transgene was amplified from fly complementary DNA with an isoform-specific primer (5'-TATAAAGCTTAAGCCACCATGATTACAGCTCCGG CCACGGCCA-3') and a reverse primer (5'-GAGACTCGAGCTACATGCTCTTAT TGAAGCTCAGGGCG-3'). As detailed in Methods, the UAS-TrpA1(A) transgene was inserted in the same genomic location used for the UAS-TrpA1(B) transgene to control for transgene position effects. Anti-TRPA1 immunohistochemistry was as described (Kang et al. 2010), except that the secondary antibody was incubated for 3 days.

### Behavior

The proboscis extension assay was conducted as previously described (Kang et al. 2010), with seven flies per experiment, three experiments per genotype. For heat-sensitive regurgitation, >20 flies per genotype (2–3 days old) were starved overnight with water, then glued to glass slides. After 2–3 h recovery, flies were satiated with water. Only flies drinking longer than 5 s were tested. Drinking times did not significantly differ between wild-type and rescue flies (E.C.C. and P.A.G., unpublished data), consistent with similar ingestion behaviors. Flies were heated with a radiant heater at 800 W (H-4438, Optimus) and temperature was monitored by adjacent thermocouple microprobe

(IT-23, Physitemp Instruments) wrapped in fly cuticle. Chemicals used in incapacitation assays were sucrose (Calbiochem LC8510), sorbitol (Sigma S-1876), ficoll (Sigma F-4375), agarose (Invitrogen 15510-027), caffeine (Sigma C0750), NMM (Sigma 389412), isopropanol (100%, J. T. Baker 9083-03), ethanol (100%, Decon Lab 2716) and allyl isothiocyanate (95%, Sigma 377430).

### **Characterization of TRPA1 isoforms in *Xenopus* oocytes**

TRPA1 currents were recorded as described (Kang et al. 2010; Hamada et al. 2008). To evaluate temperature sensitivities, oocytes were perfused in the recording buffer (96 mM NaCl, 1 mM MgCl<sub>2</sub>, 4 mM KCl, and 5 mM HEPES, pH 7.6), the temperature of which was increased  $\sim 0.5$  °C s<sup>-1</sup> from 10 to 45 °C by SC-20 in-line heater/cooler (Warner Instruments) with a CL100 bipolar temperature controller (Warner Instruments). Temperature-evoked current was recorded at -60 mV. From the recorded current,  $Q_{10}$  was calculated as described (Vyklícky et al. 1999; Gracheva et al. 2010). Arrhenius  $Q_{10} = 10^{(10(-S_{\text{arrhe}})/(T_2-T_1))}$ , where  $S_{\text{arrhe}}$  is the slope of linear phase of an Arrhenius plot between absolute temperatures,  $T_1$  and  $T_2$ . Transition temperature was assessed as the temperature at which the least-squares fit lines from the two linear phases intersect (Vyklícky et al. 1999; Gracheva et al. 2010).  $Q_{10}$  from 27–37 °C was calculated from currents at temperatures of interest using the equation,  $Q_{10} = (I_2/I_1)^{10/(T_2-T_1)}$  where  $I_1$  and  $I_2$  are currents observed at temperatures of  $T_1$  and  $T_2$ , respectively.  $Q_{10}$  determinations were validated by using *Crotalus atrox* TRPA1 (Gracheva et al. 2010) as a control with known  $Q_{10}$  (K.K. and P.A.G., unpublished data).



To assess sensitivity to NMM, voltage across the membrane was initially held at  $-80$  mV, and a 300-ms voltage ramp ( $-80$  mV to  $80$  mV) per second was applied. The oocytes were perfused for 1 min with the recording buffer containing indicated concentrations of NMM with 30-s washes between NMM applications. Current amplitudes at  $-80$  mV after application of each NMM concentration were fitted to the Hill equation through Sigmaplot 10. The first coding exon of *A. gambiae* *TrpA1(B)* was chemically synthesized (Genscript).

### **Gustatory neuron electrophysiology**

Extracellular recordings of gustatory neurons were obtained using the tip-recording method<sup>9</sup>. Adult female flies, aged 1–4 days, were prepared by inserting a glass reference electrode containing *Drosophila* Ringer's solution into the thorax and advancing the electrode through the head to the labellum. A glass recording electrode with an  $\sim 15$ - $\mu$ m opening was used to apply tastants to individual sensilla. Raw signals were amplified using a TasteProbe preamplifier (Syntech) and were digitized and analysed using a PowerLab data-acquisition system with LabChart software (ADInstruments). Amplified signals were digitized at a rate of  $20$  kb  $s^{-1}$  and filtered using a  $100$ – $3,000$  Hz band-pass filter before analysis. Individual action potentials were sorted using a visually adjusted threshold and average spike rate was calculated beginning 200 ms after electrode contact. Recording times varied by experiment: berberine chloride and sucrose positive controls, 5 s; electrolyte only, 20 s; NMM on i-type bristles, 60 s; NMM on L-type bristles, 120 s; heat ramps,  $>60$  s. For heat-ramp experiments, recordings were performed using

electrolyte only as tastant. After ~30 s of recording to determine baseline activity, heat was applied manually to the fly using a radiant heater (PRESTO HeatDish, National Presto Industries). Application of heat was maintained for ~10–30 s and the distance between the heat source and the preparation was reduced to obtain a temperature of  $\geq 39$  °C. Bristle temperature was estimated using thermocouple microprobe (IT-23, Physitemp Instruments) wrapped in fly cuticle. All tastants were dissolved in 30 mM tricholine citrate as the electrolyte to inhibit the activity of the water cell in L-type bristle (Weiczorek & Wolff 1988). Tastants were stored at  $-20$  °C and aliquots maintained at  $4$  °C for up to 1 week. For all experiments, a positive control was used to confirm the viability of the target bristle. For i-type bristles, 1 mM berberine chloride was used as control. For L-type bristles, 30 mM sucrose was used. Individual tastant presentations were separated by a minimum delay of 60 s. At least two animals and six bristles were examined for each condition.

## **Molecular Biology**

Primers for RT-PCR reactions: *D. melanogaster TrpA1(A)* forward, 5'-GCCGG AACAGCAAGTATT3-3'; *D. melanogaster TrpA1(B)* forward, 5'-GTGGACTATCTG GAGGCG-3'; *D. melanogaster TrpA1* common reverse, 5'-TATCCTTCGCATTAA AGTCGC-3'. Mutagenesis of *Drosophila* TRPA1 was performed as described. Briefly, for a desired mutation, each of two mutually complementary mutant primers was paired for PCR with a primer (outer primer) that anneals outside of either *Sall* or *HpaI* restriction recognition site. The two resulting PCR fragments that overlap only in the

region of the two mutant primers were combined and served as template for the next PCR reaction that contained only outer primers. The second PCR product was digested by *Sall* and *HpaI*, and subsequently replaced the corresponding wild type region of TRPA1 cDNA. The fragment between the two restriction sites was sequenced. Sequences were aligned using MUSCLE 3.7 (Edgar 2004).

## D. TABLES, FIGURES AND LEGENDS

**Figure A1.1.** Reactive electrophiles cause incapacitation in *Drosophila*. In all experiment, 15-30 flies were exposed to chemicals in 15 mL conical tubes. **a**, Solid chemicals were administered as ~50 mg powder for 5 min, tubes containing flies for testing were briefly vortexed to maximize exposure. “No Chemical” tubes were also vortexed as control. **a**, Undiluted Liquids were administered as ~50 $\mu$ l drop applied to KimWipes for 1 min. b.p. = boiling point. a-b,  $**\alpha=0.01$ , Turkey HSD. All data are mean  $\pm$  s.e.m. 15-30 flies/experiment, n=3 experiments/condition.

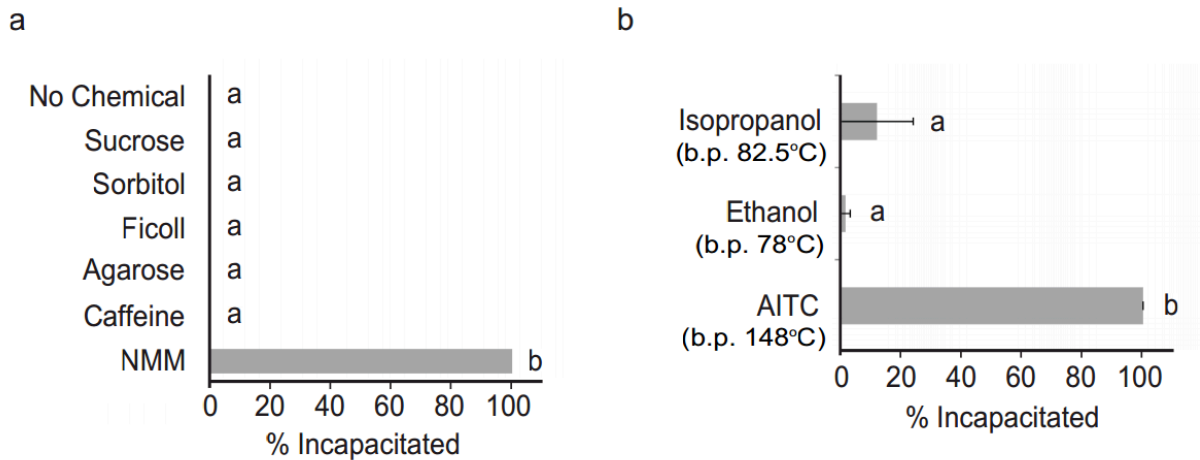


**Figure A1.2. TRPA1-dependent gustatory neurons do not respond to heat.** **a.** TRPA1 immunostaining of wild-type (top) and *TrpA1<sup>ins</sup>* (bottom) labella. Right, differential interference contrast overlay of labellar structures. Arrowheads, chemosensor cell bodies. Scale bar, 20  $\mu$ m. **b.** Top, *Drosophila* gustatory organs: LSO, labral sense organ; OES, oesophagus. Bottom, labellar bristles. Brown, s-type; grey, L-type; black, i-type; berberine-sensitive bristles were targeted for electrophysiology. **c-d.** Bristle responses to: berberine (1 mM) and NMM (10 mM) (c); warming (d). Temp., temperature. **e.** Average spike rate after subtracting electrolyte-only baseline. freq., frequency. \*\* $P < 0.01$ ; NS, not significant ( $P > 0.05$ ), t-test. All data are mean  $\pm$  standard error of the mean (s.e.m.). Warming reached an average maximum temperature of  $39.0 \pm 0.6^\circ\text{C}$  (mean  $\pm$  standard deviation).

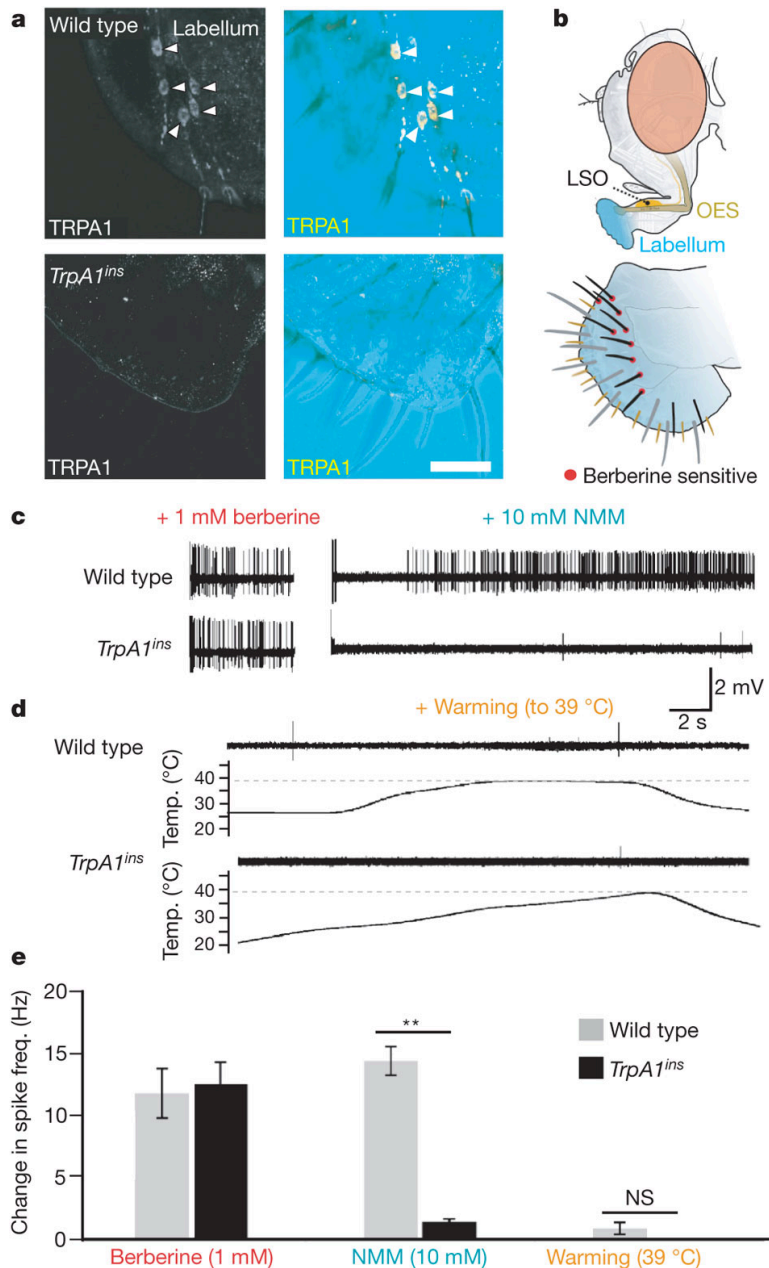


**Figure A1.3.** Example response from labellar gustatory bristles to electrolyte-only solution in wild type and *TrpA1<sup>ins</sup>* mutants. Responses from berberine-sensitive i-type bristles. Arrow: artifact caused by initial contact with bristle.

Electrolyte Only (30 mM Tricholine Citrate)

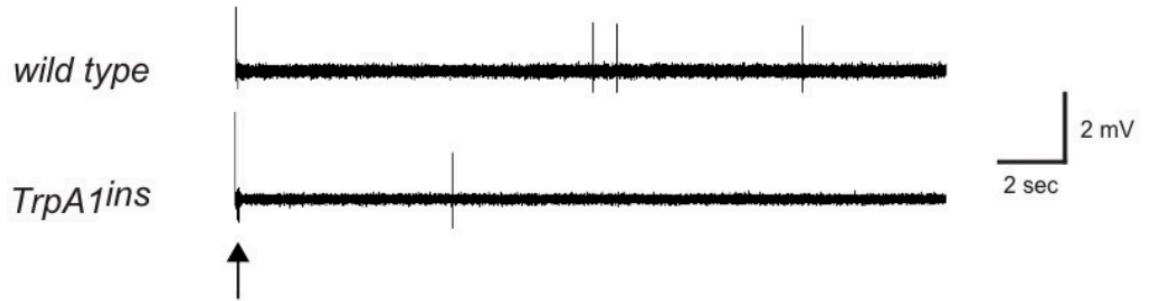


**Figure A1.4. TRPA1 isoform diversity yields tissue-specific channels with different thermal sensitivities.** **a.** *TrpA1* gene structure and primer locations. **b.** TRPA1 proteins. Dark red and blue boxes denote isoform-specific sequences. Dark grey, transmembrane (TM) region. a, ankyrin repeat; aa, amino acids. **c.** RT-PCR analysis of dissected tissue. **d-e.** TRPA1(A)- and TRPA1(B)-dependent currents (d) and Arrhenius plots (e) in oocytes.  $T_{tr}$ , transition temperature. **f.**  $Q_{10}$  values from Arrhenius plot (left) or 27–37°C (right). **g-h.** Left panels, NMM responsiveness of TRPA1(A) (g) and TRPA1(B) (h). Right panels,  $I-V$  relationships at points marked at left. **i.** Mean amplitudes at 300  $\mu$ M NMM (left) and NMM dose-response (right). All data, mean  $\pm$  s.e.m. **\*\*** $P < 0.01$ ; NS, not significant, t-test.

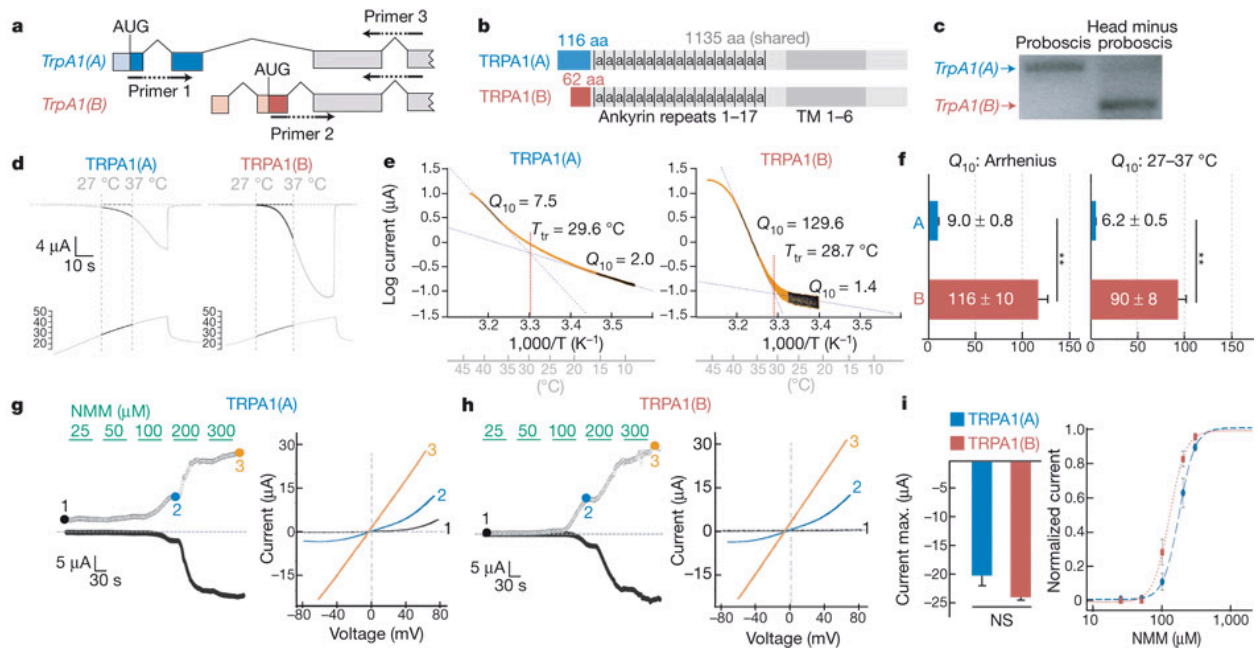


**Figure A1.5. TRPA1(A) currents below and above the transition temperature show similar reversal potentials and voltage dependences.***a.* Temperature-dependent activity of TRPA1(A) at 80 and -80 mV in *Xenopus* oocytes. Voltage ramps between -80 and 80 mV were applied for 300 msec every second via two-electrode voltage clamp. Temperature was increased at  $\sim 0.5$  °C/sec. *Light blue line* indicates current at 15 °C, while *purple and orange lines* currents at 25 and 30 °C, respectively. *b.* Current-voltage relationships of TRPA1(A) activity at 15, 25 and 30 °C marked in (*a*).

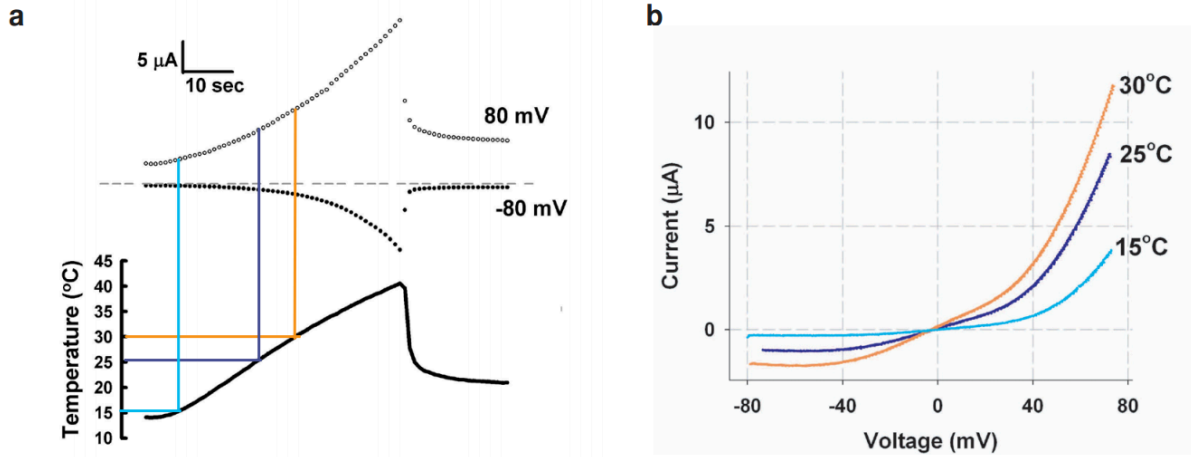




**Figure A1.6. Comparison of maximum heat-responsive current amplitudes for wild type TRPA1(A) and TRPA1(B) channels from *Drosophila melanogaster* and *Anopheles gambiae*.** **a, b,** Maximum TRPA1-dependent currents generated by temperature increase for *Drosophila* (**a**) and *Anopheles* (**b**) channels. Statistical comparisons by unpaired t-test

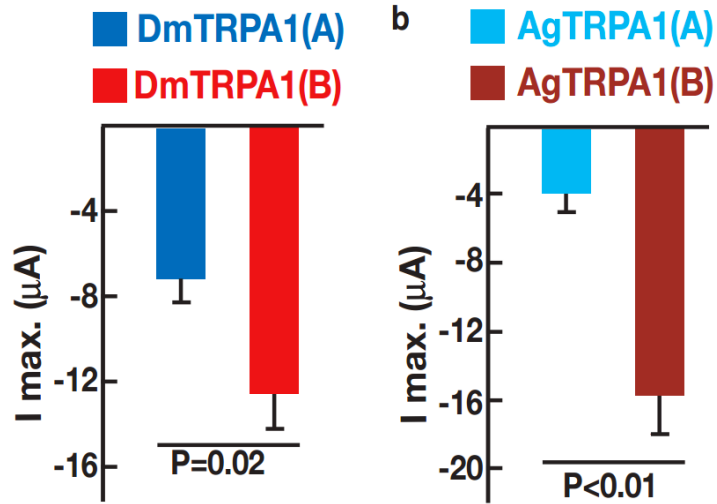


**Figure A1.7. TRPA1 isoform diversity determines sensory specificity of gustatory neurons.** **a-c.** TrpA1 mutant, berberine-sensitive i-type bristles expressing different TRPA1 isoforms. **a, b,** Electrophysiological responses to NMM (**a**) and warming (**b**). **c.** Quantification. **d-f.** L-type bristles expressing TRPA1 isoforms. Responses to NMM (**d**) and warming (**e**). **f.** Quantification. **g.** Rescue of TrpA1 mutant behavioral response to NMM-containing food. PER, proboscis extension response. **h.** Warmth-induced regurgitation in *TrpA1* mutant rescued with TRPA1(B). **i.** Regurgitation upon warming from room temperature (~23°C) to 32°C. In (c, f, g and i, statistically distinct groups are marked by a, b and c. (Tukey honestly significant difference (HSD) test,  $\alpha = 0.01$ ). Data are mean  $\pm$  s.e.m.

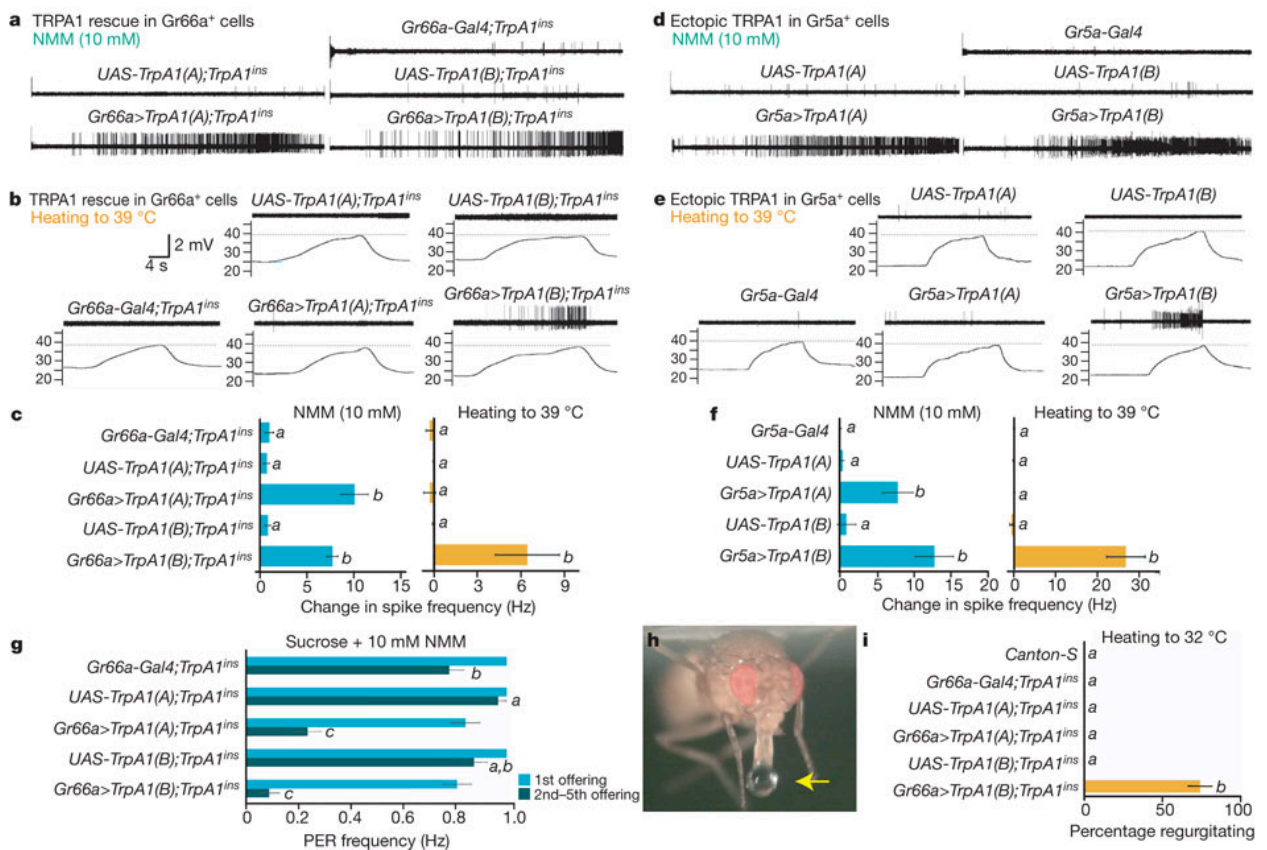


**Figure A1.8.** Supplementary Figure 5: Example responses from labellar gustatory bristles for TRPA1 rescue and gain-of-function. a, b, Responses of *TrpA1<sup>ins</sup>* mutant, berberine-sensitive i-type bristles expressing different TRPA1 isoforms. a, c, Typical responses of bristles to electrolyte-only solution (30 mM tricholine citrate). b, d, Typical responses to positive control solutions used to confirm preparation viability. Berberine-sensitive i-type bristles confirmed with 1 mM berberine chloride (b) and L-type bristles confirmed with 30 mM sucrose (d).

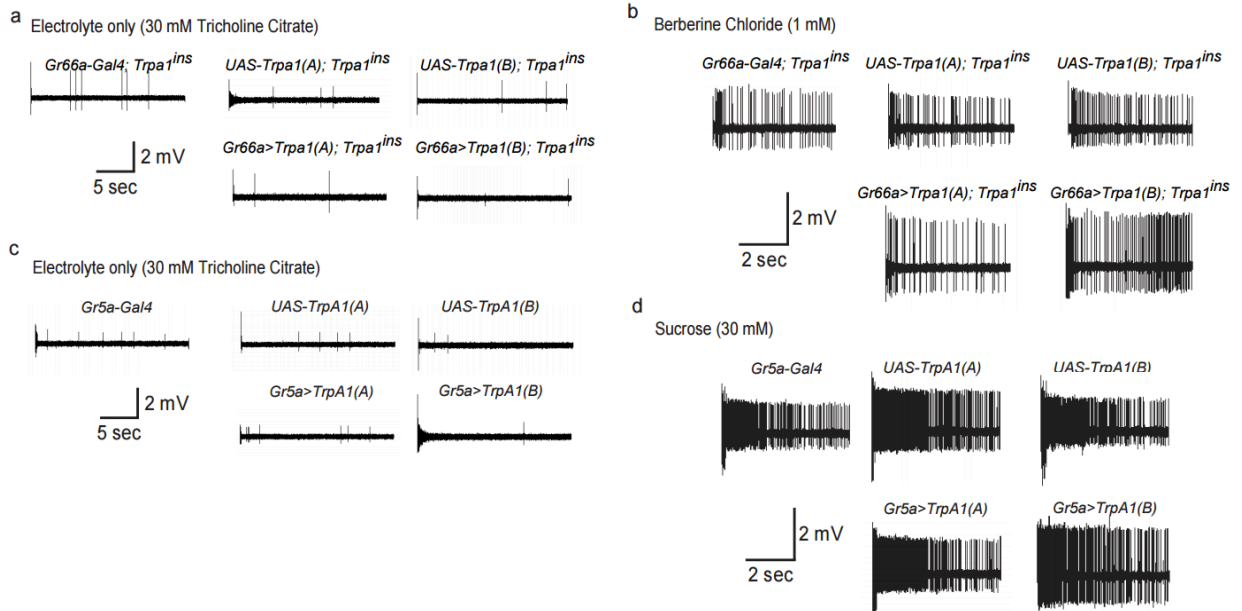


**Figure A1.9. Regulation of insect TRPA1 thermosensitivity by alternative N termini.** **a.** TRPA1 sequence alignments. *Acyr. pisum*, *Acyrthosiphon pisum*; *Aedes ag.*, *A. aegypti*; *Anopheles g.*, *A. gambiae*; *Dros. mel.*, *D. melanogaster*; *Dros. vir.*, *D. virilis*. **b.**  $Q_{10}$  values and transition temperatures (Trans. temp.) of wild-type (WT) and mutant TRPA1. *Dm*, *D. melanogaster*. a, b and c denote statistically distinct groups (Tukey HSD,  $\alpha = 0.02$ ). **c.** Arrhenius plots of indicated channels. **d.** *A. gambiae* (Ag)TrpA1 gene structure. **e.** AgTRPA1 isoforms. a, ankyrin repeat; aa, amino acids. Blue and dark red indicate isoform-specific amino acids. Dark grey indicates transmembrane (TM) region. **f-h.** Temperature sensitivity of AgTRPA1(A) and AgTRPA1(B). **f, g.** Traces (f) and Arrhenius plots (g) of temperature-dependent current recordings at 260 mV in *Xenopus* oocytes. **h.**  $Q_{10}$  values from Arrhenius plot (left) or 27–37°C (right) (\*\* $P < 0.01$ , t-test). Error bars,  $\pm$  s.e.m.

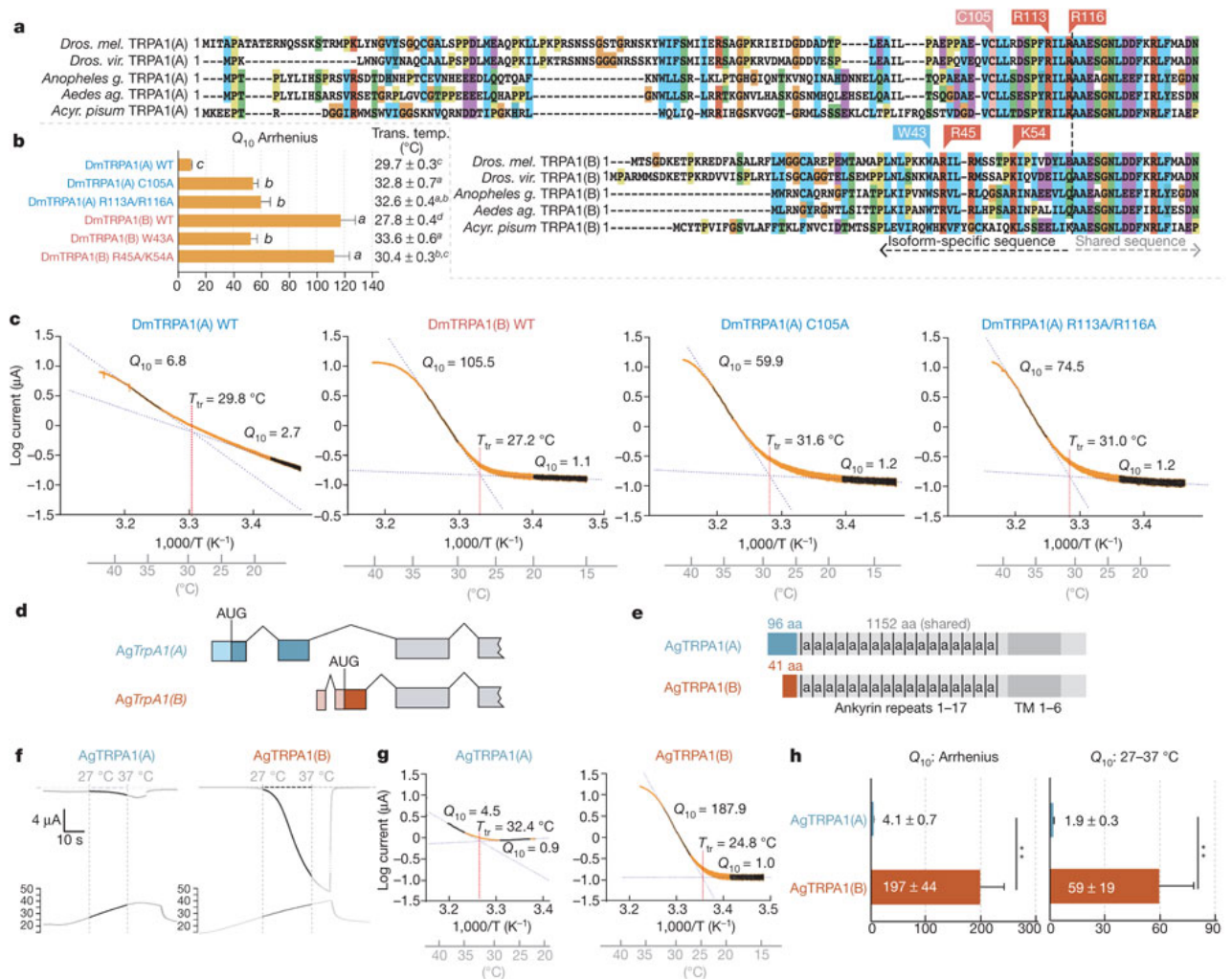


**Figure A1.10. Representative current recordings of wild type TRPA1 isoforms and TRPA1(A) mutants.** Lower traces show temperature ramps from 15 to 45 °C (~0.5 °C/sec) applied to frog oocytes expressing TRPA1 channels as indicated. Currents were recorded at -60 mV held by two-electrode voltage clamp. *a-d*. The corresponding arrhenius plots are presented in Figure 4.

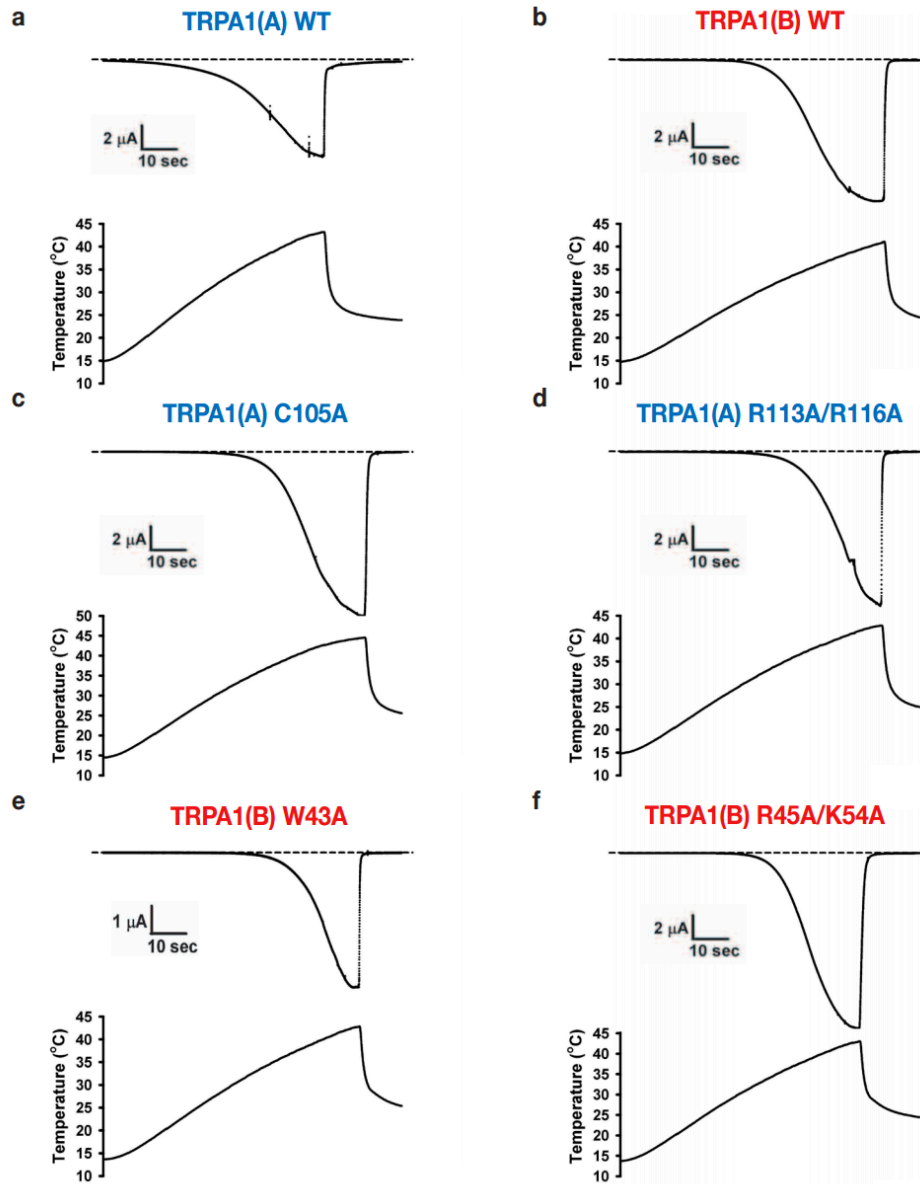


**Figure A1.11. Comparison of maximum current responses for wild-type and mutant TRPA1 channels.** Maximum TRPA1-dependent currents generated by temperature increase and by 300  $\mu$ M NMM application in oocytes. For comparison to wild type channels, the heat responses of mutant channels that exhibited increased thermal sensitivity by Q10 (TRPA1(A)C105A and TRPA1(A) R113A/R116A) were normalized by dividing maximum heat responses by maximum NMM responses.

	<b>I<sub>max</sub> (heat)</b>	<b>I<sub>max</sub> (NMM)</b>	<b>I<sub>max</sub> (heat)/I<sub>max</sub> (NMM)</b>
<b>TRPA1(A) WT</b>	<b>-7.3 +/- 1.1</b>	<b>-20.3 +/- 2.1</b>	<b>0.36</b>
<b>TRPA1(A) C105A</b>	<b>-7.9 +/- 2.1</b>	<b>-14.1 +/- 2.4</b>	<b>0.56</b>
<b>TRPA1(A) R113A/R116A</b>	<b>-7.8 +/- 1.4</b>	<b>-13.1 +/- 1.9</b>	<b>0.59</b>
<b>TRPA1(B) WT</b>	<b>-12.4 +/- 1.7</b>	<b>-24.2 +/- 0.6</b>	<b>0.51</b>
<b>TRPA1(B) W43A</b>	<b>-3.7 +/- 0.4</b>	nd	---
<b>TRPA1(B) R45A/K54A</b>	<b>-8.7 +/- 1.5</b>	nd	---

**Figure A1.12. NMM sensitivities of TRPA1(A) mutants are similar to that of wild type TRPA1(A).** A series of NMM concentrations from 50 to 300  $\mu\text{M}$  was applied to *Xenopus* oocytes expressing wild type and mutant forms of TRPA1(A). The data were collected following 1-min perfusion of each NMM concentration at -80 mV, and fitted to the Hill equation. All data are means; error bars indicate +/-SEM

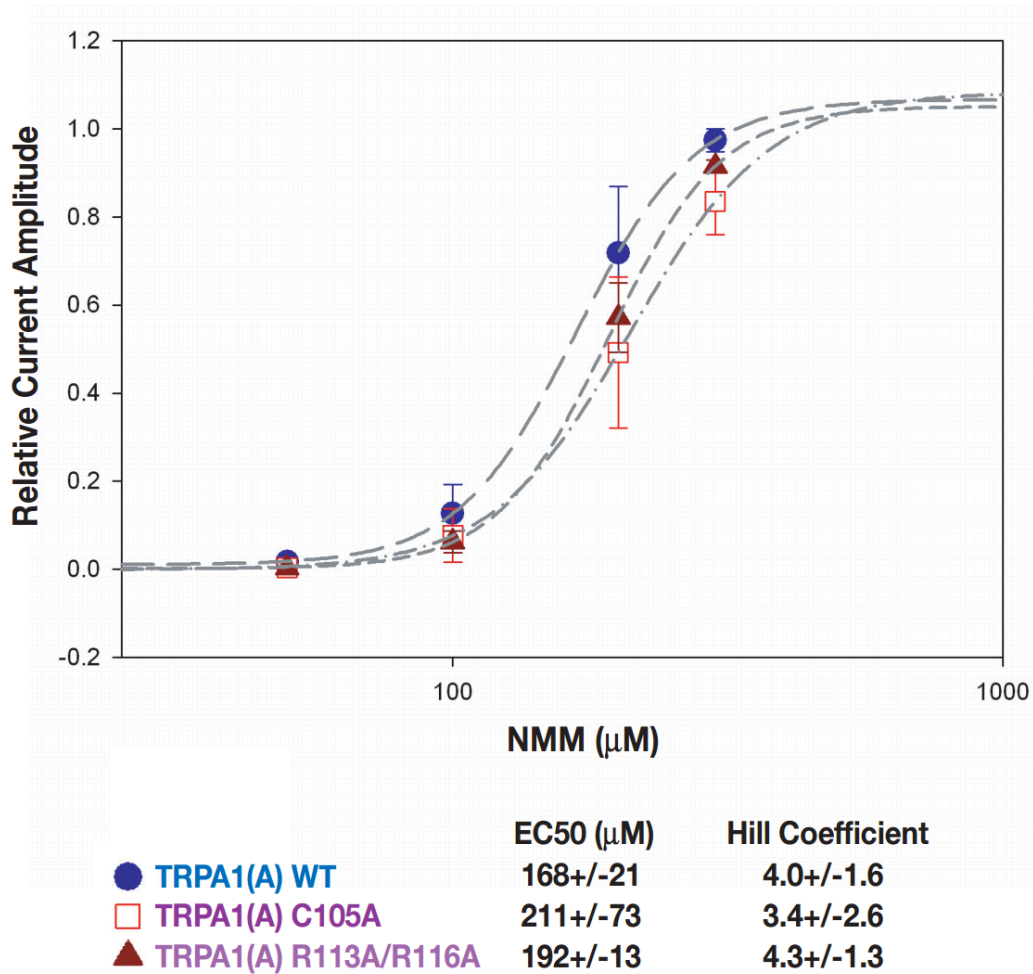


**Figure A1.13. Both agTRPA1(A) and agTRPA1(B) robustly respond to reactive electrophiles. a.** A frog oocyte expressing agTRPA1(A) was perfused with 40  $\mu\text{M}$  allylthiocyanate (AITC) for 1 min, and washed for 30 sec. Subsequently, the AITC-evoked current was blocked by 100  $\mu\text{M}$  ruthenium red (RuR). The current was recorded at -60 mV held by two-electrode voltage clamp (TEVC). **b.** Three concentrations of NMM from 50 to 200  $\mu\text{M}$  were sequentially exposed to a oocyte expressing agTRPA1(B) with 30 sec washing intervals as indicated. Currents were recorded while 300 msec-voltage swipes between -80 and 80 mV were applied every second via TEVC.

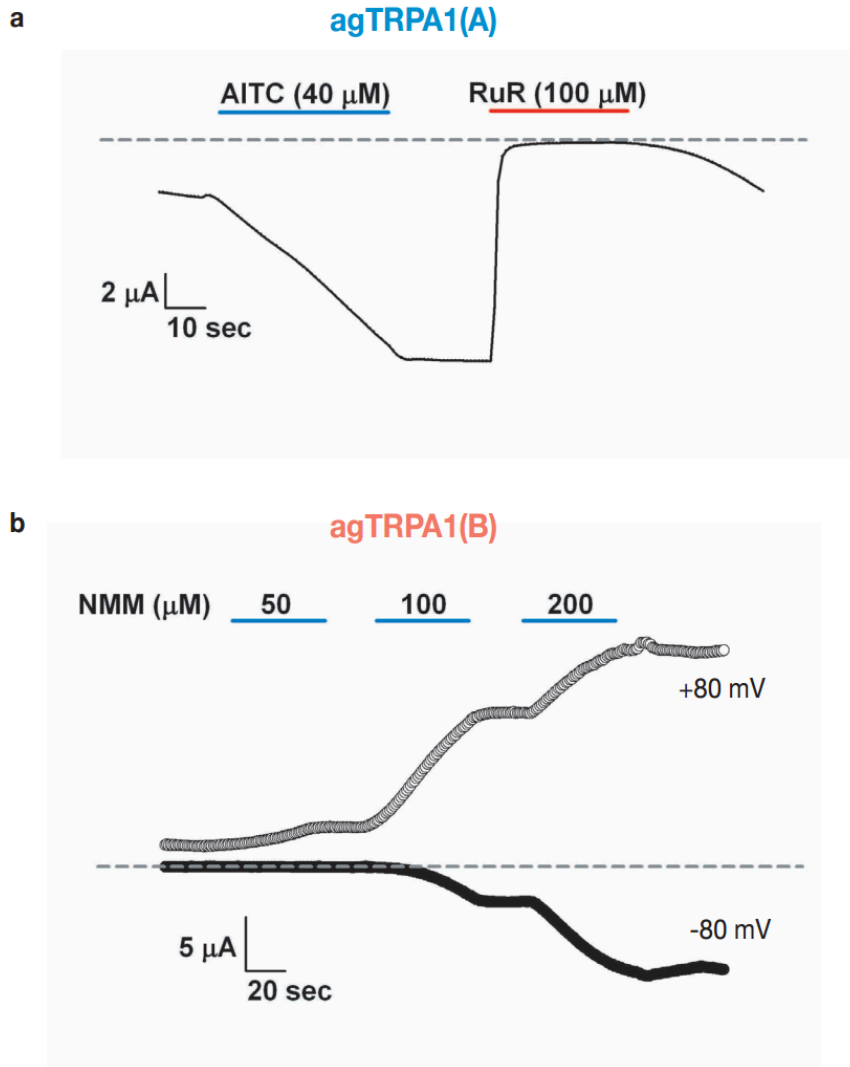
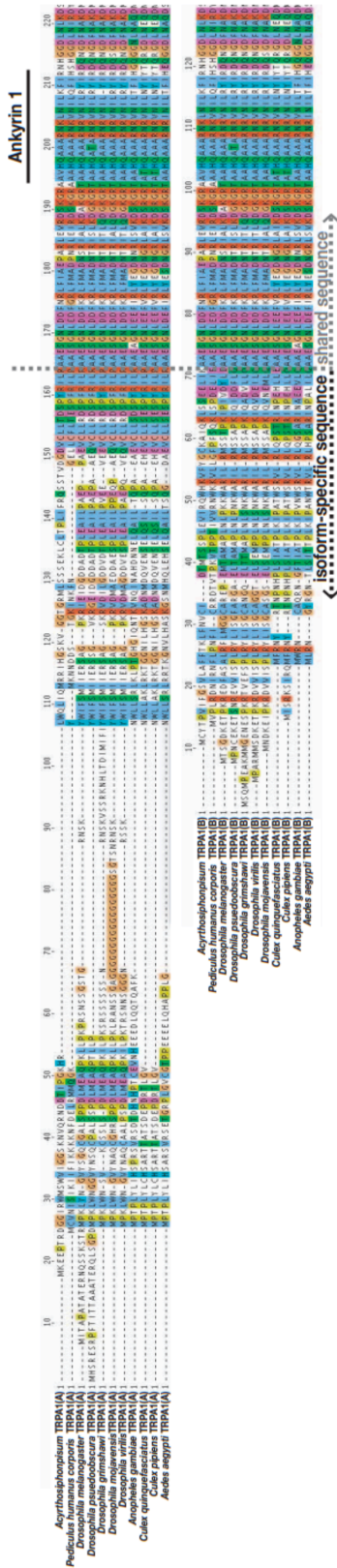




**Figure A1.14. Conservation of TRPA1 diversity in insect pests.** Multiple sequence alignments of insect TRPA1 isoforms. Position of ankyrin repeat #1 in TRPA1 is noted.



## **CHAPTER AII**

**CYP6 P450 Enzymes and *ACE-1* Duplication Produce Extreme and Multiple  
Insecticide Resistance in the Malaria Mosquito *Anopheles gambiae***

Constant V. Edi, Luc Djogbénou, Adam M. Jenkins, Kimberly Regna, Marc A. T. Muskavitch, Rodolphe Poupardin, Christopher M. Jones, John Essandoh, Guillaume K. Kétoh, Mark J. I. Paine, Benjamin G. Koudou, Martin J. Donnelly Hilary Ranson, David Weetman. CYP6 P450 Enzymes and ACE-1 Duplication Produce Extreme and Multiple Insecticide Resistance in the Malaria Mosquito *Anopheles gambiae*. *PLoS Genet* **10**, e1004236 (2014).

## **A. ABSTRACT**

Malaria control relies heavily on pyrethroid insecticides, to which susceptibility is declining in *Anopheles* mosquitoes. To combat pyrethroid resistance, application of alternative insecticides is advocated for indoor residual spraying (IRS), and carbamates are increasingly important. Emergence of a very strong carbamate resistance phenotype in *Anopheles gambiae* from Tiassalé, Côte d'Ivoire, West Africa, is therefore a potentially major operational challenge, particularly because these malaria vectors now exhibit resistance to multiple insecticide classes. We investigated the genetic basis of resistance to the most commonly-applied carbamate, bendiocarb, in *An. gambiae* from Tiassalé. Geographically-replicated whole genome microarray experiments identified elevated P450 enzyme expression as associated with bendiocarb resistance, most notably genes from the CYP6 subfamily. P450s were further implicated in resistance phenotypes by induction of significantly elevated mortality to bendiocarb by the synergist piperonyl butoxide (PBO), which also enhanced the action of pyrethroids and an organophosphate. *CYP6P3* and especially *CYP6M2* produced bendiocarb resistance via transgenic expression in *Drosophila* in addition to pyrethroid resistance for both genes, and DDT resistance for *CYP6M2* expression. *CYP6M2* can thus cause resistance to three distinct

classes of insecticide although the biochemical mechanism for carbamates is unclear because, in contrast to CYP6P3, recombinant CYP6M2 did not metabolize bendiocarb in vitro. Strongly bendiocarb resistant mosquitoes also displayed elevated expression of the acetylcholinesterase *ACE-1* gene, arising at least in part from gene duplication, which confers a survival advantage to carriers of additional copies of resistant *ACE-1* G119S alleles. Our results are alarming for vector-based malaria control. Extreme carbamate resistance in Tiassalé *An. gambiae* results from coupling of over-expressed target site allelic variants with heightened CYP6 P450 expression, which also provides resistance across contrasting insecticides. Mosquito populations displaying such a diverse basis of extreme and cross-resistance are likely to be unresponsive to standard insecticide resistance management practices.

## **B. INTRODUCTION**

Malaria mortality has decreased substantially in sub-Saharan Africa over the last decade, attributed in part to a massive scale-up in insecticide-based vector control interventions (WHO World Health Organization 2011). As the only insecticide class approved for treatment of bednets (ITNs) and the most widely used for indoor residual spraying (IRS), pyrethroids are by far the most important class of insecticides for control of malaria vectors (van den Berg et al. 2012). Unfortunately pyrethroid resistance is now widespread and increasing in the most important malaria-transmitting *Anopheles* species (Badolo et al. 2012; Ranson et al. 2009; Ranson et al. 2011) and catastrophic consequences are predicted for disease control if major pyrethroid failure occurs (WHO World Health Organization 2012). With no entirely new insecticide classes for public

health anticipated for several years (Ranson et al. 2011; WHO World Health Organization 2012) preservation of pyrethroid efficacy is critically dependent upon strategies such as rotation or combination of pyrethroids with just three other insecticide classes, organochlorines, carbamates and organophosphates (WHO World Health Organization 2012; Insecticide Resistance Action Committee 2011). In addition to logistical and financial issues, insecticide resistance management suffers from knowledge-gaps concerning mechanisms causing cross-resistance between available alternative insecticides, and more, generally how high-level resistance arises (Namountougou et al. 2012). With strongly- and multiply-resistant phenotypes documented increasingly in populations of the major malaria vector *Anopheles gambiae* in West Africa (Namountougou et al. 2012; Corbel et al. 2007; Edi et al. 2012) such information is urgently required.

Of the four classes of conventional insecticide licensed by the World Health Organization (WHO), pyrethroids and DDT (the only organochlorine) both target the same *para*-type voltage-gated sodium channel (VGSC). This creates an inherent vulnerability to cross-resistance via mutations in the VGSC target site gene (Martinez-Torres et al. 1998; H Ranson et al. 2000; Jones, Liyanapathirana, et al. 2012a), which are now widespread in *An. gambiae* (Ranson et al. 2011). In contrast, carbamates and organophosphates cause insect death by blocking synaptic neurotransmission via inhibition of acetylcholinesterase (AChE), encoded by the *ACE-1* gene in *An. gambiae*. Consequently, target site mutations in the VGSC gene producing resistance to pyrethroids and DDT will not cause cross-resistance to carbamates and organophosphates. The carbamate bendiocarb is being used increasingly for IRS (Akogbéto et al. 2010;

Akogbeto et al. 2011), and has proved effective in malaria control programs across Africa targeting pyrethroid- or DDT-resistant *An. gambiae* (Akogbéto et al. 2010; Akogbeto et al. 2011; Kigozi et al. 2012). A single nucleotide substitution of glycine to serine at codon position 119 (*Torpedo* nomenclature; G119S) in the *ACE-1* gene, which causes a major conformational change in AChE, has arisen multiple times in culicid mosquitoes (Weill et al. 2003; Weill et al. 2004), and is found in *An. gambiae* throughout West Africa (Djogbénoú et al. 2008; Dabire et al. 2009; Ahoua Alou et al. 2010). The G119S mutation can produce carbamate or organophosphate resistance (Djogbenou et al. 2007) but typically entails considerable fitness costs (Lenormand et al. 1999; Labbé et al. 2007; Djogbénoú et al. 2010; Labbe et al. 2007). This is beneficial for resistance management because in the absence of carbamates or organophosphates, serine frequencies should fall rapidly (Djogbénoú et al. 2010; Gassmann et al. 2009). In *Culex pipiens*, duplications of *ACE-1* create linked serine and glycine alleles, which, when combined with an unduplicated serine allele, creates highly insecticide resistant genotypes with near-full wild-type functionality, thus providing a mechanism that can compensate for fitness costs (Labbé et al. 2007; Gassmann et al. 2009). Worryingly, duplication has also been found in *An. gambiae* (Djogbénoú et al. 2008) though the consequences of copy number variation for fitness in the presence or absence of insecticide are not yet known in *Anopheles*. Though far from complete, information is available for metabolic resistance mechanisms to pyrethroids and DDT in wild populations of *An. gambiae* (Ranson et al. 2011; WHO World Health Organization 2012; Mitchell et al. 2012; Djogbénoú et al. 2008; Müller et al. 2008). Indeed, a specific P450 enzyme, CYP6M2, has been demonstrated to metabolize both of these insecticide classes, suggesting the potential to

cause cross-resistance in *An. gambiae* (Mitchell et al. 2012; Stevenson et al. 2011). By contrast little is known about metabolic mechanisms of carbamate resistance in mosquitoes and, as a consequence, potential for mechanisms of cross-resistance are unknown.

A particularly striking and potentially problematic example of insecticide resistance has been found in one of the two morphologically identical, but ecologically and genetically divergent molecular forms comprising the *An. gambiae* s.s. species pair (M molecular form, recently renamed as *An. coluzzii* (Coetzee et al. 2013)) in Tiassalé, southern Côte d'Ivoire. The Tiassalé population is resistant to all available insecticide classes, and displays extreme levels of resistance to pyrethroids and carbamates (Edi et al. 2012). The *VGSC* 1014F (*kdr*) and *ACE-1* G119S mutations are both found in Tiassalé (Edi et al. 2012; Ahoua Alou et al. 2010). Yet *kdr* shows little association with pyrethroid resistance in adult females in this population (Edi et al. 2012). *ACE-1* G119S is associated with both carbamate and organophosphate survivorship (Edi et al. 2012), but this mutation alone cannot fully explain the range of resistant phenotypes, suggesting that additional mechanisms must be involved. Here we apply whole genome microarrays, transgenic functional validation of candidates, insecticide synergist bioassays, target-site genotyping and copy number variant analysis to investigate the genetic basis of (1) extreme bendiocarb resistance and (2) cross-insecticide resistance in *An. gambiae* from Tiassalé. Our results indicate that bendiocarb resistance in Tiassalé is caused by a combination of target site gene mutation and duplication, and by specific P450 enzymes which produce resistance across other insecticide classes.

## C. RESULTS

### Whole Genome Transcription Analysis

Our study involved two microarray experiments (hereafter referred to as Exp1 and Exp2), involving solely M molecular form *An. gambiae*, to identify candidate genes involved in bendiocarb resistance. In Exp1 gene expression profiles of female mosquitoes from bendiocarb-susceptible laboratory strains (NGousso and Mali-NIH) and a bendiocarb-susceptible field population (Okyereko, Ghana), none of which were exposed to insecticide, were compared to those of Tiassalé females. Two Tiassalé groups were used: either without insecticide exposure (Figure A2.1A), or the survivors of bendiocarb exposure selecting for the 20% most resistant females in the population (Edi et al. 2012) (Figure 2.1B). We used a stringent filtering process to determine significant differential expression (detailed in the legend to Figure A2.1), which included criteria on both the probability and consistency of direction of differential expression, and also required a more extreme level of differential expression in the Tiassalé-selected than Tiassalé (unexposed) vs. susceptible comparisons. Inclusion of this third criterion enhanced the likelihood that genes exhibiting differential expression are associated with bendiocarb resistance, rather than implicated via indirect association with another insecticide. Moreover, the requirement for significance in comparisons involving both bendiocarb-exposed and unexposed Tiassalé samples (Figure A2.1A, B) negates the possibility that any differential expression identified was a result solely of induction of gene expression by insecticide exposure.



In Exp1 145 probes were significant, out of a total of 14 914 non-control probes, with almost all (143/145) expressed at a higher level in the resistant samples. Functional annotation clustering analysis detected two significant clusters within the significantly over-expressed genes. The larger cluster was enriched for several P450s and the functionally-related genes cytochrome b5 and cytochrome P450 reductase. Of these, *CYP6P3*, *CYP6P4*, *CYP6M2* and cytochrome b5 are evident amongst the most significant and/or over-expressed probes in Figure A2.2A. Of the five physically-adjacent CYP6P subfamily genes in *An. gambiae*, *CYP6P1* and *CYP6P2* were also significant, and *CYP6P5* only marginally non-significant according to our strict criteria (five out of the six comparisons  $q < 0.05$ ). The four probes for the *ACE-1* target site gene exhibited the strongest statistical support (lowest q-values) for resistance-associated overexpression in the Exp1 dataset (Figure A2.2A).

Experiment 2 employed a simpler design in which bendiocarb resistant samples from Kovié (Togo) were compared to the same Okyereko field samples used in Exp1 and to a second field population from Malanville (Benin). Significant differential expression was determined according to the first two criteria employed for analysis of Exp1 (Figure A2.1). The likelihood of specificity of results to the bendiocarb resistance phenotype was enhanced because all three populations used in Exp2 exhibit resistance to pyrethroids and DDT, all are susceptible to organophosphates, but only the Kovié population is resistant to bendiocarb. In Exp2 2453 probes were significantly differentially expressed; likely reflecting the lower number of pairwise comparisons available for stringent filtering than in Exp1. Consequently we do not consider results from Exp2 alone in detail. Nevertheless it is interesting to note that the lowest q-values and highest fold-changes were both for

alcohol dehydrogenase genes (Figure A2.3), and the latter is the physical neighbor and closest paralogue of the highly overexpressed alcohol dehydrogenase in Exp1 (Figure A2.2A). Sixteen probes, representing only seven genes, were significant in both Exp1 and Exp2 (Figure A2.2B), including all replicate probes for three of the CYP6 P450 genes highlighted previously. Of these, *CYP6M2* was most highly over-expressed, second only to *Ribonuclease t2*. However, results for *Ribonuclease t2* were much more variable, with differential expression dramatically high compared to lab strains, but moderate or low compared to wild populations. Evidence for specific involvement in bendiocarb resistance is suggested by significance of two of the *CYP6M2* probes in the (relatively low-powered) direct comparison of bendiocarb selected vs. unselected samples within Exp1; the other two *CYP6M2* probes and two of those for *ACE-1* were marginally non-significant ( $0.05 < q < 0.10$ ; Figure A2.4).

### **qRT-PCR Expression of Candidate Genes**

Five genes were chosen for further analysis: *ACE-1* and *CYP6P3* from Exp1; *CYP6M2* and *CYP6P4* from Exp1+Exp2; and *CYP6P5*, which we included because of a suspected type II error in the microarray analysis (see above). qRT-PCR estimates of expression, relative to the susceptible Okyereko population, showed reasonable agreement with microarray estimates albeit with some lower estimates (Figure A2.5). *CYP6M2* and *CYP6P4* exhibited up to eight and nine-fold overexpression, and *ACE-1* six-fold compared to Okyereko, though high variability among biological replicates for the P450 genes resulted in relatively few significant pairwise comparisons (Figure A2.6). Nevertheless the hypothesis that fold-changes should follow the rank order predicted by

the level of bendiocarb resistance in each comparison (i.e. Tiassalé selected>Tiassalé unexposed>Kovié) was met qualitatively for all genes (Figure A2.6).

### **Insecticide Resistance Phenotypes of CYP6 Genes in *Drosophila***

For functional validation via transgenic expression in *D. melanogaster*, we chose *CYP6P3* and *CYP6M2*; both of which have been shown to metabolize pyrethroids (Müller et al. 2008; Stevenson et al. 2011), and *CYP6M2* also DDT (Mitchell et al. 2012). The capacity of each gene to confer resistance to bendiocarb, to the class I and II pyrethroids permethrin and deltamethrin, respectively, and to DDT and was assessed by comparing survival of transgenic *D. melanogaster*, exhibiting ubiquitous expression of *CYP6M2* or *CYP6P3* (e.g. UAS-*CYP6M2*/ACT5C-GAL4 experimental class flies), to that of flies carrying the UAS-*CYP6M2* or *CYP6P3* responder, but lacking the ACT5C-GAL4 driver (e.g. UAS-*CYP6M2*/CyO control class flies). For *CYP6M2* the relative expression level of the experimental flies was 4.0 and for *CYP6P3* 4.3 (Table A2.2). As indicated by elevated LC<sub>50</sub> values (Figure 2.7), expression of either *CYP6M2* or *CYP6P3* produced pyrethroid resistant phenotypes, and *CYP6M2* expression also induced significant DDT resistance (Table A2.1). Assays for *CYP6P3* with DDT did not produce reproducible results (data not shown). Flies expressing the candidate genes exhibited greater survival across a narrow range of bendiocarb concentrations (Figure A2.7). However, at a discriminating dosage of 0.1 mg/ vial (NPIC 2002) a resistance ratio of approximately seven was exhibited for *CYP6M2*/ACT5C: *CYP6M2*/CyO flies (Mann-Whitney, P=0.0002; Figure A2.8) with a much smaller, but still significant, ratio of approximately 1.4 (Mann-Whitney, P = 0.019) for *CYP6P3*/ACT5C: *CYP6P3*/CyO flies.

Caution is required in quantitative interpretation of the resistance levels generated, both because of the non-native genetic background and also ubiquitous expression of genes that may be expressed in a tissue-specific manner (Baker et al. 2011). Nevertheless, the bioassays on transgenic *Drosophila* show that each P450s can confer resistance to more than one insecticide class.

### ***In vitro* Metabolism Assays**

Recombinant *CYP6M2* and *CYP6P3* were expressed in *E. coli* with *An. gambiae* NADPH P450 reductase and cytochrome b5. An initial experiment, using 0.1 mM P450 and 2 hour incubation with bendiocarb, demonstrated metabolism of bendiocarb by *CYP6P3* (64.2% mean depletion 64.0% st.dev) but no metabolic activity of *CYP6M2* (0611.0%). Further investigation of *CYP6P3* activity across a range of incubation times (Figure A2.9A) and enzyme concentrations (Figure A2.9B) supported the initial observation, with metabolism plateauing at a maximum of 50%.

### **Resistance Phenotypes and Inhibition**

*An. gambiae* from Tiassalé are classified as resistant to all classes of WHO-approved insecticides (<90% bioassay mortality 24 hours after a 60 min exposure), with resistance phenotypes stable across wet and dry seasons (Figure A2.10, Table A2.3). Nevertheless, resistance varies markedly among insecticides (Table A2.3), with notably higher prevalence for bendiocarb and DDT than the organophosphate fenitrothion. The synergist PBO, which is primarily considered an inhibitor of P450 enzymes, exerted a

significant influence on bioassay mortality (Table A2.3) for four of the five insecticides tested, with only DDT not significantly impacted (Figure A2.10). The synergizing effect of PBO was strongest for bendiocarb, with a near five-fold increase in mortality, equivalent to an odds ratio for PBO-induced insecticidal mortality exceeding ten (Figure A2.10). However, for all of the insecticides, apart from fenitrothion, over 20% of the population survived even with PBO pre-exposure.

### **AChE Target Site Resistance**

The *ACE-1* G119S substitution is the only non-synonymous target site mutation known in *An. gambiae* (Djogbénu et al. 2008), and the resistant (serine) allele is common in Tiassalé with an estimated frequency of 0.46 (N=306). All occurrences of serine are in heterozygotes (95% confidence limits for heterozygote frequency: 0.87–0.94), which underlies a dramatic deviation of genotype frequencies from Hardy-Weinberg equilibrium ( $\chi^2 = 135.5$ ,  $P < 0$ ). To examine the independence of putatively P450-mediated resistance and AChE target site insensitivity, we typed the G119S locus in females from the diagnostic (60 min) bendiocarb assays with and without pre-exposure to PBO. In either case absence of the 119 serine allele appears to almost guarantee mortality to bendiocarb (Table A2.4), as previously observed for fenitrothion bioassays in Tiassalé (Edi et al. 2012). However, the strong bendiocarb resistance association of G119S was reduced significantly by PBO pre-exposure (homogeneity  $\chi^2 = 8.3$ ,  $P = 0.004$ ) with the probability of survival for heterozygotes reduced to approximately 50% (Table A2.4). To investigate whether heterozygote survivorship might be linked to copy number variation, via a difference in numbers of serine and

glycine alleles, we examined the qPCR dye balance ratio for live and dead individuals within the heterozygote genotype call cluster (Figure A2.11A). In many individuals called as heterozygotes, a markedly higher ratio of 119S: 119G dye label than the 1:1 expected for a true heterozygote is evident (Figure A2.11A), and surviving heterozygotes exhibited a significantly higher serine: glycine dye signal ratio than those killed (t-test,  $P = 1.5 \times 10^{-5}$ ). We designed an additional qRT-PCR diagnostic to investigate copy number more directly in a portion of the surviving and dead individuals typed as G119S heterozygotes. The difference in copy number was highly significant between survivors and dead (Figure A2.11B), with 15/16 survivors but only 5/16 dead females exhibiting a copy number ratio in excess of 1.5 (Table A2.4), consistent with possession of an additional allele. These results show that independent of the enzymes inhibited by PBO survival, females heterozygous for the G119S mutation (i.e. most individuals in Tiassalé) depends upon *Ace-1* copy number variation and possession of additional resistant serine alleles.

#### **D. DISCUSSION**

Bendiocarb is an increasingly important alternative to pyrethroids for IRS, but with carbamate resistant malaria vectors now established in West Africa (Namountougou et al. 2012; Corbel et al. 2007; Edi et al. 2012; Oduola et al. 2012; Okoye et al. 2008) detailed understanding of the underlying mechanisms is urgently required to combat resistance and avoid cross-resistance (WHO World Health Organization 2012). Exhibiting the most extreme carbamate resistance and multiple insecticide resistance

phenotypes documented to date in *An. gambiae* (Edi et al. 2012), the Tiassalé population represents an especially suitable model to address this question. Our results show how P450s contribute to multiple resistance in Tiassalé, and couple with overexpression of *ACE-1* resistant alleles to produce extreme bendiocarb resistance.

### **P450s in Carbamate Resistance and Cross-resistance**

The major biochemical mechanisms of carbamate resistance in mosquitoes have previously been identified as modified AChE (via point substitutions, most notably G119S) and less frequently esterase-mediated metabolism (Insecticide Resistance Action Committee 2011). PBO-induced increases in carbamate mortality have been reported in wild mosquito populations exhibiting low to moderate resistance levels, including M form *An. gambiae* from West Africa (Oduola et al. 2012; Koffi et al. 2013; Brooke et al. 2001). The significant synergizing effect of PBO in the present work and these previous studies is consistent with a role of P450s in carbamate resistance, but should not be taken alone as direct proof (Farnham 2015) because PBO exposure can also inhibit some esterases (Young et al. 2005; Gunning et al. 1998). However, our microarray data clearly identified over-expression of multiple *CYP6* P450 genes, whereas only a single carboxylesterase gene (*COEAE6G*) was significant, and expressed at a lower level. Taken together, the synergist data and transcriptional profiles indicate that a substantial proportion of the Tiassalé population is dependent upon the action of P450s for resistance to bendiocarb. Near-equivalent synergism of permethrin and deltamethrin, coupled with identification and functional validation of shared candidate genes, suggests the same conclusion for pyrethroids. For fenitrothion, the effect of PBO is also consistent with

P450 involvement, but in the absence of specific candidate genes, additional supporting evidence will be required to confirm this hypothesis.

Genes from the CYP6P cluster emerged as strong candidates for involvement in P450-mediated detoxification. *CYP6P3* overexpression has been linked repeatedly with pyrethroid resistance in *An. gambiae* (Djogbénou et al. 2008; Müller et al. 2008), as has its ortholog in *An. funestus* *CYP6P9* (Wondji et al. 2009; Riveron et al. 2013) and both enzymes can metabolize class I and II pyrethroids (Müller et al. 2008; Stevenson et al. 2011; Riveron et al. 2013). We demonstrate that *CYP6P3* can produce significant resistance to both classes of pyrethroid and, to a lesser extent bendiocarb, in *D. melanogaster*. We also show that recombinant *CYP6P3* can metabolize bendiocarb *in vitro*; the third mosquito P450 to metabolize a carbamates, after *An. gambiae* CYP6Z1 and CYP6Z2 which have been demonstrated to metabolize the insecticide carbaryl (Chiu et al. 2008). Interestingly *CYP6P4*, which, in contrast to *CYP6P3*, was also significantly overexpressed in the Togolese Kovié population, is the ortholog of the resistance-associated *CYP6P4* gene in *An. funestus* (Wondji et al. 2009), and along with *CYP6P3* was recently found to be overexpressed in DDT-resistant samples of both M and S molecular forms of *An. gambiae* from Cameroon (Fossog Tene et al. 2013). Although we were unable to obtain data for the impact of *CYP6P3* expression on survival with DDT exposure in *D. melanogaster*, the potential of *CYP6P* genes to act on DDT merits further investigation. It is also interesting to note that both cytochrome b5 and cytochrome P450 reductase, both important for P450-mediated insecticidal detoxification (Liu & Scott 1996) are overexpressed in Tiassalé, suggesting a possible role in resistance for co-expression of these genes with the CYP6 P450s.



*CYP6M2* was overexpressed in Tiassalé, Kovié, and also in the Tiassalé bendiocarb-selected vs. control comparison. *CYP6M2* expression generated *Drosophila* phenotypes significantly resistant to bendiocarb, DDT, and class I and II pyrethroids. Overexpression of *CYP6M2* has been linked repeatedly to pyrethroid (Djogbénu et al. 2008; Müller et al. 2008) and DDT resistance (Mitchell et al. 2012; Fossog Tene et al. 2013) in *An. gambiae*, and is known to metabolize both these classes of insecticide (Mitchell et al. 2012; Stevenson et al. 2011). Our data now suggest a role in bendiocarb resistance, and overall provide strong evidence for involvement in resistance to three classes of insecticide. The biochemical mechanism of involvement remains unclear however because *CYP6M2* did not metabolize bendiocarb *in vitro*, though we cannot rule out the possibility that some unknown, and thus currently, absent co-factor might be required. Sequestration also seems unlikely since *CYP6M2* does not appear to bind bendiocarb. A role in breakdown of secondary bendiocarb metabolites certainly remains plausible, though at present knowledge of such mechanisms for any insecticide in mosquitoes is very limited (David et al. 2013; Chandor Proust et al. 2013). High variability in *CYP6M2* expression among biological replicates, especially evident in qRT-PCR, suggests that the regulatory mechanism(s) generating overexpression is far from fixation in Tiassalé. Further work is required to determine whether the cause of overexpression might be gene amplification, as seen for insecticide-linked *CYP6P* genes in *An. funestus* (Wondji et al. 2009) and *CYP6Y3* in the aphid *Myzus persicae* (Puinean et al. 2010) or a cis regulatory variant, or both, as documented for *CYP6G1* in *D. melanogaster* (Schmidt et al. 2010). In either case, the actual level of expression in individuals possessing causal regulatory variant(s) may be much higher than we detected

from pooled biological replicates. As a consequence, it is possible that *CYP6M2* (and other key P450s) might be expressed at too high a level for PBO to fully inhibit at the dosage applied, resulting in only partial synergy. Indeed it is interesting that *CYP6M2* generated significant DDT resistance in transformed *Drosophila* in our study and has been shown metabolize DDT (Mitchell et al. 2012) yet PBO provided only very slight and non-significant synergy for DDT-exposed Tiassalé females. An inadequate concentration of PBO might be important, but it is worth noting that levels of DDT resistance in West African *An. gambiae* can be extreme and are likely to be underpinned by additional mechanisms (Mitchell et al. 2012) such as the significantly resistance-associated *kdr* L1014F target site mutation in Tiassalé (Edi et al. 2012). Whilst incomplete synergy of highly expressed P450 enzymes might be a partial explanation, our results point to target site mechanisms as a key factor underpinning survival following PBO and bendiocarb exposure.

### **Target Site Insensitivity and Amplification**

Possession of the *ACE-1* 119 serine variant appears to be a near-prerequisite for bendiocarb-survival in Tiassalé, as documented previously for fenitrothion (Edi et al. 2012). This is apparently not the case in all *An. gambiae* populations, with some individuals lacking the serine mutation surviving a standard 60 min exposure (Oduola et al. 2012; Koffi et al. 2013). Over 90% of Tiassalé mosquitoes are heterozygous for G119S, which could be consistent with fitness costs for individuals lacking a fully-functional wild-type allele since the serine allele exhibits lowered activity (Labbé et al. 2007). It is apparent though that possession of the *ACE-1* G119S mutation represents

only a portion of the target site mediated resistance mechanism. Tiassalé females generally showed much higher expression of *ACE-1* than all other populations in our experiments, reaching approximately six-fold in the highly resistant bendiocarb-selected group compared to the Okyereko susceptible group. Following PBO-mediated P450 inhibition, survival of G119S heterozygotes was reduced to approximately 50% and our results show that individuals exhibiting a higher *ACE-1* copy number and more copies of the serine allele had a significant survival advantage. Together these results indicate that the primary explanation for the ubiquitous heterozygosity found in Tiassalé is an elevated copy number of expressed *ACE-1* alleles. At least in individuals possessing additional serine alleles, this enhances carbamate resistance, and can apparently generate resistance independently of P450 activity.

Extra copies of *ACE-1* alleles have been found in West African *An. gambiae*, and lack of sequence variation suggests that duplication is a very recent event (Djogbénu et al. 2008). Consequences of *ACE-1* duplication have not been documented previously in *Anopheles* but *Cx. pipiens* possessing two G119S resistant alleles and a wild type susceptible allele can exhibit near maximal fitness in the presence and absence of organophosphate treatment (Labbé et al. 2007). If this fitness scenario is similar in *An. gambiae* *ACE-1* duplicates could spread rapidly, or may have already done so but have been largely undetected by available diagnostics. The estimated copy numbers we detected in some individuals suggests that more *ACE-1* copies may be present in *An. gambiae* than are known in *Cx. pipiens*, perhaps more akin to the high level of amplification found in spider mites *Tetranychus evansi* (Carvalho et al. 2012). This raises the possibility of a potentially multifarious set of resistant phenotypes dependent upon the

number and G119S genotype of the copies possessed by an individual, understanding of which will benefit from further application of the DNA-based qPCR diagnostic we have developed.

## **Conclusion**

Extreme levels of resistance to single insecticides, and multiple resistance across different insecticidal classes represent major problems for control of disease vectors, and pest insects generally. Tiassalé *An. gambiae* show exceptionally high-level carbamate resistance and the broadest insecticide resistance profile documented to date. Our results indicate that overexpression of specific CYP6 enzymes and duplicated resistant *ACE-1* alleles are major factors contributing to this resistance profile. Results from the less resistant Kovié population show that at least some of the mechanisms are not restricted to Tiassalé and could be quite widespread in West Africa. The involvement of *CYP6P3* and *CYP6M2* in resistance to multiple insecticide classes parallels the cross resistance engendered by *CYP6* genes in other insect taxa (Daborn et al. 2001; Lin & Scott 2011) and is extremely concerning because resilience to standard resistance management strategies is likely to be increased greatly. Further work is now required to understand the biochemical role of *CYP6M2* in detoxification of bendiocarb and also to better understand any associated fitness costs of elevated *CYP6P* gene expression. In addition, whilst we have demonstrated involvement of elevated expression of the CYP6 P450s in insecticide resistance, the impact of structural variants within these genes remains to be investigated and is very poorly understood for P450-mediated insecticide resistance in mosquitoes. In spite of a major impact of PBO on three distinct insecticide classes, too

many females remained alive to suggest that PBO provides a resistance-breaking solution. Nevertheless, we suggest that this preliminary conclusion may be worth further testing: (i) using higher PBO concentrations; (ii) in females old enough to transmit malaria, which are usually less insecticide resistant (Chouaibou et al. 2012; Jones, Sanou, et al. 2012b; Lines & Nassor 1991); or (iii) in less resistant populations. Monitoring the spread of *ACE-I* duplications should be an immediate priority, whereas modification of AChE-targeting insecticides to reduce sensitivity to the G119S substitution (Alout et al. 2012; Wong et al. 2012) represents an important longer-term goal.

## **E. METHODS**

### **Study Design and Samples**

Our study involved *Anopheles gambiae* samples for bioassays coupled with target site genotyping and copy number analysis, and two microarray experiments. The first (Exp1; see Figure A2.1A,B) compared samples from laboratory strains or field populations entirely susceptible to carbamates, with bendiocarb-resistant females from Tiassalé, which were also the subject of bioassays. Exp2 (see Figure A2.1C) involved a comparison of a population moderately resistant to bendiocarb (Kovié) with two fully carbamate susceptible field populations. For field populations, larvae were collected and provided with ground TetraMin fish food. Emerged adults were provided 10% sugar solution. All 3–5 day old females for subsequent gene expression analysis were preserved in RNALater (Sigma). With the exception of a selected group from the Tiassalé

population (below), all samples were preserved without exposure to insecticide. The Tiassalé selected group were survivors of exposure to 0.1% bendiocarb (using WHO tubes and papers) for 360 min which induces approximately 80% mortality after 24 h (11); unexposed controls were held for 360 min with control paper, which did not induce mortality. All mosquitoes used in the study were identified as *An. gambiae* s.s. M molecular form using the SINE-PCR method (Santolamazza et al. 2008).

### **Synergist Bioassays, ACE-1 G119S Genotyping and Copy Number Analysis**

The effect of the insecticide synergist piperonyl butoxide (PBO), a primary action of which is to inhibit P450 monooxygenase enzymes (Farnham 2015), was evaluated using WHO bioassays. Eight replicates of 25 adult female *An. gambiae* emerging from larvae obtained from an irrigated rice field in Tiassalé were exposed to five insecticides (permethrin, deltamethrin, DDT, bendiocarb and fenitrothion). Immediately prior to each 60 min insecticide exposure, mosquitoes were exposed to 4% PBO paper for 60 min. 100 females were exposed to PBO alone as control. Chi-squared tests were used to compare the mortality with and without PBO. A TaqMan qPCR assay (Bass et al. 2010) run on an Agilent Stratagene real-time thermal cycler was used to genotype PBO-exposed samples for the *ACE-1* G119S polymorphism, with qualitative calling of genotypes based on clustering in endpoint scatterplots. G119S genotype call data for samples not exposed to PBO was taken from a prior publication (Edi et al. 2012). Following qualitative genotype calling, endpoint dR values for each dye were exported, and the data from individuals called as heterozygotes was analyzed quantitatively to investigate the possibility of sub-grouping within this genotype cluster. Specifically we tested whether surviving and dead

mosquitoes, heterozygous for G119S, might possess different numbers of serine and alleles by comparing FAM (serine label)/VIC (glycine label) dye ratios using an unequal variance t-test. To further quantify the copy number variation suggested by the TaqMan genotyping results we designed a qRT-PCR to amplify fragments from three different exons of the *ACE-1* gene, with normalization (for varying gDNA concentration among samples) provided via comparison with amplification of a fragment from each of two single-copy genes *CYP4G16* and *Elongation Factor*. Primer details are given in Table A2.5 and qRT-PCR conditions are the same as listed below for gene expression analysis. Relative copy number levels for *Ace-1* were estimated relative to two pools of samples (N = 4 each) from the Kisumu laboratory strain by the  $\Delta\Delta\text{CT}$  method (Schmittgen & Livak 2008).  $\Delta\Delta\text{CT}$  values for each test sample are the mean for the three *ACE-1* amplicons following normalization to both single copy genes and subtraction of the average normalized Kisumu values. Test samples were 16 *ACE-1* G119S heterozygote survivors and 16 dead, chosen at random from those genotyped by the TaqMan assay.  $\Delta\Delta\text{CT}$  values were compared between survivors and dead using an unequal variance t-test.

## **Microarrays**

Total RNA was extracted from batches of 10 mosquitoes using the Ambion RNAqueous-4PCR Kit. RNA quantity and quality was assessed using a NanoDrop spectrophotometer (Thermo Fisher Scientific) and a 2100 Bioanalyzer (Agilent Technologies) before further use. Three biological replicate extractions of total RNA from batches of 10 mosquitoes for each sample population or colony (except Ngouso where there were N = 2 replicates) were labelled and hybridized to *Anopheles gambiae* 8615 k whole genome microarrays

using previously described protocols (Mitchell et al. 2012). Exp 2 employed a fully-interwoven loop design (Figure 2.12), optimal for study power (Cui & Churchill 2003) whilst, owing to the large number of comparisons and unbalanced replication, a pairwise full dye-swap design was used for Exp1 with indirect connection through the (resistant) Tiassalé groups (Fig. A2.1 A,B). Exp1 was analyzed using GeneSpring GX v9.0 software (Agilent), which is readily applied to dye swap experiments, while the R program MAANOVA (Wu et al. 2003), with LIMMA (Koooperberg et al. 2005) for normalization prior to ANOVA, was used to analyze the interwoven loop in Exp2, using previously-described custom R-scripts (Mitchell et al. 2012). For both experiments, the basic significance threshold for any single pairwise comparison was a q-value with false discovery rate (FDR) set at 0.05 (i.e. an FDR-corrected threshold for multiple testing). Full details of the criteria applied to determine overall significance within and across Exp1 and 2 are given in Figure A2.1. Within Exp1, the direct comparison of Tiassalé bendiocarb-selected vs. Tiassalé control comparison was analyzed separately and not used to determine overall significance, owing to the lower power expected for a within-population experiment involving the same level of replication as the cross-population comparisons (Müller et al. 2008). Significantly over-expressed genes emerging from Exp1 were studied at functional level using the software DAVID Bioinformatics resources 6.7 (Huang et al. 2007). Microarray data are deposited with ArrayExpress under accession numbers E-MTAB- 1903 (Exp1) and E-MTAB-1889 (Exp2).



## qRT-PCR

Quantitative real-time PCR was used to provide technical replication of results from the microarray experiments for a subset of significantly over-expressed genes. Samples were converted to cDNA using oligo(dT)<sub>20</sub> (Invitrogen) and Superscript III (Invitrogen) according to the manufacturer's instructions and purified with the QIAquick PCR Purification Kit. Three pairs of exon-spanning primers were designed for each gene of interest and from each triplicate a pair was chosen that produced a single peak from melt curve analysis, and PCR efficiency closest to 100%, determined using a cDNA dilution series obtained from a single sample. Primers details are listed in Table A2.6. All qRT-PCR reactions were run on an Agilent Stratagene real-time thermal cycler and analyzed using Agilent's MXPro software (Mx3005P). The PCR conditions used throughout were 10 min for 95°C, 40 cycles of 10 s at 95°C and 60°C respectively, with melting curves run after each end point amplification at 1 min for 95°C, followed by 30 s increments of 1°C from 55°C to 95°C. The same RNA samples used for microarrays from Tiassalé (selected and unexposed), Kovié and Okyereko plus an additional two replicates (N = 5 for all but the Tiassalé selected group where N = 3) were used. Expression levels for each gene of interest were estimated relative to the Okyereko population (chosen as the reference bendiocarb susceptible group because it was present in both microarray experiments) by the  $\Delta\Delta\text{CT}$  method following correction for variable PCR efficiency (Schmittgen & Livak 2008), and normalization using two stably-expressed genes (*Rsp7* and *Elongation Factor*); primers listed in Table A2.6. Statistical significance of over-expression of each group relative to Okyereko was assessed using equal or unequal variance t-tests as appropriate, depending on results of F-tests for homoscedasticity.

## **Production of Transgenic *Drosophila melanogaster***

cDNA clones containing the open reading frames for *CYP6M2* and *CYP6P3* (sequences from the *An. gambiae* Kisumu laboratory strain) were PCR-amplified using high fidelity AccuPrime Pfx polymerase (Invitrogen). PCR primers contained EcoRI and NotI restriction sites within the forward and reverse primers, respectively. PCR products were gel-purified using the GenElute Gel Extraction Kit (Sigma) and subsequently digested with the aforementioned restriction enzymes (New England Biolabs). The pUAST-attB plasmid (obtained from Dr. Konrad Basler, University of Zurich) digested with EcoRI and NotI was gel purified, as noted above, and incubated with PCR-amplified, restriction enzyme-digested products of the *CYP6M2* or *CYP6P3* clone and T4 DNA ligase (New England Biolabs). Ligation mixtures were transformed into competent DH5 $\alpha$  cells, and individual colonies were verified using PCR. The EndoFree Plasmid Maxi Kit (Qiagen) was utilized to obtain large amounts of plasmids for subsequent steps. pUAST-attB clones containing the *CYP6M2* or *CYP6P3* insertion were sent to Rainbow Transgenic Flies, Inc. (Camarillo, CA, USA) for injection into Bloomington Stock #9750 ( $y^1 w^{1118}$ ; PBac{y<sup>+</sup>-attP-3B}VK00033) embryos. The PhiC31 integration system in this stock enables site-specific recombination between the integration vector (pUAST-attB) and a landing platform in the fly stock (attP) (Wang et al. 2012). Upon receiving the injected embryos, survivors were kept at 25°C, and G<sub>0</sub> flies that eclosed were sorted by sex prior to mating. To establish families of homozygous transgenic flies, G<sub>0</sub> flies were crossed with  $w^{1118}$  flies, and G<sub>1</sub> flies were sorted based on  $w^+$  eye color (as a marker for insertion events). G<sub>1</sub>  $w^+$  flies were crossed *inter se* to obtain homozygous insertion lines. The following *D. melanogaster* stocks were obtained from the Bloomington *Drosophila* Stock

Center (Bloomington, IN, USA):  $y^1 w^1$ ; P{Act5C-GAL4}25FO1/CyO,  $y^+$ ,  $w^*$  (BL4414); P{GawB}Aph-4c232 (BL30828), and  $w^{1118}$  (BL3605). Virgin females from *CYP6M2* or *CYP6P3* insertion stocks were crossed with Act5C-GAL4/CyO (ubiquitous Actin5C driver) flies for expression studies.

### **Transcript Expression Analysis**

For each class within a cross (control and experimental), 8–10 two-day-old flies were obtained and flash-frozen in liquid nitrogen, and then stored at  $-80^\circ\text{C}$  in triplicate. Total RNA was extracted using TRI Reagent (Sigma), and 1  $\mu\text{g}$  of RNA was treated with RNase-Free DNaseI (Fisher Scientific). For each synthesis, a 10  $\mu\text{L}$  reaction was created using 1  $\mu\text{L}$  DNase-treated RNA; three technical replicates were performed for each biological replicate. Primers for amplification of cDNA product, used at a concentration of 0.75  $\mu\text{M}$ , were: Cyp6M2\_Forward: 5'-ACGAGTTCGAGCTGAAGGAT-3', Cyp6M2\_Reverse: 5'-GTTACTCAATGCCGAACG-3', Cyp6P3\_Forward: 5'-TATTGCAGAGAACGGTGGAG-3', Cyp6P3\_Reverse: 5'-TACTTCCGAAGGGTTTCGTC-3'. Relative expression was compared using Actin primers (Ponton et al. 2011) at a concentration of 0.50  $\mu\text{M}$ . qRT-PCR reactions were performed using USB VeriQuest SYBR Green One-Step qRT-PCR Master Mix (2X) on a 7500 Fast Real-Time PCR System (Applied Biosystems). Cycling conditions used were  $50^\circ\text{C}$  for 10 minutes and  $95^\circ\text{C}$  for 10 minutes, followed by 40 cycles of  $90^\circ\text{C}$  for 15 seconds and  $56^\circ\text{C}$  for 30 seconds, with the fluorescence measured at the end of each cycle.

## **Bendiocarb Metabolism Assays**

Recombinant *CYP6M2* and *CYP6P3* were commercially co-expressed with *An. gambiae* NADPH P450 reductase and cytochrome b5 in an *E. coli* system by Cypex (Dundee, UK). Using previously described methodologies (Stevenson et al. 2011) a first experiment showed that *CYP6M2* was unable to metabolize bendiocarb (10  $\mu$ M) after a 2 hour incubation and thus only *CYP6P3* was investigated in subsequent experiments. For time course measurements, reactions were performed in 200  $\mu$ L with 10  $\mu$ M insecticide, 0.1  $\mu$ M *CYP6P3* membrane in 200 mM Tris-HCl pH 7.4 and started by adding the NADPH regenerating system (1 mM glucose-6-phosphate (G6P), 0.25 mM MgCl<sub>2</sub>, 0.1 mM NADP<sup>+</sup>, and 1 U/mL glucose-6-phosphate dehydrogenase (G6PDH)). Reactions were incubated for a specified time at 30°C with 1200 rpm orbital shaking and stopped by adding 0.2 mL of acetonitrile. Shaking was carried for an additional 10 min before centrifuging the reactions at 20000 g for 20 min. 200  $\mu$ l of supernatant was used for HPLC analysis. Reactions were performed in triplicate and compared against a negative control with no NADPH regenerating system to calculate substrate depletion. An additional experiment with different enzyme concentrations was performed, using the methods above, for 20 mins with P450 concentrations of: 0.2, 0.1, 0.075, 0.05, 0.025 and 0.0125 mM. The reactions were performed in parallel against a negative control (2NADPH). In each experiment the supernatants were analyzed by reverse-phase HPLC with a 250 mm C18 column (Acclaim 120, Dionex) and a mobile phase consisting of 35% acetonitrile and 65% water. The system was run at a controlled temperature of 42°C with 1 ml/min flow rate. Bendiocarb insecticide was monitored at 205 nm and quantified by measuring peak areas using OpenLab CDS (Agilent Technologies).

## **Insecticide Exposure Assays**

An appropriate amount of insecticide was added to 100  $\mu$ l of acetone and placed into individual 16x200 mm glass disposable culture tubes (VWR Scientific). Tubes were then placed on their sides and rotated continuously, coating the entire interior of the tube, until all acetone was evaporated. A total of 8–12 control and 8–12 experimental transgenic flies, aged 3–5 days post-eclosion, were added to each tube. Flies from experimental and control classes were mixed in single insecticide-coated vials for assays, to ensure equivalent exposure to insecticide. The tubes were capped with cotton balls saturated with a 10% (w/v) glucose/water solution. Tubes were then incubated at 25°C for 24 h, after which mortality was assessed. Linear regression models were used to fit dose-response curves, from which LC<sub>50</sub> values (and confidence intervals) were estimated using Prism v5.0. However, for bendiocarb this was not possible owing to a very sharp inflection in the dose-response profile. Instead differences between lines were assessed at a diagnostic dose of 0.1  $\mu$ g bendiocarb/vial, applied previously to *Apis mellifera* (Dulin et al. 2012; NPIC 2002), using Mann-Whitney U tests.

## F. TABLES, FIGURES AND LEGENDS

**Figure A2.1. Microarray Experimental Design.** Arrows indicate pairwise comparisons with direction indicating an increasing level of bendiocarb resistance, which was used to predict the expected direction of differential gene expression (only solid arrows were used to determine significance). Coloured boxes indicate samples resistant to bendiocarb; the red box indicates the only bendiocarb-selected sample. **C.** In Exp2 microarray probes were considered significantly differentially expressed in resistant samples if: (i) each sus vs. res comparisons showed a consistent direction of expression as predicted by arrow direction; and (ii) each sus vs. res comparison yielded corrected  $P < 0.05$ . **A-B.** In Exp1 an additional criteria for significance was applied to increase specificity of results to the bendiocarb phenotype: (iii) fold-change for each Tiassalé-selected vs. sus comparison must be more extreme than the corresponding Tiassalé vs. sus comparison. Overall significance required significance in both Exp1 and Exp2.

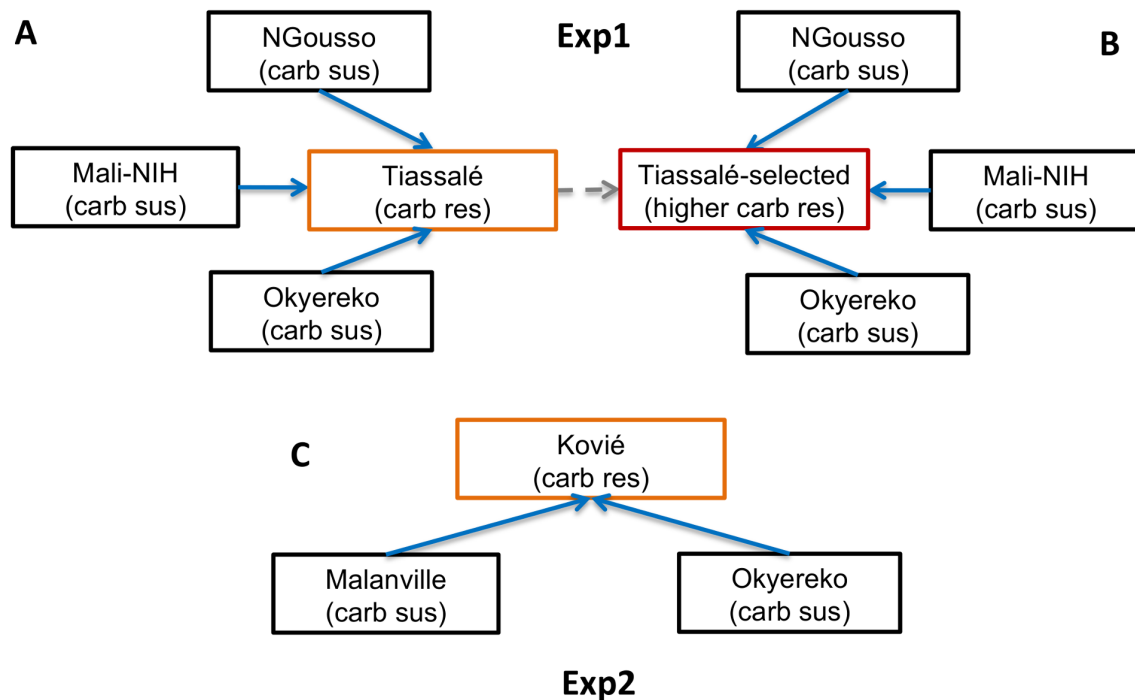


**Figure A2.2. Genes Significantly Overexpressed (Relative to Susceptible Samples) in (A) Tiassalé Bendiocarb Resistant Samples in Exp1, and (B) Both Tiassalé and Kovié Samples.** Plots show: **A.** Log<sub>2</sub>-transformed fold-changes (FC) plotted against –log<sub>10</sub> transformed q-values (multiple-testing-corrected probabilities) for bendiocarb-selected Tiassalé samples versus the average of the three susceptible populations; **B.** Comparison of Kovié FC against Tiassalé-selected FC for probes significant in both experiments. For genes represented by multiple probes, numbers in parentheses indicate the number of probes significant/total.

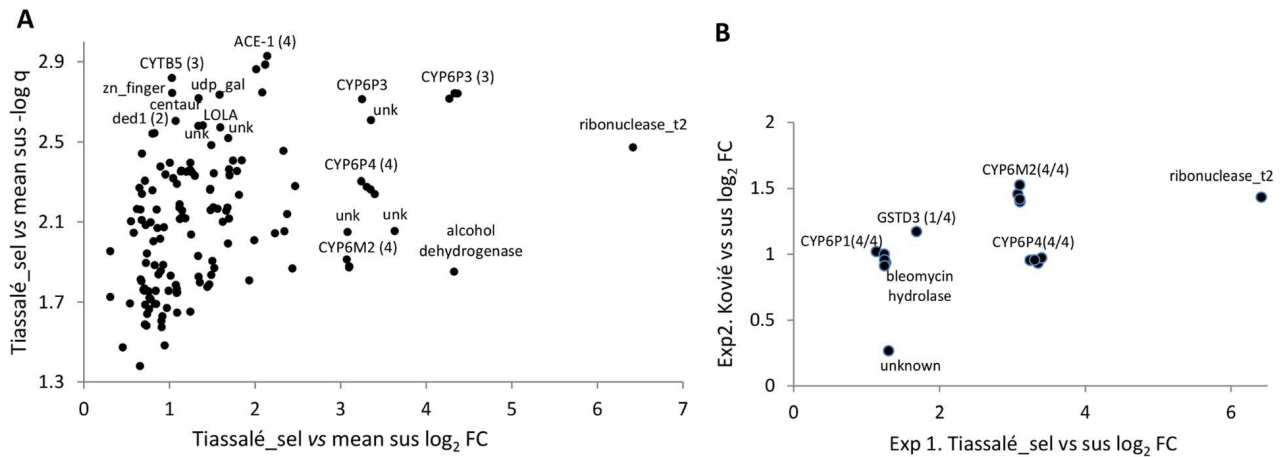


**Figure A2.3. Probes significantly over-expressed in Kovié.** Relative to Okyereko and Malanville (Exp2). Average  $\log_2$ -transformed fold- changes are plotted against average  $-\log_{10}$ -transformed q-values (multiple-testing-corrected probabilities). An arbitrary cut-off of  $\log_2FC = 2$  and  $-\log q = 3$  was used to determine probes to be labelled.

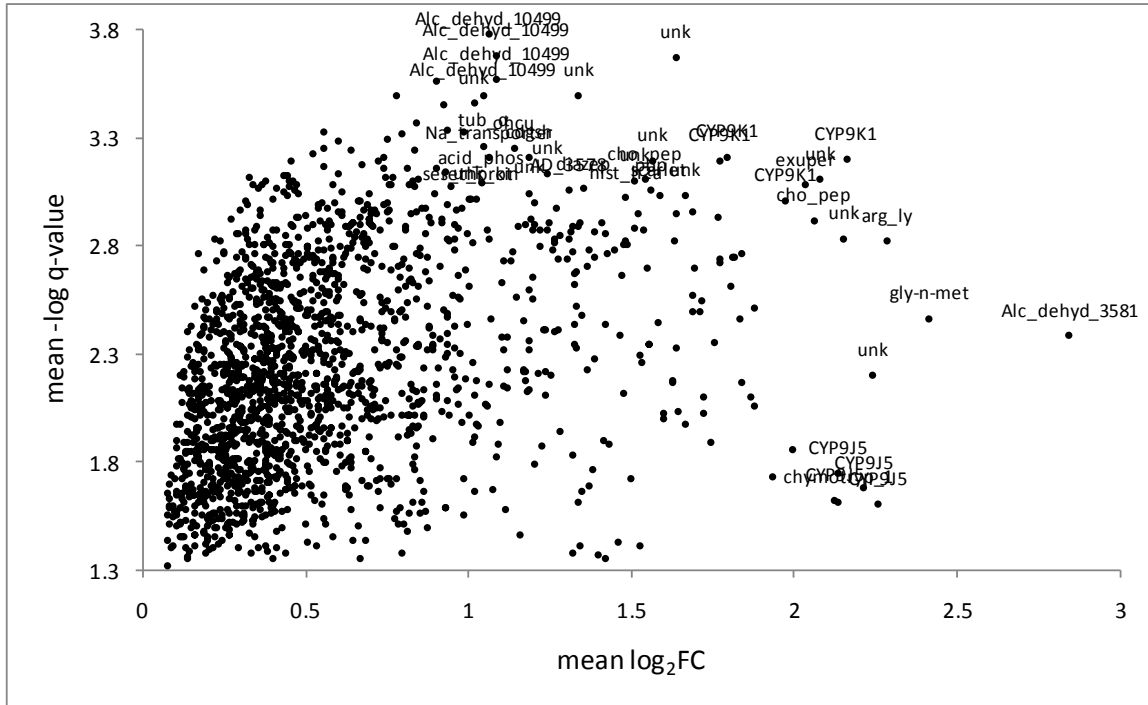




**Figure A2.4. Microarray results for Tiassalé selected vs unexposed controls.** Arbitrary cut-offs of  $\log_2FC = 0.6$  and  $-\log q = 1$  are used to determine points to label. (n) indicates label represents >1 replicate probes.

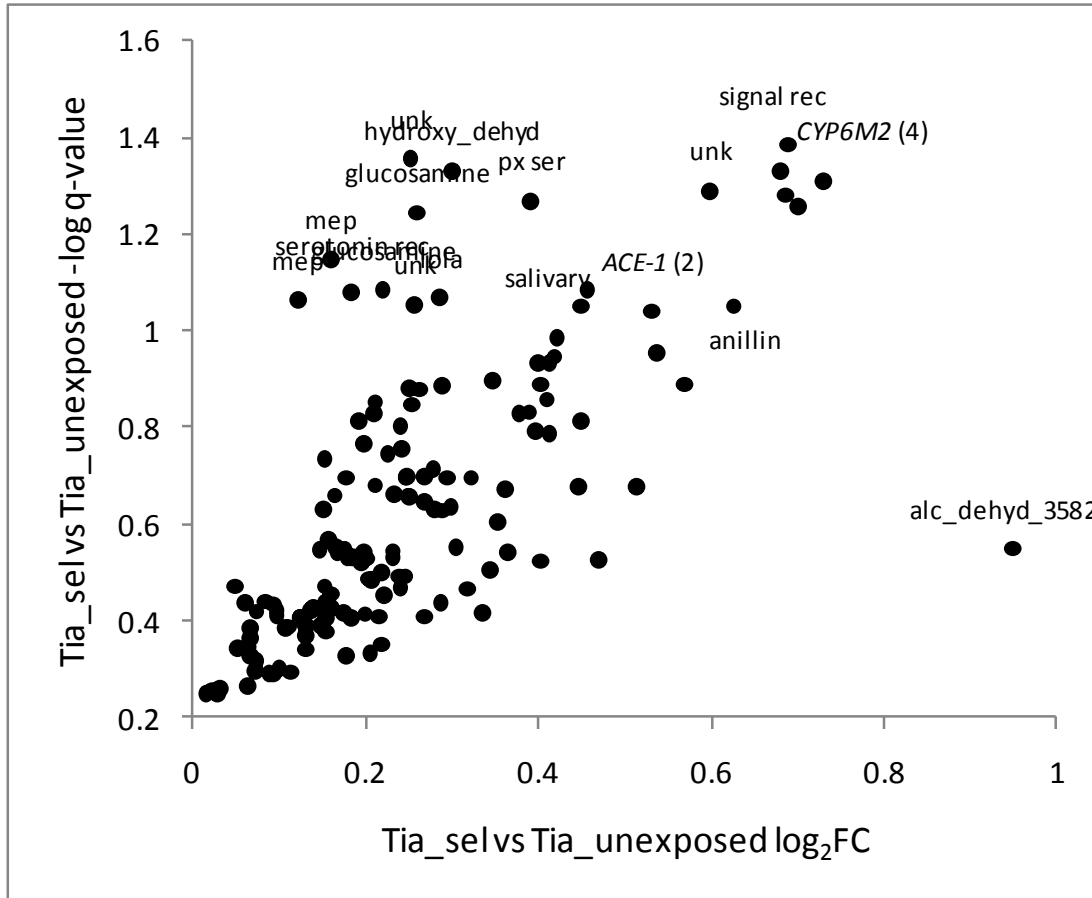


**Figure A2.5. Relationship between expression measured by qRT-PCR and microarrays for candidate genes.** The overall correlation is  $r = 0.50$  ( $P = 0.056$ ).

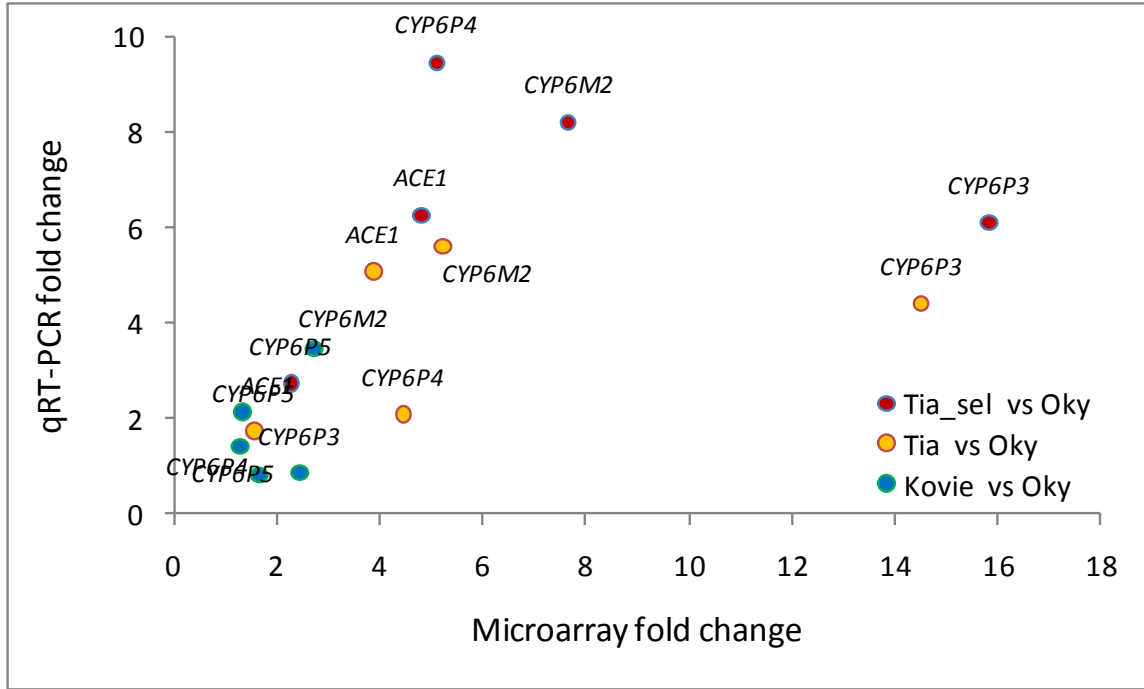


**Figure A2.6. qRT-PCR Expression Analysis of Candidate Genes.** Bars show mean fold changes relative to the bendiocarb and organophosphate susceptible Okyereko population. Asterisks indicate significant over-expression. Expression differences between pairs of populations are significant where error bars do not overlap. N = 5 biological replicates except for Tiassalé (N = 3).

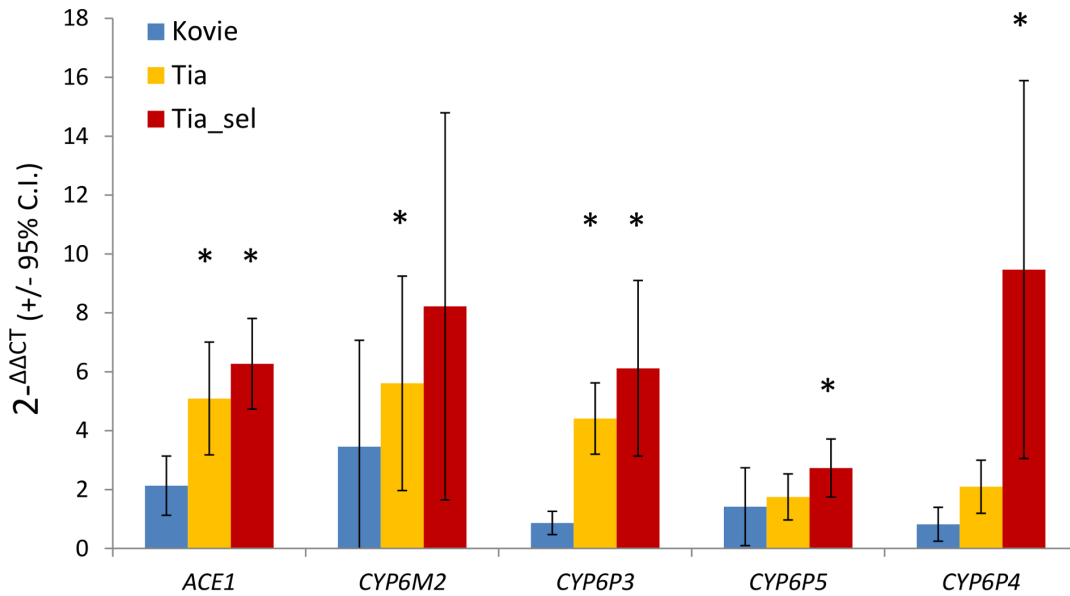


**Figure A2.7. Survival of transgenic *D. melanogaster* that express *CYP6M2* or *CYP6P3* in the presence of varied amounts of insecticides.** Log-linear plots of insecticide concentration vs. survival are shown. Blue points show survival of transformed flies with the *Act5C* driver which exhibit ubiquitous expression; red points show *CyO* control class flies. Bars show SEM of percent survival. Owing to the sharp inflection for both bendiocarb plots the regression model could not be applied to either *Act5C* or *CyO* data. N = 5 for all insecticides and concentrations other than bendiocarb at 0.1  $\mu\text{g}$ , for which N = 8 (see Fig. 4). The gap in the x-axis results from use of a log scale on which control vials (zero insecticide) have no value.

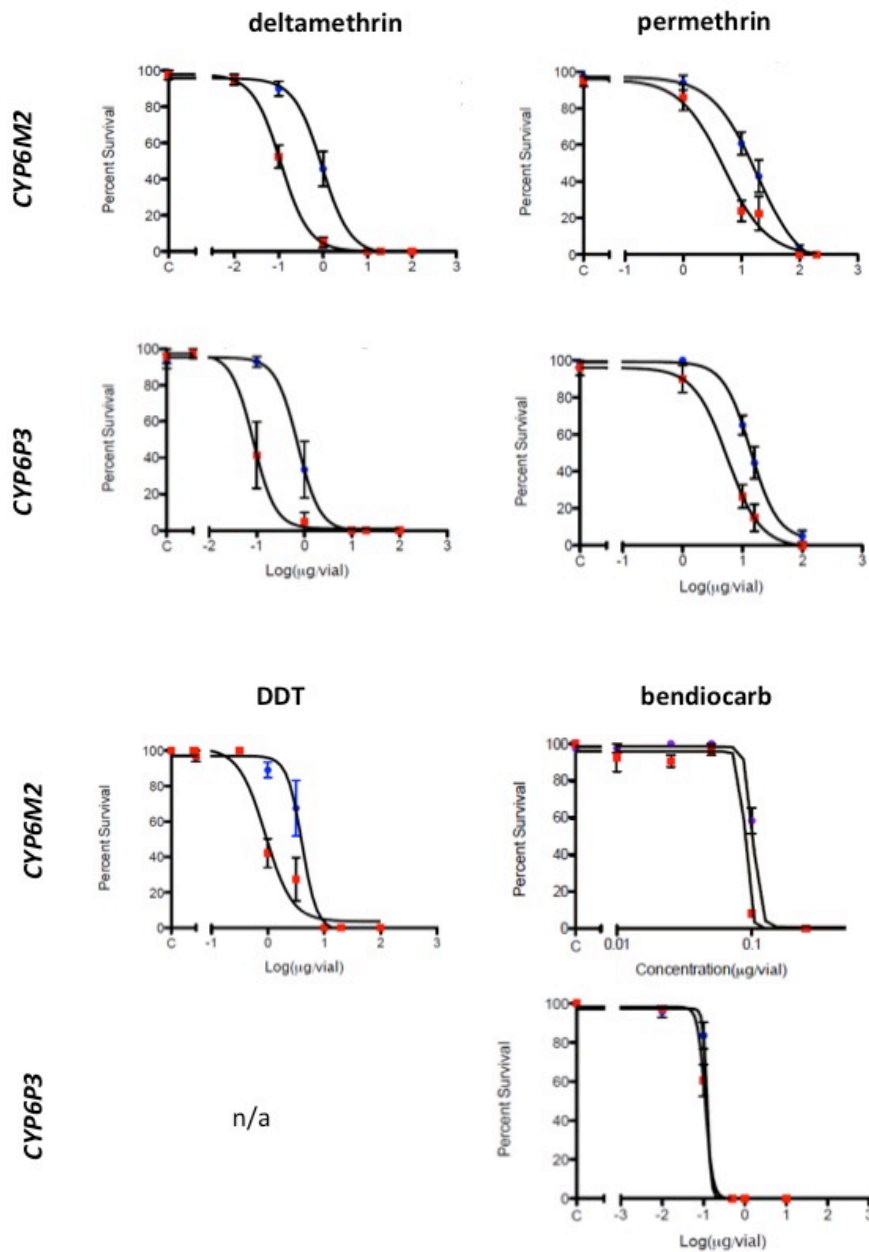


**Figure A2.8. Survival of Transgenic *Drosophila* Expressing *An. gambiae* *Cyp6M2* or *CYP6P3* in the Presence of Bendiocarb.** Boxes show interquartile ranges with median lines and whiskers (error bars) show 95<sup>th</sup> percentiles for test (Act5C driver) or control (CyO) lines following exposure to 0.1  $\mu$ g bendiocarb. Note that whiskers and median lines coincident with interquartile limits are not visible. Individual points falling outside percentiles are marked as dots. Mann-Whitney tests: \*\*\*P<0.001; \*P<0.05.

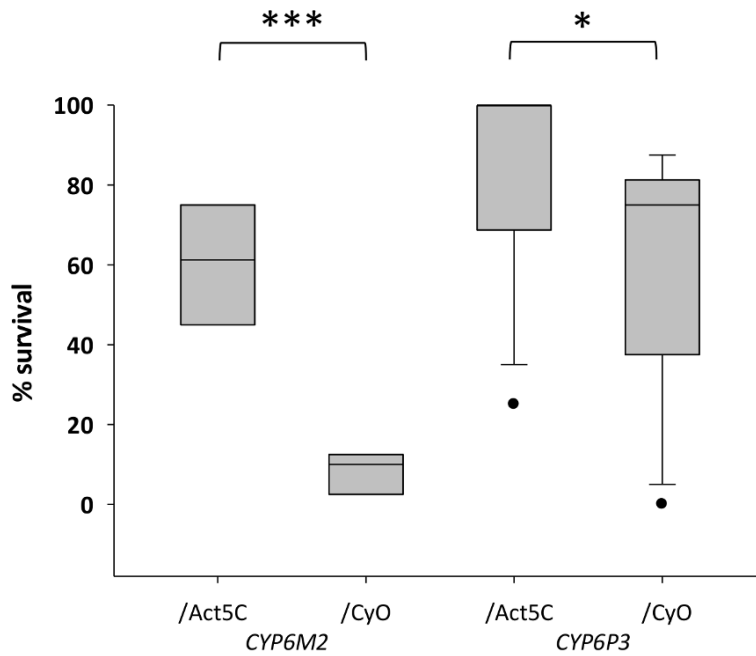


**Figure A2.9. *In vitro* Metabolism of Bendiocarb by Recombinant CYP6P3 Expressed in *E. coli*.** In both plots, which show the effect of (A) incubation time and (B) enzyme concentration, points show the mean of three replicates (following subtraction of no-NADPH negative control values)  $\pm$  one standard error.

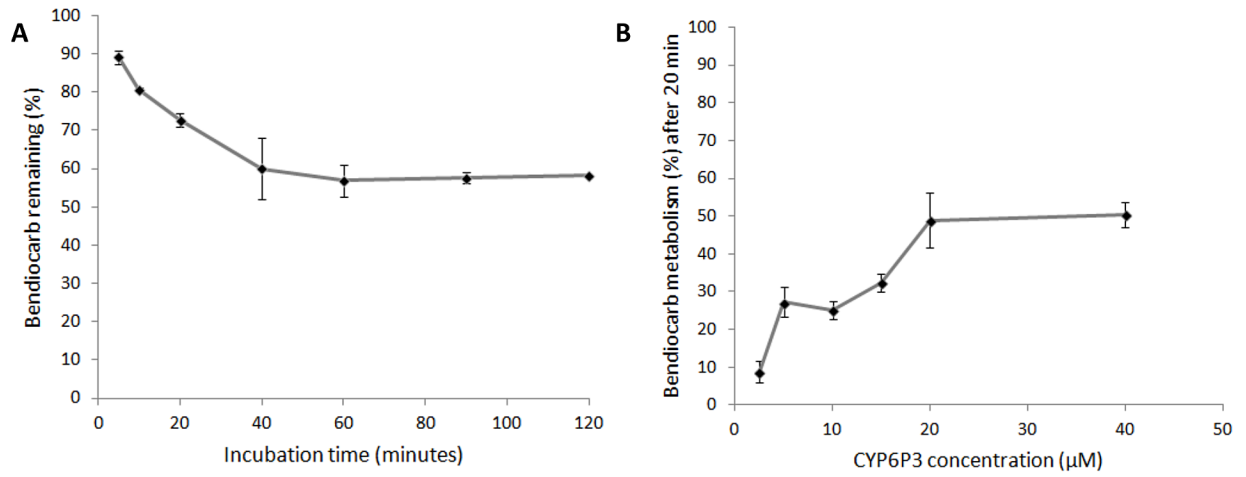


**Figure A2.10. Insecticide Resistance Phenotypes From Dry (Blue) and Wet (Red) Seasons With and Without the Synergist PBO.** Bars are mean mortalities from four replicate bioassays (N = 25 each), with 95% binomial confidence limits. Odds ratios are shown above bars and represent the odds of mortality with PBO pre-exposure, compared to the odds of mortality with insecticide alone (data from the two seasons are pooled). \* $P < 0.001$ ; <sup>NS</sup> not significant ( $X^2$ -test).

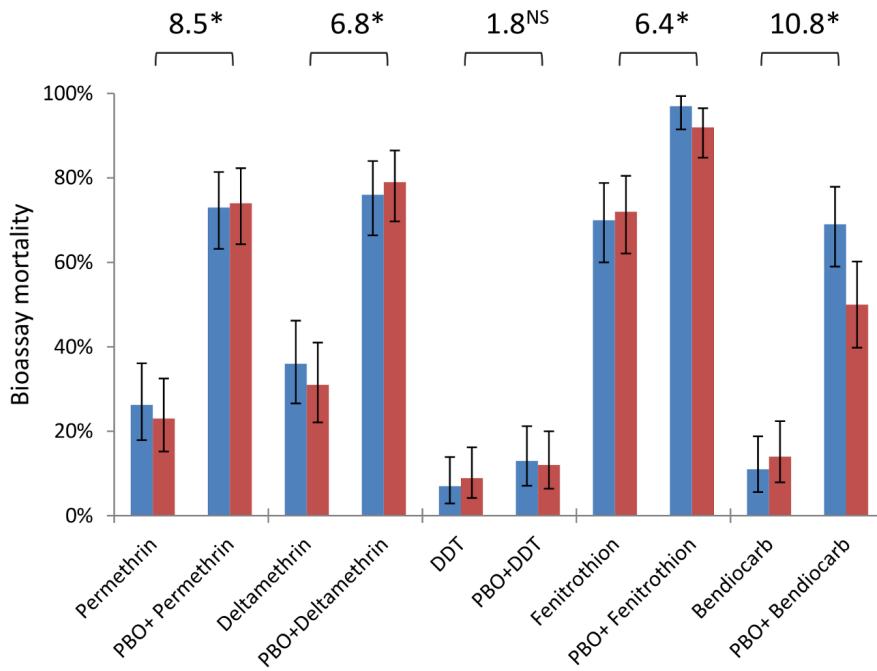


**Figure A2.11. Role of Target Site Allelic Variation and Copy Number Variation in Bendiocarb Resistance.** **A.** *ACE-1* G119S TaqMan genotyping scatterplot of females exposed to bendiocarb, following PBO synergist exposure. Filled dots are genotypes called, unfilled are those excluded owing to ambiguous position. The line illustrates a 1:1 Glycine (G): Serine (S) allele balance. Triangles are controls: S/S = mutant (resistant) allele homozygote; G/G = wild type (susceptible) allele homozygote. The line illustrates a 1:1 Gly:Ser allele balance. The dashed circle illustrates heterozygous genotypes. **B.** *Ace-1* genomic DNA copy number ratio of survivors and dead (N = 16 each) from the heterozygote genotype cluster. Bars show mean  $\Delta\Delta$ CT values relative to a standard susceptible laboratory strain (Kisumu) following normalisation against reference genes; error bars are 95% confidence intervals. In both plots blue denotes bioassay survivors and red denotes dead.

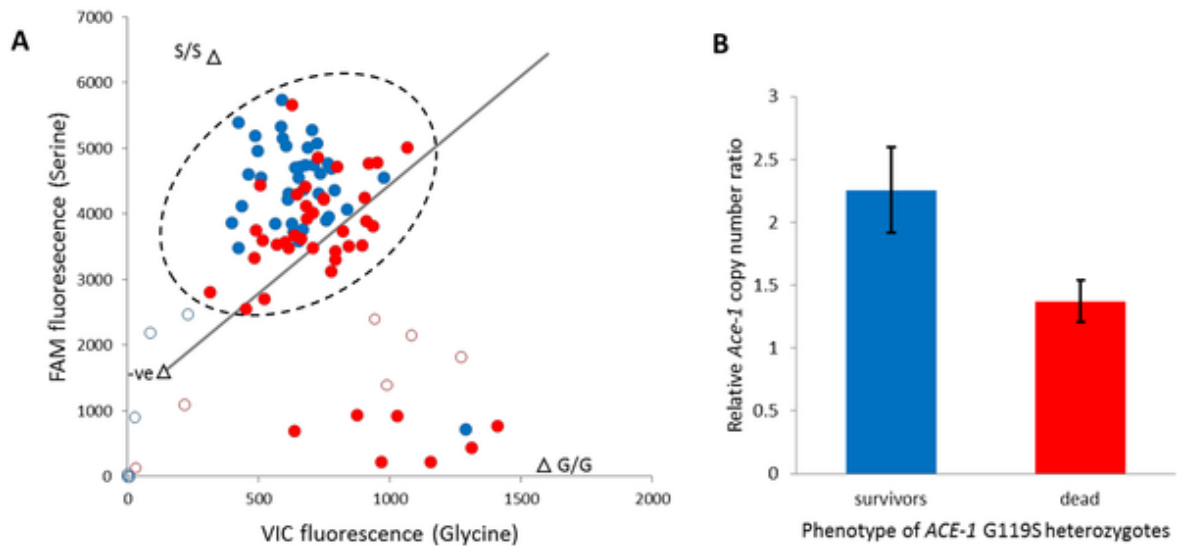






**Table A2.1. Survival of transformed *D. melanogaster* expressing *CYP6M2* and *CYP6P3* exposed to the pyrethroids permethrin and deltamethrin, and for *CYP6M2* also DDT.**

	<b>CYP6M2</b>		<b>CYP6P3</b>	
	<b>/Act5C</b>	<b>/Cy0</b>	<b>/Act5C</b>	<b>/Cy0</b>
perm	<b>18.37</b>	4.97	<b>13.74</b>	5.56
	9.71–34.75	2.72–9.11	10.74–17.58	3.08–10.02
delta	<b>0.94</b>	0.11	<b>0.72</b>	0.09
	0.71–1.25	0.09–0.14	0.41–1.28	0.05–0.15
DDT	<b>4.04</b>	0.91		
	3.09–5.28	0.70–1.17		

LC<sub>50</sub> estimates (μg) and 95% confidence limits are shown, in bold type where Act5C test line LC<sub>50</sub>s are significantly greater than CyO controls.

**Table A2.2. qRT-PCR expression results for transformed *Drosophila melanogaster*.** Relative fold differences in expression between experimental and control flies ( $\Delta\Delta\text{CT}$ ) are highlighted for each gene. Biological replicates are in rows and technical replicates in columns.

<b>CYP6M2</b>		CYP6M2/Act5C-Actin Primers				CYP6M2 Primers				Experimental
Replicate	Tech 1	Tech 2	Tech 3	mean	Tech 1	Tech 2	Tech 3	mean	$\Delta\text{CT}$	
1	24.19	24.62	24.71	24.51	26.57	26.68	26.61	26.62	-2.11	
2	20.24	21.43	21.79	21.15	27.31	27.29	27.20	27.27	-6.11	
3	20.94	21.97	22.70	21.87	27.63	27.56	27.51	27.57	-5.70	
								mean	-4.64	
		CYP6M2/CyO-Actin Primers				CYP6M2 Primers				Control
Replicate	Tech 1	Tech 2	Tech 3	mean	Tech 1	Tech 2	Tech 3	mean	$\Delta\text{CT}$	
1	18.97	21.18	21.05	20.40	27.04	26.92	27.07	27.01	-6.61	
2	21.48	21.94	22.49	21.97	29.40	29.62	29.73	29.58	-7.61	
3	24.35	24.15	23.41	23.97	29.56	29.54	29.90	29.67	-5.70	
								mean	-6.64	
								<b><math>\Delta\Delta\text{CT}</math></b>	<b>4.00</b>	
<b>CYP6P3</b>		CYP6P3/Act5C-Actin Primers				CYP6P3 Primers				Experimental
Replicate	Tech 1	Tech 2	Tech 3	mean	Tech 1	Tech 2	Tech 3	mean	$\Delta\text{CT}$	
1	n/a	26.10	26.51	26.31	24.20	24.06	24.26	24.17	2.13	
2	22.80	22.98	23.88	23.22	24.55	24.81	24.67	24.68	-1.46	
3	17.24	18.25	18.23	17.91	24.93	25.48	24.65	25.02	-7.11	
								mean	-2.15	
		CYP6P3/CyO-Actin Primers				CYP6P3 Primers				Control
Replicate	Tech 1	Tech 2	Tech 3	mean	Tech 1	Tech 2	Tech 3	mean	$\Delta\text{CT}$	
1	24.05	24.79	24.37	24.40	26.67	26.66	26.96	26.76	-2.36	
2	18.97	19.41	19.32	19.23	25.68	25.70	25.67	25.68	-6.45	
3	21.10	21.49	21.66	21.42	24.80	25.63	25.77	25.40	-3.98	
								mean	-4.26	
								<b><math>\Delta\Delta\text{CT}</math></b>	<b>4.34</b>	

**Table A2.3. Generalized linear model testing the effects of insecticide type, season and PBO on bioassay mortality**

Model terms included	$\chi^2$	d.f.	P-value
insecticide	5353.2	4	$\approx 0$
PBO	2101.2	1	$\approx 0$
season	0.6		0.42
insecticide x PBO	902.7	4	$\approx 0$
season x PBO	12.7	1	0.0004
insecticide x season	5.0	4	0.29
insecticide x season x PBO	65.1	4	$2 \times 10^{-13}$

Intercept included in model but not shown ( $P \approx 0$ ). Full model shown: removal of the non-significant insecticide x season interaction term had negligible impact on the results.

**Table A2.4. Resistance association of the G119S target site mutation, in the presence and absence of PBO following 60 min bendiocarb exposure.**

		ACE-1 G119S genotype			$\chi^2$	P
		S/S	G/S	G/G		
bendiocarb	alive	0	49	0	43.46	$10^{-12}$
	dead	0	12	25		
bendiocarb + PBO	alive	0	38	1	3.07	0.08
	dead	0	35	7		
Homogeneity test					8.28	0.004

**Table A2.5. qRT-PCR primer details for copy number variant analysis.**

gene	AGAP	primer name	primer sequence	efficiency (%)
<i>Elongation Factor</i>	AGAP005128	EF_gq_1F	AGCAGCTGTTTCAGCAAACG	93.5
		EF_gq_1R	TCTCCCGCACAGTGAAAGAC	
<i>CYP4G16</i>	AGAP001076	CYP4G16gq_5F	ATTGCGCATACAGATGGCCT	95.5
		CYP4G16gq_5R	CGGTCCAGGTATCCGTTTCAG	
<i>ACE-1</i>	AGAP001356	Ace-1_gq_5F	CCATGTGGAACCCGAACACG	93.8
		Ace-1_gq_5R	GTCGTACACGTCCAGGGTG	
<i>ACE-1</i>	AGAP001356	Ace1_gq_12_F	TATCTGTACACGCACCGCAG	97.2
		Ace1_gq_12_R	TTCGCCGAACACGTAGTTGA	
<i>ACE-1</i>	AGAP001356	Ace1_gq_1bF	CGGCGACCGTCAGATTCATA	96.9
		Ace1_gq_1bR	GTCCGCCACCACTTGTTTTTC	

**Table A2.6. qRT-PCR primer details for gene expression analysis.**

gene	AGAP	primer name	primer sequence	efficiency (%)
<i>Rps7</i>	AGAP010592	S7qf1	AGAACCAGCAGACCACCATC	106.4
		S7qR1	GCTGCAAACCTTCGGCTATTC	
<i>Elongation Factor</i>	AGAP005128	EFf1	GGCAAGAGGCATAACGATCAATGCG	91.1
		EFr1	GTCCATCTGCGACGCTCCGG	
<i>ACE-1</i>	AGAP001356	Ace-1_q3_F	CACGGCGACGAGATCAACTA	106.3
		Ace-1_q3_R	TGGGATTTGGATTGCCGGTT	
CYP6M2	AGAP008212	M2qf1	TACGATGACAACAAGGGCAAG	104.4
		M2qr1	GCGATCGTGGAAGTACTGG	
CYP6P3	AGAP002865	P3qf2	TGTGATTGACGAAACCTTCGGAAG	105.4
		P3qr2	ATAGTCCACAGACGGTACGCGGG	
CYP6P5	AGAP002866	CYP6P5_q3_F	AACCCGGACATTCAGGATCG	90.7
		CYP6P5_q3_R	TGCGTAACGTTTCGTTGATTACG	
CYP6P4	AGAP002867	CYP6P4_9b_F	GTCTGCGGGAGGAAATCGAG	102.3
		CYP6P4_9b_R	TACTTGCGCAGGGTTTCATTG	

## **CHAPTER AIII**

### **Metabolic and Target-Site Mechanisms Combine to Confer Strong DDT Resistance in *Anopheles gambiae***



Sara N. Mitchell, Daniel J. Rigden, Andrew J. Dowd, Fang Lu, Craig S. Wilding, David Weetman, Samuel Dadzie, Adam M. Jenkins, Kimberly Regna, Pelagie Boko, Luc Djogbenou, Marc A. T. Muskavitch, Hilary Ranson, Mark J. I. Paine, Olga Mayans, Martin J. Donnelly. Metabolic and Target-Site Mechanisms Combine to Confer Strong DDT Resistance in *Anopheles gambiae*. *PLoS ONE* **9**, e92662 (2014).

## A. ABSTRACT

The development of resistance to insecticides has become a classic exemplar of evolution occurring within human time scales. In this study we demonstrate how resistance to DDT in the major African malaria vector *Anopheles gambiae* is a result of both target-site resistance mechanisms that have introgressed between incipient species (the M- and S-molecular forms) and allelic variants in a DDT-detoxifying enzyme. Sequencing of the detoxification enzyme, *Gste2*, from DDT resistant and susceptible strains of *An. gambiae*, revealed a non-synonymous polymorphism (I114T), proximal to the DDT binding domain, which segregated with strain phenotype. Recombinant protein expression and DDT metabolism analysis revealed that the proteins from the susceptible strain lost activity at higher DDT concentrations, characteristic of substrate inhibition. The effect of I114T on GSTE2 protein structure was explored through X-ray crystallography. The amino acid exchange in the DDT-resistant strain introduced a hydroxyl group nearby the hydrophobic DDT-binding region. The exchange does not result in structural alterations but is predicted to facilitate local dynamics and enzyme activity. Expression of both wild-type and 114T alleles the allele in *Drosophila* conferred an increase in DDT tolerance. The 114T mutation was significantly associated with DDT resistance in wild caught M-form populations and acts in concert with target-site mutations in the voltage gated

sodium channel (*Vgsc-1575Y* and *Vgsc-1014F*) to confer extreme levels of DDT resistance in wild caught *An. gambiae*.

## B. INTRODUCTION

Physiological resistance to insecticides often involves either mutations in the insecticide target site (target-site resistance), or elevated activity of detoxifying enzymes that metabolize and/or sequester insecticides (metabolic resistance). Resistance may result from selection upon standing genetic variation (Newcomb et al. 1997) or from a *de novo* mutation (French-Constant et al. 1993). In *Anopheles gambiae*, a primary African malaria vector, a third route has been described, involving introgression of resistance mutation-bearing haplotypes between molecular forms which are thought to be in the process of speciation (Weill et al. 2000). There is overwhelming evidence that the mutation *L1014F*, a replacement change in the voltage-gated sodium channel (*Vgsc*), the target of both DDT and pyrethroid insecticides, is significantly associated with increased phenotypic resistance in both the donor S- and recipient M-form populations across Africa (Reimer et al. 2008; Jones et al. 2012; Weetman et al. 2010). However, what remains unknown is whether such introgressed resistance alleles interact with allelic variants in the recipient genetic background.

In *An. gambiae* metabolic resistance has been linked to elevated expression of detoxifying enzymes through microarray-based analyses and quantitative PCR (David et al. 2005; Mitchell et al. 2012; Müller et al. 2008). An epsilon-class glutathione-S-transferase in *An. gambiae*, *GSTE2*, and its ortholog in the dengue and yellow fever

vector *Aedes aegypti*, have been linked to DDT resistance through elevated gene expression (Prapanthadara et al. 1993; Lumjuan et al. 2005). Recombinant protein expression and *in vitro* assays also support a role for this enzyme in DDT metabolism (Lumjuan et al. 2005; Ranson et al. 2001). In previous studies, *Gste2* was found to be 5–8 fold over-expressed in *An. gambiae* of the ZAN/U strain, which displays DDT resistance in the absence of mutations in the voltage-gated sodium channel, compared to a susceptible East African mosquito colony (Kisumu) (Ranson et al. 2001; Ding et al. 2003; Ding et al. 2005).

The rationale for the current study arose from the serendipitous discovery of allelic differences in *Gste2* in recently re-established colonies of Kisumu and ZAN/U (source [www.MR4.org](http://www.MR4.org)), which exhibited the expected DDT susceptibility/resistance profiles but not the level of differential expression observed previously (Ranson et al. 2001; Ding et al. 2003). The ZAN/U colony showed only a 2.34-fold greater expression of *Gste2* and less than a 2-fold difference in protein expression compared with the Kisumu colony (Figure A3.1 and Figure A3.2). Upon review of the crystal structure that was already resolved for GSTE2 from the susceptible Kisumu strain (Wang et al. 2008), it appeared that the alleles differed in codons proximal to the putative DDT-binding site, a hydrophobic pocket adjacent to the glutathione (GSH) binding site.

Our study demonstrates how one substitution (I114T) is found commonly, and inferred to originate, in M-molecular form populations of *An. gambiae* where it is significantly associated with DDT resistance. In concert with target-site resistance mechanisms (*Vgsc-1014F* and *Vgsc-1575Y*), it explains a substantial fraction of the observed variation in DDT resistance. Recombinant protein expression, X-ray

crystallography and transgenic expression of allelic variants in *Drosophila* are also presented to provide a mechanistic insight.

## C. RESULTS

### **Recombinant protein expression and DDTase activity screens**

Based upon amino acid sequence, three allelic variants were identified, two within the Kisumu colony and one in the ZAN/U colony (Table A3.1; GenBank accession numbers: JX840597-JX840599). The three alleles were expressed in *E.coli* and each exhibited activity with the substrate CDNB in the presence of GSH; confirming that the expressed proteins were glutathione-S-transferases (Table A3.1). DDT metabolism assays were performed to determine optimal conditions for kinetic analysis of each variant *GSTE2* enzyme with a substrate (DDT) dilution series. At lower concentrations all three variant enzymes displayed comparable activity (Figure A3.3). However, the ZAN/U-derived *GSTE2* protein displayed a significantly higher mean enzyme rate than the two Kisumu proteins at the higher concentrations tested (Figure A3.3). Enzyme kinetic measurements did not produce markedly different values for maximum enzyme rate ( $V_{max}$ ) and the  $K_M$  (substrate concentration at half maximum velocity) for the three variants (Table A3.2). However, the Kisumu alleles did not exhibit standard Michaelis-Menten kinetics (Figure A3.3), but rather displayed profiles typical of enzymes experiencing substrate inhibition (Vincent 2005; Lin et al. 2001).

## Structural analysis of non-synonymous changes in *GSTE2*

Molecular modeling was used initially to investigate the mechanistic effect of the amino acid replacements on catalysis. Previously, Wang et al. (Wang et al. 2008) proposed that a hydrophobic pocket in close proximity to the GSH binding site was the site of DDT binding. Predicted to be of particular importance was the inclination of the C-terminal section of helix H4, which brought residues 112, 116 and 120 closer to the GSH cofactor. These residues also helped to form a pocket 'cap' for the putative DDT binding site, which would potentially increase hydrophobicity and therefore affinity for the highly hydrophobic DDT molecule. Our study focused upon two residue exchanges, I114T and F120L, which are located in the C-terminal section of helix H4 and, thus, have the potential to influence DDT binding.

The variable mutation found at position 120, F120L, in the Kisumu strain had potential to affect the formation of the putative DDT pocket cap as the aromatic phenylalanine is replaced with the shorter aliphatic chain of leucine. F120 is predicted to make hydrophobic contact with one of the aromatic rings of the DDT molecule. A leucine residue at this position, being smaller, may not form as tight an interaction with the DDT and, thereby, weaken its binding. The importance of the phenylalanine residue at this position is supported by the likelihood that this is the ancestral allele, as it is fixed in an extensive collection of *An. arabiensis* from Sudan, Ethiopia, Tanzania and Malawi (collection details in (Donnelly & Townson 2000) (GenBank accession numbers: JX627247-JX627266). However, enzyme kinetics parameters (Table A3.2) indicate that the F120L exchange has little influence on substrate affinity or catalysis, suggesting that the aromatic group of phenylalanine is dispensable at this position and not deterministic

of DDT affinity.

Position 114 is also situated in close proximity to the predicted DDT binding pocket. The effect of the change from isoleucine, inferred to be ancestral from comparisons with the same *An. arabiensis* data, to threonine at position 114 was difficult to estimate through modeling. In this case, a destabilizing polar hydroxyl group is introduced in a hydrophobic core region of the protein in ZAN/U, with the potential for marked effects on protein conformation. To better understand the effect of this substitution in enzyme activation, we elucidated the structure of ZAN/U:GSH using X-ray crystallography (Figure A3.4). The structure, determined to 2.3 Å resolution (R-factor/R-free 17.57/22.78 %), closely resembles that of the Kisumu enzyme previously reported (PDB entry 2IMI; (Wang et al. 2008)) (0.5 Å overall rmsd calculated using RAPIDO (Vincent 2005) (Figure A3.2) as well as that of *GSTE2* from *An. funestus* most recently elucidated (PDB entry 3ZML). Similar to the Kisumu variant from *An. gambiae*, the latter carries Ile at position 114. Both enzymes share 93% sequence identity and their structures superimpose with an rmsd of 0.3 Å. The model of ZAN/U calculated in this study shows that the introduced hydroxyl group is stabilized by hydrogen bond formation to the main chain carbonyl group of R110 (calculated using HBOND, J. Overington, unpublished), so that the presence of this polar group in the hydrophobic core does not lead to structural alterations in the enzyme (Figure A3.4A; a comparison to *GSTE2* from *An. funestus* is shown in Figure A3.5). Interestingly, inspection of electron density maps for all *GSTE2* enzymes (Figure A3.6), calculated using PDB\_REDO (Joosten et al. 2012), reveal a disorder of residues F113 and Y133, which are involved in the mutual packing of two H4 helices across the dimer interface, at a spot that is immediately local

to the predicted DDT pocket. This suggests that this region, which constitutes the DDT pocket ‘cap’, has high intrinsic dynamics. Such dynamics could facilitate the motions that take place during substrate binding and/or product release and, thereby, influence catalytic turn-over. Our data suggest that mutations can influence catalysis even when not resulting in detectable structural alterations, most likely by affecting the molecular dynamics of this region.

### **Heterologous expression of *GSTE2* in *Drosophila melanogaster***

Heterologous expression in *Drosophila melanogaster* was achieved for both the *Gste2*-ZAN/U and *Gste2*-Kisumu1B alleles (Figure A3.7). For both alleles ubiquitous expression of *An. gambiae Gste2* resulted in an increase in resistance to DDT as assessed by resistance ratio of  $LC_{50s}$  ( $LC_{50}$  transformed line/ $LC_{50}$  control). Although, contrary to the recombinant *E.coli* work (Figure A3.3), and our a priori expectations, the resistance ratios were apparently higher for *Gste2*-Kisumu1B (15.15) than *Gste2*-ZAN/U (5.24).

### **Screening of I114T and Vgsc variants in wild-caught, DDT-phenotyped specimens of *An. gambiae***

We screened for the presence of the I114T mutations in a number of collections of both molecular forms of *An. gambiae*. Unexpectedly, given that the ZAN/U colony is of the S-molecular form and originates from East Africa, the 114T allele was most common in M-form populations from West Africa (Figure A3.8). For example in both Benin and Burkina Faso 114T allele was significantly more frequent in M-form (Benin Freq = 0.79;

95% CIs 0.75–0.83: Burkina Faso Freq = 0.59; 95% CIs 0.54–0.63) than sympatric S-form populations (Benin Freq = 0.05; 95% CIs 0.03–0.09: Burkina Faso Freq = 0.12; 95% CIs 0.08–0.17) suggestive that the mutation originated in M-form populations. Consequently we focused genotype: phenotype studies on West African populations, where in addition we were able to investigate potential interactions between the *Gste2* variant and two known DDT-linked *Vgsc* variants that are rare or absent in East Africa. Female *An. gambiae* from Benin and Burkina Faso that survived or were killed by 60 minute DDT exposure in standard WHO susceptibility tests (World Health Organization 2012), were genotyped at the *Gste2*-114 codon and at the resistance-associated mutations in the voltage gated sodium channel (*Vgsc*-1014F, commonly termed *kdr*, and *Vgsc* - 1575Y)(Jones et al. 2012). In the M-form specimens from Benin there was a significant association between 114T and DDT survival (allelic test of association  $p = 8 \times 10^{-4}$ : Odds Ratio (OR) = 2.35 ; 95% CIs 1.42–3.88). The trend was similar in Burkinabe specimens but did not reach statistical significance ( $p = 0.28$ : OR = 1.27; 95% CIs 0.83–1.93). As expected the *Vgsc*-1014F mutation was associated with DDT resistance in both locations, Benin ( $p = 6 \times 10^{-4}$ : OR = 2.21; 95% CIs 1.40–3.50) and Burkina Faso ( $p = 5 \times 10^{-7}$ ; OR = 3.05 95% CIs 1.97–4.74).

For the Benin data, where both *Gste2*-114T and *Vgsc*-1014F were significantly associated with DDT resistance in univariate analyses, we fitted a general linear model with a logistic link function. In this analysis both mutations remained significantly associated with the ability of mosquitoes to survive DDT exposure (*Gste2*-114T  $p = 0.002$ ; *Vgsc*-1014F  $p = 0.018$ ). The additive effects of the resistance loci was revealed in both Benin and Burkina Faso by elevated odds ratio for a double mutant haplotype



relative to wildtype (OR Benin = 3.13 (95% CIs 1.59–6.15;  $p = 0.0012$ ; OR Burkina Faso 5.00 (95% CIs 2.51–9.98;  $p < 0.001$ ; Figure A3.9). The third mutation, *Vgsc*-1575Y, is at low frequency in Benin (Freq = 0.035; 95% CIs 0.02–0.06) precluding association analysis but at a higher frequency in Burkina Faso (Freq = 0.12; 95% CIs 0.09–0.16). In Burkina Faso *Vgsc*-1014F was strongly resistance-associated ( $p = 6.6 \times 10^{-7}$ ) whereas both *Gste2*-114T ( $p = 0.051$ ) and *Vgsc*-1575Y ( $p = 0.039$ ) were on the margins of significance. However, for the triple mutant (*Gste2*-114T: *Vgsc*-1014F : *Vgsc*-1575Y) the odds ratio relative to wild type rose to 12.99 (95% CIs 2.55–66.10;  $p < 0.001$ ; Dataset S2), which translates into an increase in probability of surviving a one hour DDT exposure from 50% to 93%. Nonetheless, over 50% of the variation remained to be explained and may reflect the effects of environmental factors or additional resistance mechanisms (e.g. (Mitchell et al. 2012)).

Full-length *Gste2* sequences were obtained from 18 M-form individuals used in the Burkinabe genotype: phenotype tests (Genbank accession numbers: KC533009–KC533026). There were no additional non-synonymous mutations that segregated with the 114T mutation providing further evidence that mutation is causal, rather than merely a marker of DDT resistance.

## D. DISCUSSION

Our data demonstrate how introgression of adaptively advantageous alleles between the molecular forms of *An. gambiae* can bring together combinations of alleles that enhance insecticide resistance phenotypes. This is yet another example of the

evolutionary plasticity of this species complex and vividly illustrates why its members are so extremely difficult to control. The triple mutant described in this study is almost completely resistant to DDT, as assessed using the standard World Health Organization exposure assay. There is no simple association between resistance phenotype and epidemiological outcomes but these data raise concerns about the efficacy of indoor residual spraying with DDT in parts of West Africa for controlling malaria.

Insecticide resistance in mosquitoes (David et al. 2005; Müller et al. 2008; Lumjuan et al. 2005; Ranson et al. 2001; Djogbénou et al. 2008; Amenya et al. 2008), and other insects (Le Goff et al. 2003; Puinean et al. 2010), is commonly linked to elevated expression of detoxifying enzymes. Indeed *Gste2* was first implicated in DDT resistance as a result of elevated expression rather than allelic variation (Ranson et al. 2001; Ding et al. 2003). However, it seems that the ZAN/U strain used in earlier work bears little relation to that used in this study: in addition to the higher levels of *Gste2* expression observed, the amino acid at codon 114 was an asparagine (N) (Ranson et al. 2001; Ding et al. 2003; Orтели et al. 2003) not the threonine we identify here. The occurrence of the I114T mutant in our ZAN/U strain is probably a result of a contamination event, most likely from an M form colony, followed by selection during routine colony husbandry to maintain the DDT-resistant phenotype. Such inter-colony contamination events are a major problem when rearing morphologically identical mosquito strains (Wilkins et al. 2009). The involvement of metabolic allelic variants in conferring an insecticide resistance phenotype is not without precedent. In the sheep blowfly, *Lucilia cuprina*, Newcomb et al. (Newcomb et al. 1997) highlighted a G137D substitution within a carboxylesterase gene, E3, which conferred broad-spectrum

organophosphate (OP) hydrolase activity. The same mutation was subsequently found to confer OP resistance in the housefly *Musca domestica* (Claudianos et al. 1999). Next generation sequencing of individual *An. gambiae* (<http://www.malariagen.net/node/287>) will permit genome-wide association studies of insecticide resistance phenotypes to simultaneously uncover coding and regulatory variants.

The data that were obtained from the heterologous expression of Kisumu and ZAN/U alleles in *D. melanogaster* are somewhat at odds with our contention that the ZAN/U allelic variant is DDT-resistance associated. However, these data may point to the influence of genotypic background in the penetrance of a resistance-associated variant, as has been observed previously in both *An. gambiae* and *D. melanogaster* (Weetman et al. 2010; Smith et al. 2011). In an earlier study *Drosophila* transformed with the *Gste2*-ZAN/U allele showed DDT LC<sub>50</sub> values in excess of those observed here (Daborn et al. 2012).

### **Mechanism of action of *Gste2-114T***

The importance of mutation I114T most likely arises from the creation of an enzyme with increased catalytic activity through predicted increased conformation dynamics and reduced product affinity, facilitating metabolic turnover. The relationship between structure, stability and catalysis of enzymes has been studied extensively in the context of protein thermostability (Sterner & Liebl 2001). Enzymes from hyperthermophiles, which grow optimally at elevated temperatures, are often barely active at room temperature but are as active as their mesophilic homologues at high

temperatures. It has been proposed that the low activity of the thermostable enzymes at mesophilic temperatures is due to a high structural rigidity, which is relieved at their elevated physiological temperatures. This concept of “corresponding states” highlights the importance of protein dynamics in catalysis (Jaenicke 1991). In agreement with this concept, rational protein design and directed evolution have shown that enzyme mutants with reduced stability often exhibit improved catalytic activity compared to the wild-type form, even though structural alterations are often minimal or undetectable (e.g. (Schlee et al. 2009; Merz et al. 2000)). The lack of notable structural differences between the Kisumu 2B and ZAN/U 1C variants and the intrinsic dynamics of the region vicinal to the catalytic site in *GSTE2* enzymes led us to speculate an effect of the residue exchanges in protein stability. We predicted changes in stability that might result from mutation of amino acids, I114 and F120, to their smaller replacements, T114 in ZAN/U 1C and L120 in Kisumu 1B. The I114T change was predicted as strongly destabilizing at 2.85 kcal/mol (Dehouck et al. 2011), while the F120L was classified as neutral at -0.98 kcal/mol. The destabilizing effect of the T114 exchange is likely due to the reduction in side chain volume, with the introduced polarity apparently well accommodated in the local environment. The change in volume is greater for position 120, but volume changes in protein cores are especially disruptive (Dehouck et al. 2011) and I114 is buried while F120 is largely solvent-accessible. It is position 114 that correlates better with activity and which was shown to associate with phenotype in the phenotypic work conducted in Benin and Burkina Faso (Figure A3.9). It appears that the 114 mutant drives DDT resistance through dynamic rather than static conformational changes.

## Conclusion

We describe a variant *Gste2*-114T that is significantly associated with DDT resistance in M molecular form females from West Africa. This mutation in concert with *Vgsc* mutations confers highly elevated resistance to DDT. Whilst individually the mutations may have a modest effect on resistance phenotype the effect of acquisition of these incremental changes relative to wild-type may be large.

## E. METHODS

### Strains

The DDT resistant ZAN/U strain was derived from the ZANDS strain, colonized from Zanzibar and displaying resistance to DDT as larvae (Prapanthadara et al. 1993; Prapanthadara et al. 1995). ZAN/U was derived from this strain via selection of 1-day old adults with 4% DDT (Ranson et al. 2000). ZAN/U displays DDT resistance in the absence of known knockdown resistance (*kdr*) mutations in the sodium channel. The Kisumu strain is fully susceptible to DDT and originates from Kisumu in Western Kenya. Both of these laboratory colonies are of the S molecular form and originate from East Africa. These studies did not involve human participants or endangered or protected species and therefore no ethical clearance or specific permissions were required.

## Sequencing of *Gste2*

*Gste2* (GenBank accession number XM319968.3), for which only a single transcript has been reported, is situated on chromosome 3R at position 28,597,686–28,598,594 (AgamP3.5 genome assembly of *An. gambiae* see [www.vectorbase.org](http://www.vectorbase.org)). To investigate non-synonymous changes between the strains, sequence data were obtained from ten individual female mosquitoes from both ZAN/U and Kisumu. Primers were designed to amplify a 680bp fragment encompassing the majority of the three exons. Total DNA was purified from single insects using the DNeasy Blood and Tissue spin column kit (Qiagen). All twenty DNA extracts were confirmed as the S-form of *An. gambiae* using a PCR-RFLP approach (Fanello et al. 2002). *Gste2* amplicons were sent for direct sequencing (Macrogen, South Korea). Those individuals yielding poor quality data from direct sequencing were re-amplified and cloned in *Escherichia coli* using a pGEM-T Easy Vector (Promega) prior to sequencing. All sequences were aligned versus the full *Gste2* genomic sequence obtained from VectorBase (<http://www.vectorbase.org/>) using CodonCode Aligner software (CodonCode Corporation) and synonymous and non-synonymous polymorphisms identified.

Full-length cDNA sequences for Kisumu and ZAN/U *Gste2* were produced from RNA extracted from three batches of ten female mosquitoes from each strain using the PicoPure RNA Isolation Kit (Arcturus). RNA concentration was measured (NanoDrop spectrophotometer, Thermo) and approximately 2 µg from each pool used for cDNA synthesis (SuperScript III Reverse Transcriptase, Invitrogen). The cDNA sequence was amplified from cDNA pools using primers situated in the 5' and 3' untranslated regions (Table A3.3) to produce a 683 bp fragment. The amplified *Gste2* fragment from each

cDNA pool was then cloned into a pGEM-T Easy holding vector (Promega) using 1 µl of PCR product. Positive clones from each cDNA pool were selected for sequencing. Selected clones were used to inoculate a 5 ml, over-night culture from which plasmid DNA was extracted (QIAprep Spin Miniprep Kit, Qiagen). An aliquot of each plasmid was then sent for sequencing (Macrogen, South Korea; GenBank accession numbers: JX840597- JX840599).

### **Modeling of non-synonymous changes on to the *GSTE2* protein structure**

The amino acid changes identified in the ZAN/U and Kisumu sequence data were interpreted in the context of the Kisumu *GSTE2* crystal structure [ProteinDataBank (PDB) accession code 2IL3] and their potential importance in DDT binding inferred with respect to the residues highlighted by Wang et al. (Wang et al. 2008) as amino acid positions likely to be involved with DDT binding/metabolism, henceforth termed the catalytic triad. This *in silico* approach was used to select *Gste2* haplotypes that were likely to have differing DDT-ase activity for further recombinant protein and crystallography work. PoPMuSiC (Dehouck et al. 2009; Dehouck et al. 2011) was used to predict protein stability changes occurring as a result of amino acid changes between the polymorphisms.

### **Recombinant protein expression and DDTase activity screens**

Recombinant protein expression was performed for three *Gste2* allelic variants that had non-synonymous changes proximal to the DDT binding site. *Gste2* was re-

amplified from clones of the cDNA extracts using primers that incorporated a 3' *NdeI* site and a 5' *BamHI* restriction site (Table A3.3). These restriction sites were exploited to clone the *Gste2* alleles into protein expression vector pET15b (Novagen) before transformation into *E. coli* BL21 (DE3) (New England Biolabs). Cultures were incubated at 37°C (150RPM) until an optical density of  $\approx 0.8$  (wavelength 600 nm) was reached, then protein production was induced by addition of 1 mM isopropyl- $\beta$ -D-thiogalactoside (IPTG) at 30°C (150RPM). A pET15b encoded polyhistidine (6XHis) tag was exploited for purification of GSTE2 using nickel affinity chromatography. Bacterial lysates were prepared by sonication in buffer TSE (50 mM Tris-HCl pH 7.4, 1 mM EDTA, 150 mM NaCl, 10 mM  $\beta$ -mercaptoethanol ( $\beta$ -ME), 1.25 mM MgCl<sub>2</sub> and 250 U benzonase) and cell debris removed through centrifugation (10,000 g for 20 minutes at 4°C) and filtration (0.2  $\mu$ m filter). Crude cell lysate was then applied to a 1 ml nickel-nitrilotriacetate (Ni-NTA) agarose (Qiagen) column and washed with 10 column volumes of buffer A (50 mM sodium phosphate, 200 mM NaCl, pH 8.0) containing 20 mM imidazole. Protein was eluted in 10 ml of buffer B (50 mM sodium phosphate, 300 mM NaCl, pH 8.0) containing 250 mM imidazole. Purified *GSTE2* was then applied to a PD-10 Desalting Column (GE Healthcare) and eluted in storage buffer [50 mM sodium phosphate, 20 mM Dithiothreitol (DTT), pH 7.4].

Protein concentration was determined using a commercial protein quantification kit (Fluka – Sigma-Aldrich) based on the Bradford protein assay (Bradford 1976) and GST activity confirmed for each purified recombinant variant using the GST substrate 1-chloro-2, 4-dinitrobenzene (CDNB) in a standard colorimetric activity assay (Harbig et al. 1974). The recombinant proteins produced for each of the three *GSTE2* variants were



of extremely high and consistent purity (Figure A3.10).

The DDT dehydrochlorinase activity of all *GSTE2* variants was assessed using an enzymatic assay and High Performance Liquid Chromatography (Prapanthadara et al. 1993). *GSTE2* catalyzes the dehydrochlorination of DDT in the presence of glutathione (GSH) to produce 1,1-dichloro-2,2-bis(p-chlorophenyl) ethylene (DDE) (Ranson et al. 2001). Reverse-phase HPLC using a silica based stationary phase and a 90%:10% methanol:water mobile phase was used to separate DDT, DDE and the spike-in control dicofol according to their polarity. Standard curves were produced for DDT, DDE and dicofol using a doubling dilution series (200–12.5 µg/ml). The mobile solvent phase was pumped through the HPLC system (Ultimate 3000) at a rate of 1 ml/minute and 20 µl of each sample injected. Data acquisition was set at 18 minutes as DDE elutes at approximately 14 minutes with DDT eluting at ≈ 12 minutes, and the UV wavelength 232 nm selected. Compound concentration (µg/ml) was then plotted against the HPLC peak area to produce a standard curve with the intercept fixed at zero. The equation of this curve was employed to assess DDT, DDE and dicofol concentration in subsequent assays.

### **Enzyme kinetics**

To compare enzyme activity between variants, a doubling dilution series of DDT from 200–3.125 µg/ml was employed using optimized reaction parameters. Each assay contained 60 mg of *GSTE2* enzyme. All variant *GSTE2* proteins were assayed at each DDT concentration and a series of three technical replicates performed. The DDE peak

area from the HPLC trace was normalised against the dicofol spike-in area and the adjusted area used to calculate micrograms of DDE produced per ml reaction using the DDE standard curve. The DDE concentration was used to calculate the enzyme rate, expressed as mmol DDE/mg *GSTE2* protein/min. Michaelis-Menten and substrate inhibition plots were produced to compare the kinetics of each *GSTE2* allele based upon initial substrate concentration (DDT) and rate of product (DDE) formation in R (R-Core-Team 2012). The maximum enzyme rate ( $V_{\max}$ ), the point at which all enzyme active sites are bound to substrate, the Michaelis-Menten constant ( $K_M$ ), which is the substrate concentration for an enzyme at half its maximum velocity and  $K_{\text{cat}}$ , a measurement of overall catalytic turn-over rate, were derived from the fitted equations.

### **X-ray crystallography and corresponding recombinant protein production**

The *Gste2* variant ZAN/U was cloned into the expression vector pOPIN (Oxford Protein Production Facility-UK) via the In-Fusion PCR cloning system (Clontech). This vector incorporates His<sub>6</sub>- and SUMO-tags, as well as a SUMO protease cleavage site, N-terminal to the target insert. Protein expression was in *E. coli* BL21(DE3) Rosetta2 (Novagen). Cultures were grown at 37°C up to an OD<sub>600</sub> of 0.6 in Terrific broth supplemented with 50 µg/ml kanamycin and 34 µg/ml chloramphenicol. Expression was induced with 1 mM IPTG and cultures grown for a further 18hr at 25°C. Cells were harvested by centrifugation. The bacterial pellet was re-suspended in lysis buffer (25 mM Tris- HCl pH 8.0, 500 mM NaCl, 5 mM β-ME) and supplemented with 1.25 mM MgCl<sub>2</sub> and 250 units of benzonase before sonication on ice. The homogenate was clarified by centrifugation and affinity purified using a 3 ml Ni-NTA agarose (Qiagen)

column equilibrated in wash buffer (lysis buffer supplemented with 20 mM imidazole). Protein was eluted using 250 mM imidazole before over-night dialysis at 4°C against 25 mM Tris-HCl pH 8.0, 200 mM NaCl, 5 mM  $\beta$ -ME to remove imidazole and reduce salt concentration. Tags were removed by incubation with SUMO protease overnight at 4°C (1.7  $\mu$ l SUMO protease/mg fusion protein). Further purification used subtractive metal affinity and size exclusion chromatography in a Superdex 75 HR16/60 column (GE Healthcare) equilibrated in dialysis buffer. Purified samples were concentrated to 13 mg/ml via Vivaspin column (GE Healthcare). As the apo enzyme was unstable and degraded rapidly, it was supplemented with GSH (1:1.2 molar ratio) and the stabilized complex stored at 4°C until further use.

Crystals of ZAN/U:GSH were grown at 22°C in VDX 24-well plates in hanging drops. Drops consisted of 1  $\mu$ l protein solution and 1  $\mu$ l mother liquor containing 30% PEG 6000, 0.1 M Bis-Tris pH 6.5, 1 mM  $\beta$ -ME. Crystals grew within 3 days and exhibited rod morphologies with approximate dimensions of 0.2x0.05x0.05 mm<sup>3</sup>. Crystals were then soaked in mother liquor supplemented with 40% PEG 400 and DDE at saturation for 2 days. For X-ray data collection, crystals were retrieved and shock-frozen in liquid nitrogen. Diffraction data were collected at 100 K on beamline I04 at Diamond (Didcot, UK) and processed using XDS/XSCALE (McCoy et al. 2007). Processing statistics and crystallographic parameters are given in Table A3.4. The crystal form used in this study contained two biological dimers in its asymmetric unit (four molecular copies). Phasing was by molecular replacement in Phaser (McCoy et al. 2007) using a single molecular copy (A) from PDB entry 2IL3 (Wang et al. 2008). The model was manually rebuilt in COOT (Adams et al. 2002; Emsley & Cowtan 2004) and TLS refined

in Refmac5 using local NCS restraints (Murshudov et al. 2011). Solvent building was in Phenix and COOT. In the final model, the four molecular copies of ZAN/U:GSH were virtually identical (0.42 Å overall rmsd calculated with RAPIDO (Mosca & Schneider 2008)). DDE binding could not be identified in electron density maps. Model and refinement statistics are given in Table A3.4. Model coordinates and diffraction data have been deposited with the ProteinDataBank (PDB accession code 4GSN).

### **Heterologous expression of GSTE2 in *Drosophila melanogaster***

cDNA clones including the open reading frames for *Gste2*- ZAN/U and *Gste2*-Kisumu1B, were PCR-amplified using high fidelity AccuPrime Pfx polymerase (Invitrogen). The PCR primers used contained *EcoRI* and *NotI* restriction sites within the forward and reverse primers, respectively (Table A3.3). PCR products were gel-purified using the GenElute Gel Extraction Kit (Sigma) and subsequently ligated into a pUASTattB plasmid (obtained from Dr. Konrad Basler, University of Zurich) using T4 DNA ligase (New England Biolabs). Ligation mixtures were transformed into competent DH5 $\alpha$  cells for plasmid production, and individual colonies were verified using PCR. The EndoFree Plasmid Maxi Kit (Qiagen) was utilized to obtain purified plasmid DNA for subsequent steps. pUAST-attB clones containing *Gste2* inserts were sent to Rainbow Transgenic Flies, Inc. (Camarillo, CA, USA) for injection into Bloomington stock #9750 ( $y^1 w^{1118}$ ; PBac{ $y^+$ -attP-3B}VK00033) embryos. This Phi integration system enables site-specific recombination between the integration vector (pUAST-attB) and a landing platform in the fly stock (attP)(Venken et al. 2006).

Larvae were kept at 25°C, and G<sub>0</sub> flies that eclosed were sorted by sex prior to mating. To establish families of homozygous transgenic flies, G<sub>0</sub> flies were crossed with w<sup>1118</sup> flies and G<sub>1</sub> flies were sorted based on w<sup>+</sup> eye color (as a marker for insertion events). G<sub>1</sub> w<sup>+</sup> flies were crossed *inter se* to obtain homozygous insertion lines. The following *D. melanogaster* stocks were obtained from the Bloomington *Drosophila* Stock Center (Bloomington, IN, USA): y<sup>1</sup> w<sup>1</sup>; P{Act5C-GAL4}25FO1/CyO, y<sup>+</sup> and w<sup>1118</sup> (BL3605). Virgin females from both types of *Gste2* insertion stocks were crossed with *Act5C-GAL4/CyO* (ubiquitous Actin5C driver) flies. Control crosses were set up in parallel by crossing heterozygous (*Act5C*) GAL4 driver males to virgin w<sup>1118</sup> females.

To create dose response curves *Drosophila* adults were exposed to a range of DDT concentrations (Figure A3.7). DDT, dissolved in 100 µl of acetone, was added to 16x100 mm glass disposable culture tubes (VWR Scientific). Tubes were placed on their sides and continually oscillated until the entirety of the interior of tube was coated and all acetone had evaporated. A total of 8–12 control and 8–12 experimental transgenic flies were added to each tube. The tubes were capped with cotton wool saturated with a 10% (w/v) glucose/water solution. Tubes were then incubated at 25°C for 24 hr. After 24 hr, mortality, (as indicated by absence of movement) was recorded and LC<sub>50</sub> values calculated in the R language (R-Core-Team 2012).

## **Screening of allelic variants in wild-caught, DDT-phenotyped specimens of *Anopheles gambiae***

Data from catalytic assays, modeling and X-ray crystallography suggested that one of the non-synonymous changes had a marked effect on DDTase activity. A TaqMan SNP genotyping assay was designed to screen for the mutation in individual mosquitoes (see Table A3.3 for primer and probe sequences). DNA extracts from adult female mosquitoes from a number of locations in sub-Saharan Africa were genotyped for the *Gste2* allelic variants. In addition female mosquitoes with known DDT susceptibility phenotypes, as defined by the standard WHO protocol, were obtained from Burkina Faso (Badolo et al. 2012) and Benin. SNP genotyping assays were performed in 10 ml volume containing 1x Sensimix (Bioline), 1x primer/probe mix and 1  $\mu$ l template DNA with a temperature profile of 95°C for 10min followed by 40 cycles of 92°C for 15s and 60°C for 1min on an Agilent MX3005 real-time PCR machine. VIC and FAM fluorescence was captured at the end of each cycle and genotypes called from endpoint fluorescence using the Agilent MXPro software. Specimens from Benin and Burkina Faso were also screened for known DDT-resistance associated variants in the voltage-gated sodium channel (Bass et al. 2007; Jones et al. 2012). Genotype: phenotype associations were assessed using a generalized linear model with a logit link function (R-Core-Team 2012), chi-squared tests Poptools 3.2 (Hood 2010), and sample haplotype frequencies estimated using Haploview 4.2 (Barrett et al. 2005).

## F. TABLES, FIGURES AND LEGENDS

**Figure A3.1. Mean normalized expression of *GSTe2* in female *An. gambiae* s.s. of the DDT resistant ZAN/U strain and susceptible Kisumu strain.** Expression of *GSTe2* and ribosomal S7 were assessed from ten RNA pools comprised of ten 3 day old female mosquitoes using the GeXP quantitative PCR system (Beckman-Coulter). The ZAN/U colony showed 2.34 fold greater expression of *Gste2* compared with the Kisumu colony. *GSTe2* expression was normalized against housekeeping gene ribosomal S7. Standard error of the normalized mean expression is also indicated.

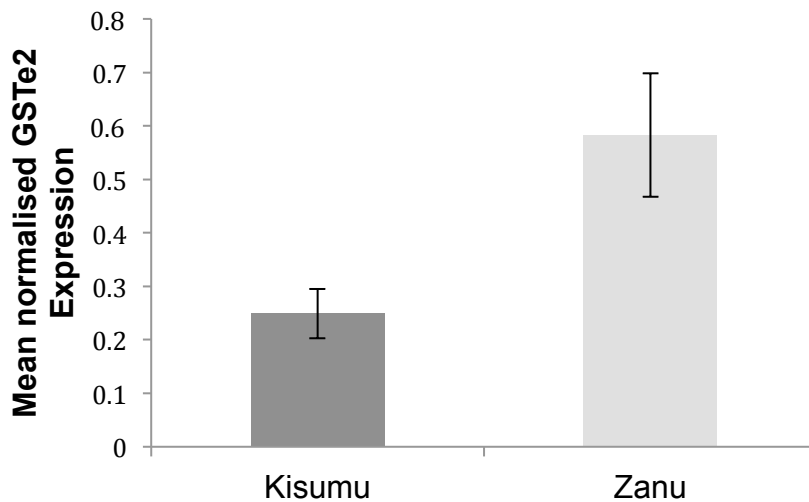


**Figure A3.2. Western blot comparison of *GSTe2* protein level in the Kisumu (Kis) and ZAN/U (Zan) *An. gambiae* s.s. strains.** Whole mosquito extracts from 10 unmated 3 day old female mosquitoes from each strain was probed with *An. gambiae* *GSTe2* polyclonal antibody. Approximately 1.7 times more *GSTe2* protein was present in the ZAN/U extract as determined by background corrected pixel intensities using the ImageJ v1.43 software. *Ae. aegypti* recombinant *GSTe2* was run as a positive control (+).

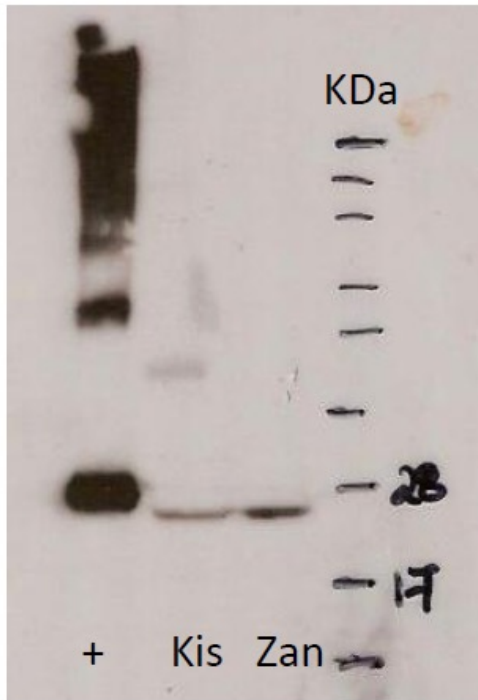




**Figure A3.3. Comparison of *GSTE2* catalyzed DDT metabolism for three variant recombinant proteins over a DDT dilution series.** Three allelic variants of enzyme *GSTE2* from *An. gambiae* are compared over a range of DDT concentrations and the mean production of DDE plotted from three replicate assays. Fitted curves used the Michaelis-Menten equation for the ZAN/U allele and a substrate inhibition equation for the two Kisumu alleles

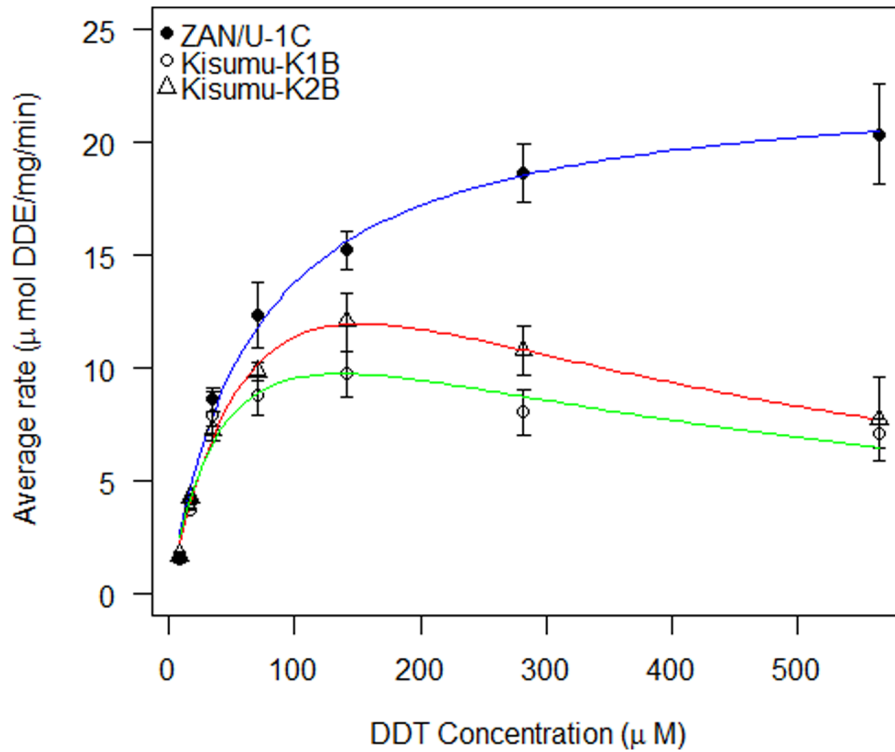


**Figure A3.4. Crystal structure of *GSTE2* ZAN/U variant.** a. Superposition of the crystal structure of ZAN/U determined in this study (orange) and the Kimusu 1B variant (grey; PDB entry IMI). A high degree of local and overall structural agreement is clearly noticeable. The location of the docked DDT is based on the computational prediction of Wang et al. (Wang et al. 2008). Some manual adjustments were made to relieve steric clashes and to better superimpose the DDT on the position of the hexyl group of bound S-hexylglutathione. b. Close-up detail of the ZAN/U active site. c. Superposition of structure of ZAN/U and Kimusu 1B variant local to position 114 (colour code as in a. A superimposition of ZAN/U from *An. gambiae* with the *GSTE2* from *An. funestus* is provided in Figure A3.5).

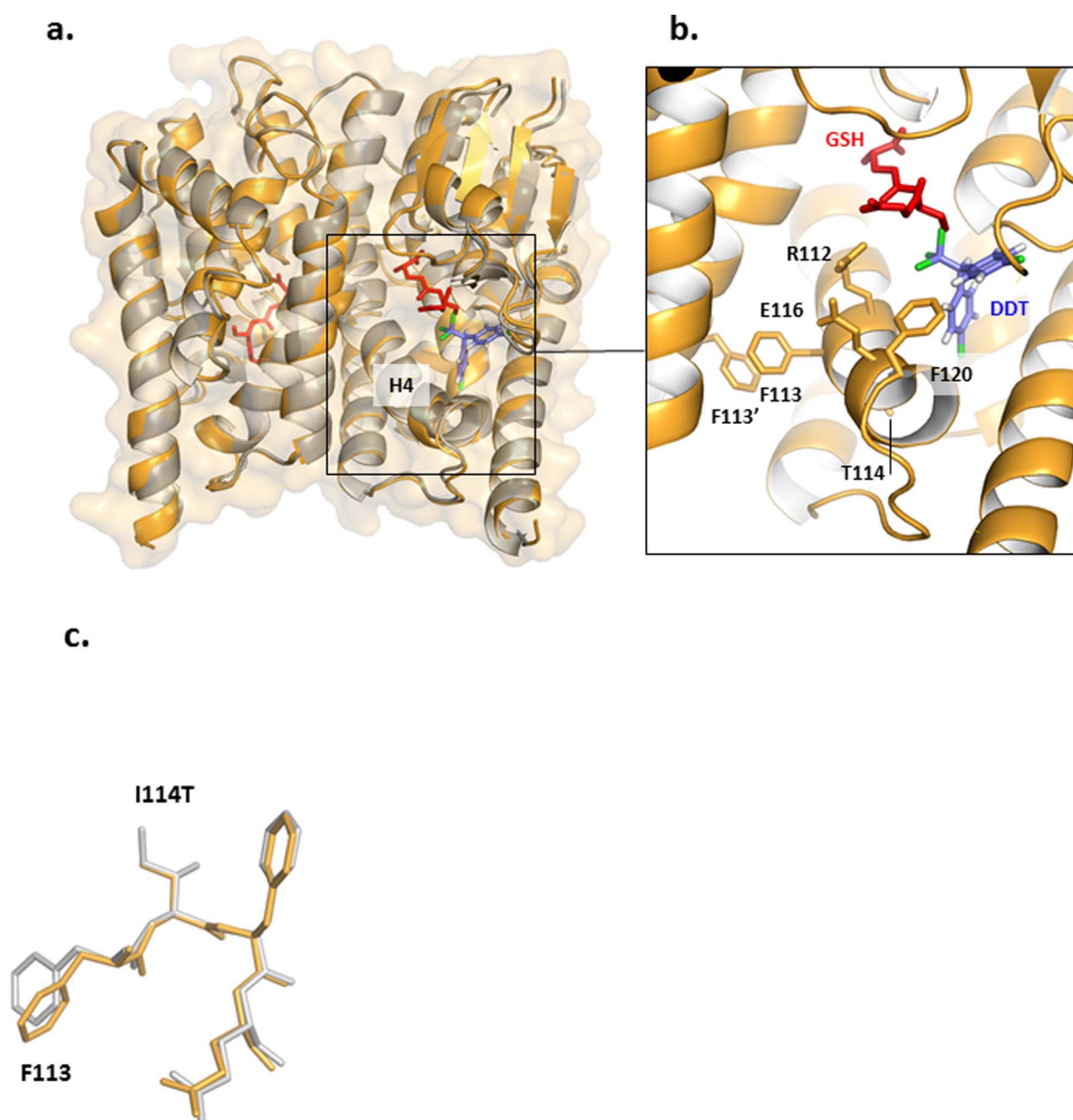


**Figure A3.5.** Superimposition of the *GSTE2* enzymes of *An. gambiae* (ZAN/U variant generated in this study containing Thr114; orange) and *An. funestus* (containing Ile114; blue). The GSH ligand is shown in red. a. Overall view; b. close-up of the mutated region of helix H4 showing the altered residue in position 114, and Phe113 at the dimer interface.

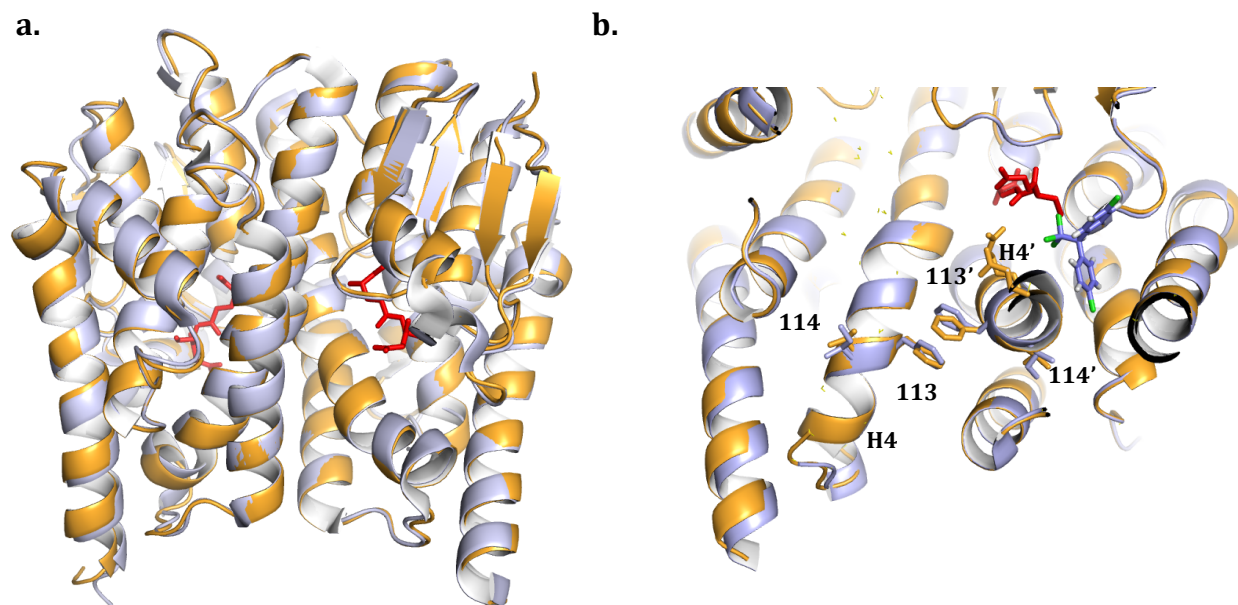


**Figure A3.6. Subunit Interface in *GSTE2* variants.** a. Close-up detail of interface groups in the *GSTE2* dimer. Phenylalanine residues F113 contributed by the respective helices H4 as well as tyrosines Y133 from neighboring helices pack together to form a linear stack. b. Electron density map (contoured at 1.0  $\sigma$ ) for the *GSTE2* ZAN/U variant. The mutated residue T114 is shown. The preceding residue F113 is poorly ordered and has been modeled as adopting two alternate conformations (towards the front and back of the paper plane).

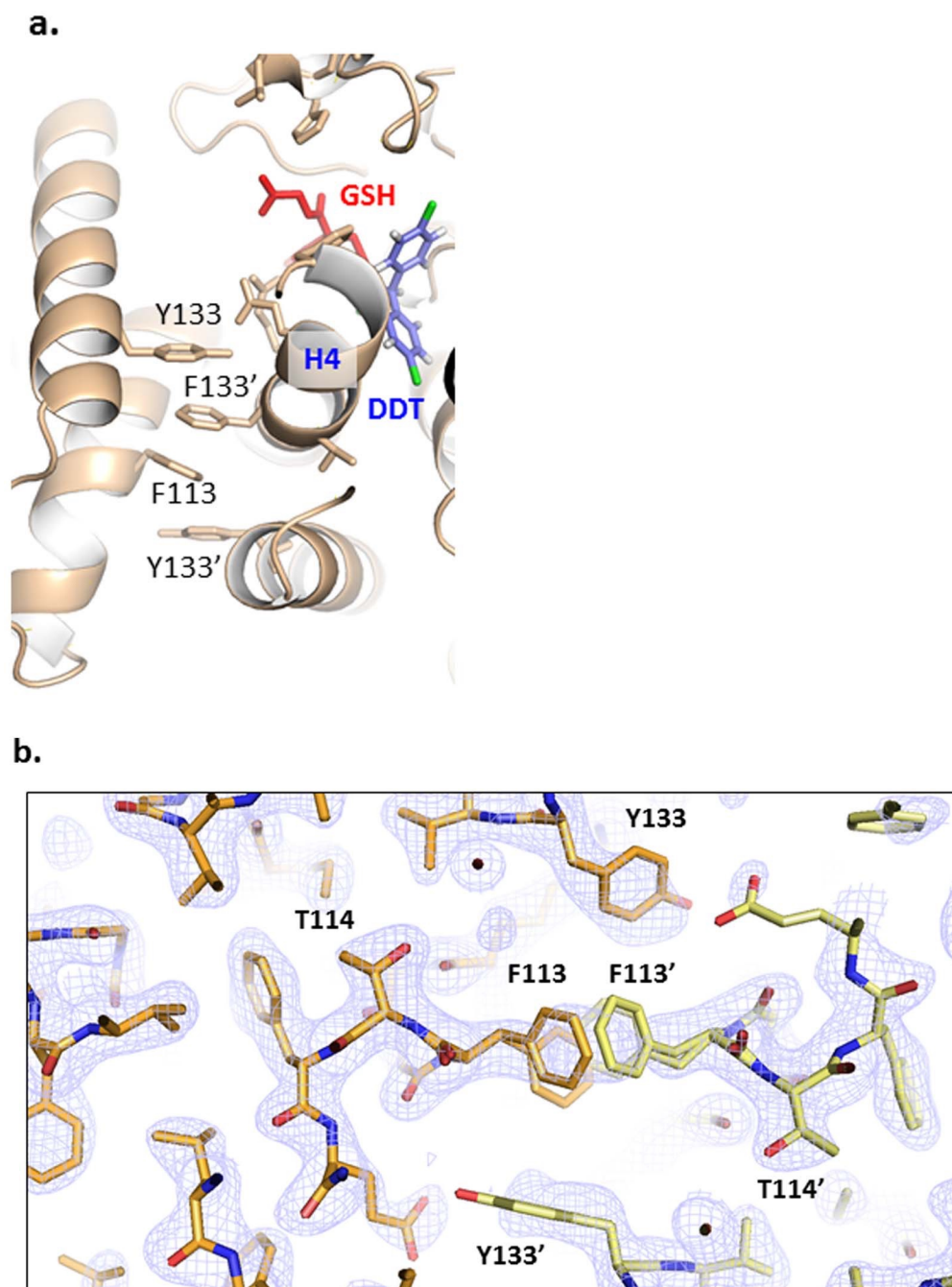


**Figure A3.7. Dose-response curves for *Drosophila melanogaster* adults transformed with *Anopheles gambiae* *Gste2* alleles.** The left panel shows survival of control (CyO x UAS+*Gste2*-Kisumu1B; black circles) and Kisumu allele expressing lines (Actin-Gal4 x UAS+*Gste2*-Kisumu1B; open circle) together with 95% confidence intervals. The right panel shows survival of control (CyO x UAS+*Gste2*-ZANU; black circles) and ZAN/U allele (Actin-Gal4 x UAS+*Gste2*-ZANU; open circle) together with 95% confidence intervals.

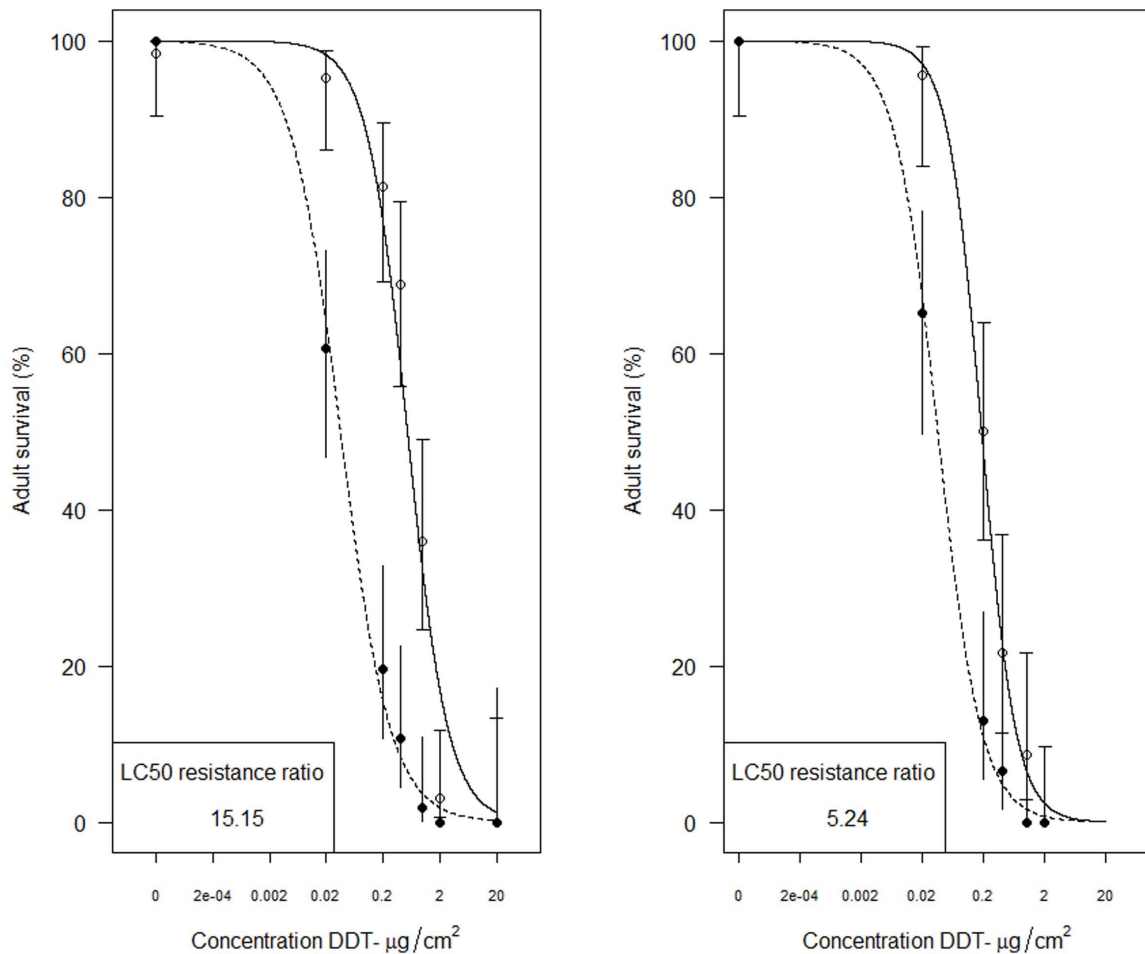


**Figure A3.8. Geographical variation in frequency of *Gste2*-I114T in the S and M molecular forms of *An. gambiae* across Africa.** Blue represents the I114 and red the T114 frequency. The molecular form of the collection is indicated by the letter overlaid on each chart. Samples were from: Benin S-form n = 111; M-form n = 223. Burkina Faso S-form n = 115; M-form n = 216. Cameroon S-form n = 55; M-form n = 652. Ghana S-form n = 29; M-form n = 758. Guinea-Bissau S-form n = 38; M-form n = 39. Mali S-form n = 31; M-form n = 26. Uganda S-form n = 207. The base map was obtained from [http://en.wikipedia.org/wiki/File:Africa\\_satellite\\_orthographic.jpg](http://en.wikipedia.org/wiki/File:Africa_satellite_orthographic.jpg) and was created by NASA. Details of the locations are given in Table A3.5.



**Figure A3.9. Summary of haplotypic association tests for the combination of four possible allele combinations at the *Vgsc*-1014 (*kdr*) and *Gste2*-114 loci with DDT susceptibility in *An. gambiae* M-form females from Benin (Panel A) and Burkina Faso (Panel B). Susceptibility to 4% DDT, was determined following a 1hr exposure to followed by 24hr recovery. Odds ratios are given with significance indicated by asterisks (\* $P = 0.0502$ , \* $P < 0.05$ , \*\* $P < 0.01$ , \*\*\* $P < 0.001$ ). The arrow is oriented from least to most resistant. The allele combination in bold (*Gste2*-114T: *kdr*-Phe) is the double mutant which is significantly associated with DDT resistance. wt = wildtype.**

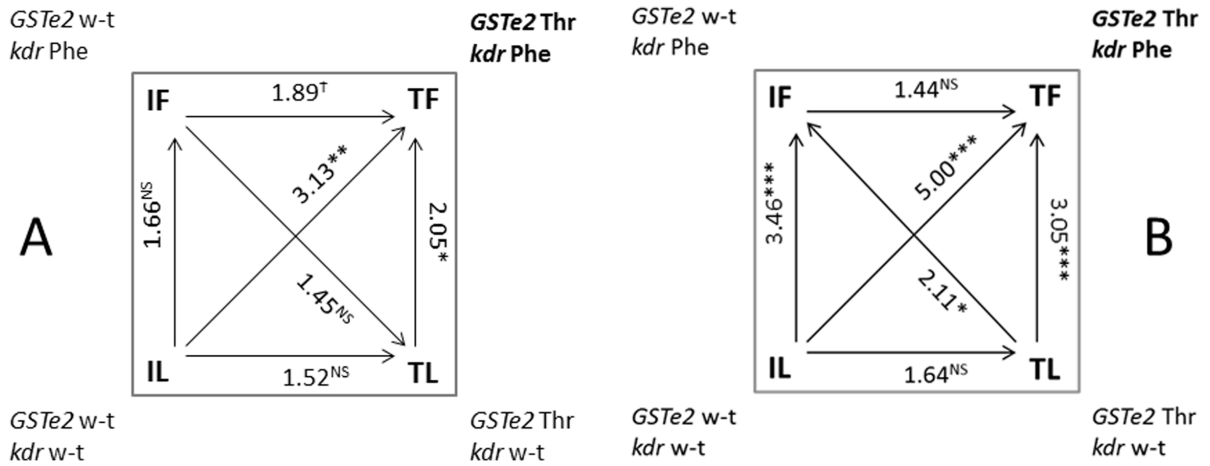




**Figure A3.10. SDS PAGE gel illustrating the purity of three recombinant variants of *Gste2* isolated from *An. gambiae* s.s.** The left panel represents 2.5  $\mu$ g and the right 1.25  $\mu$ g of each glycerol stored protein. SDS PAGE performed as previously outlined.

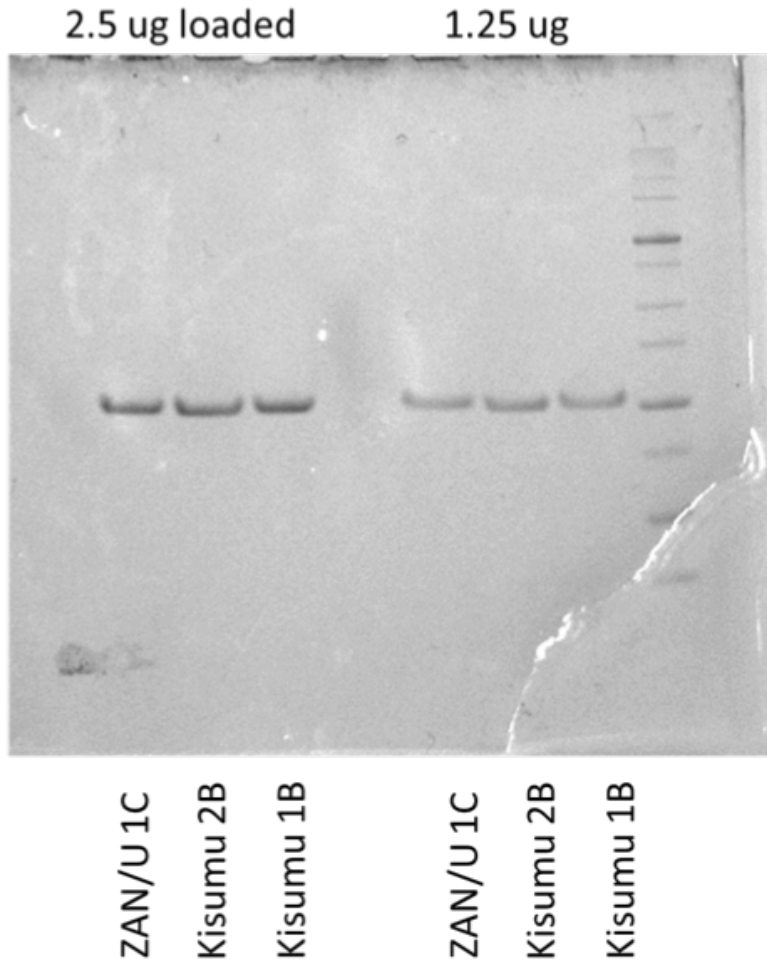




**Table A3.1. *GSTE2* allelic variants from the *An. gambiae* Kisumu and ZAN/U strain used for recombinant protein expression.**

<b>Cloned variant</b>	<b>Amino acid position</b>		<b>Specific activity (<math>\mu</math>moles/mg)</b>
	114	120	
Kisumu 1B	Isoleucine	Leucine	15.85
Kisumu 2B	Isoleucine	Phenylalanine	21.33
ZAN/U 1C	Threonine	Phenylalanine	7.10

The position of variant amino acids proximal to the putative DDT binding site are shown; together with the specific activity of the recombinant *GSTE2* with substrate CDNB. Protein concentrations were determined using a commercial assay (Fluka – Sigma-Aldrich) based on Bradford assay chemistry[40]. CDNB activity was determined by colorimetric assay and spectrophotometric reading.

**Table A3.2. Enzyme kinetic parameters of three *GSTE2* alleles with substrate DDT.**

	<b>Kisumu 1B</b>	<b>Kisumu 2B</b>	<b>ZAN/U 1C</b>
$K_M^{DDT}$ ( $\mu\text{M}$ )	50.9	97.8	66.4
$V_{max}$ ( $\mu\text{mol DDE}/\text{min}/\text{mg}$ )	17.0	27.2	22.9
$K_{cat}$ ( $\text{s}^{-1}$ )	14.1	22.5	18.9

Three variant *GSTE2* proteins were expressed from a DDT resistant (ZAN/U) and susceptible (Kisumu) strain of *An. gambiae* and assayed with substrate DDT over a range of concentrations. The maximum enzyme rate ( $V_{max}$ ), substrate concentration at half the maximum rate ( $K_M$ ) and catalytic turn-over ( $K_{cat}$ ) were calculated for each protein from a Michaelis-Menten or substrate inhibition equation (Figure 1).

**Table A3.3. PCR primers.** Numbers 1 and 2 - *Gste2* promoter region amplification and sequencing. Numbers 3 and 4-amplification of the *Gste2* coding region. Numbers 5 and 6- amplification of the coding region of *Gste2* incorporating the *NdeI* and *BamHI* restriction enzyme sites for subsequent cloning into expression vector pET-15b (Novagen). Numbers 7 and 8 Heterologous expression of *GSTE2* in *Drosophila melanogaster*. Numbers 9–12 primers and probes used in the Taqman assay for variants at the 114 codon. Probes 11 and 12 carried a non-fluorescent quencher at the 3'end.

	Primer/ probe name	Primer/ probe sequence
1	AGU1 F	5'-TTGCCGTACTATGAGGAGATCAAC-3'
2	AGU1 R	5'-TCTCTCTCAATCCCTTTACGTACC-3'
3	GSTe2 cDNA F	5'-CGCTGCGAAAATGTCCAACC-3'
4	GSTe2 cDNA Rb	5'-TACCTTTTTTAAGCCTAGCATTC-3'
5	GSTe2 cDNA_RE_F	5'-TTT <b>CATATG</b> TCCAACCTTGAC-3'
6	GSTe2 cDNA_RE_R	5'-TTT <b>GGATCCT</b> AAGCCTTAGCATTC-3'
7	GSTe2_ <i>fEcoRI</i>	5'-GAATTCATGTCCAACCTTGACTGTACACC-3'
8	GSTe2_ <i>rNotI</i> :	5'-GCGGCCGCTTAAGCCTTAGCATTCTCCTCCTT - 3'
9	114-Taqman primer F	5'-CGAGTCCGGCGTACTGTT-3'
10	114-Taqman primer R	5'-GGCGTTATGCTGGAAGTGGAA
11	114 Taqman probe ILE	5'-6FAM-ACGAAAATGAATCTC-3'
12	114 Taqman probe THR	5'-VIC-ACGAAAGTGAATCTC-3'

**Table A3.4. Statistics for X-ray data and model refinement.** The model contains all protein residues with the exception of Ala221 in chain A and C and Lys220-Ala221 in chain D that were disordered in the electron density maps.

<i>Diffraction data</i>		
X-ray source	I04, Diamond (Didcot)	
Detector	ADSC Quantum 315	
Wavelength (Å)	0.9763	
Spacegroup	P2 <sub>1</sub>	
Unit cell	a=51.33 Å, b=86.38 Å, c=92.85 Å, β=90.73	
Molecules a.u. / solvent content	4 / 40%	
Resolution	20.0-2.3 (2.35-2.30)	
Unique reflections	35941	(2245)
R <sub>sym</sub> (I) [%]	10.4	(50.7)
I/σ (I)	10.4	(3.3)
Multiplicity	3.72	(3.82)
Completeness (%)	99.4	(99.2)
<i>Refinement statistics</i>		
Nr Reflections in working / test sets	34800 / 1123	
R-factor/R <sub>free</sub> (%)	17.57 / 22.78	
Nr protein residues <sup>a</sup> / ligands / solvent atoms	878 / 4 x GSH / 198	
Total number of atoms	7260	
Average B-factors (Å <sup>2</sup> )	38.0	
rmsd bond / angle (°)	0.002 / 0.636	
Ramachandran analysis		
Favoured / Allowed / Outlier (%)	97.7 / 1.8 / 0.5	

**Table A3.5. Exact collection latitudes and longitudes of the collections used in figure A3.8.**

<b>Country</b>	<b>Location name/comment</b>	<b>Latitude</b>	<b>Longitude</b>
Benin	Cotonou	06°21'45"N	02°25'32"E
Benin	Pahou	06°22'60"N	02°13'00"E
Benin	Tori-Bossito	06°30'11"N	02°08'42"E
Benin	Bohicon	07°10'08"N	02°04'01"E
Benin	Sekou	06°37'00"N	02°13'00"E
Benin	Glazoue	07°58'25"N	02°14'24"E
Benin	Kandi	11°07' 43"N	02°56'13"E
Benin	Malanville	11°52'00"N	03°22'60"E
Burkina Faso	Soumosso	11° 01' 12"N	04° 03' 00"W
Burkina Faso	Goundry	12° 30' 00"N	01° 20' 00"W
Burkina Faso	Koupela	12° 11' 50"N	00° 21' 21"W
Burkina Faso	Kuinima	11° 08' 49"N	04° 17' 00"W
Cameroon		03° 52' 00"N	11° 31' 0"E
Ghana		05° 53' 00"N	00°00' 00"W
Guinea Bissau		11° 53' 28"N	15° 34' 55"W
Mali		13° 24' 00"N	7° 7' 48"W
Uganda		00° 41' 34"N	34° 10' 52"E

## **REFERENCES**

- Abdelsadik, A. & Roeder, T., 2010. Chronic activation of the epithelial immune system of the fruit fly's salivary glands has a negative effect on organismal growth and induces a peculiar set of target genes. *BMC Genomics*, 11, pp.1471–2164.
- Adams, P.D. et al., 2002. PHENIX: building new software for automated crystallographic structure determination. *Biological Crystallography*, D58, p.1948±1954.
- Ahoua Alou, L.P. et al., 2010. Distribution of ace-1R and resistance to carbamates and organophosphates in *Anopheles gambiae* s.s. populations from Côte d'Ivoire. *Malaria Journal*, 9(1), p.167.
- Abrieux, A. et al., 2014. The GPCR membrane receptor, DopEcR, mediates the actions of both dopamine and ecdysone to control sexpheromone perception in an insect. *Frontiers in Behavioral Neuroscience*, 8, pp.1–9.
- Ahmad, M., Denholm, I. & Bromilow, R.H., 2006. Delayed cuticular penetration and enhanced metabolism of deltamethrin in pyrethroid-resistant strains of *Helicoverpa armigera* from China and Pakistan. *Pest Management Science*, 62(9), pp.805–810.
- Akogbeto, M. et al., 2011. Dramatic Decrease in Malaria Transmission after Large-Scale Indoor Residual Spraying with Bendiocarb in Benin, an Area of High Resistance of *Anopheles gambiae* to Pyrethroids. *American Journal of Tropical Medicine and Hygiene*, 85(4), pp.586–593.
- Akogbéto, M.C. et al., 2010. Bendiocarb, a potential alternative against pyrethroid resistant *Anopheles gambiae* in Benin, West Africa. *Malaria Journal*, 9(1), p.204.
- Alfredo Ulloa-Aguirre et al., 1999. Structure-Activity Relationships of G Protein-Coupled Receptors. *Archives of Medical Research*, 30, pp.420–435.
- Alout, H. et al., 2012. Novel AChE Inhibitors for Sustainable Insecticide Resistance Management B. Brooke, ed. *PLoS ONE*, 7(10), p.e47125.
- Ali, D.W., Orchard, I. & Lange, A.B., 1993. The Aminergic Control of Locust (*Locusta migratoria*) Salivary Glands: Evidence for Dopaminergic and Serotonergic Innervation. *Journal of Insect Physiology*, 39, pp.623–632.
- Allen, J.A. & Roth, B.L., 2011. Strategies to Discover Unexpected Targets for Drugs Active at G Protein-Coupled Receptors. *Annual Review of Pharmacology and Toxicology*, 51(1), pp.117–144.
- Alonso, P.L. et al., 2011. A Research Agenda to Underpin Malaria Eradication. *PLoS Medicine*, 8(1), p.e1000406.
- Altschul, S.F. et al., 1990. Basic Local Alignment Search Tool undefined author, ed. *J. Mol. Biol.*, 215, pp.403–410.

- Amenya, D.A. et al., 2008. Over expression of a Cytochrome P450 (CYP6P9) in a Major African Malaria Vector, *Anopheles Funestus*, Resistant to Pyrethroids. *Insect Molecular Biology*, 17, pp.19–25.
- An, C. et al., 2011. Characterization of a regulatory unit that controls melanization and affects longevity of mosquitoes. *Cellular and Molecular Life Sciences*, 68(11), pp.1929–1939.
- Andretica, R. et al., 2008. *Drosophila* D1 dopamine receptor mediates caffeine-induced arousal. *PNAS*, 105, pp.20392–20397.
- Andrews, J.M., Quinby, G.E. & Langmuir, A.D., 1950. Malaria Eradication in the United States. *American Journal of Public Health*, 40, pp.1405–1411.
- Aparicio, R. et al., 2013. dRYBP Contributes to the Negative Regulation of the *Drosophila* Imd Pathway F. Leulier, ed. *PLoS ONE*, 8(4), p.e62052.
- Apple, R.T. & Fristrom, J.W., 1991. 20-Hydroxyecdysone Is Required for, and Negatively Regulates, Transcription of *Drosophila* Pupal Cuticle Protein Genes. *Developmental Biology*, 146, pp.569–582.
- Araujo, R.N. et al., 2006. RNA interference of the salivary gland nitrophorin 2 in the triatomine bug *Rhodnius prolixus* (Hemiptera: Reduviidae) by dsRNA ingestion or injection. *Insect Biochemistry and Molecular Biology*, 36(9), pp.683–693.
- Awolola, T.S. et al., 2009. Evidence of multiple pyrethroid resistance mechanisms in the malaria vector *Anopheles gambiae sensu stricto* from Nigeria. *Transactions of the Royal Society of Tropical Medicine and Hygiene*, 103(11), pp.1139–1145.
- Ayala, D. et al., 2009. Habitat suitability and ecological niche profile of major malaria vectors in Cameroon. *Malaria Journal*, 8(1), p.307.
- Ayme, A. & Tissieres, A., 1985. Locus 67B of *Drosophila melanogaster* contains seven, not four, closely related heat shock genes. *The EMBO Journal*, 4, pp.2949–2954.
- Åkerfelt, M., Morimoto, R.I. & Sistonen, L., 2010. Heat shock factors: integrators of cell stress, development and lifespan. *Nature Reviews Molecular Cell Biology*, 11(8), pp.545–555.
- Badenhorst, P., 2005. The *Drosophila* nucleosome remodeling factor NURF is required for Ecdysteroid signaling and metamorphosis. *Genes & Development*, 19(21), pp.2540–2545.
- Badolo, A. et al., 2012. Three years of insecticide resistance monitoring in *Anopheles gambiae* in Burkina Faso: resistance on the rise? *Malaria Journal*, 11(1), pp.1–1.
- Bai, H. & Palli, S.R., 2015. Advanced Technologies for Managing Insect Pest. *Advanced Technologies for Managing Insect Pests*, pp.57–82.



- Bai, H. et al., 2011. Large-scale RNAi screen of G protein-coupled receptors involved in larval growth, molting and metamorphosis in the red flour beetle. *BMC Genomics*, 12(1), p.388.
- Baldini, F. et al., 2013. The Interaction between a Sexually Transferred Steroid Hormone and a Female Protein Regulates Oogenesis in the Malaria Mosquito *Anopheles gambiae* D. S. Schneider, ed. *PLoS Biology*, 11(10), p.e1001695.
- Baker, D.A. et al., 2011. A comprehensive gene expression atlas of sex- and tissue-specificity in the malaria vector, *Anopheles gambiae*. *BMC Genomics*, 12(1), p.296.
- Bang, S. et al., 2011. Dopamine Signalling in Mushroom Bodies Regulates Temperature-Preference Behaviour in *Drosophila*. *PLoS Genetics*, 7(3), p.e1001346.
- Bargmann, C.I., 2006. Comparative chemosensation from receptors to ecology. *Nature*, 444(7117), pp.295–301.
- Barrett, J.C. et al., 2005. Haploview: analysis and visualization of LD and haplotype maps. *Bioinformatics*, 21(2), pp.263–265.
- Bartoloni, A. & Zammarchi, L., 2012. Clinical Aspects of Uncomplicated and Severe Malaria. *Mediterranean Journal of Hematology and Infectious Diseases*, 4(1), p.2012026.
- Bashar, K. et al., 2012. Blood-feeding patterns of *Anopheles* mosquitoes in a malaria-endemic area of Bangladesh. *Parasites & Vectors*, 5(1), p.39.
- Bass, C. et al., 2007. Detection of knockdown resistance (kdr) mutations in *Anopheles gambiae*: a comparison of two new high-throughput assays with existing methods. *Malaria Journal*, 6(1), p.111.
- Bass, C. et al., 2010. Pesticide Biochemistry and Physiology. *Pesticide Biochemistry And Physiology*, 96(2), pp.80–85.
- Baumann, O. et al., 2002. Distribution of serotonergic and dopaminergic nerve fibers in the salivary gland complex of the cockroach *Periplaneta americana*. *BMC Physiology*, 2, pp.1–15.
- Beare, N.A.V. et al., 2006. Malarial Retinopathy: A Newly Established Diagnostic Sign in Severe Malaria. *Am J Trop Med Hyg*, 75, pp.790–797.
- Beggs, K.T., Tyndall, J.D.A. & Mercer, A.R., 2011. Honey Bee Dopamine and Octopamine Receptors Linked to Intracellular Calcium Signaling Have a Close Phylogenetic and Pharmacological Relationship I. A. Hansen, ed. *PLoS ONE*, 6(11), p.e26809.

- Behrens, M. et al., 2007. Gustatory Expression Pattern of the Human TAS2R Bitter Receptor Gene Family Reveals a Heterogenous Population of Bitter Responsive Taste Receptor Cells. *Journal of Neuroscience*, 27(46), pp.12630–12640.
- Beier, J.C. et al., 2012. Attractive toxic sugar bait (ATSB) methods decimate populations of Anopheles malaria vectors in arid environments regardless of the local availability of favoured sugar-source blossoms. *Malaria Journal*, 11(1), p.31.
- Benedict, M.Q., 2014. Methods in Anopheles Research. pp.1–419.
- Benjamini, Y. et al., 2001. Controlling the false discovery rate in behavior genetics research. *Behavioural Brain Research*, 125, pp.279–284.
- Benton, R., 2009. Molecular Basis of Odor Detection in Insects. *Annals of the New York Academy of Sciences*, 1170(1), pp.478–481.
- Benton, R. et al., 2006. Atypical Membrane Topology and Heteromeric Function of Drosophila Odorant Receptors In Vivo. *PLoS Biology*, 4(2), p.e20.
- Besansky, N.J., Hill, C.A. & Costantini, C., 2004. No accounting for taste: host preference in malaria vectors. *Trends in Parasitology*, 20(6), pp.249–251.
- Biamonte, M.A., Wanner, J. & Le Roch, K.G., 2013. Recent advances in malaria drug discovery. *Bioorganic & Medicinal Chemistry Letters*, 23(10), pp.2829–2843.
- Birman, S. et al., 1994. A Novel and Major Isoform of Tyrosine Hydroxylase in Drosophila Is Generated by Alternative RNA Processing. *The Journal of Biological Chemistry*, 269(12), pp.26559–26567.
- Blenau, W. & Baumann, A., 2001. Molecular and Pharmacological Properties of Insect Biogenic Amine Receptors: Lessons From Drosophila melanogaster and Apis mellifera. *Archives of Insect Biochemistry and Physiology*, 48, pp.13–38.
- Blenau, W., Erber, J. & Baumann, A., 1998. Characterization of a Dopamine D1 Receptor from Apis mellifera: Cloning, Functional Expression, Pharmacology, and mRNA Localization in the Brain. *Journal of Neurochemistry*, 70, pp.15–23.
- Boivin, B. et al., 2008. G Protein-Coupled Receptors in and on the Cell Nucleus: A New Signaling Paradigm? *Journal of Receptors and Signal Transduction*, 28(1-2), pp.15–28.
- Bradford, M.M., 1976. A Rapid and Sensitive Method for the Quantitation of Microgram Quantities of Protein Utilizing the Principle of Protein-Dye Binding. *Analytical Biochemistry*, 72, pp.248–254.
- Brand, A.H. & Perrimon, N., 1993. Targeted gene expression as a means of altering cell fates and generating dominant phenotypes. *Development*, 118, pp.401–415.

- Brauchi, S., Orio, P. & Latorre, R., 2004. Clues to understanding cold sensation: Thermodynamics and electrophysiological analysis of the cold receptor TRPM8. *PNAS*, 101(43), pp.15494–15499.
- Bray, P.G. et al., 1998. Access to Hematin: The Basis of Chloroquine Resistance. *Molecular Pharmacology*, 54, pp.170–179.
- Bray, S. & Amrein, H., 2003. A Putative *Drosophila* Pheromone Receptor Expressed in Male-Specific Taste Neurons Is Required for Efficient Courtship. *Neuron*, 39, pp.1019–1029.
- Broderick, N.A., Buchon, N. & Lemaitre, B., 2014. Microbiota-Induced Changes in *Drosophila melanogaster* Host Gene Expression and Gut Morphology. *mBio*, 5(3), pp.e01117–14–e01117–14.
- Brody, T. & Cravchik, A., 2000. *Drosophila melanogaster* G Protein–coupled Receptors. *The Journal of Cell Biology*, 150(2), pp.F83–F88.
- Brooke, B.D. et al., 2001. Bioassay and biochemical analyses of insecticide resistance in southern African *Anopheles funestus* (Diptera: Culicidae). *Bulletin of entomological research*, 91(04), pp.265–272.
- Buchon, N. et al., 2009. *Drosophila* Intestinal Response to Bacterial Infection: Activation of Host Defense and Stem Cell Proliferation. *Cell Host and Microbe*, 5(2), pp.200–211.
- Buck, L. & Axel, R., 1991. A Novel Multigene Family May Encode Odorant Receptors: A Molecular Basis for Odor Recognition. *Cell*, 65, pp.175–187.
- Budnik, V. & White, K., 1987. Genetic dissection of dopamine and serotonin synthesis in the nervous system of *Drosophila melanogaster*. *Journal of Neurogenetics*, 4, pp.309–314.
- Burand, J.P. & Hunter, W.B., 2013. RNAi: Future in insect management. *Journal of Invertebrate Pathology*, 112(S1), pp.S68–S74.
- Butcher, G.A., Cohen, S. & Garnham, P., 1970. Passive immunity in *Plasmodium knowlesi* malaria. *Transactions of the Royal Society of Tropical Medicine and Hygiene*, 64(6), pp.1–8.
- Carvalho, R. et al., 2012. Pesticide Biochemistry and Physiology. *Pesticide Biochemistry And Physiology*, 104(2), pp.143–149.
- Cator, L.J. et al., 2010. Sizing up a mate: variation in production and response to acoustic signals in *Anopheles gambiae*. *Behavioral Ecology*, 21(5), pp.1033–1039.

- Catteruccia, F. & Levashina, E. A. 2009. RNAi in the Malaria Vector, *Anopheles gambiae*: Therapeutic Applications of RNAi: Methods and Protocols. *Methods Mol. Biol.* **555**, 63–75.
- Chandor Proust, A. et al., 2013. The central role of mosquito cytochrome P450 CYP6Zs in insecticide detoxification revealed by functional expression and structural modelling. *Biochem. J.*, 455(1), pp.75–85.
- Chareonviriyaphap, T. et al., 2013. Review of insecticide resistance and behavioral avoidance of vectors of human diseases in Thailand. *Parasites & Vectors*, 6(1), pp.1–28.
- Charles, J.P., 2010. The regulation of expression of insect cuticle protein genes. *Insect Biochemistry and Molecular Biology*, 40(3), pp.205–213.
- Charlwood, J.D. & Jones, M.D.R., 1980. Mating in the mosquito, *Anopheles gambiae* s.l. *Physiological Entomology*, 5, pp.315–320.
- Charlwood, J.D. et al., 1997. Survival and infection probabilities of anthropophilic anophelines from an area of high prevalence of *Plasmodium falciparum* in humans. *Bulletin of entomological research*, 87, pp.445–453.
- Charroux, B. & Royet, J., 2012. Gut-microbiota interactions in non-mammals: What can we learn from *Drosophila*? *Seminars in Immunology*, 24(1), pp.17–24.
- Cheruiyot, J. et al., 2014. Polymorphisms in *Pfmdr1*, *Pfcrt*, and *Pfnhe1* Genes Are Associated with Reduced In Vitro Activities of Quinine in *Plasmodium falciparum* Isolates from Western Kenya. *Antimicrobial Agents and Chemotherapy*, 58(7), pp.3737–3743.
- Chiu, T.-L. et al., 2008. Comparative molecular modeling of *Anopheles gambiae* CYP6Z1, a mosquito P450 capable of metabolizing DDT. *PNAS*, 105(26), pp.8855–8860.
- Choi, C. et al., 2012. Autoreceptor Control of Peptide/Neurotransmitter Corelease from PDF Neurons Determines Allocation of Circadian Activity in *Drosophila*. *Cell Reports*, 2(2), pp.332–344.
- Chouaibou, M.S. et al., 2012. Increase in susceptibility to insecticides with aging of wild *Anopheles gambiae* mosquitoes from Côte d'Ivoire. *BMC Infectious Diseases*, 12(1), pp.1–11.
- Chyb, S. et al., 2003. *Drosophila* Gr5a encodes a taste receptor tuned to trehalose. *PNAS*, 100, pp.14526–14530.
- Claudianos, C., Russell, R.J. & Oakeshott, J.G., 1999. The same amino acid substitution in orthologous esterases confers organophosphate resistance on the house fly and a blowfly. *Insect Biochemistry and Molecular Biology*, 29, pp.675–686.

- Clements, A.N., 1992. *The Biology of Mosquitoes. Volume I. Chapman & Hall, New York.*
- Clements, A.N., 1999. *The Biology of Mosquitoes. Volume II. Cabi, Wallingford.*
- Clements, A.N., 1955. The Sources of Energy for Flight in Mosquitoes. *Exp. Biol.*, 32, pp.1–8.
- Clyne, P.J., 2000. Candidate Taste Receptors in *Drosophila*. *Science*, 287(5459), pp.1830–1834.
- Clyne, P.J. et al., 1999. A Novel Family of Divergent Seven-Transmembrane Proteins: Candidate Odorant Receptors in *Drosophila*. *Neuron*, 22, pp.327–338.
- Coetzee, M. et al., 2013. *Anopheles coluzzii* and *Anopheles amharicus*, new members of the *Anopheles gambiae* complex. *Zootaxa*, 3619(3).
- Cohet, Y., 1975. Epigenetic influences on the lifespan of the *Drosophila*: existence of an optimal growth temperature for adult longevity. *Exp. Geront.*, 10, pp.181–184.
- Conley, J.M. et al., 2015. Evaluation of AaDOP2 Receptor Antagonists Reveals Antidepressants and Antipsychotics as Novel Lead Molecules for Control of the Yellow Fever Mosquito, *Aedes aegypti*. *Journal of Pharmacology and Experimental Therapeutics*, 352(1), pp.53–60.
- Cook, P.E. & Sinkins, S.P., 2010. Transcriptional profiling of *Anopheles gambiae* mosquitoes for adult age estimation. *Insect Molecular Biology*, 19(6), pp.745–751.
- Corbel, V. et al., 2007. Multiple insecticide resistance mechanisms in *Anopheles gambiae* and *Culex quinquefasciatus* from Benin, West Africa. *Acta Tropica*, 101(3), pp.207–216.
- Cowman, A.F. et al., 1988. Amino acid changes linked to pyrimethamine resistance in the dihydrofolate reductase-thymidylate synthase gene of *Plasmodium falciparum*. *PNAS*, 85, pp.9109–9113.
- Crosnier, C. et al., 2011. Basigin is a receptor essential for erythrocyte invasion by *Plasmodium falciparum*. *Nature*, 480(7378), pp.534–537.
- Crossgrove, K. et al., 1996. The *Drosophila* Broad-Complex Early Gene Directly Regulates Late Gene Transcription during the Ecdysone-Induced Puffing Cascade. *Developmental Biology*, 180, pp.745–758.
- Cui, X. & Churchill, G.A., 2003. Statistical tests for differential expression in cDNA microarray experiments. *Genome Biology*, 4(4), pp.210.1–210.10.

- Dabire, K.R. et al., 2009. Distribution of insensitive acetylcholinesterase (ace-1R) in *Anopheles gambiae*s.l. populations from Burkina Faso (West Africa). *Tropical Medicine & International Health*, 14(4), pp.396–403.
- Dabire, K.R. et al., 2013. Assortative mating in mixed swarms of the mosquito *Anopheles gambiae* s.s. M and S molecular forms, in Burkina Faso, West Africa. *Medical and Veterinary Entomology*, 27(3), pp.298–312.
- Daborn, P. et al., 2001. DDT resistance in correlates with over-expression and confers cross-resistance to the neonicotinoid imidacloprid. *Molecular Genetics and Genomics*, 266(4), pp.556–563.
- Daborn, P.J. et al., 2002. A Single P450 Allele Associated with Insecticide Resistance in *Drosophila*. *Science*, 297, pp.2253–2256.
- Daborn, P.J. et al., 2012. Using *Drosophila melanogaster* to validate metabolism-based insecticide resistance from insect pests. *Insect Biochemistry and Molecular Biology*, 42(12), pp.918–924.
- Dahanukar, A. et al., 2001. A Gr receptor is required for response to the sugar trehalose in taste neurons of *Drosophila*. *Nature Neuroscience*, 4(12), pp.1182–1186.
- Dahanukar, A. et al., 2007. Two Gr genes underlie sugar reception in *Drosophila*. *Neuron*, 56(3), pp.503–516.
- Daniels, R.L. & McKemy, D.D., 2007. Mice left out in the cold: commentary on the phenotype of TRPM8-nulls. *Molecular Pain*, 3(1), p.23.
- David, J.-P. et al., 2005. The *Anopheles gambiae* detoxification chip: A highly specific microarray to study metabolic-based insecticide resistance in malaria vectors. *PNAS*, 102(11), pp.4080–4084.
- David, J.P. et al., 2013. Role of cytochrome P450s in insecticide resistance: impact on the control of mosquito-borne diseases and use of insecticides on Earth. *Philosophical Transactions of the Royal Society B: Biological Sciences*, 368(1612), pp.1–12.
- Davies, T.G.E. et al., 2007. DDT, pyrethrins, pyrethroids and insect sodium channels. *IUBMB Life*, 59(3), pp.151–162.
- Davis, M.B. et al., 2005. Phenotypic analysis of EcR-A mutants suggests that EcR isoforms have unique functions during *Drosophila* development. *Developmental Biology*, 282(2), pp.385–396.
- Davis, M.M. et al., 2007. A neuropeptide hormone cascade controls the precise onset of post-eclosion cuticular tanning in *Drosophila melanogaster*. *Development*, 134(24), pp.4395–4404.

- de Bruyne, M., Clyne, P.J. & Carlson, J.R., 1999. Odor Coding in a Model Olfactory Organ: The *Drosophila* Maxillary Palp. *The Journal of Neuroscience*, 19, pp.4520–4532.
- Dehouck, Y. et al., 2009. Fast and accurate predictions of protein stability changes upon mutations using statistical potentials and neural networks: PoPMuSiC-2.0. *Bioinformatics*, 25(19), pp.2537–2543.
- Dehouck, Y. et al., 2011. PoPMuSiC 2.1: a web server for the estimation of protein stability changes upon mutation and sequence optimality. *BMC Bioinformatics*, 12(1), p.151.
- Detinova, T.S., 1962. Age-grouping methods in Diptera of medical importance. *WHO Monograph Series*, 47, pp.1–216.
- Dewey, E.M. et al., 2004. Identification of the Gene Encoding Bursicon, an Insect Neuropeptide Responsible for Cuticle Sclerotization and Wing Spreading. *Current Biology*, 14(13), pp.1208–1213.
- Dhaka, A., Viswanath, V. & Patapoutian, A., 2006. TRP Ion Channels and Temperature Sensation. *Annu. Rev. Neurosci.*, 29, pp.135–161.
- Ding, Y. et al., 2003. The *Anopheles gambiae* glutathione transferase supergene family: annotation, phylogeny and expression profiles. *BMC Genomics*, 4(1), p.35.
- Dinio, T. et al., 2012. Investigating the activity of quinine analogues versus chloroquine resistant *Plasmodium falciparum*. *Bioorganic & Medicinal Chemistry*, 20(10), pp.3292–3297.
- Ditzen, M., Pellegrino, M. & Vosshall, L.B., 2008. Insect Odorant Receptors Are Molecular Targets of the Insect Repellent DEET. *Science*, 319(5871), pp.1838–1842.
- Djogbenou, L. et al., 2007. Characterization of insensitive acetylcholinesterase (ace-1(R)) in *Anopheles gambiae*(Diptera: Culicidae): resistance levels and dominance. *J. Med Entomol.*, 44(5), pp.805–810.
- Djogbénou, L. et al., 2008. Evidence of Introgression of the ace-1R Mutation and of the ace-1 Duplication in West African *Anopheles gambiae* s. s D. A. Carter, ed. *PLoS ONE*, 3(5), p.e2172.
- Djogbénou, L., Noel, V. & Agnew, P., 2010. Costs of insensitive acetylcholinesterase insecticide resistance for the malaria vector *Anopheles gambiae* homozygous for the G119S mutation. *Malaria Journal*, 9(1), p.12.
- Doctor, J., Fristrom, D.K. & Fristrom, J.W., 1985. The pupal cuticle of *Drosophila*: biphasic synthesis of pupal cuticle proteins in vivo and in vitro in response to 20-hydroxyecdysone. *The Journal of Cell Biology*, 101, pp.189–200.

- Dondorp, A.M. et al., 2009. Artemisinin Resistance in Plasmodium falciparum Malaria. *N Engl J Med*, 361(5), pp.455–467.
- Donnelly, M.J. & Townson, H., 2000. Evidence for extensive genetic differentiation among populations of the malaria vector *Anopheles arabiensis* in Eastern Africa. *Insect Molecular Biology*, 9(4), pp.357–367.
- Dotson, E.M. et al., 1998. A family of pupal-specific cuticular protein genes in the mosquito *Anopheles gambiae*. *Insect Biochemistry and Molecular Biology*, 28, pp.459–472.
- Draper, I. et al., 2007. Locomotor activity is regulated by D2-like receptors in *Drosophila*: An anatomic and functional analysis. *Developmental Neurobiology*, 67(3), pp.378–393.
- Duffy, J.B., 2002. GAL4 system in *Drosophila*: A fly geneticist's swiss army knife. *genesis*, 34(1-2), pp.1–15.
- Dulin, F. et al., 2012. Ecotoxicology and Environmental Safety. *Ecotoxicology and Environmental Safety*, 79(C), pp.13–21.
- Dunipace, L. et al., 2001. Spatially restricted expression of candidate taste receptors in the *Drosophila* gustatory system. *Current Biology*, 11, pp.822–835.
- Durand, R. et al., 2001. Analysis of pfcrt point mutations and chloroquine susceptibility in isolates of *Plasmodium falciparum*. *Molecular and Biochemical Parasitology*, 114, pp.95–102.
- Eckstein-Ludwig, U. et al., 2003. Artemisinins target the SERCA of *Plasmodium falciparum*. *Nature*, 424, pp.957–961.
- Edgar, R., Domrachev, M. & Lash, A.E., 2002. Gene Expression Omnibus: NCBI gene expression and hybridization array data repository. *Nucleic Acids Research*, 30, pp.207–210.
- Edgar, R.C., 2004. MUSCLE: multiple sequence alignment with high accuracy and high throughput. *Nucleic Acids Research*, 32(5), pp.1792–1797.
- Edi, C.V. et al., 2014. CYP6 P450 Enzymes and ACE-1 Duplication Produce Extreme and Multiple Insecticide Resistance in the Malaria Mosquito *Anopheles gambiae* J. Zhang, ed. *PLoS Genetics*, 10(3), p.e1004236.
- Emsley, P. & Cowtan, K., 2004. Coot: model-building tools for molecular graphics. *Acta Crystallographica Section D Biological Crystallography*, 60(12), pp.2126–2132.
- Enayati, A. & Hemingway, J., 2010. Malaria Management: Past, Present, and Future. *Annual Review of Entomology*, 55(1), pp.569–591.



- Erturk-Hasdemira, D. et al., 2009. Two roles for the *Drosophila* IKK complex in the activation of Relish and the induction of antimicrobial peptide genes. *PNAS*, 106(24), pp.9779–9784.
- Essandoh, J., Yawson, A.E. & Weetman, D., 2013. Acetylcholinesterase (Ace-1) target site mutation 119S is strongly diagnostic of carbamate and organophosphate resistance in *Anopheles gambiae* s.s. and *Anopheles coluzzii* across southern Ghana. *Malaria Journal*, 12, pp.1–10.
- Evans, P.D., Bayliss, A. & Reale, V., 2014. GPCR-mediated rapid, non-genomic actions of steroids: Comparisons between DmDopEcR and GPER1 (GPR30). *General and comparative endocrinology*, 195(C), pp.157–163.
- Eveleth, D.D. et al., 1986. Sequence and structure of the dopa decarboxylase gene of *Drosophila*: evidence for novel RNA splicing variants. *The EMBO Journal*, 5, pp.2663–2672.
- Falk, R., Bleiser-Avivi, N. & Atidia, J., 1976. Labellar Taste Organs of *Drosophila melanogaster*. *Journal of Morphology*, 150, pp.327–341.
- Fanello, C., Santolamazza, F. & Torre, Della, A., 2002. Simultaneous identification of species and molecular forms of the *Anopheles gambiae* complex by PCR-RFLP. *Medical and Veterinary Entomology*, 16, pp.461–464.
- Farnham, A.W., 2015. The mode of action of piperonyl butoxide with reference to studying pesticide resistance. *Piperonyl Butoxide*, pp.199–213.
- Fechtel, K., Fristrom, D.K. & Fristrom, J.W., 1989. Prepupal differentiation in *Drosophila*: distinct cell types elaborate a shared structure, the pupal cuticle, but accumulate transcripts in unique patterns. *Development*, 106, pp.649–656.
- Feng, G. et al., 1996. Cloning and Functional Characterization of a Novel Dopamine Receptor from *Drosophila melanogaster*. *The Journal of Neuroscience*, 16(12), pp.3925–3933.
- Fernando, M.D.A., Kounatidis, I. & Ligoxygakis, P., 2014. Loss of Trabid, a New Negative Regulator of the *Drosophila* Immune-Deficiency Pathway at the Level of TAK1, Reduces Life Span. E. Rulifson, ed. *PLoS Genetics*, 10(2), p.e1004117.
- Ferreira, A. et al., 2011. Sick Hemoglobin Confers Tolerance to Plasmodium Infection. *Cell*, 145(3), pp.398–409.
- French-Constant, R.H. et al., 1993. A point mutation in a *Drosophila* GABA receptor confers insecticide resistance. *Nature*, 363, pp.449–451.
- French-Constant, R.H., Daborn, P.J. & Goff, G.L., 2004. The genetics and genomics of insecticide resistance. *Trends in Genetics*, 20(3), pp.163–170.

- Field, L.M. et al., 1999. Relationship between amount of esterase and gene copy number in insecticide-resistant *Myzus persicae* (Sulzer). *Biochem. J.*, 339, pp.737–742.
- Fire, A. et al., 1998. Potent and specific genetic interference by double-stranded RNA in *Caenorhabditis elegans*. *Nature*, 391, pp.806–811.
- Fossog Tene, B. et al., 2013. Resistance to DDT in an Urban Setting: Common Mechanisms Implicated in Both M and S Forms of *Anopheles gambiae* in the City of Yaoundé Cameroon J. Vontas, ed. *PLoS ONE*, 8(4), p.e61408.
- Foster, W.A., 1995. Mosquito Sugar Feeding and Reproductive Energetics. *Annual Review of Entomology*, 40, pp.433–474.
- Freeman, E.G., Wisotsky, Z. & Dahanukar, A., 2014. Detection of sweet tastants by a conserved group of insect gustatory receptors. *PNAS*, 111(4), pp.1598–1603.
- Friggi-Grelin, F., Ich, M. & Birman, S., 2003. Tissue-specific developmental requirements of *Drosophila* tyrosine hydroxylase isoforms. *genesis*, 35(4), pp.260–269.
- Fujishiro, N., Kijima, H. & Morita, H., 1984. Impulse frequency and action potential amplitude in labellar chemosensory neurons of *Drosophila melanogaster*. *Journal of Insect Physiology*, 30, pp.317–325.
- Galindo, K. & Smith, D.P., 2001. A Large Family of Divergent *Drosophila* Odorant-Binding Proteins Expressed in Gustatory and Olfactory Sensilla. *Genetics*, 159, pp.1059–1072.
- Garcia-Sainz, J.A., Vieira, F.G. & Rozas, J., 2009. Molecular evolution of the major chemosensory gene families in insects. *Heredity*, 103(3), pp.208–216.
- Garrett-Jones, C. & Shidrawi, G.R., 1969. Malaria Vectorial Capacity of a Population of *Anopheles gambiae*. *Bulletin of the World Health Organization*, 40, pp.531–545.
- Garver, L. & Dimopoulos, G., 2007. Protocol for RNAi Assays in Adult Mosquitoes (*A. gambiae*). *Journal of Visualized Experiments*, (5), p.e230.
- Gary, R.E., Jr & Foster, W.A., 2004. *Anopheles gambiae* feeding and survival on honeydew and extra-floral nectar of peridomestic plants. *Medical and Veterinary Entomology*, 18, pp.102–107.
- Gassmann, A.J., Onstad, D.W. & Pittendrigh, B.R., 2009. Evolutionary analysis of herbivorous insects in natural and agricultural environments. *Pest Management Science*, 65(11), pp.1174–1181.

- GBD 2013 Mortality and Causes of Death Collaborators, 2015. Global, regional, and national age–sex specific all-cause and cause-specific mortality for 240 causes of death, 1990–2013: a systematic analysis for the Global Burden of Disease Study 2013. *The Lancet*, 385(9963), pp.117–171.
- Gelbart, W.M. & Emmert, D.B., 2013. FlyBase High Throughput Expression Pattern Data.
- Gething, P.W. et al., 2011. A new world malaria map: Plasmodium falciparum endemicity in 2010. *Malaria Journal*, 10(1), p.378.
- Ghosh, E. et al., 2015. Methodological advances: the unsung heroes of the GPCR structural revolution. *Nature Reviews Molecular Cell Biology*, 16(2), pp.69–81.
- Gibson, G. & Russell, I., 2006. Flying in Tune: Sexual Recognition in Mosquitoes. *Current Biology*, 16(13), pp.1311–1316.
- Gifford, A.N., 1991. The dopamine and 5-hydroxytryptamine content of locust and cockroach salivary neurones. *J. Exp. Biol.*, (161), pp.405–414.
- Gillies, M.T., 1954. The recognition of age-groups within populations of *Anopheles gambiae* by the pre-gravid rate and the sporozoite rate. *Annals of tropical medicine and parasitology*, 48(1), pp.58–74.
- Giraldo-Calderon, G.I. et al., 2015. VectorBase: an updated bioinformatics resource for invertebrate vectors and other organisms related with human diseases. *Nucleic Acids Research*, 43(D1), pp.D707–D713.
- Githeko, A.K. et al., 1996. Some Observations on the Biting Behavior of *Anopheles gambiae* s.s., *Anopheles arabiensis*, and *Anopheles funestus* and Their Implications for Malaria Control. *Experimental Parasitology*, 82, pp.306–315.
- Glendinning, J.I., 2008. Insect Gustatory Systems. *The Senses: A Comprehensive Reference*, 4, pp.75–95.
- Gobeil, F. et al., 2006. G-protein-coupled receptors signalling at the cell nucleus: an emerging paradigm. *Canadian Journal of Physiology and Pharmacology*, 84(3-4), pp.287–297.
- Gonzalez-Arenas, A. et al., 2006. Estrogens Cross-Talk to  $\alpha 1b$ -Adrenergic Receptors. *Molecular Pharmacology*, 70, pp.154–162.
- Goodisman, M.A.D. et al., 2005. Evolution of Insect Metamorphosis: a Microarray-Based Study of Larval and Adult Gene Expression in the Ant *Camponotus festinatus*. *Evolution*, 59(4), pp.858–870.
- Gorski, S.M. et al., 2003. A SAGE Approach to Discovery of Genes Involved in Autophagic Cell Death. *Current Biology*, 13, pp.358–363.

- Gotzes, F., Balfanz, S. & Baumann, A., 1994. Receptors & channels.: Primary structure and functional characterization of a *Drosophila* dopamine receptor with high homology to human D1/5 receptors. *Receptors and Channels*, 2, pp.131–141.
- Gracheva, E.O. et al., 2011. Ganglion-specific splicing of TRPV1 underlies infrared sensation in vampire bats. *Nature*, 476(7358), pp.88–91.
- Gracheva, E.O. et al., 2010. Molecular basis of infrared detection by snakes. *Nature*, 464(7291), pp.1006–1011.
- Grandl, J. et al., 2008. Pore region of TRPV3 ion channel is specifically required for heat activation. *Nature Neuroscience*, 11(9), pp.1007–1013.
- Grandl, J. et al., 2010. Temperature-induced opening of TRPV1 ion channel is stabilized by the pore domain. *Nature Publishing Group*, 13(6), pp.708–714.
- Granger, N.A., Ebersohl, R. & Sparks, T.C., 2000. Pharmacological characterization of dopamine receptors in the corpus allatum of *Manduca sexta* larvae. *Insect Biochemistry and Molecular Biology*, 30, pp.755–766.
- Granier, S. & Kobilka, B., 2012. A new era of GPCR structural and chemical biology. *Nature Chemical Biology*, 8(8), pp.670–673.
- Graveley, B.R. et al., 2011. The developmental transcriptome of *Drosophila melanogaster*. *Nature*, 471(7339), pp.473–479.
- Greenwood, B.M. et al., 2008. Malaria: progress, perils, and prospects for eradication. *Journal of Clinical Investigation*, 118(4), pp.1266–1276.
- Griebler, M. et al., 2008. RNA interference with the allatoregulating neuropeptide genes from the fall armyworm *Spodoptera frugiperda* and its effects on the JH titer in the hemolymph. *Journal of Insect Physiology*, 54(6), pp.997–1007.
- Gunning, R.V., Moores, G.D. & Devonshire, A.L., 1998. Inhibition of resistance-related esterase by piperonyl butoxide in *Helicoverpa armigera* (Hübner) (Lepidoptera: Noctuidae) and *Aphis gossypii* (Homoptera: Aphididae). *Piperonyl Butoxide*, pp.215–226.
- Hamada, F.N. et al., 2008. An internal thermal sensor controlling temperature preference in *Drosophila*. *Nature*, 454(7201), pp.217–220.
- Han, K.-A. et al., 1996. DAMB, a Novel Dopamine Receptor Expressed Specifically in *Drosophila* Mushroom Bodies. *Neuron*, 16, pp.1127–1135.
- Harbig, W.H., Pabst, M.J. & Jakoby, W.B., 1974. Glutathione S-Transferases. *The Journal of Biological Chemistry*, 249, pp.7130–7139.

- Harker, B.W. et al., 2012. Transcription Profiling Associated With Life Cycle of *Anopheles gambiae*. *Journal of Medical Entomology*, 49(2), pp.316–325.
- Harwood, B.N. et al., 2013. Membrane Tethered Bursicon Constructs as Heterodimeric Modulators of the *Drosophila* G Protein-Coupled Receptor Rickets. *Molecular Pharmacology*, 83(4), pp.814–821.
- Hauser, F. et al., 2006. A review of neurohormone GPCRs present in the fruitfly *Drosophila melanogaster* and the honey bee *Apis mellifera*. *Progress in Neurobiology*, 80(1), pp.1–19.
- Hearn, M.G. et al., 2002. A *Drosophila* dopamine 2-like receptor: Molecular characterization and identification of multiple alternatively spliced variants. *PNAS*, 99, pp.14554–14559.
- Heimbeck, G. et al., 1999. Smell and Taste Perception in *Drosophila melanogaster* Larva: Toxin Expression Studies in Chemosensory Neurons. *The Journal of Neuroscience*, 19(15), pp.6599–6609.
- Hemingway, J. & Ranson, H., 2000. Insecticide Resistance in Insect Vectors of Human Disease. *Annual Review of Entomology*, 45, pp.371–391.
- Hempelmann, E., 2006. Hemozoin Biocrystallization in *Plasmodium falciparum* and the antimalarial activity of crystallization inhibitors. *Parasitology Research*, 100(4), pp.671–676.
- Hill, C.A. et al., 2002. G Protein-Coupled Receptors in *Anopheles gambiae*. *Science*, 298(5591), pp.176–178.
- Hill, C.A. et al., 2013. Pesticide Biochemistry and Physiology. *Pesticide Biochemistry And Physiology*, 106(3), pp.141–148.
- Hiroi, M. et al., 2004. Two antagonistic gustatory receptor neurons responding to sweet-salty and bitter taste in *Drosophila*. *Journal of Neurobiology*, 61(3), pp.333–342.
- Hiroi, M., Marion-Poll, F. & Tanimura, T., 2002. Differentiated Response to Sugars among Labellar Chemosensilla in *Drosophila*. *Zoological Science*, 19(9), pp.1009–1018.
- Hodgson, E.S., Lettvin, J.Y. & Roeder, K.D., 1955. Physiology of a primary chemoreceptor unit. *Science*, 122, pp.417–418.
- Hodgson, E.S., Lettvin, J.Y. & Roeder, K.R., 1955. Physiology of a Primary Chemoreceptor Unit. *Science*, 122, pp.417–418.
- Hood, G.M., 2010. *PopTools version 3.2.5. Available on the internet. URL <http://www.poptools.org>.*

- Hopkins, T.L. et al., 1999. Pupal cuticle proteins of *Manduca sexta*: characterization and profiles during sclerotization. *Insect Biochemistry and Molecular Biology*, 30, pp.19–27.
- Horn, T. & Boutros, M., 2010. E-RNAi: a web application for the multi-species design of RNAi reagents--2010 update. *Nucleic Acids Research*, 38, pp.W332–W339.
- Howes, R.E. et al., 2011. The global distribution of the Duffy blood group. *Nature Communications*, 2, pp.270–10.
- Huang, D.W. et al., 2007. DAVID Bioinformatics Resources: expanded annotation database and novel algorithms to better extract biology from large gene lists. *Nucleic Acids Research*, 35(Web Server), pp.W169–W175.
- Huang, D.W., Sherman, B.T. & Lempicki, R.A., 2009. Bioinformatics enrichment tools: paths toward the comprehensive functional analysis of large gene lists. *Nucleic Acids Research*, 37(1), pp.1–13.
- Huvenne, H. & Smagghe, G., 2010. Mechanisms of dsRNA uptake in insects and potential of RNAi for pest control: A review. *Journal of Insect Physiology*, 56(3), pp.227–235.
- Hyde, J.E., 2002. Mechanisms of resistance of *Plasmodium falciparum* to antimalarial drugs. *Microbes and Infection*, 4, pp.165–174.
- Ibraheem, Z.O. et al., 2014. Role of Different Pfcrt and Pfmdr-1 Mutations in Conferring Resistance to Antimalaria Drugs in *Plasmodium falciparum*. *Malaria Research and Treatment*, 2014(1), pp.1–17.
- Ignell, R. et al., 2010. Assessment of diet choice by the yellow fever mosquito *Aedes aegypti*. *Physiological Entomology*, 35(3), pp.274–286.
- Inagaki, H.K. et al., 2012. Visualizing Neuromodulation In Vivo: TANGO-Mapping of Dopamine Signaling Reveals Appetite Control of Sugar Sensing. *Cell*, 148(3), pp.583–595.
- Insecticide Resistance Action Committee, 2011. Prevention and Management of Insecticide Resistance in Vectors of Public Health Importance. pp.1–72.
- Irland, R. et al., 1982. Ecdysterone Induces the Transcription of Four Heat-Shock Genes in *Drosophila* S3 Cells and Imaginal Discs. *Developmental Biology*, 93, pp.498–507.
- Ishimoto, H. et al., 2005. G-protein gamma subunit 1 is required for sugar reception in *Drosophila*. *The EMBO Journal*, 24, pp.3259–3265.
- Isono, K. & Morita, H., 2010. Molecular and cellular designs of insect taste receptor system. *Frontiers in Cellular Neuroscience*.

- Jackson, C.J. et al., 2013. Structure and function of an insect  $\alpha$ -carboxylesterase ( $\alpha$ Esterase7) associated with insecticide resistance. *PNAS*, 110, pp.10177–10182.
- Jaenicke, R., 1991. Protein stability and molecular adaptation to extreme conditions. *Eur. J. Biochem.*, 202, pp.715–728.
- Jones, C.M., Liyanapathirana, M., et al., 2012a. Footprints of positive selection associated with a mutation (N1575Y) in the voltage-gated sodium channel of *Anopheles gambiae*. *PNAS*, 109(17), pp.6614–6619.
- Jones, C.M., Sanou, A., et al., 2012b. Aging partially restores the efficacy of malaria vector control in insecticide-resistant populations of *Anopheles gambiae* s.l. from Burkina Faso. *Malaria Journal*, 11(1), p.24.
- Joosten, R.P. et al., 2012. PDB\_REDO: constructive validation, more than just looking for errors. *Acta Cryst (2012). D68*, pp. 484-496.
- Kang, K. et al., 2010. Analysis of *Drosophila* TRPA1 reveals an ancient origin for human chemical nociception. *Nature*, 464(7288), pp.597–600.
- Kang, K. et al., 2011. Modulation of TRPA1 thermal sensitivity enables sensory discrimination in *Drosophila*. *Nature*, 481(7379), pp.76–80.
- Katritch, V., Cherezov, V. & Stevens, R.C., 2013. Structure-Function of the G Protein–Coupled Receptor Superfamily. *Annual Review of Pharmacology and Toxicology*, 53(1), pp.531–556.
- Kelly-Hope, L.A. & McKenzie, F.E., 2009. The multiplicity of malaria transmission: a review of entomological inoculation rate measurements and methods across sub-Saharan Africa. *Malaria Journal*, 8(1), pp.1–16.
- Kent, L.B., Walden, K.K.O. & Robertson, H.M., 2007. The Gr Family of Candidate Gustatory and Olfactory Receptors in the Yellow-Fever Mosquito *Aedes aegypti*. *Chemical Senses*, 33(1), pp.79–93.
- Kessler, S., Vlimant, M. & Guerin, P.M., 2013. The sugar meal of the African malaria mosquito *Anopheles gambiae* and how deterrent compounds interfere with it: a behavioural and neurophysiological study. *Journal of Experimental Biology*, 216(7), pp.1292–1306.
- Kigozi, R. et al., 2012. Indoor Residual Spraying of Insecticide and Malaria Morbidity in a High Transmission Intensity Area of Uganda P. J. Milligan, ed. *PLoS ONE*, 7(8), p.e42857.
- Kim, Y.C., Lee, H.G. & Han, K.A., 2007. D1 Dopamine Receptor dDA1 Is Required in the Mushroom Body Neurons for Aversive and Appetitive Learning in *Drosophila*. *Journal of Neuroscience*, 27(29), pp.7640–7647.

- Klabunde, T. & Hessler, G., 2002. Knowledge for GPCR Lead Finding & Optimization. *ChemBioChem*, 3, pp.928–944.
- Koffi, A.A. et al., 2013. Insecticide resistance status of *Anopheles gambiae* s.s population from M'Bé: a WHOPEs-labelled experimental hut station, 10 years after the political crisis in Côte d'Ivoire. *Malaria Journal*, 12, pp.1–8.
- Kooperberg, C. et al., 2005. Significance testing for small microarray experiments. *Statistics in Medicine*, 24(15), pp.2281–2298.
- Knox, T.B. et al., 2014. An online tool for mapping insecticide resistance in major *Anopheles* vectors of human malaria parasites and review of resistance status for the Afrotropical region. *Parasites & Vectors*, 7, pp.1–14.
- Kobilka, B.K., 2007. G Protein Coupled Receptor Structure and Activation. *Biochim. Biophys. Acta.*, 1768(4), pp.794–807.
- Kong, E.C. et al., 2010. A Pair of Dopamine Neurons Target the D1-Like Dopamine Receptor DopR in the Central Complex to Promote Ethanol-Stimulated Locomotion in *Drosophila*. M. A. Frye, ed. *PLoS ONE*, 5(4), p.e9954.
- Korsinczky, M. et al., 2004. Sulfadoxine Resistance in *Plasmodium vivax* Is Associated with a Specific Amino Acid in Dihydropteroate Synthase at the Putative Sulfadoxine-Binding Site. *Antimicrobial Agents and Chemotherapy*, 48(6), pp.2214–2222.
- Krebs, R.A. & Feder, M.E., 1997. Deleterious consequences of Hsp70 overexpression in *Drosophila melanogaster* larvae. *Cell Stress & Chaperones*, 2, pp.60–71.
- Kristiansen, K., 2004. Molecular mechanisms of ligand binding, signaling, and regulation within the superfamily of G-protein-coupled receptors: molecular modeling and mutagenesis approaches to receptor structure and function. *Pharmacology & Therapeutics*, 103(1), pp.21–80.
- Kriventseva, E.V. et al., 2015. OrthoDB v8: update of the hierarchical catalog of orthologs and the underlying free software. *Nucleic Acids Research*, 43(D1), pp.D250–D256.
- Krogh, A. et al., 2001. Predicting transmembrane protein topology with a hidden markov model: application to complete genomes. *Journal of Molecular Biology*, 305(3), pp.567–580.
- Kwon, H.-W. et al., 2006. Olfactory responses in a gustatory organ of the malaria vector mosquito *Anopheles gambiae*. *PNAS*, 103, pp.13526–13531.
- Labbe, P. et al., 2007. Independent Duplications of the Acetylcholinesterase Gene Conferring Insecticide Resistance in the Mosquito *Culex pipiens*. *Molecular Biology and Evolution*, 24(4), pp.1056–1067.



- Labbé, P. et al., 2007. Forty Years of Erratic Insecticide Resistance Evolution in the Mosquito *Culex pipiens*. *PLoS Genetics*, 3(11), p.e205.
- Lacaille, F. et al., 2007. An Inhibitory Sex Pheromone Tastes Bitter for *Drosophila* Males Y. Rao, ed. *PLoS ONE*, 2(8), p.e661.
- Lagerström, M.C. & Schiöth, H.B., 2008. Structural diversity of G protein-coupled receptors and significance for drug discovery. *Nature Reviews Drug Discovery*, 7(4), pp.339–357.
- Laishram, D.D. et al., 2012. The complexities of malaria diseasemanifestations with a focus on asymptomaticmalaria. *Malaria Journal*, 11(1), p.29.
- Larkin, M.A. et al., 2007. Clustal W and Clustal X version 2.0. *Bioinformatics*, 23(21), pp.2947–2948.
- Lebestky, T. et al., 2009. Two Different Forms of Arousal in *Drosophila* Are Oppositely Regulated by the Dopamine D1 Receptor Ortholog DopR via Distinct Neural Circuits. *Neuron*, 64(4), pp.522–536.
- Le Goff, G. et al., 2003. Microarray analysis of cytochrome P450 mediated insecticide resistance in *Drosophila*. *Insect Biochemistry and Molecular Biology*, 33(7), pp.701–708.
- Lee, K.-Z. & Ferrandon, D., 2011. Negative regulation of immune responses on the fly. *The EMBO Journal*, 30(6), pp.988–990.
- Lee, Y. et al., 2012. Gustatory Receptors Required for Avoiding the Insecticide L-Canavanine. *Journal of Neuroscience*, 32(4), pp.1429–1435.
- Lee, Y., Moon, S.J. & Montella, C., 2009. Multiple gustatory receptors required for the caffeine response in *Drosophila*. *PNAS*, 106, pp.4495–4450.
- Lenormand, T. et al., 1999. Tracking the evolution of insecticide resistance in the mosquito *Culex pipiens*. *Nature*, 400, pp.861–864.
- Levy, F., 2003. Proteomic Analysis of the Systemic Immune Response of *Drosophila*. *Molecular & Cellular Proteomics*, 3(2), pp.156–166.
- Lhocine, N. et al., 2008. PIMS Modulates Immune Tolerance by Negatively Regulating *Drosophila* Innate Immune Signaling. *Cell Host and Microbe*, 4(2), pp.147–158.
- Liang, J. et al., 2010. Expression profile of cuticular genes of silkworm, *Bombyx mori*. *BMC Genomics*, 11, pp.1–13.
- Liapakis, G. et al., 2000. The forgotten serine. A critical role for ser-203<sup>5.42</sup> in ligand binding to and activation of the beta 2-adrenergic receptor. *Journal of Biological Chemistry*, 275(48), pp.37779–37788.

- Lin, G.G.-H. & Scott, J.G., 2011. Pesticide Biochemistry and Physiology. *Pesticide Biochemistry And Physiology*, 100(2), pp.130–134.
- Lin, Y. et al., 2001. Substrate Inhibition Kinetics for Cytochrome P450-Catalyzed Reactions. *Drug Metabolism and Disposition*, 29(1), pp.368–374.
- Lines, J.D. & Nassor, N.S., 1991. DDT resistance in *Anopheles gambiae* declines with mosquito age. *Medical and Veterinary Entomology*, 5, pp.261–265.
- Ling, F. et al., 2014. The Molecular and Cellular Basis of Taste Coding in the Legs of *Drosophila*. *Journal of Neuroscience*, 34(21), pp.7148–7164.
- Liu, B., Hui, K. & Qin, F., 2003. Thermodynamics of Heat Activation of Single Capsaicin Ion Channels VR1. *Biophysical Journal*, 85(5), pp.2988–3006.
- Liu, N. & Scott, J.G., 1996. Genetic analysis of factors controlling high-level expression of cytochrome P450, CYP6D1, cytochrome b5, P450 reductase, and monooxygenase activities in LPR house flies, *Musca domestica*. *Biochem Genet*, 34, pp.133–148.
- Livingstone, M.S. & Tempel, B.L., 1983. Genetic dissection of monoamine neurotransmitter synthesis in *Drosophila*. *Nature*, 303, pp.67–70.
- Lo, E. et al., 2015. Molecular epidemiology of *Plasmodium vivax* and *Plasmodium falciparum* malaria among Duffy-positive and Duffy-negative populations in Ethiopia. *Malaria Journal*, pp.1–10.
- Louis-Clement Gouagna et al., 2010. Patterns of sugar feeding and host plant preferences in adult males of *An. gambiae* (Diptera: Culicidae). *Journal of Vector Ecology*, 35, pp.267–276.
- Lu, G., 2005. TRPV1b, a Functional Human Vanilloid Receptor Splice Variant. *Molecular Pharmacology*, 67(4), pp.1119–1127.
- Lumjuan, N. et al., 2005. Elevated activity of an Epsilon class glutathione transferase confers DDT resistance in the dengue vector, *Aedes aegypti*. *Insect Biochemistry and Molecular Biology*, 35(8), pp.861–871.
- Luna, C. et al., 2002. Characterization of four Toll related genes during development and immune responses in *Anopheles gambiae*. *Insect Biochemistry and Molecular Biology*, 32, pp.1171–1179.
- Lyimo, E.O., Takken, W. & Koella, J.C., 1992. Effect of rearing temperature and larval density on larval survival, age at pupation and adult size of *Anopheles gambiae*. *Entomologia Experimentalis et Applicata*, 63, pp.265–271.
- Maekawa, E. et al., 2011. The role of proboscis of the malaria vector mosquito *Anopheles stephensi* in host-seeking behavior. *Parasites & Vectors*, 4(1), p.10.

- Maillet, F. et al., 2008. The *Drosophila* Peptidoglycan Recognition Protein PGRP-LF Blocks PGRP-LC and IMD/JNK Pathway Activation. *Cell Host and Microbe*, 3(5), pp.293–303.
- Makler, M.T., Piper, R.C. & Milhous, W.K., 1998. Lactate Dehydrogenase and the Diagnosis of Malaria. *Parasitology Today*, 14(9), pp.376–377.
- Marella, S. et al., 2006. Imaging Taste Responses in the Fly Brain Reveals a Functional Map of Taste Category and Behavior. *Neuron*, 49(2), pp.285–295.
- Martens, W.J., 1998. Health impacts of climate change and ozone depletion: an ecoepidemiologic modeling approach. *Environmental Health Perspectives*, 106, pp.241–251.
- Martinez-Torres, D. et al., 1998. Molecular characterization of pyrethroid knockdown resistance (*kdr*) in the major malaria vector *Anopheles gambiae* s.s. *Insect Molecular Biology*, 7(2), pp.179–184.
- Mason, P.J., Hall, L.M.C. & Gausz, J., 1984. The expression of heat shock genes during normal development in *Drosophila melanogaster* (heat shock/abundant transcripts/developmental regulation). *Mol Gen Genet*, 194, pp.73–78.
- McCoy, A.J. et al., 2007. Phaser crystallographic software. *Journal of Applied Crystallography*, 40(4), pp.658–674.
- McIver, S.B., Wilkes, T.J. & Gillies, M.T., 1980. Attraction to mammals of male *Mansonia (Mansonioides)* (Diptera: Culicidae). *Bulletin of entomological research*, 70(1), pp.11–16.
- Merz, A. et al., 2000. Improving the Catalytic Activity of a Thermophilic Enzyme at Low Temperatures †. *Biochemistry*, 39(5), pp.880–889.
- Meunier, N. et al., 2003. Peripheral coding of bitter taste in *Drosophila*. *Journal of Neurobiology*, 56(2), pp.139–152.
- Meyer, J.M. et al., 2012. A “Genome-to-Lead” Approach for Insecticide Discovery: Pharmacological Characterization and Screening of *Aedes aegypti* D1-like Dopamine Receptors R. R. Dinglasan, ed. *PLoS Neglected Tropical Diseases*, 6(1), p.e1478.
- Meyerhof, W. et al., 2010. The Molecular Receptive Ranges of Human TAS2R Bitter Taste Receptors. *Chemical Senses*, 35(2), pp.157–170.
- Michel, K. et al., 2005. *Anopheles gambiae* SRPN2 facilitates midgut invasion by the malaria parasite *Plasmodium berghei*. *EMBO Reports*, 6(9), pp.891–897.
- Michel, K. et al., 2006. Increased melanizing activity in *Anopheles gambiae* does not affect development of *Plasmodium falciparum*. *PNAS*, 103, pp.16858–16863.

- Mitchell, A. et al., 2015a. The InterPro protein families database: the classification resource after 15 years. *Nucleic Acids Research*, 43(D1), pp.D213–D221.
- Mitchell, B.K., Itagaki, H. & Rivet, M.-P., 1999. Peripheral and Central Structures Involved in Insect Gustation. *Microscopy research and technique*, 47, pp.401–415.
- Mitchell, S.N. et al., 2012. Identification and validation of a gene causing cross-resistance between insecticide classes in *Anopheles gambiae* from Ghana. *PNAS*, 109(16), pp.6147–6152.
- Mitchell, S.N. et al., 2015b. Evolution of sexual traits influencing vectorial capacity in anopheline mosquitoes. *Science*, 347(6225), pp.985–988.
- Mitchell, S.N. et al., 2014. Metabolic and Target-Site Mechanisms Combine to Confer Strong DDT Resistance in *Anopheles gambiae* K. Michel, ed. *PLoS ONE*, 9(3), p.e92662.
- Miyazaki, T. & Ito, K., 2010. Neural architecture of the primary gustatory center of *Drosophila melanogaster* visualized with GAL4 and LexA enhancer-trap systems. *The Journal of Comparative Neurology*, 518(20), pp.4147–4181.
- Monastirioti, M., 1999. Biogenic amine systems in the fruit fly *Drosophila melanogaster*. *Microscopy research and technique*, 45, pp.106–121.
- Moon, S.J. et al., 2009. A *Drosophila* Gustatory Receptor Essential for Aversive Taste and Inhibiting Male-to-Male Courtship. *Current Biology*, 19(19), pp.1623–1627.
- Moon, S.J. et al., 2006. A Taste Receptor Required for the Caffeine Response In Vivo. *Current Biology*, 16(18), pp.1812–1817.
- Mosca, R. & Schneider, T.R., 2008. RAPIDO: a web server for the alignment of protein structures in the presence of conformational changes. *Nucleic Acids Research*, 36(Web Server), pp.W42–W46.
- Müller, P. et al., 2008. Field-Caught Permethrin-Resistant *Anopheles gambiae* Overexpress CYP6P3, a P450 That Metabolises Pyrethroids D. L. Stern, ed. *PLoS Genetics*, 4(11), p.e1000286.
- Muller, G.C. et al., 2010. Successful field trial of attractive toxic sugar bait (ATSB) plant-spraying methods against malaria vectors in the *Anopheles gambiae* complex in Mali, West Africa. *Malaria Journal*, 9(210), pp.1–7.
- Murray, C.K. & Bennett, J.W., 2009. Rapid Diagnosis of Malaria. *Interdisciplinary Perspectives on Infectious Diseases*, 2009(1), pp.1–7.
- Murshudov, G.N. et al., 2011. REFMAC5 for the refinement of macromolecular crystal structures. *Acta Cryst (2011). D67*, 355-367, pp.1–13.

- Mustard, J.A. et al., 2003. Analysis of two D1-like dopamine receptors from the honey bee *Apis mellifera* reveals agonist-independent activity. *Molecular Brain Research*, 113(1-2), pp.67–77.
- Mustard, J.A., Beggs, K.T. & Mercer, A.R., 2005. Molecular biology of the invertebrate dopamine receptors. *Archives of Insect Biochemistry and Physiology*, 59(3), pp.103–117.
- Myllymaki, H. & Ramet, M., 2013. Transcription factor *zfh1* downregulates *Drosophila* Imd pathway. *Developmental and Comparative Immunology*, 39(3), pp.188–197.
- Mysore, K. et al., 2014. Chitosan/siRNA nanoparticle targeting demonstrates a requirement for single-minded during larval and pupal olfactory system development of the vector mosquito *Aedes aegypti*. *BMC Developmental Biology*, 14, pp.1–16.
- Mysore, K. et al., 2013. Disruption of *Aedes aegypti* Olfactory System Development through Chitosan/siRNA Nanoparticle Targeting of semaphorin-1a J. M. C. Ribeiro, ed. *PLoS Neglected Tropical Diseases*, 7(5), p.e2215.
- Napoli, C., Lemieux, C. & Jorgensen, R., 2002. Introduction of a Chimeric Chalcone Synthase Gene into *Petunia* Results in Reversible Co-Suppression of Homologous Genes. *The Plant Cell*, 2, pp.279–289.
- Nájera, J.A., González-Silva, M. & Alonso, P.L., 2011. Some Lessons for the Future from the Global Malaria Eradication Programme (1955–1969). *PLoS Medicine*, 8(1), p.e1000412.
- Namoutougou, M. et al., 2012. Multiple Insecticide Resistance in *Anopheles gambiae* s.l. Populations from Burkina Faso, West Africa J. Vontas, ed. *PLoS ONE*, 7(11), p.e48412.
- Neafsey, D.E. et al., 2015. Highly evolvable malaria vectors: The genomes of 16 *Anopheles* mosquitoes. *Science*, 347(6217), pp.1258522–1258522.
- Neckameyer, W. et al., 2001. Dopamine and Sensory Tissue Development in *Drosophila melanogaster*. *Developmental Neurobiology*, 47, pp.280–294.
- Neckameyera, W.S. & Quinna, W.G., 1989. Isolation and characterization of the gene for *Drosophila* tyrosine hydroxylase. *Neuron*, 2, pp.1167–1175.
- NPIC, 2002. Bendiocarb technical fact sheet. National Pesticide Information Centre, Oregon State University. Available at: <http://npic.orst.edu/factsheets/bendiotech.pdf>. pp.1–5.
- Neubig, R.R. & Siderovski, D.P., 2002. Regulators of G-protein Signalling as New Central Nervous System Drug Targets. *Nature Reviews Drug Discovery*, 1(3), pp.187–197.

- Newby, L. & Jackson, R.F., 1991. *Drosophila* Ebony Mutants Have Altered Circadian Activity Rhythms but Normal Eclosion Rhythms. *Journal of Neurogenetics*, 7, pp.85–101.
- Newcomb, R.D. et al., 1997. A single amino acid substitution converts a carboxylesterase to an organophosphorus hydrolase and confers insecticide resistance on a blowfly. *PNAS*, 94, pp.7464–7468.
- Nuss, A.B. et al., 2015. Dopamine Receptor Antagonists as New Mode-of-Action Insecticide Leads for Control of *Aedes* and *Culex* Mosquito Vectors P. J. McCall, ed. *PLoS Neglected Tropical Diseases*, 9(3), p.e0003515.
- Oduola, A.O. et al., 2012. Evidence of carbamate resistance in urban populations of *Anopheles gambiae* s.s. mosquitoes resistant to DDT and deltamethrin insecticides in Lagos, South-Western Nigeria. *Parasites & Vectors*, 5(1), pp.1–8.
- Okoye, P.N. et al., 2008. Characterisation of DDT, pyrethroid and carbamate resistance in *Anopheles funestus* from Obuasi, Ghana. *Transactions of the Royal Society of Tropical Medicine and Hygiene*, 102(6), pp.591–598.
- Ortelli, F. et al., 2003. Heterologous expression of four glutathione transferase genes genetically linked to a major insecticide-resistance locus from the malaria vector *Anopheles gambiae*. *Biochem. J.*, 373, pp.957–963.
- Overington, J.P., Al-Lazikani, B. & Hopkins, A.L., 2006. How many drug targets are there? *Nature Reviews*, 5, pp.993–996.
- O'Neill, P.M., Barton, V.E. & Ward, S.A., 2010. The Molecular Mechanism of Action of Artemisinin—The Debate Continues. *Molecules*, 15(3), pp.1705–1721.
- Pandey, A.V. et al., 1999. Artemisinin, an Endoperoxide Antimalarial, Disrupts the Hemoglobin Catabolism and Heme Detoxification Systems in Malarial Parasite. *The Journal of Biological Chemistry*, 274(27), pp.19383–19388.
- Pappas, L.G. & Larsen, J.R., 1976. Gustatory Hairs on the Mosquito, *Culiseta inornata*. *The Journal of Experimental Zoology*, 196, pp.351–360.
- Pappas, L.G. & Larsen, J.R., 1978. Gustatory mechanisms and sugar-feeding in the mosquito, *Culiseta inornata*. *Physiological Entomology*, 3, pp.115–119.
- Park, D. et al., 2004. Ap-let neurons—a peptidergic circuit potentially controlling ecdysial behavior in *Drosophila*. *Developmental Biology*, 269(1), pp.95–108.
- Patapoutian, A., Tate, S. & Woolf, C.J., 2009. Transient receptor potential channels: targeting pain at the source. *Nature Reviews Drug Discovery*, 8(1), pp.55–68.
- Perry, T., Batterham, P. & Daborn, P.J., 2011. The biology of insecticidal activity and resistance. *Insect Biochemistry and Molecular Biology*, 41(7), pp.411–422.

- Petersen, I., Eastman, R. & Lanzer, M., 2011. Drug-resistant malaria: Molecular mechanisms and implications for public health. *FEBS Letters*, 585(11), pp.1551–1562.
- Philipsborn, von, A.C. et al., 2011. Neuronal Control of *Drosophila* Courtship Song. *Neuron*, 69(3), pp.509–522.
- Pinto, J. et al., 2007. Multiple Origins of Knockdown Resistance Mutations in the Afrotropical Mosquito Vector *Anopheles gambiae* N. Ahmed, ed. *PLoS ONE*, 2(11), p.e1243.
- Pitts, R.J. et al., 2011. pitts\_chemosensorytranscriptome\_2011. *BMC Genomics*, 12(1), p.271.
- Pitts, R.J., Fox, A.N. & Zwiebel, L.J., 2004. A highly conserved candidate chemoreceptor expressed in both olfactory and gustatory tissues in the malaria vector *Anopheles gambiae*. *PNAS*, 101(14), pp.5058–5063.
- Polerstock, A.R., Eigenbrode, S.D. & Klowden, M.J., 2002. Mating Alters the Cuticular Hydrocarbons of Female *Anopheles Gambiae* Sensu Stricto and *Aedes Aegypti* (Diptera: Culicidae). *Journal of Medical Entomology*, 39(3), pp.545–552.
- Ponton, F. et al., 2011. Journal of Insect Physiology. *Journal of Insect Physiology*, 57(6), pp.840–850.
- Prapanthadara, L., Hemingway, J. & Ketterman, A., 1993. Partial purification and characterization of glutathione S-transferases involved in DDT resistance from the mosquito *Anopheles gambiae*. *Pesticide biochemistry and physiology*, 47, pp.119–133.
- Prapanthadara, L.-A., Hemingway, J. & Ketterman, A.J., 1995. DDT resistance in *Anopheles gambiae* (Diptera, Culicidae) from Zanzibar, Tanzania, based on increased DDT dehydrochlorinase activity of Glutathione S-Transferases. *Bulletin of entomological research*, 85, pp.267–274.
- Puinean, A.M. et al., 2010. Amplification of a Cytochrome P450 Gene Is Associated with Resistance to Neonicotinoid Insecticides in the Aphid *Myzus persicae* D. L. Stern, ed. *PLoS Genetics*, 6(6), p.e1000999.
- R-Core-Team, 2012. R: A Language and Environment for Statistical Computing. pp.1–3604.
- Ramphul, U. et al., 2009. Insecticide resistance and its association with target-site mutations in natural populations of *Anopheles gambiae* from eastern Uganda. *Transactions of the Royal Society of Tropical Medicine and Hygiene*, 103(11), pp.1121–1126.

- Ranson, H. et al., 2000. Identification of a point mutation in the voltage-gated sodium channel gene of Kenyan *Anopheles gambiae* associated with resistance to DDT and pyrethroids. *Insect Molecular Biology*, 9(5), pp.491–497.
- Ranson, H. et al., 2000. Genetic mapping of two loci affecting DDT resistance in the malaria vector *Anopheles gambiae*. *Insect Molecular Biology*, 9(5), pp.499–507.
- Ranson, H. et al., 2001. Identification of a novel class of insect glutathione S-transferases involved in resistance to DDT in the malaria vector *Anopheles gambiae*. *Biochem. J.*, 359, pp.295–304.
- Ranson, H. et al., 2009. Insecticide resistance in *Anopheles gambiae*: data from the first year of a multi-country study highlight the extent of the problem. *Malaria Journal*, 8(1), p.299.
- Ranson, H. et al., 2011. Pyrethroid resistance in African anopheline mosquitoes: what are the implications for malaria control? *Trends in Parasitology*, 27(2), pp.91–98.
- Reale, V. et al., 1997. Agonist-Specific Coupling of a Cloned *Drosophila melanogaster* D1-Like Dopamine Receptor to Multiple Second Messenger Pathways by Synthetic Agonists. *The Journal of Neuroscience*, 17, pp.6545–6553.
- Reimer, L. et al., 2008. Relationship Between *kdr* Mutation and Resistance to Pyrethroid and DDT Insecticides in Natural Populations of *Anopheles gambiae*. *J. Med Entomol.*, 45(2), pp.260–266.
- Riehle, M.A. et al., 2002. Neuropeptides and Peptide Hormones in *Anopheles gambiae*. *Science*, 298, pp.172–175.
- Riemensperger, T. et al., 2010. Behavioral consequences of dopamine deficiency in the *Drosophila* central nervous system. *PNAS*, 108, pp.834–839.
- Ringo, J., 1996. Sexual Receptivity in Insects. *Annual Review of Entomology*, 41, pp.473–494.
- Ritter, S.L. & Hall, R.A., 2009. Fine-tuning of GPCR activity by receptor-interacting proteins. *Nature Reviews Molecular Cell Biology*, 10(12), pp.819–830.
- Riveron, J.M. et al., 2013. Directionally Selected Cytochrome P450 Alleles Are Driving the Spread of Pyrethroid Resistance in the Major Malaria Vector *Anopheles funestus*. *PNAS*, 110(1), pp.252–257.
- Robertson, H.M., Warr, C.G. & Carlson, J.R., 2003. Molecular evolution of the insect chemoreceptor gene superfamily in *Drosophila melanogaster*. *PNAS*, 100, pp.14537–14542.
- Rodrigues, V. & Siddiqi, O., 1978. Genetic analysis of chemosensory pathway. *Proceedings B. Indian Academy of Sciences*, 87, pp.147–160.



- Rogers, D.W. et al., 2009. Transglutaminase-Mediated Semen Coagulation Controls Sperm Storage in the Malaria Mosquito D. S. Schneider, ed. *PLoS Biology*, 7(12), p.e1000272.
- Romano, N. & Macino, G., 1992. *Quelling: transient inactivation of gene expression in Neurospora crassa by transformation with homologous sequences*, Mol Microbiol.
- Rosenbaum, D.M., Rasmussen, S.G.F. & Kobilka, B.K., 2009. The structure and function of G-protein-coupled receptors. *Nature*, 459(7245), pp.356–363.
- Rozenfeld, R. & Devi, L.A., 2010. Receptor heteromerization and drug discovery. *Trends in Pharmacological Sciences*, 31(3), pp.124–130.
- Rubin, G.M. & Spradling, A.C., 1982. Genetic Transformation of Drosophila with Transposable Element Vectors. *Science*, 218, pp.348–353.
- Russell, C.B. & Hunter, F.F., 2002. Analysis of nectar and honeydew feeding in Aedes and Ochlerotatus mosquitoes. *Journal of American Mosquito Control Association*, 18(2), pp.86–90.
- Rynes, J. et al., 2012. Activating Transcription Factor 3 Regulates Immune and Metabolic Homeostasis. *Molecular and Cellular Biology*, 32(19), pp.3949–3962.
- Ryu, J.H. et al., 2004. The Homeobox Gene Caudal Regulates Constitutive Local Expression of Antimicrobial Peptide Genes in Drosophila Epithelia. *Molecular and Cellular Biology*, 24(1), pp.172–185.
- Saavedra-Rodriguez, K. et al., 2007. A mutation in the voltage-gated sodium channel gene associated with pyrethroid resistance in Latin American Aedes aegypti. *Insect Molecular Biology*, 16(6), pp.785–798.
- Sala Junior, V. et al., 2008. Floral nectar chemical composition of floral nectar in conventional and transgenic sweet orange, Citrus sinensis (L.) Osbeck, expressing an antibacterial peptide. *Plant Systematics and Evolution*, 275(1-2), pp.1–7.
- Sanford, J.L., Shields, V.D.C. & Dickens, J.C., 2013. Gustatory receptor neuron responds to DEET and other insect repellents in the yellow-fever mosquito, Aedes aegypti. *Naturwissenschaften*, 100(3), pp.269–273.
- Santolamazza, F. et al., 2008. Insertion polymorphisms of SINE200 retrotransposons within speciation islands of Anopheles gambiae molecular forms. *Malaria Journal*, 7(1), p.163.
- Schlee, S. et al., 2009. Activation of Anthranilate Phosphoribosyltransferase from Sulfolobus solfataricus by Removal of Magnesium Inhibition and Acceleration of Product Release. *Biochemistry*, 48(23), pp.5199–5209.

- Schmidt, J.M. et al., 2010. Copy Number Variation and Transposable Elements Feature in Recent, Ongoing Adaptation at the Cyp6g1 Locus D. J. Begun, ed. *PLoS Genetics*, 6(6), p.e1000998.
- Schmittgen, T.D. & Livak, K.J., 2008. Analyzing real-time PCR data by the comparative CT method. *Nature Protocols*, 3(6), pp.1101–1108.
- Schneider, K.A. & Escalante, A.A., 2013. Fitness components and natural selection: why are there different patterns on the emergence of drug resistance in *Plasmodium falciparum* and *Plasmodium vivax*? *Malaria Journal*, 12(15), pp.1–11.
- Scott, J.G. et al., 2013. Towards the elements of successful insect RNAi. *Journal of Insect Physiology*, 59(12), pp.1212–1221.
- Scott, K. et al., 2001. A Chemosensory Gene Family Encoding Candidate Gustatory and Olfactory Receptors in *Drosophila*. *Cell*, 104, pp.661–673.
- Scuderi, A. & Letsou, A., 2005. Amnioserosa is required for dorsal closure in *Drosophila*. *Developmental Dynamics*, 232(3), pp.791–800.
- Seenivasagan, T. et al., 2009. Surface morphology and morphometric analysis of sensilla of Asian tiger mosquito, *Aedes albopictus* (Skuse): an SEM investigation. *J Vector Borne Dis*, 46, pp.125–135.
- Sen, G.L. & Blau, H.M., 2006. A brief history of RNAi: the silence of the genes. *The FASEB Journal*, 20(9), pp.1293–1299.
- Seugnet, L. et al., 2008. D1 Receptor Activation in the Mushroom Bodies Rescues Sleep-Loss-Induced Learning Impairments in *Drosophila*. *Current Biology*, 18(15), pp.1110–1117.
- Shakhmantsir, I., Massad, N.L. & Kennell, J.A., 2013. Regulation of cuticle pigmentation in *drosophila* by the nutrient sensing insulin and TOR signaling pathways. *Developmental Dynamics*, 243(3), pp.393–401.
- Shanbhag, S. et al., 2001. Gustatory organs of *Drosophila melanogaster* : fine structure and expression of the putative odorant-binding protein PBPRP2. *Cell and Tissue Research*, 304(3), pp.423–437.
- Shandilya, A. et al., 2013. A plausible mechanism for the antimalarial activity of artemisinin: A computational approach. *Scientific Reports*, 3.
- Shin, S.C. et al., 2011. *Drosophila* Microbiome Modulates Host Developmental and Metabolic Homeostasis via Insulin Signaling. *Science*, 334(6056), pp.670–674.
- Sibley, C.H. et al., 2001. Pyrimethamine–sulfadoxine resistance in *Plasmodium falciparum*: what next? *Trends in Parasitology*, 17(12), pp.582–588.

- Sinden, R.E., 2002. Molecular interactions between Plasmodium and its insect vectors. *Cellular Microbiology*, 4(11), pp.713–724.
- Singh, B. & Daneshvar, C., 2013. Human Infections and Detection of Plasmodium knowlesi. *Clinical Microbiology Reviews*, 26(2), pp.165–184.
- Singh, N.R., 1997. Neurobiology of the Gustatory Systems of Drosophila and Some Terrestrial Insects. *Microscopy research and technique*, 39, pp.547–563.
- Sinka, M.E. et al., 2012. A global map of dominant malaria vectors. *Parasites & Vectors*, 5, pp.1–11.
- Sirotkin, K. & Davidson, N., 1982. Developmentally Regulated Transcription from Drosophila melanogaster Chromosomal Site 67B. *Developmental Biology*, 89, pp.196–210.
- Smillie, W.G., 1952. *The period of great epidemics in the United States (1800-1875). The history of American epidemiology.* C.V. Mosby. St. Louis, Missouri.
- Smith, D.L. & Ellis McKenzie, F., 2004. Statics and dynamics of malaria infection in Anopheles mosquitoes. *Malaria Journal*, 3(1), p.13.
- Smith, D.T. et al., 2011. DDT resistance, epistasis and male fitness in flies. *Journal of Evolutionary Biology*, 24(6), pp.1351–1362.
- Snow, R.W. et al., 1999. Estimating mortality, morbidity and disability due to malaria among Africa's non-pregnant population. *Bulletin of the World Health Organization*, 77, pp.624–640.
- Sparks, J.T., Vinyard, B.T. & Dickens, J.C., 2013. Insect Biochemistry and Molecular Biology. *Insect Biochemistry and Molecular Biology*, 43(12), pp.1161–1171.
- Srivastava, D.P., 2005. Rapid, Nongenomic Responses to Ecdysteroids and Catecholamines Mediated by a Novel Drosophila G-Protein-Coupled Receptor. *Journal of Neuroscience*, 25(26), pp.6145–6155.
- St Pierre, S.E. et al., 2014. FlyBase 102--advanced approaches to interrogating FlyBase. *Nucleic Acids Research*, 42, pp.D780–D788. Available at: <http://nar.oxfordjournals.org/lookup/doi/10.1093/nar/gkt1092>.
- Stark, K.R. & James, A.A., 1996. Anticoagulants in Vector Arthropods. *Parasitology Today*, 12(11), pp.430–437.
- Sterner, R. & Liebl, W., 2001. Thermophilic Adaptation of Proteins. *Critical Reviews in Biochemistry and Molecular Biology*, 36(1), pp.1–68.
- Stevenson, B.J. et al., 2011. Insect Biochemistry and Molecular Biology. *Insect Biochemistry and Molecular Biology*, 41(7), pp.492–502.

- Stocker, R.F., 1994. The organization of the chemosensory system in *Drosophila melanogaster*: a review. *Cell and Tissue Research*, 275, pp.3–26.
- Stone, C.M., Jackson, B.T. & Foster, W.A., 2012. Effects of Plant-Community Composition on the Vectorial Capacity and Fitness of the Malaria Mosquito *Anopheles gambiae*. *American Journal of Tropical Medicine and Hygiene*, 87(4), pp.727–736.
- Storelli, G. et al., 2011. Lactobacillus plantarum Promotes *Drosophila* Systemic Growth by Modulating Hormonal Signals through TOR-Dependent Nutrient Sensing. *Cell Metabolism*, 14(3), pp.403–414.
- Sugamori, K.S. et al., 1995. A primordial dopamine D1-like adenylyl cyclase-linked receptor from *Drosophila melanogaster* displaying poor affinity for benzazepines. *FEBS*, 362, pp.131–138.
- Sumba, L.A. et al., 2008. Regulation of Oviposition in *Anopheles gambiae* s.s.: Role of Inter- and Intra-Specific Signals. *Journal of Chemical Ecology*, 34(11), pp.1430–1436.
- Suwanchaichinda, C. & Kanost, M.R., 2009. The serpin gene family in *Anopheles gambiae*. *Gene*, 442(1-2), pp.47–54.
- Szklarczyk, D. et al., 2010. The STRING database in 2011: functional interaction networks of proteins, globally integrated and scored. *Nucleic Acids Research*, 39(Database), pp.D561–D568.
- Šimo, L. et al., 2011. Evidence for D1 Dopamine Receptor Activation by a Paracrine Signal of Dopamine in Tick Salivary Glands I. Hansen, ed. *PLoS ONE*, 6(1), p.e16158.
- Šimo, L. et al., 2014. Invertebrate specific D1-like dopamine receptor in control of salivary glands in the black-legged tick *Ixodes scapularis*. *The Journal of Comparative Neurology*, 522(9), pp.2038–2052.
- Tadevosyan, A. et al., 2012. G protein-coupled receptor signalling in the cardiac nuclear membrane: evidence and possible roles in physiological and pathophysiological function. *The Journal of Physiology*, 590(6), pp.1313–1330.
- Takahashi, K.H. et al., 2010. Effects of small Hsp genes on developmental stability and microenvironmental canalization. *BMC Evolutionary Biology*, 10(1), p.284.
- Takken, W. et al., 2006. Mosquito mating behaviour. pp.183–188.
- Takken, W., van Loon, J.J. & Adam, W., 2001. Inhibition of host-seeking response and olfactory responsiveness in *Anopheles gambiae* following blood feeding. *Journal of Insect Physiology*, 47, pp.303–310.

- Talavera, K. et al., 2005. Heat activation of TRPM5 underlies thermal sensitivity of sweet taste. *Nature*, 438(7070), pp.1022–1025.
- Tauszig, S. et al., 2000. Toll-related receptors and the control of antimicrobial peptide expression in *Drosophila*. *PNAS*, 97, pp.10520–10525.
- Tautermann, C.S. & Pautsch, A., 2011. The Implication of the First Agonist Bound Activated GPCR X-ray Structure on GPCR in Silico Modeling. *ACS Medicinal Chemistry Letters*, 2(6), pp.414–418.
- The malERA Consultative Group on Vector Control, 2011. A Research Agenda for Malaria Eradication: Vector Control. *PLoS Medicine*, 8(1), p.e1000401.
- Thorne, N. et al., 2004. Taste Perception and Coding in *Drosophila*. *Current Biology*, 14(12), pp.1065–1079.
- Tracey, W.D. et al., 2003. *painless*, a *Drosophila* Gene Essential for Nociception. *Cell*, 113, pp.261–273.
- Tripet, F. et al., 2003. Frequency of Multiple Inseminations in Field-Collected *Anopheles gambiae* Females Revealed by DNA Analysis of Transferred Sperm. *Am J Trop Med Hyg*, 68(1), pp.1–5.
- Troppmann, B. et al., 2014. Characterization of an Invertebrate-Type Dopamine Receptor of the American Cockroach, *Periplaneta americana*. *International Journal of Molecular Sciences*, 15(1), pp.629–653.
- Truman, J.W. & Riddiford, L.M., 2007. The morphostatic actions of juvenile hormone. *Insect Biochemistry and Molecular Biology*, 37(8), pp.761–770.
- Tryselius, Y. et al., 1992. *CecC*, a cecropin gene expressed during metamorphosis in *Drosophila* pupae. *Eur. J. Biochem.*, 204, pp.1–5.
- Uchida, K. & Tominaga, M., 2011. The role of thermosensitive TRP (transient receptor potential) channels in insulin secretion. *Endocrine Journal*, 58(12), pp.1021–1028.
- Ueno, T. & Kume, K., 2014. Functional characterization of dopamine transporter in vivo using *Drosophila melanogaster* behavioral assays. *Frontiers in Behavioral Neuroscience*, 8, pp.1–11.
- Valles, A.M. & White, K., 1986. Development of serotonin-containing neurons in *Drosophila* mutants unable to synthesize serotonin. *The Journal of Neuroscience*, 6, pp.1482–1491.
- van den Berg, H. et al., 2012. Global Trends in the Use of Insecticides to Control Vector-Borne Diseases. *Environmental Health Perspectives*, 120(4), pp.577–582.

- Vanden Broeck, J., 2001. Insect G Protein-Coupled Receptors and Signal Transduction. *Archives of Insect Biochemistry and Physiology*, 48, pp.1–12.
- Vaniotis, G. et al., 2011. Cellular Signalling. *Cellular Signalling*, 23(1), pp.89–98.
- Venken, K.J.T. et al., 2006. P[acman]: A BAC Transgenic Platform for Targeted Insertion of Large DNA Fragments in *D. melanogaster*. *Science*, 314, pp.1747–1751.
- Verleyen, P. et al., 2006. Identification of new immune induced molecules in the haemolymph of *Drosophila melanogaster* by 2D-nanoLC MS/MS. *Journal of Insect Physiology*, 52(4), pp.379–388.
- Vincent, F., 2005. Structure and Kinetics of a Monomeric Glucosamine 6-Phosphate Deaminase: Missing link of the NagB superfamily? *Journal of Biological Chemistry*, 280(20), pp.19649–19655.
- Viswanath, V. et al., 2003. Opposite thermosensor in fruitfly and mouse. *Nature*, 423, pp.822–823.
- Vontas, J. et al., 2007. Transcriptional analysis of insecticide resistance in *Anopheles stephensi* using cross-species microarray hybridization. *Insect Molecular Biology*, 16(3), pp.315–324.
- Vos, M.H. et al., 2006. TRPV1b overexpression negatively regulates TRPV1 responsiveness to capsaicin, heat and low pH in HEK293 cells. *Journal of Neurochemistry*, 99(4), pp.1088–1102.
- Vosshall, L.B. et al., 1999. A Spatial Map of Olfactory Receptor Expression in the *Drosophila* Antenna. *Cell*, 96, pp.725–736.
- Vyklicky, L. et al., 1999. Temperature coefficient of membrane currents induced by noxious heat in sensory neurones in the rat. *The Journal of Physiology*, 517, pp.181–192.
- Wada-Katsumata, A., Silverman, J. & Schal, C., 2013. Changes in Taste Neurons Support the Emergence of an Adaptive Behavior in Cockroaches. *Science*, 340(6135), pp.972–975.
- Waddell, S., 2013. Reinforcement signalling in *Drosophila*; dopamine does it all after all. *Current Opinion in Neurobiology*, 23(3), pp.324–329.
- Wang, G. et al., 2009. *Anopheles gambiae* TRPA1 is a heat-activated channel expressed in thermosensitive sensilla of female antennae. *European Journal of Neuroscience*, 30(6), pp.967–974.
- Wang, J. et al., 2013a. WEB-based GENE SeT AnaLYsis Toolkit (WebGestalt): update 2013. *Nucleic Acids Research*, 41(W1), pp.W77–W83.

- Wang, J.-W., Beck, E.S. & McCabe, B.D., 2012. A Modular Toolset for Recombination Transgenesis and Neurogenetic Analysis of *Drosophila*. G. Roman, ed. *PLoS ONE*, 7(7), p.e42102.
- Wang, P.-H. et al., 2013b. Analysis of Expression, Cellular Localization, and Function of Three Inhibitors of Apoptosis (IAPs) from *Litopenaeus vannamei* during WSSV Infection and in Regulation of Antimicrobial Peptide Genes (AMPs) S. D. Fugmann, ed. *PLoS ONE*, 8(8), p.e72592.
- Wang, Y. et al., 2008. Journal of Structural Biology. *Journal of Structural Biology*, 164(2), pp.228–235.
- Wang, Z. et al., 2004. Taste Representations in the *Drosophila* Brain. *Cell*, 117, pp.981–991.
- Warhurst, D.C., 2001. A Molecular Marker for Chloroquine-Resistant *Falciparum Malaria*. 344(4), pp.299–302.
- Watts, R.J. et al., 2004. Glia Engulf Degenerating Axons during Developmental Axon Pruning. *Current Biology*, 14(8), pp.678–684.
- Weetman, D. et al., 2010. Association Mapping of Insecticide Resistance in Wild *Anopheles gambiae* Populations: Major Variants Identified in a Low-Linkage Disequilibrium Genome K. Y. K. Chan, ed. *PLoS ONE*, 5(10), p.e13140.
- Weiczorek, H. & Wolff, G., 1988. The labellar sugar receptor of *Drosophila*. *Journal of Comparative Physiology A*, 164, pp.825–834.
- Weill, M. et al., 2000. The *kdr* mutation occurs in the Mopti form of *Anopheles gambiae* s.s. through introgression. *Insect Molecular Biology*, 9(5), pp.451–455.
- Weill, M. et al., 2003. Insecticide resistance in mosquito vectors. *Nature*, 423, pp.136–137.
- Weill, M. et al., 2004. The unique mutation in *ace-1* giving high insecticide resistance is easily detectable in mosquito vectors. *Insect Molecular Biology*, 13(1), pp.1–7.
- Weiss, L.A. et al., 2011. The Molecular and Cellular Basis of Bitter Taste in *Drosophila*. *Neuron*, 69(2), pp.258–272.
- Wheatley, M. et al., 2012. Lifting the lid on GPCRs: the role of extracellular loops. *British Journal of Pharmacology*, 165(6), pp.1688–1703.
- Wheeler, D.L. et al., 2007. Database resources of the National Center for Biotechnology Information. *Nucleic Acids Research*, 35(Database), pp.D5–D12.

- White, N.J. et al., 2014. Malaria. *The Lancet*, 383, pp.723–735.
- Wilkins, E.E. et al., 2009. Authentication scheme for routine verification of genetically similar laboratory colonies: a trial with *Anopheles gambiae*. *BMC Biotechnology*, 9(1), p.91.
- Williams, L.L., 1963. Malaria Eradication in the United States. *American Journal of Public Health*, 53(1), pp.1–5.
- Williams, T.N., 2006. Human red blood cell polymorphisms and malaria. *Current Opinion in Microbiology*, 9(4), pp.388–394.
- Wittkopp, P.J., Carroll, S.B. & Kopp, A., 2003. Evolution in black and white: genetic control of pigment patterns in *Drosophila*. *Trends in Genetics*, 19(9), pp.495–504.
- Wodarz, A. et al., 1995. Expression of Crumbs Confers Apical Character on Plasma Membrane Domains of Ectodermal Epithelia of *Drosophila*. *Cell*, 82, pp.67–76.
- World Health Organization, 2014. World Malaria Report: 2014. pp.1–142.
- World Health Organization, 2011. World Malaria Report: 2011. pp.1–107.
- World Health Organization, 2012. World Malaria Report: 2012. pp.1–124.
- Wong, D.M. et al., 2012. Select Small Core Structure Carbamates Exhibit High Contact Toxicity to “Carbamate-Resistant” Strain Malaria Mosquitoes, *Anopheles gambiae* (Akron) I. Silman, ed. *PLoS ONE*, 7(10), p.e46712.
- Wright, C.D. et al., 2012. Nuclear localization drives  $\alpha$ 1-adrenergic receptor oligomerization and signaling in cardiac myocytes. *Cellular Signalling*, 24(3), pp.794–802.
- Wright, L.G. et al., 1996. Molecular Characterization of the 71E Late Puff in *Drosophila melanogaster* Reveals a Family of Novel Genes. *J. Mol. Biol.*, 255, pp.387–400.
- Wright, T.R.F., 1987. The genetics of biogenic amine metabolism, sclerotization, and melanization in *Drosophila melanogaster*. *Advances in Genetics*, 24, pp.127–222.
- Wright, T.R.F., Hodgetts, R.B. & Sherald, A.F., 1976. The Genetics of Dopa Decarboxylase in *Drosophila melanogaster*. *Genetics*, 84, pp.267–285.
- Wu, H. et al., 2003. MAANOVA: A Software Package for the Analysis of Spotted cDNA Microarray Experiments. *The Analysis of Gene Expression Data: Methods and Software*, pp.313–341.
- Wu, L.J., Sweet, T.B. & Clapham, D.E., 2010. International Union of Basic and Clinical Pharmacology. LXXVI. Current Progress in the Mammalian TRP Ion Channel Family. *Pharmacological Reviews*, 62(3), pp.381–404.



- Yamamoto, S. & Seto, E.S., 2014. Dopamine Dynamics and Signaling in *Drosophila*: An Overview of Genes, Drugs and Behavioral Paradigms. *Exp. Anim.*, 63(2), pp.107–119.
- Yang, C.H. et al., 2008. *Drosophila* Egg-Laying Site Selection as a System to Study Simple Decision-Making Processes. *Science*, 319(5870), pp.1679–1683.
- Yang, F. et al., 2010. Thermosensitive TRP channel pore turret is part of the temperature activation pathway. *PNAS*, 107(15), pp.7083–7088.
- Yao, J., Liu, B. & Qin, F., 2011. Modular thermal sensors in temperature-gated transient receptor potential (TRP) channels. *PNAS*, 108(27), pp.11109–11114.
- Young, S.J., Gunning, R.V. & Moores, G.D., 2005. The effect of piperonyl butoxide on pyrethroid-resistance-associated esterases in *Helicoverpa armigera* (Hubner) (Lepidoptera: Noctuidae). *Pest Management Science*, 61(4), pp.397–401.
- Zhang, B., Kirov, S. & Snoddy, J., 2005. WebGestalt: an integrated system for exploring gene sets in various biological contexts. *Nucleic Acids Research*, 33(Web Server), pp.W741–W748.
- Zhang, H.-J. et al., 2011. Topological and Functional Characterization of an Insect Gustatory Receptor F. Marion-Poll, ed. *PLoS ONE*, 6(8), p.e24111.
- Zhang, K. et al., 2007. Dopamine-Mushroom Body Circuit Regulates Saliency-Based Decision-Making in *Drosophila*. *Science*, 316(5833), pp.1901–1904.
- Zhang, R. & Xie, X., 2012. Tools for GPCR drug discovery. *Nature Publishing Group*, pp.1–13.
- Zhang, X. et al., 2015. Chitosan/Interfering RNA Nanoparticle Mediated Gene Silencing in Disease Vector Mosquito Larvae. *Journal of Visualized Experiments*, (97).
- Zhang, X., Zhang, J. & Zhu, K.Y., 2010. Chitosan/double-stranded RNA nanoparticle-mediated RNA interference to silence chitin synthase genes through larval feeding in the African malaria mosquito (*Anopheles gambiae*). *Insect Molecular Biology*, 19(5), pp.683–693.
- Zhang, Z. & Palli, S.R., 2009. Identification of a cis-regulatory element required for 20-hydroxyecdysone enhancement of antimicrobial peptide gene expression in *Drosophila melanogaster*. *Insect Molecular Biology*, 18(5), pp.595–605.
- Zhou, X. & Riddiford, L.M., 2002. Broad specifies pupal development and mediates the “status quo” action of juvenile hormone on the pupal-adult transformation in *Drosophila* and *Manduca*. *Development*, 129, pp.2259–2269.

- Zraly, C.B., Middleton, F.A. & Dingwall, A.K., 2006. Hormone-response Genes Are Direct in Vivo Regulatory Targets of Brahma (SWI/SNF) Complex Function. *Journal of Biological Chemistry*, 281(46), pp.35305–35315.
- Zucker, J.R., 2009. Changing Patterns of Autochthonous Malaria Transmission in the United States: A Review of Recent Outbreaks. *Emerging Infectious Diseases*, 2, pp.37–43.